PHOTOCATALYTIC STRATEGIES FOR THE FUNCTIONALIZATION OF PYRIDINES

Eleni Georgiou

UNIVERSITAT ROVIRA i VIRGILI

Photocatalytic Strategies for the Functionalization of Pyridines

ELENI GEORGIOU

DOCTORAL THESIS
2023

Eleni Georgiou

Photocatalytic Strategies for the Functionalization of Pyridines

Doctoral Thesis

Supervised by Prof. Paolo Melchiorre and Prof. Kilian Muñiz

ICIQ – Institut Català d'Investigació Química

Tarragona

2023

UNIVERSITAT ROVIRA i VIRGILI

ICIQ Institut Català d'Investigació Química

Prof. Paolo Melchiorre, ICREA Research Professor & ICIQ Group Leader

I STATE that the present study, entitled "Photocatalytic Strategies for the Functionalization of Pyridines", presented by ELENI GEORGIOU for the award of the degree of Doctor, has been carried out under the supervision of Prof. Kilian Muñiz, in memoriam, and under my supervision at the Institut Català d'Investigació Química (ICIQ).

Tarragona, May 3rd 2023

Doctoral Thesis Supervisor

Prof. Paolo Melchiorre

Acknowledgements

I would like to thank my PhD supervisors, Prof. Kilian Muñiz, and Prof. Paolo Melchiorre for both giving me the opportunity to join their research groups and for their continuous support and guidance.

Next, I would like to thank Sorania Jiménez for the administrative support through the all the years of my doctoral studies. Apart from her exceptional work, she has also been supportive in many other ways.

I would also like to thank all past members of the Muñiz group and all past and present members of the Melchiorre group and for the scientific and personal support and for all the beautiful moments spent together inside and outside the lab. I had the opportunity to meet people from both research groups, which have been excellent colleagues and friends. During the first one and half years of my PhD studies as a member of the Muñiz group I shared a lot of moments with the rest of the group. I had the pleasure of working with great scientists where we exchanged advice and ideas. A huge thanks is going to Alexandra Bosnidou (Anda), Estefanía Del Castillo (Estefi), Thomas Duhamel, Daniel Bafaluy (Bafa), Èric Cots, Alienor Jeandin, Jiayu Zhang and Jixiang Ni. I also thank Dr. Kang Chen, which I had the opportunity to work with. After the unexpected and dramatic loss of Kilian, I had a warm welcome from the Melchiorre group. Thanks to our laboratory technician Miguel Sellés. Next, I would like to thank colleagues and friends which I had shared with a lot: Yann Baumgartner, Jan Vilím (Yann & Jan), Eduardo de Pedro Beato (Edu), Martin Berger, Vasileios Tseliou, Adriana Faraone, Wei Zhou, Laura Kqiku, Thomas H.-F. Wong, Florian Schiel and Shuo Wu. In addition, I would like to thank Davide Spinnato, Emilien Le Saux, Will Hartley and Igor Dmitriev which I had a great collaboration with. I take the chance to thank also all the people that welcomed me during my short research stay in ETH Zurich and Prof. Bill Morandi.

I would like to thank all the research support units at ICIQ, in particular the Spectroscopy and Material Characterization Unit (especially Dr. Georgiana Stoica), the NMR unit, the HRMS unit, the Chemical Reaction Technologies unit, and the HTE Laboratory (especially Dr. Xisco Caldentey).

I would like to acknowledge the financial support from Institute of Chemical Research of Catalonia (ICIQ) and the Spanish Ministry of Science for a FPI predoctoral fellowship (CTQ2017-88158-R).

Finally, deepest gratitude to my family, my fiancé and my friends.

Ευχαριστώ!

List of Publications

Some of the results presented in this thesis have been published:

- Georgiou, E.;[+] Spinnato, D.;[+] Chen, K.; Melchiorre, P.; Muñiz, K. "Switchable photocatalysis for the chemodivergent benzylation of 4-cyanopyridines" *Chem. Sci.* **2022**, *13,* 8060−8064.

- Le Saux, E.; Georgiou, E.; Dmitriev, I. A.; Hartley, W. C.; Melchiorre, P. "Photochemical Organocatalytic Functionalization of Pyridines via Pyridinyl Radicals" *J. Am. Chem. Soc.* **2023**, *145,* 47–52.

Στην οικογένεια μου.

Table of Contents

Chapter I

Introduction

This doctoral study focuses on the functionalization of pyridines and related azaarenes using new photochemical organocatalytic processes. The aim of this chapter is to provide the readers with a general overview of the conventional methods to functionalize pyridines and recent advances in the field along with the challenges that have been addressed and those that remain. In particular, I will discuss the more useful reactions for pyridine functionalization based on both polar and radical mechanisms (Figure 1.1).

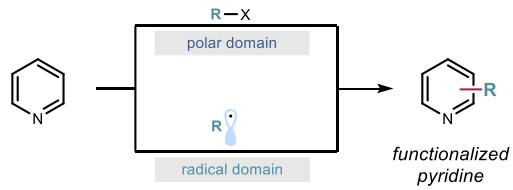

Figure 1.1. Functionalization of pyridine and other azaarenes in polar and radical domain.

1.1 Importance and Ubiquity of Pyridines and other Azaarenes

Nitrogen-containing heterocycles are ubiquitous structural motifs in pharmaceuticals and naturally occurring bioactive compounds.[1] *N*-heterocycles also found broad application in material sciences and as ligands in metal catalysis.[2] According to a survey published in 2021, pyridine is ranked no. 1 in FDA approved drugs within all *N*-heterocycles (Figure 1.2).[3] This trend continues today, with new entries added in the FDA approved drugs list and other pyridine-based structures being at phase III of clinical trials.

---

[1] (a) Baumann, M.; Baxendale, I. R. "An overview of the synthetic routes to the best selling drugs containing 6-membered heterocycles" *Beilstein J. Org. Chem.* **2013**, *9*, 2265–2319; (b) Vitaku, E.; Smith, D. T.; Njardarson, J. T. "Analysis of the structural diversity, substitution patterns, and frequency of nitrogen heterocycles among U.S. FDA approved pharmaceuticals" *J. Med. Chem.* **2014**, *57*, 10257–10274.

[2] (a) Matolscy, G. *Pesticide Chemistry.*; Elsevier Scientific: Amsterdam, **1988**; (b) Leclerc, N.; Sanaur, S.; Galmiche, L.; Mathevet, F.; Attias, A.-J.; Fave, J.-L.; Roussel, J.; Hapiot, P.; Lemaître, N.; Geffroy, B. C "6-(Arylvinylene)-3-bromopyridine Derivatives as Lego Building Blocks for Liquid Crystal, Nonlinear Optical, and Blue Light Emitting Chromophores" *Chem. Mater.* **2005**, *17*, 502–513; (c) Zafar, M. N.; Atif, A. H.; Nazar, M. F.; Sumrra, S. H.; Gul-E-Saba; Paracha, R. "Pyridine and related ligands in transition metal homogeneous catalysis" *Russ. J. Coord. Chem.* **2016**, *42*, 1–18.

[3] Bhutani, P.; Joshi, G.; Raja, N.; Bachhav, N.; Rajanna, P. K.; Bhutani, H.; Paul, A. T.; Kumar, R. "U.S. FDA Approved Drugs from 2015-June 2020: A Perspective" *J. Med. Chem.* **2021**, *64*, 2339-2381.

The prevalence of pyridines and other azaarenes in pharmaceuticals largely depend on their unique properties. Pyridines are often chosen as bioisosters to replace certain arenes or other heteroarenes on a drug candidate, including isoxazoles, pyrazoles, nitrophenols, indanones or even benzene.[4]

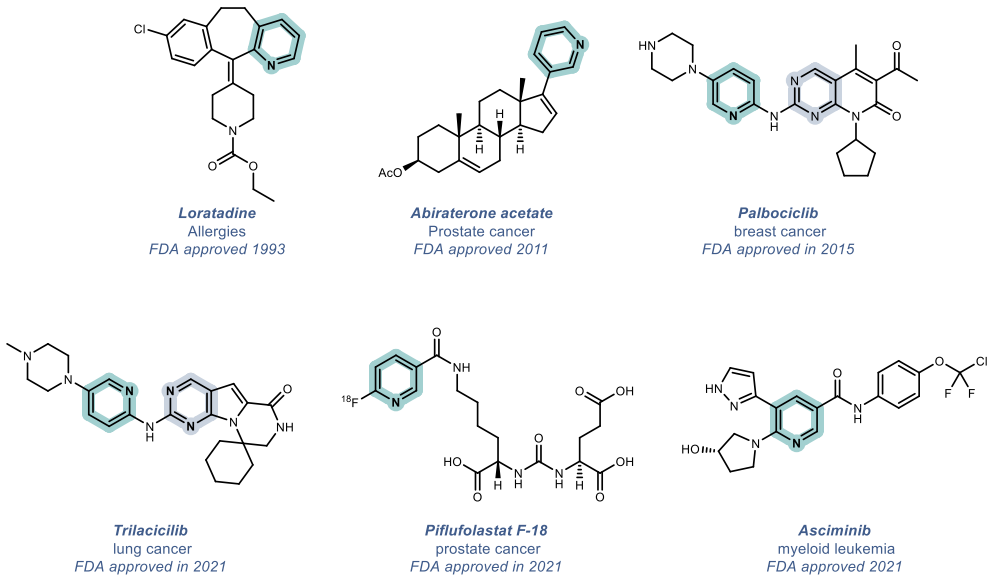

Figure 1.2. Examples of pyridine- and other azaarene-containing pharmaceuticals.

Pyridines can also affect solubility, metabolic stability, binding affinity, cellular penetrance, and target engagement of a drug to a specific target.[5] The nitrogen lone pair is a key component of the pyridine properties. The lone pair has the ability to act as a hydrogen donor acceptor, increasing the binding affinity in protein active sites.[6] Increased aqueous solubility can also be observed in the presence of azaarenes within drug molecules, which can improve the overall bioavailability and uptake in the circulatory system. It is therefore no surprise that the discovery and development of new drugs rely heavily on chemists' ability to modify/diversify these commonly occurring structures. Expanding beyond known methodologies for pyridine functionalization is of great value to the toolkit of medicinal chemists and more broadly within the chemical industry.

[4] Gaikwad, P. L.; Gandhi, P. S.; Jagdale, D. M.; Kadam, V. "The use of bioisosterism in drug design and molecular modification" J. *Am. J. PharmTech Res.* **2012**, *2*, 1−23.
[5] Smith, D. A. in *Metabolism, Pharmacokinetics, and Toxicity of Functional Groups: Impact of the Building Blocks of Medicinal Chemistry in ADMET*.; Royal Society of Chemistry, 2010.
[6] Serafim, R.A.M.; de Souza Gama, F.H.; Dutra, L.A.; Dos Reis, C.V.; Vasconcelos, S.N.S.; da Silva Santiago, A.; Takarada, J.E.; Di Pillo, F.; Azevedo, H.; Mascarello, A.; *et al.* "Development of Pyridine-based Inhibitors for the Human Vaccinia-related Kinases 1 and 2" *ACS Med. Chem. Lett.* **2019**, *10*, 1266–1271.

1.2 Conventional Methodologies for the Functionalization of Pyridines

Pyridine is often compared to the structurally similar benzene. The replacement of a carbon atom of an aryl ring with nitrogen comes with several changes in reactivity. The nitrogen in a pyridine ring is sp^2 hybridized and its lone pair is perpendicular to the π-system, therefore the electrons cannot be donated to the ring. In addition, nitrogen is more electronegative than carbon, resulting in a more electron-deficient π-system. Those characteristics make pyridines attractive for drug design. However, the functionalization of pyridines is challenging. Some of the main issues in pyridine chemistry are the control of regioselectivity, the undesirable coordination of the Lewis basic nitrogen to metal complexes, and the susceptibility to oxidation (Figure 1.3).[7, 8]

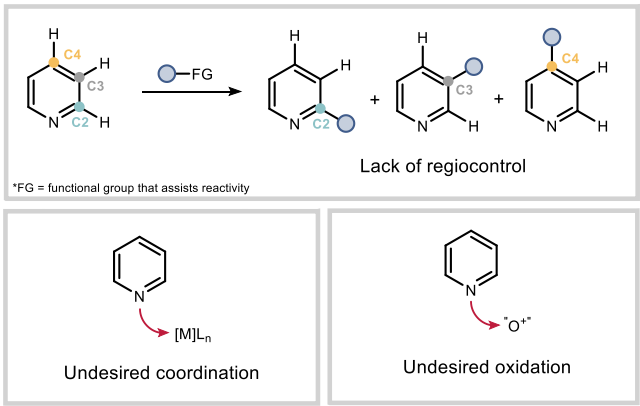

Figure 1.3. Challenges associated with the direct functionalization of pyridines using traditional methods.

Despite these challenges, the direct functionalization of the pyridine core is attractive, and significant progress has been made. The electrophilic aromatic substitution (EAS) reactions, including halogenation, are classic ways to functionalize aromatic compounds. Introduction of a halogen on the aromatic ring through EAS then allowed its use as a handle for further reactions, including cross coupling and radical processes. Halogenation through EAS is generally conducted at room temperature for electron rich arenes; however, pyridine requires much harsher conditions due to its π-electron deficiency. The bromination reaction of pyridine **1a** requires strong thermal conditions, a strong acid (such as sulfuric acid), and elemental bromine (Scheme 1.1).[9] The severity of those conditions hampers the applicability to

[7] Brahmachari, G. in *Green Synthetic Approaches for Biologically Relevant Heterocycles*. Elsevier, 2014.
[8] Joule, J. A.; Mills, K. in *Heterocyclic Chemistry, 5th ed.*; Wiley/Blackwell Publishing Ltd., 2010.
[9] Grimmett, M. R. *Adv. Heterocycl. Chem.* "Halogenation of Heterocycles: II. Six- and Seven-Membered Rings" **1993**, *58*, 271−345.

functionalized pyridines with labile functional groups or moieties that can react with bromine. The brominated product **2a** is formed with C3 selectivity, however the dibrominated adduct **2a'** can also be observed. A common strategy to increase the electron density of the pyridine ring is *via* oxidative activation to form the corresponding *N*-oxide **3**.[10] In this case, C4-bromination is achieved at the cost of two additional steps: installation and removal of the *N*-oxide group.

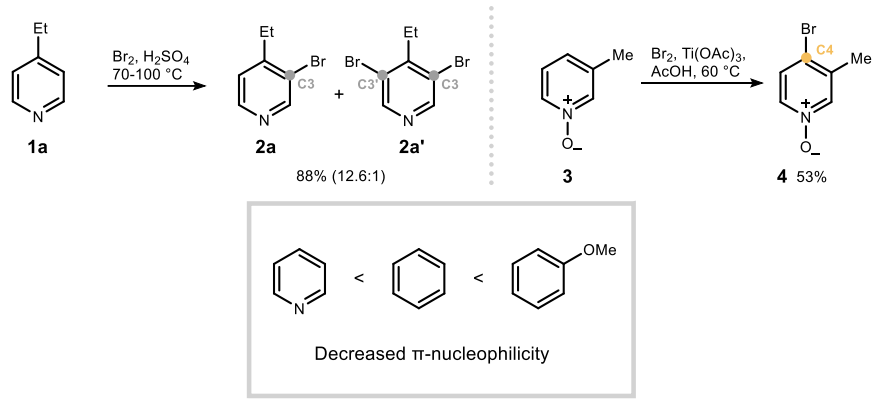

Scheme 1.1. The electrophilic aromatic substitution (bromination) of pyridine requires harsh conditions.

The Chichibabin reaction, reported in 1914, is one of the oldest methods to functionalize pyridines (Scheme 1.2).[11,12] Chichibabin *et al*. described the C2-amination of pyridine **1** using sodium amide that proceeds through an addition/elimination mechanism. First, the nucleophilic attack of sodium amide at the C2 position forms a Meisenheimer σ-adduct intermediate, followed by the loss of hydride to restore aromaticity affording product **5**. While effective, one major disadvantage of the method is the necessity of the strongly basic $NaNH_2$ and high temperatures, conditions which limit the functional group tolerance.[13]

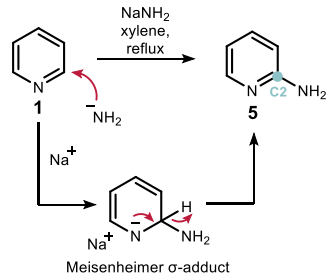

Scheme 1.2. The Chichibabin reaction and the proposed intermediate.

[10] Mosher, H. S.; Turner, L.; Carlsmith, A. "Pyridine-*N*-oxide" *Org. Synth.* **1953**, *33*, 79.
[11] Chichibabin, A. E.; Zeide, O. A. "New Reaction for Compounds Containing the Pyridine Nucleus". *J. Russ. Phys. Chem. Soc.* **1914**, *46*, 1216–36.
[12] Wang, Z. in *Comprehensive Organic Name Reactions and Reagents*.; John Wiley and Sons, Inc., 2010.
[13] McGill, C. K.; Rappa, A. *Adv. Heterocycl. Chem.* "Advances in the Chichibabin reaction" **1988**, *44*, 1−79.

Another classical approach to functionalize pyridines and other azaarenes is through direct metalation followed by trapping of an electrophile (Scheme 1.3).[14] This process requires a strong lithium or magnesium base to first deprotonate the pyridine (**1b**) to form a metalated species (not shown). Regiocontrol over the deprotonation step can be gained using pre-installed directing groups on the pyridine moiety.[15] The directing group coordinates the metal ion, which brings the base in close proximity to a specific C−H bond, resulting in C4 functionalized product **6**.

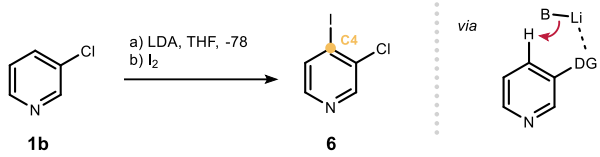

Scheme 1.3. Direct metalation followed by trapping with electrophile.

Radical chemistry offered new opportunities for the functionalization of pyridines.[16] The first example of radical-based pyridine functionalization was reported by Lynch (Scheme 1.4a).[17] Lynch observed that aryl radical addition into pyridines **1** gave a mixture of C2, C3, and C4 regioisomers **7**. It was also observed that the product distribution of the arylated pyridines changed when acetic acid was added in the reaction mixture.[18] Addition of acetic acid increased the selectivity towards the C2 product. In 1968, Minisci and coworkers demonstrated with their pioneering work that alkyl radicals, generated using strongly acidic conditions, could add into pyridine **1** at C2 and C4 positions (products **8**, Scheme 1.4b).[19,20] In 1971, Minisci *et al.* further expanded upon this observation, reporting a defining protocol, known today as the "*Minisci reaction*" (Scheme 1.4c). The chemistry relied on the generation

[14] Schlosser, M.; Mongin, F. "Pyridine elaboration through organometallic intermediates: regiochemical control and completeness" *Chem. Soc. Rev.* **2007**, *36*, 1161−1172.
[15] Rocca, P.; Marsais, F.; Godard, A.; Quéguiner, G. "Connection between metalation and cross-coupling strategies. A new convergent route to azacarbazoles" *Tetrahedron* **1993**, *49*, 49−64.
[16] Yan, M.; Lo, J. C.; Edwards, J. T.; Baran, P. S. "Radicals: Reactive Intermediates with Translational Potential" *J. Am. Chem. Soc.* **2016**, *138*, 12692−12714.
[17] Lynch, B. M.; Chang, H. S. "Concentration-dependent orientations in free-radical phenylations of heteroaromatic compounds" *Tetrahedron Lett.* **1964**, *5*, 2965–2968.
[18] Dou, H. J. M.; Lynch, B. M. "Selective free-radical phenylations: Nitrogen-heteroaromatic compounds in acidic media" *Tetrahedron Lett.* **1965**, *6*, 897–901.
[19] Minisci, F.; Galli, R.; Cecere, M.; Malatesta, V.; Caronna, T. "Nucleophilic character of alkyl radicals: new syntheses by alkyl radicals generated in redox processes" *Tetrahedron Lett.* **1968**, *9*, 5609–5612.
[20] Minisci, F.; Galli, R.; Malatesta, V.; Caronna, T. "Nucleophilic character of alkyl radicals–II: Selective alkylation of pyridine, quinoline and acridine by hydroperoxides and oxaziranes" *Tetrahedron* **1970**, *26*, 4083–4091.

of alkyl radicals through decarboxylation of various carboxylic acids under oxidative conditions (silver catalyst in combination with persulfate).[21]

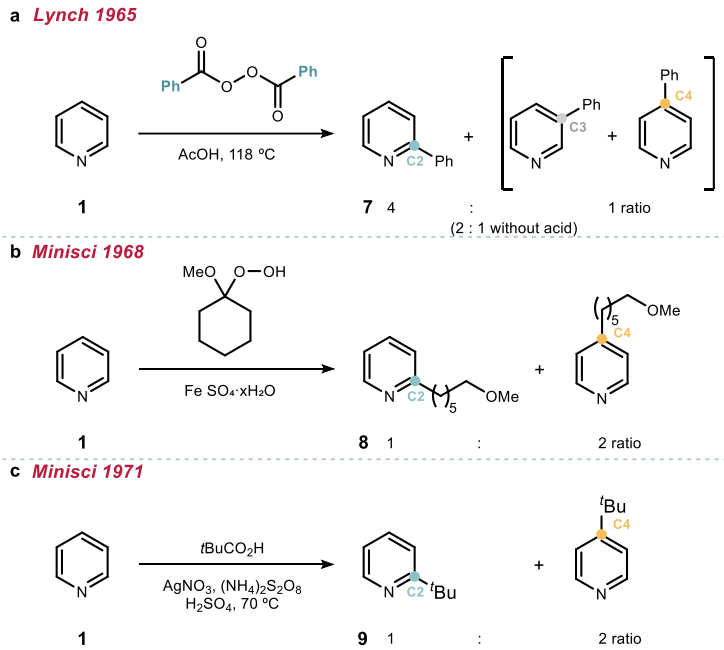

Scheme 1.4. Pioneering works for the radical addition to pyridines.

The Minisci protocol has been applied for the functionalization of both pyridines and quinolines. The mechanism of the nucleophilic addition of a carbon-centered radical into a heteroarene consists of four individual steps (Scheme 1.5). First, the commonly used stoichiometric acid leads to protonation of the heteroarene. The protonated heteroarene **1'** has lower LUMO energy, which facilitates the radical addition. Since the LUMO coefficients at the C2 and C4 of pyridine and quinoline moieties are similar, regioisomeric mixtures of the resulting radical cations are obtained (intermediates **I**).[22] A deprotonation step at the more acidic position, α (or γ) to the nitrogen radical cation **I**, leads to a neutral radical **II**. Finally, an oxidation step by the external oxidant restores the aromaticity affording products **9**.

[21] Minisci, F.; Bernardi, R.; Bertini, F.; Galli, R.; Perchinummo, M. "Nucleophilic character of alkyl radicals—VI: A new convenient selective alkylation of heteroaromatic bases" *Tetrahedron* **1971**, *27*, 3575–3579.

[22] Tauber J, Imbri D, Opatz T. "Radical Addition to Iminium Ions and Cationic Heterocycles" *Molecules* **2014**, *19*, 16190-16222.

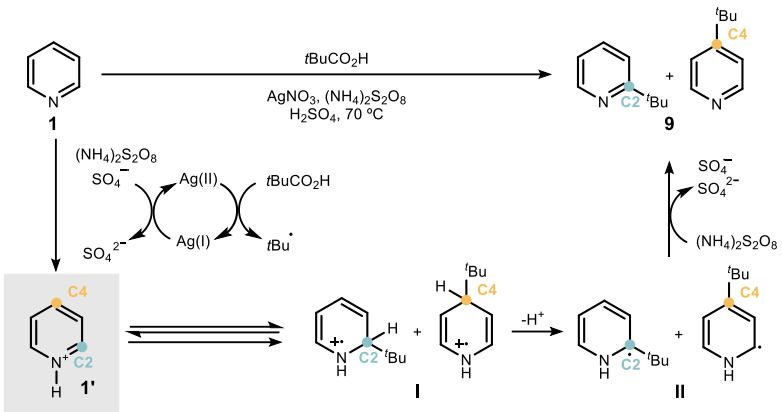

Scheme 1.5. Mechanism of the Minisci reaction.

Since the Minisci reaction does not suffer of problems often observed in metal-catalyzed functionalization of heteroarenes (inactivation of the metal catalyst upon binding of the substrate's nitrogen), this strategy is attractive for application in medicinal chemistry. In addition, a main advantage is the possibility to apply the Minisci chemistry at different stages of drug discovery (including late stage), leading to functionalized heteroarene-containing drug candidates.[23] Despite the significant advancements in pyridine functionalization using the Minisci reaction, there is still great demand to improve the regioselectivity and to expand the scope of radical precursors.[24] The following section details how photoredox catalysis contributed to achieve these goals.

1.3 Recent Developments in the Functionalization of Pyridines

1.3.1 Photoredox catalysis

The last decade has seen a resurgence of interest in photoredox catalysis.[25] As a result, a new conceptual framework and new chemical disconnections to access molecules in an efficient and sustainable manner become possible. This field has contributed significantly to the development of novel methodologies for the functionalization of pyridines *via* radical chemistry, offering milder and more benign conditions.

[23] Duncton, M. A. J. "Minisci Reactions: Versatile CH-Functionalizations for Medicinal Chemists" *Med. Chem. Commun.* **2011**, *2*, 1135–1161.
[24] Proctor, R. S. J.; Phipps, R. J. "Recent Advances in Minisci-Type Reactions" *Angew. Chem., Int. Ed.* **2019**, *58*, 13666–13699.
[25] Melchiorre, P. "Introduction: Photochemical Catalytic Processes" *Chem. Rev.* **2022**, *122*, 1483−1484.

1.3.1.1 Minisci-type reactions using photoredox catalysis

The emergence of photoredox processes led to a number of reports using Minisci-type chemistry. A seminal work was reported by the group led by DiRocco at Merck (Scheme 1.6).[26] A late-stage methylation (and cyclopropanation) of heteroarenes was achieved using an iridium photocatalyst, blue light (450 nm), and stable organic peroxides as radical precursors. The reaction development and optimization were carried out using 4-methylquionoline **10** as the model substrate.

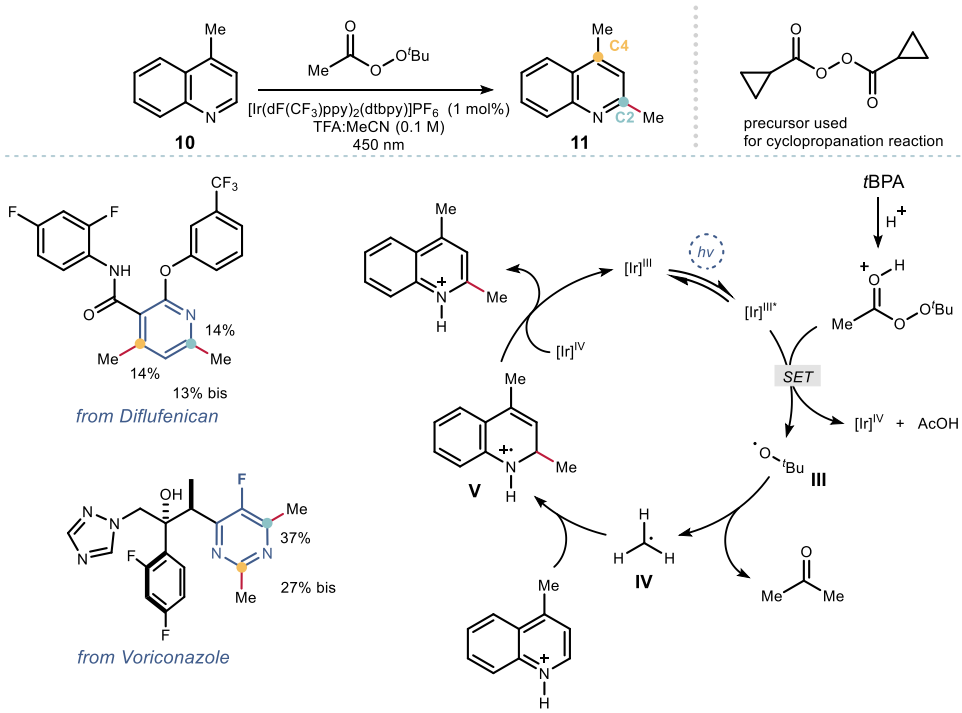

Scheme 1.6. Photoredox catalyzed methylation (and cyclopropanation) of azaarenes *via* Minisci-type mechanism.

The methodology was applicable to other molecules containing azaarenes, including pyrimidines, pyrazines, quinolines and isoquionolines. Mechanistically, the photoexcitation of the photocatalyst $[Ir(dF(CF_3)ppy)_2(dtbpy)]PF_6$ caused the decomposition of *tert*-butyl peracetate (*t*BPA) *via* single-electron transfer (SET) reduction of its protonated form, leading to the formation of *tert*-butoxy radical **III** and Ir^{IV}. Subsequent β-scission formed a methyl radical **IV** that added to the protonated azaarene. Last, a SET oxidation of the amino-radical

[26] DiRocco, D. A.; Dykstra, K.; Krska, S.; Vachal, P.; Conway, D. V.; Tudge, M. "Late-Stage Functionalization of Biologically Active Heterocycles Through Photoredox Catalysis" *Angew. Chem. Int. Ed.* **2014**, *53*, 4802–4806.

cation **V** by Ir^{IV} afforded the desired pyridine product **11**. It is noteworthy that the method was developed in a pharmaceutical company, highlighting the potential applicability of the Minisci chemistry. The methodology has been used to functionalize a number of high-value pharmaceuticals; however, the desired products were obtained along with undesired regioisomers, including the corresponding *bis*-substituent adducts.

Several researchers developed other photoredox-mediated Minisci processes, including the research teams of MacMillan, Molander, Glorius, Shang and Fu (Scheme 1.7). MacMillan *et al*. showed that ethers **A** could be used as radical precursor in a Minisci-type reaction (Scheme 1.7a).[27] This was demonstrated by generating a sulfate radical upon SET reduction from persulfate, able to act as a HAT reagent to generate α-oxo radicals **VI**. In 2017, the group of Glorius used the same sulfate radicals to generate alkyl radicals **VII** from carboxylic acids **B** upon decarboxylation (Scheme 1.7b).[28] Notably, this methodology proceeded *via* a radical chain/HAT mechanism to regenerate the sulfate radical anion. Three additional methodologies were reported on photoredox Minisci-type reaction. Shang, Fu *and co-workers* were the first to use *N*-acyloxyphthalamides **C** as radical precursors (Scheme 1.7c).[29] The phthalimide derivatives **C**, formed from *N*-protected amino acids, could be reduced *via* SET to produce α-amino radicals **VIII** for the aminoalkylation of various heteroarenes. This approach was effective with a broad variety of alkyl radicals, including primary, secondary, and tertiary ones.[30] The third Minisci protocol, developed by Molander *et al.*, used trifluoroborate salts **D** as radical precursors (Scheme 1.7d).[31] A SET oxidation by the excited Mes-Acr photocatalyst furnished a broad range of stabilized and unstabilized radicals **IX** (primary, secondary, and tertiary radicals).

[27] Jin, J.; MacMillan, D. W. C. "Direct α-Arylation of Ethers through the Combination of Photoredox-Mediated C-H Functionalization and the Minisci Reaction" *Angew. Chem. Int. Ed.* **2015**, *54*, 1565–1569.
[28] Garza-Sanchez, R. A.; Tlahuext-Aca, A.; Tavakoli, G.; Glorius, F. "Visible light-mediated direct decarboxylative C–H functionalization of heteroarenes" *ACS Catal.* **2017**, *7*, 4057–4061.
[29] Cheng, W.-M.; Shang, R.; Fu, Y. "Photoredox/Brønsted Acid Co-Catalysis Enabling Decarboxylative Coupling of Amino Acid and Peptide Redox-Active Esters with N-Heteroarenes" *ACS Catal.* **2017**, *7*, 907−911.
[30] Cheng, W.-M.; Shang, R.; Fu, M.-C.; Fu, Y. "Photoredox-Catalysed Decarboxylative Alkylation of N-Heteroarenes with N- (Acyloxy)phthalimides" *Chem. Eur. J.* **2017**, *23*, 2537−2541.
[31] Matsui, J. K.; Primer, D. N.; Molander, G. A. "Metal-free C-H alkylation of heteroarenes with alkyltrifluoroborates: a general protocol for 1°, 2° and 3° alkylation." *Chem. Sci.* **2017**, *8*, 3512−3522.

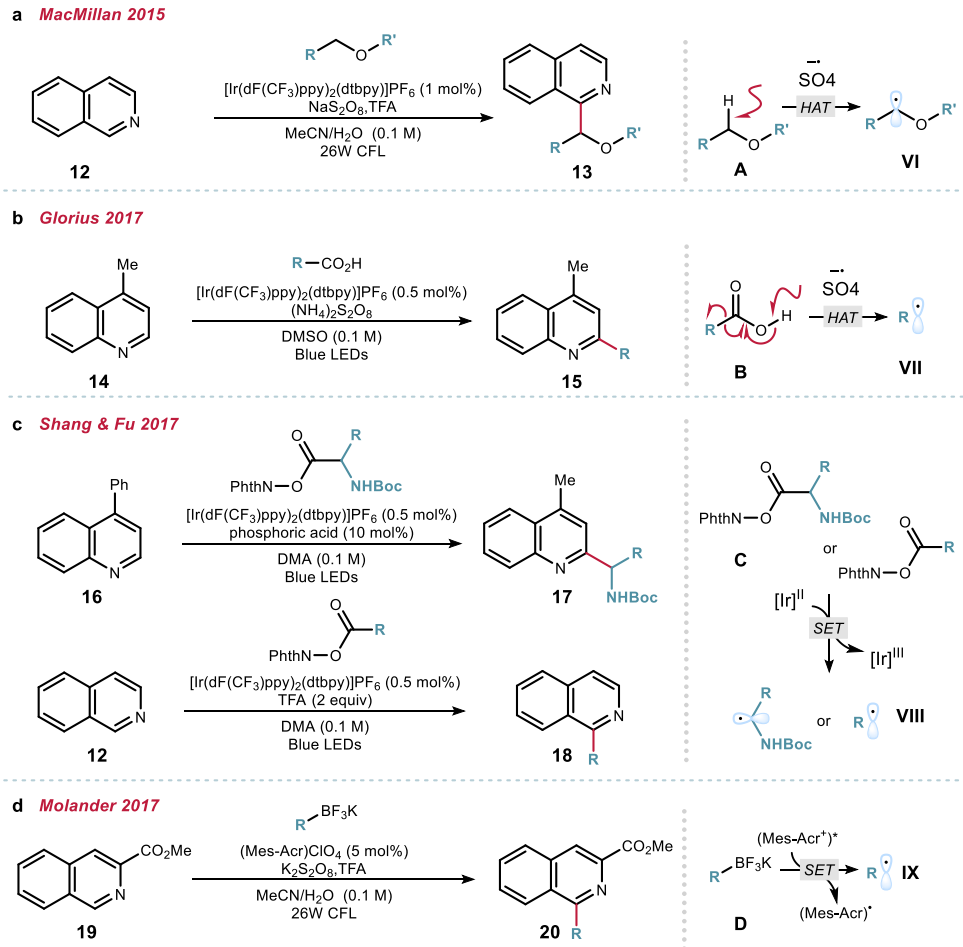

Scheme 1.7. Photochemical catalytic processes for Minisci-type reactions.

1.3.1.2 Pre-functionalized pyridines under visible-light photoredox catalysis

Minisci protocols have significantly improved with the use of photoredox catalysis, which enabled the participation of a broad spectrum of radical precursors. However, the regioselectivity issues intrinsic to the Minisci pathway remained largely unaddressed. One way to control regioselectivity under photoredox catalysis was to use pre-functionalized pyridines. These methods relied on cyanopyridines **21**, triphenylphosphonium pyridine salts **22**, and halogenated pyridines **23** (Figure 1.4).

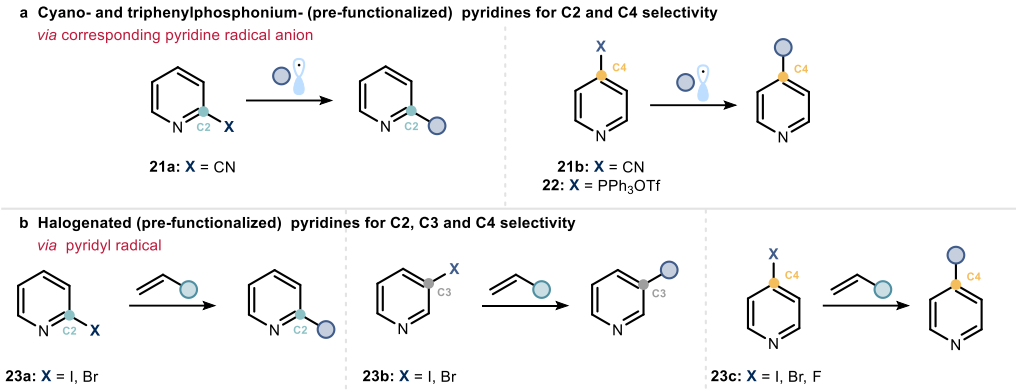

Figure 1.4. Pre-functionalized pyridines used for ensuring regiocontrol in radical functionalization processes: a) cyano- and triphenylphosphonium- pyridines; b) halogenated pyridines.

In 2011, the MacMillan group demonstrated that 4-cyanopyridine **21** are prone to SET reduction under photoredox conditions to form persistent dearomatized radical anion **X** (Scheme 1.8).[32] Upon radical coupling with α-amino radicals **XII**, generated through SET oxidation and deprotonation of amine **24**, extrusion of cyanide led to C4-functionalized pyridines **25**. The presence of the nitrile group at the C4 position of the pyridine was crucial as it stabilized the radical anion **X** formed upon reduction. While this is not a direct C-H activation method, and the installation of a nitrile is required, this protocol proved valuable for inferring regioselectivity, and quickly found broad use.

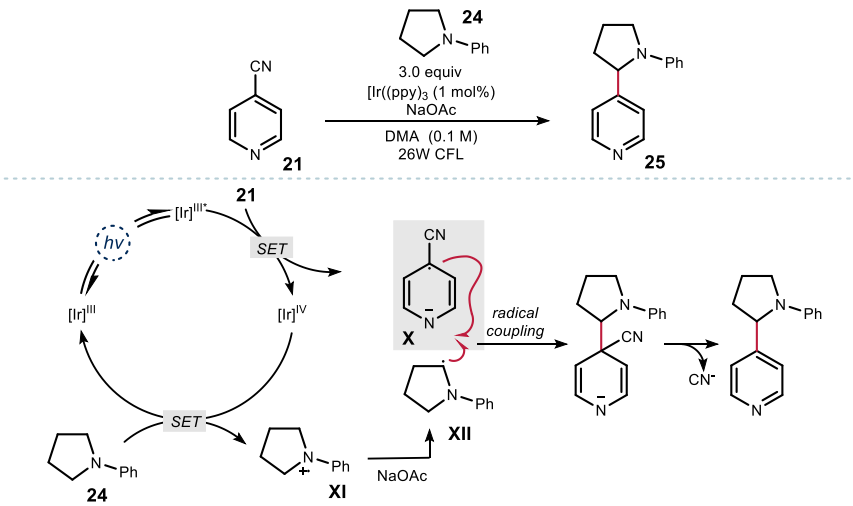

Scheme 1.8. Selective functionalization of pyridines *via* photochemical reduction of 4-cyanopyridines.

[32] McNally, A.; Prier, C. K.; MacMillan, D. W. C. "Discovery of an α-Amino C-H Arylation Reaction using the Strategy of Accelerated Serendipity" *Science* **2011**, *334*, 1114–1117.

In 2021, McNally *et al.* reported that triphenyl phosphonium salts **22** can act as an alternative to cyanopyridines under photoredox conditions (Scheme 1.9).[33] SET reduction of pyridinyltriphenyl phosphonium salts **22** formed the corresponding radical anion **XIII**, which participated in the radical coupling. In this case, extrusion of triphenylphosphine afforded the final product **27**.

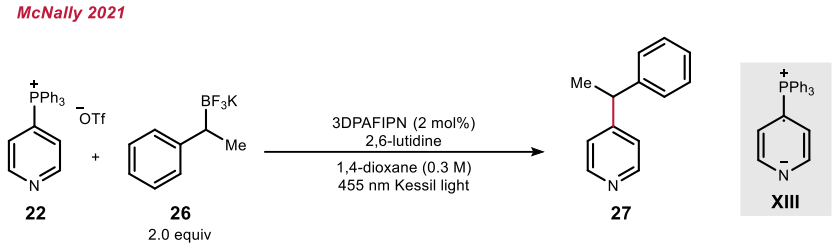

Scheme 1.9. Triphenyl phosphonium pyridine salts as alternatives of cyanopyridines.

An alternative solution to address the regioselectivity issue for the functionalization of pyridines was reported by Jui *et al.* using halogenated pyridines **23** (Scheme 1.10). A SET reduction of halogenated pyridines **23** from the excited iridium-based photocatalyst prompted the homolytic cleavage of the C−X σ bond, leading to the σ-heteroaryl radical **XIV**. It is known that aryl radicals may act as both electrophilic and nucleophilic radicals. The innovation by Jui *et al.* was the realization that also heteroaryl radicals may have an ambiphilic character, which can then be modulated based on the nature of the solvent used in the system. Jui *et al.* first reported a photoredox protocol which made use of an iridium based photocatalyst, Hantzsch ester as photochemical quencher, DMSO/H_2O as solvents under blue light irradiation (Scheme 1.10, conditions A). The authors observed that the neutral pH conditions of this system produced heteroaryl radicals **XIV** with a nucleophilic character, which were prone to Giese addition with various Michael acceptors.[34] However, when ammonium chloride in trifluoroethanol was used as the solvent mixture, an acidic medium resulted, which rendered the same radicals (protonated, **XIV'**) electrophilic,[35] and therefore reactive towards electron-neutral and electron-rich olefins (Scheme 1.10, conditions B).

[33] Greenwood, J. W.; Boyle, B. T.; McNally, A. "Pyridylphosphonium Salts as Alternatives to Cyanopyridines in Radical−Radical Coupling Reactions" *Chem. Sci.* **2021**, *12*, 10538−0543.
[34] Aycock, R. A.; Wang, H.; Jui, N. T. "A Mild Catalytic System for Radical Conjugate Addition of Nitrogen Heterocycles" *Chem. Sci.*, **2017**, *8*, 3121−3125.
[35] Byington, A. J.; Riu, M.-L. Y.; Jui, N. T. "Anti-Markovnikov Hydroarylation of Unactivated Olefins *via* Pyridyl Radical Intermediates" *J. Am. Chem. Soc.* **2017**, *139*, 6582−6585.

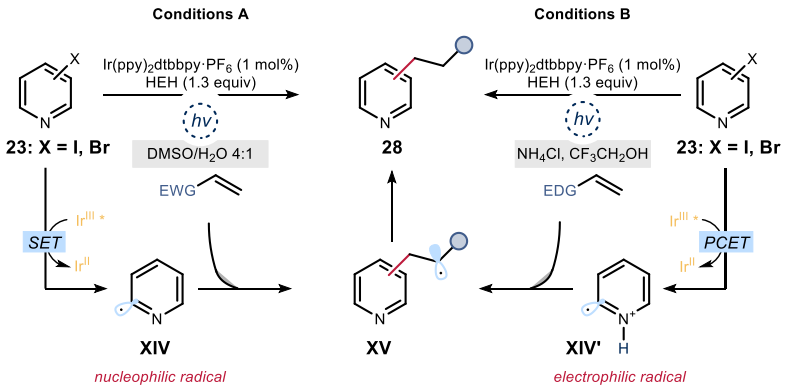

Scheme 1.10. Photoredox catalyzed C-H functionalization of pyridines *via* pyridyl radical intermediates.

1.3.2 Other methods

Outside of the photoredox domain, other advances in pyridine functionalization were reported. A C2-fluorination of pyridines was developed by the Hartwig group in 2013 (Scheme 1.11).[36] Fluorinated pyridines **29** are of very high value in pharmaceuticals and can also be used as synthetic handles for further functionalization through nucleophilic aromatic substitution (S_NAr). This method relied on the use of commercially available silver difluoride (AgF_2), which acted as an activator for pyridine **1** and as a source of fluorine. The proposed mechanism involved first the coordination of AgF_2 to the nitrogen of the pyridine moiety and the subsequent addition of a fluorine to the C2 position to give an amido silver fluoride intermediate **XVI**. Hydrogen atom abstraction from the *ipso*-position by a second molecule of AgF_2 afforded the desired fluorinated pyridine **29**. The methodology was later extended to other nucleophiles, including amines, alcohols, cyanide, and thiols, and also used for late-stage functionalization.[37]

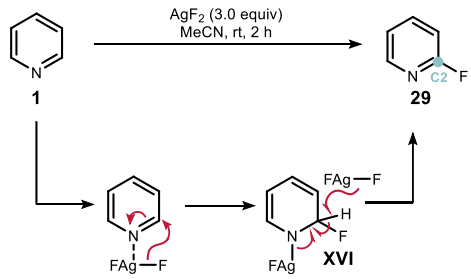

Scheme 1.11. Silver-mediated C-H fluorination of pyridines.

[36] Fier, P. S.; Hartwig, J. F. "Selective C-H fluorination of pyridines and diazines inspired by a classic amination reaction" *Science* **2013**, *342*, 956–960.
[37] Fier, P. S.; Hartwig, J. F. "Synthesis and late-stage functionalization of complex molecules through C-H fluorination and nucleophilic aromatic substitution" *J. Am. Chem. Soc.* **2014**, *136*, 10139–10147.

An additional method for the direct functionalization of pyridines was recently reported by Fier *et al*.[38] The work, developed in the Merck's R&D department, allowed the nucleophilic addition to pyridines **1** using an aldoxime reagent **30** (Scheme 1.12). A pyridinium salt intermediate **XVII** was formed upon displacement of a chloride from the α-chloro *O*-methanesulfonyl aldoxime **30**. Nucleophilic addition of a cyanide to the electrophilic intermediate **XVII**, followed by deprotonation at the *ipso*-position, resulted in the formation of the functionalized pyridine **31** along with the release of methanesulfonate salt. C2-cyanation of pyridines was achieved using NaCN as the nucleophilic source, while preliminary results highlighted the possibility to extend the chemistry to other nucleophiles, including Grignard, organozinc reagents, and malonates.

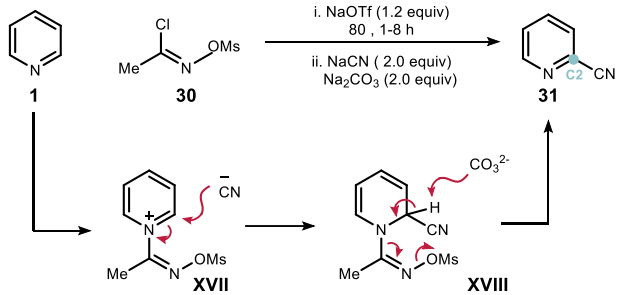

Scheme 1.12. C-H functionalization *via* nucleophilic addition to transiently generated aldoxime pyridinium salts.

Other metal-based catalytic methods have been developed for the functionalization of pyridines, using palladium, rhodium, ruthenium, iridium, and nickel catalysts.[39] In 2014, Hartwig *et al.* reported the development of an iridium catalyzed C-H borylation of heteroarenes (Scheme 1.13).[40] The commercially available [Ir(COD)Cl_2] was used as pre-catalyst in combination with B_2pin_2 and bipyridine ligand to form an active Ir^{III} species **XIX**. Upon reductive elimination, a new C−B bond was formed to furnish C3 borylated pyridine **32** along with the corresponding C4-borylated **32'** adduct in a 2:1 ratio.

[38] Fier, P. S. "A Bifunctional Reagent Designed for the Mild, Nucleophilic Functionalization of Pyridines" *J. Am. Chem. Soc.* **2017**, *139*, 9499−9502.

[39] a) Nakao, Y. "Transition-Metal-Catalyzed C-H Functionalization for the Synthesis of Substituted Pyridines" Synthesis, **2011**, 2011, 3209−3219.; b) Bull, J. A.; Mousseau, J. J.; Pelletier, G.; Charette, A. B. "Synthesis of Pyridine and Dihydropyridine Derivatives by Regio- and Stereoselective Addition to N-Activated Pyridines" *Chem. Rev.* **2012**, *112*, 2642−2713.

[40] Larsen, M. A.; Hartwig, J. F. "Iridium-catalyzed C-H borylation of heteroarenes: scope, regioselectivity, application to late-stage functionalization, and mechanism" *J. Am. Chem. Soc.* **2014**, *136*, 4287−4299.

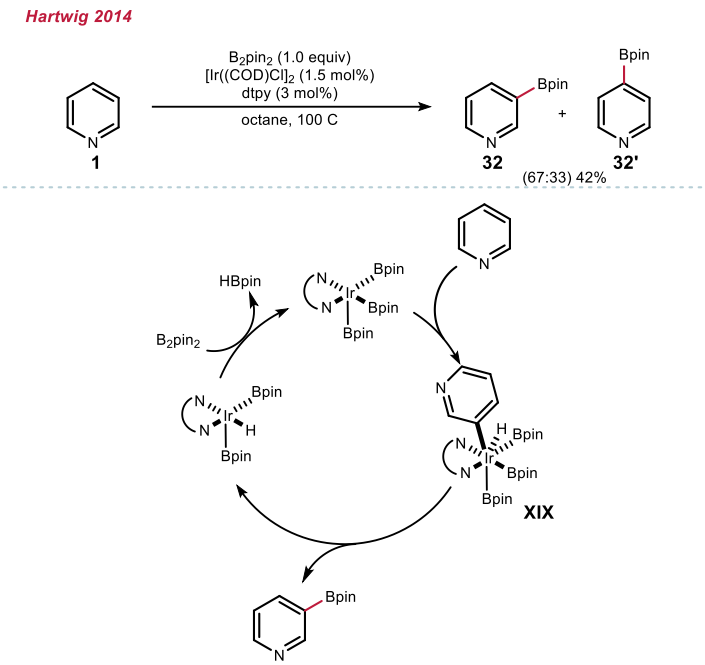

Scheme 1.13. Iridium-catalyzed borylation of pyridines.

1.4. General Objectives of the Thesis and Summary

The main objective of this doctoral thesis was to develop new photochemical strategies to functionalize pyridines and azaarenes in a regioselective manner using radical mechanisms. First, we investigated the reactivity of 4-cyanopyridines under visible-light-mediated photoredox conditions (Figure 1.5a). In this study, we developed a strategy that allowed switchable control of the chemoselectivity in the radical benzylation of 4-cyanopyridines. The process granted access *at will* to C2 and C4 functionalized pyridines using a single photoredox catalyst and changing only the nature of the photochemical quencher. In a second project, we aimed to functionalize selectively pyridines without the need of preinstalled functionalities (Figure 1.5b). Specifically, the regioselective C4 allylation of pyridines and other azaarenes was achieved using a trifunctional light-activated organocatalyst. The chemistry relied on the so-far neglected reactivity of neutral pyridinyl radical **XX** and offered a unique regioselectivity, which diverged from classical Minisci chemistry.

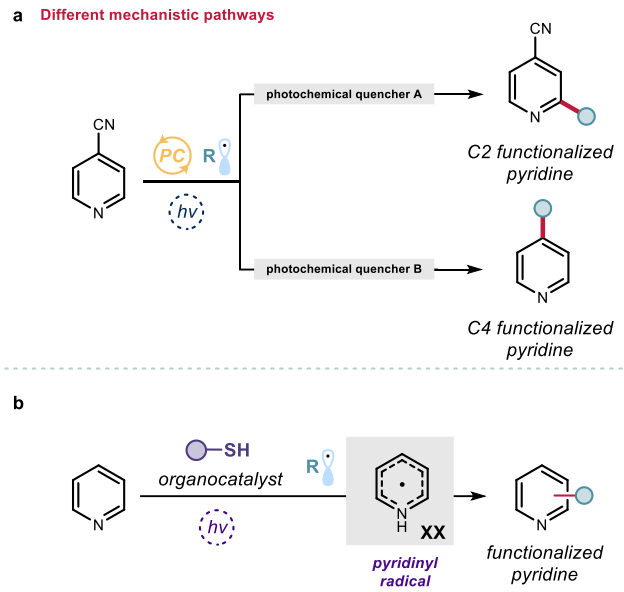

Figure 1.5. *Targets of the PhD thesis:* new photochemical strategies for the radical-based regioselective functionalization of pyridines.

1.4.1 Switchable Photocatalysis for the Chemodivergent Benzylation of Pyridines

Chapter II details the development of a selective method for the functionalization of 4-cyanopyridines with benzylic fragments bearing an amide moiety (Figure 1.6). We discuss how a serendipitous observation led to a chemodivergent protocol that enabled selective access to regioisomeric C4 or C2 benzylated pyridines. The two protocols used the same photocatalyst and reaction conditions (starting materials, solvent, temperature, light source) and diverged only on the photocatalyst quenchers (sacrificial electron donor) used. The photochemical quencher allowed us to select at will between mechanistically divergent processes: *i*) an *ipso*-substitution process, proceeding *via* radical coupling, led to C4 benzylated pyridines; *ii*) a Minisci-type addition, which afforded regioisomeric C2 functionalized pyridines.

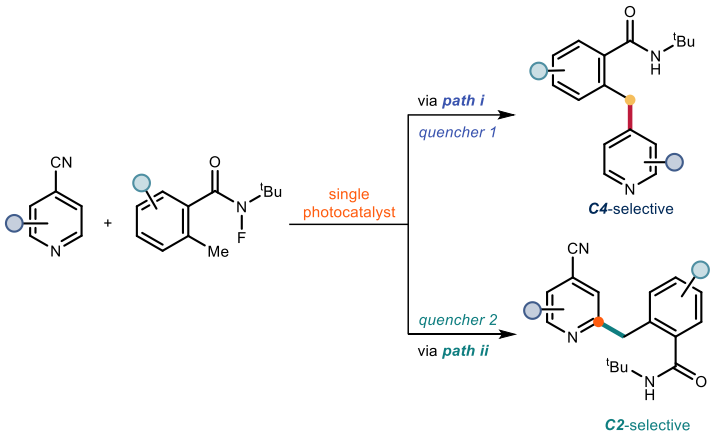

Figure 1.6. Switchable photocatalysis for the chemodivergent benzylation of 4-cyanopyridines.

This work was undertaken in collaboration with Dr. Kang Chen, who conducted the initial studies, and Davide Spinnato, who participated in the optimization of the reaction conditions, carried out part of the reaction scope, and investigated in depth the reaction mechanism. I performed extensive method development, investigated the generality and the scope of the protocol, synthesized the starting materials, and performed part of the mechanistic studies.

1.4.2 Photochemical Organocatalytic Functionalization of Pyridines *via* Pyridinyl Radicals

In chapter III, we report a photochemical organocatalytic strategy for the functionalization of pyridines with an unusual regioselectivity. In this strategy, pyridinyl radicals **XX** were generated upon SET reduction of pyridinium ions and underwent radical coupling with radicals generated from allylic C−H bonds. Overall, two substrates underwent C-H functionalization to forge a new C(sp^2)-C(sp^3) bond (Figure 1.7). The method relied on the direct excitation of a dithiphosphoric acid (DTPA, a common organocatalyst known to act as a Brønsted acid in the ground state)[41] that turned it into a strong SET reductant. The combination of these two catalytic functions (acidity and SET reducing power) led to the formation of the neutral pyridinyl radical **XX** and the corresponding thiyl radical of DTPA (not shown in the figure), which could then act as a hydrogen atom abstractor for allylic C-H bonds. Radical coupling then led to target products. This novel mechanism enabled a distinct positional selectivity for pyridine functionalisation, which diverged from classical Minisci chemistry, since it afforded mainly the C4-alkylated pyridines.

[41] Shapiro, N. D.; Rauniyar, V.; Hamilton, G. L.; Wu, J.; Toste, F. D. "Asymmetric Additions to Dienes Catalyzed by a Dithiophosphoric Acid" *Nature* **2011**, *470*, 245−249.

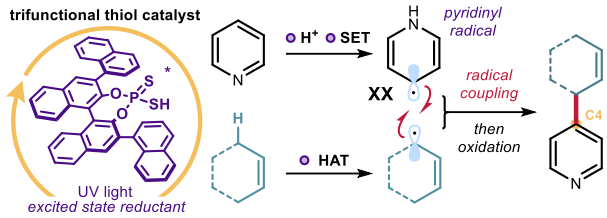

Figure 1.7. Photochemical organocatalytic functionalization of pyridines *via* pyridinyl radicals.

This work was undertaken in collaboration with Emilien Le Saux, who led the project, was involved in the discovery and optimization of the reaction, the mechanistic investigation, and reaction scope. Igor Dmtriev participated in the reaction optimization and performed part of the reaction scope. Dr. Will C. Hartley performed all the calculations. I extensively investigated the generality of the reaction scope, synthesized starting materials, and participated in the mechanistic studies.

Chapter II

Switchable Photocatalysis for the Chemodivergent Benzylation of 4-Cyanopyridines

Target

The original goal was to develop a method for the selective functionalization of pyridines with benzylic fragments containing an amide moiety. A serendipitous discovery led to two complementary and switchable methodologies for the chemodivergent functionalization of pyridines.

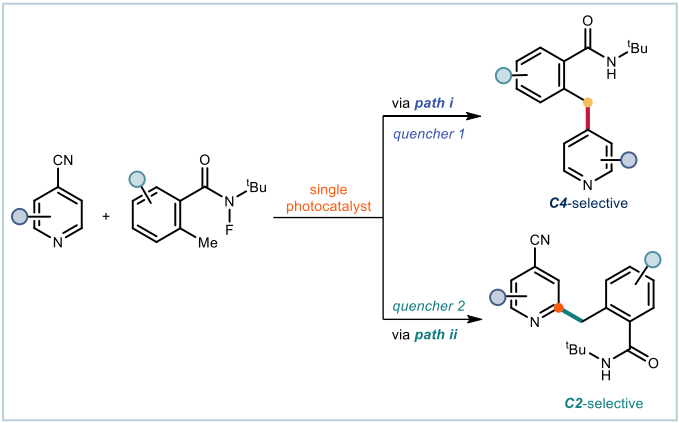

Tool

Using photoredox catalysis to generate benzyl radicals upon N−F bond activation of 2-alkyl *N*-fluorobenzamides. The judicious choice of different photocatalyst quenchers allowed us to select at will between mechanistically divergent processes, enabling selective access to regioisomeric C4 or C2 benzylated pyridines.[1]

2.1 Introduction and Target of the Project

There is significant interest in the regioselective functionalization of pyridines, particularly under mild and benign conditions. The development of a general platform that grants selective access to one position of the pyridine ring is challenging and yet to be fully realized (Figure 2.1a). In Chapter I, we discussed various methods for the functionalization of pyridines; however, they often result in undesired mixtures of products. One possibility to perform a selective pyridine functionalization relies on the use of 4-cyanopyridines **1**: in this case, the

[1] The project discussed in this chapter was conducted in collaboration with Davide Spinnato and Dr. Kang Chen under the supervision initially of Prof. Kilian Muñiz and later of Prof. Paolo Melchiorre. I (with Dr. Kang Chen) performed the initial experiments that led to the discovery of the reactions. I was involved also in the optimization, the investigation of the reaction scope, and in the mechanistic elucidation. This study has been published: Georgiou, E.; Spinnato, D.; Chen, K.; Melchiorre, P.; Muñiz, K. "Switchable photocatalysis for the chemodivergent benzylation of 4-cyanopyridines" *Chem. Sci.* **2022**, *13,* 8060−8064.

regiochemical outcome of a transformation is guaranteed (Figure 2.1b). Specifically, the installed cyano group acts as a functional handle that can be extruded upon single-electron transfer (SET) reduction and radical coupling of the resulting persistent pyridine radical anion **I** with various radical partners.

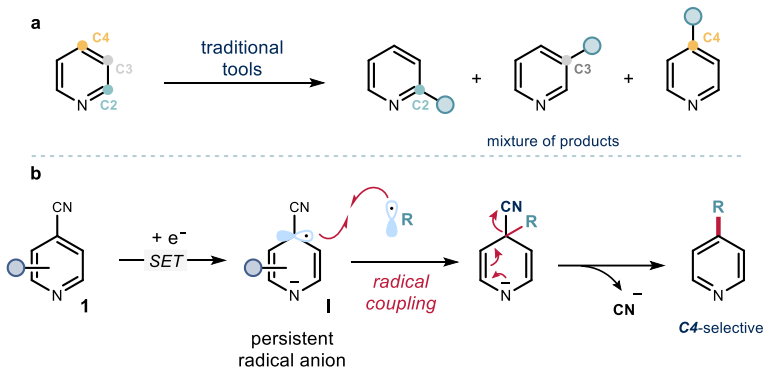

Figure 2.1. a) Lack of regiocontrol for the functionalization of pyridines using traditional tools; b) C4-selectivity using 4-cyanopyridines **1** as pyridine surrogates.

This is an effective strategy, but there is a need to broaden the scope of functional groups that can be installed, especially forging new C−C bonds within the pyridine scaffold. To achieve this goal, we sought to develop a methodology to selectively functionalize pyridines with benzylic fragments containing an amide-distal chain. The original idea was motivated by the interest of the late Professor Kilian Muñiz to react *N*-fluoroamides **2** *via* N−F bond activation (Figure 2.2). This interest originated from previous studies on the activation of other *N*-halogenated compounds for the formation of the corresponding nitrogen-centered radicals, and their further exploitation for intra- and intermolecular bond-forming transformations. [2]

Following this reasoning, we sought to develop a photoredox catalytic method for the C4-selective functionalization of pyridines. The original plan relied on the photoinduced SET reduction of 4-cyanopyridines **1** and the concomitant activation of the N−F bond within *N*-fluoroamides **2**, triggered by another SET reduction mastered by the photoredox catalyst. The two radicals ensuing from the two redox events, the pyridine radical anion **I** and the benzylic

[2] a) Martínez, C.; Muñiz, K. "An Iodine-Catalyzed Hofmann-Löffler Reaction" *Angew. Chem., Int. Ed.* **2015**, *54*, 8287−8291; b) Bosnidou, A. E.; Duhamel, T.; Muñiz, K. "Detection of the Elusive Nitrogen-Centered Radicals from Catalytic Hofmann–Löffler Reactions" *Eur. J. Org. Chem.* **2020**, *40*, 6361–6365; c) Duhamel, T.; Martínez, M. D.; Sideri, I. K.; Muñiz, K. "1,3-Diamine Formation from an Interrupted Hofmann−Löffler reaction: Iodine Catalyst Turnover through Ritter-Type Amination" *ACS Catal.* **2019**, *9*, 7741−7745; d) Bafaluy, D.; Muñoz-Molina, J. M.; Funes-Ardoiz, I.; Herold, S.; Aguirre, A. J. de; Zhang, H.; Maseras, F.; Belderrain, T. R.; Pérez, P. J.; Muñiz, K. "Copper-Catalyzed N-F Bond Activation for Uniform Intramolecular C-H Amination Yielding Pyrrolidines and Piperidines" *Angew. Chem., Int. Ed.* **2019**, *58*, 8912−8916.

radical **III**, would eventually couple to afford the target C4-functionalized pyridine **3** (Figure 2.2a). Over the course of our investigations, we serendipitously discovered that a minor change of the reaction conditions could switch the product distribution, leading to the C2-functionalized pyridines **4** (Figure 2.2b). This chemodivergent behavior was made possible by a distinct mechanistic pathway.

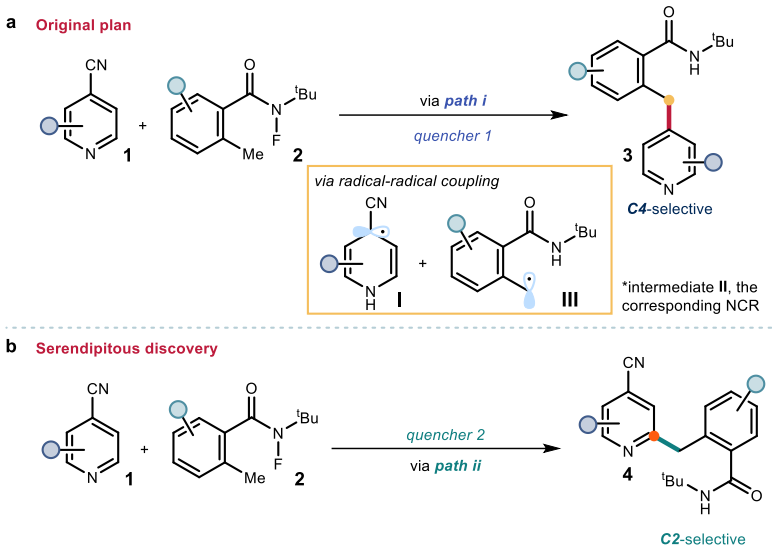

Figure 2.2. (a) Original plan and (b) serendipitously discovered method for the chemodivergent benzylation of 4-cyanopyridines.

The first part of this chapter provides an overview of the recent advances made in modern photocatalysis for the functionalization of cyanopyridines. In addition, a summary of methods suitable for the N−X bond activation to facilitate remote C(sp^3)-H functionalization of unactivated amide chain fragments is discussed. The Results and Discussion section describes our successful approach to functionalizing pyridines at the C4 position, as well as the unexpected discovery that led us to develop a complementary method for the C2-functionalization of cyanopyridines.

2.1.1 Photochemistry of cyanopyridines

The discovery of the formation of pyridine radical anion **I** derived from SET reduction of 4-cyanopyridines dates back to 1980s. Originally, these radicals could be formed under photochemical activation (UV light). This discovery represented a significant breakthrough in the field, as prior to this, the emphasis had been on the direct photoexcitation of pyridines

using high energy UV light (λ <300 nm).[3] The neutral pyridines **5** exhibited different behavior than the corresponding protonated molecule **5'**, since **5** underwent *n* → π* electronic transitions while **5'** π → π* transitions. This difference in electronic transitions dictated the chemical outcome, with **5*** exhibiting hydrogen atom transfer (HAT) reactivity, whereas **5'*** was able to act as a strong oxidant (Figure 2.3a). These approaches both delivered alkylated pyridines **6** albeit in low yield (usually <20%) and as a mixtures of regioisomers. Studies in 1981 by Caronna *et. al.* on 4-cyanopyridine **1a** under similar conditions and using alkenol **7** as reaction partner resulted in *ipso*-substituted products **8** and **9** in moderate yield (Figure 2.3b).[4] Again the acidity of the reaction media, which was modified with the addition of hydrochloric acid, played a key role to dictate the reaction outcome. Under neutral conditions, product **8** was obtained through a HAT process between excited **1a*** and alcohol **7**. When the same reaction was performed in the presence of an acid, product **9** was formed instead.

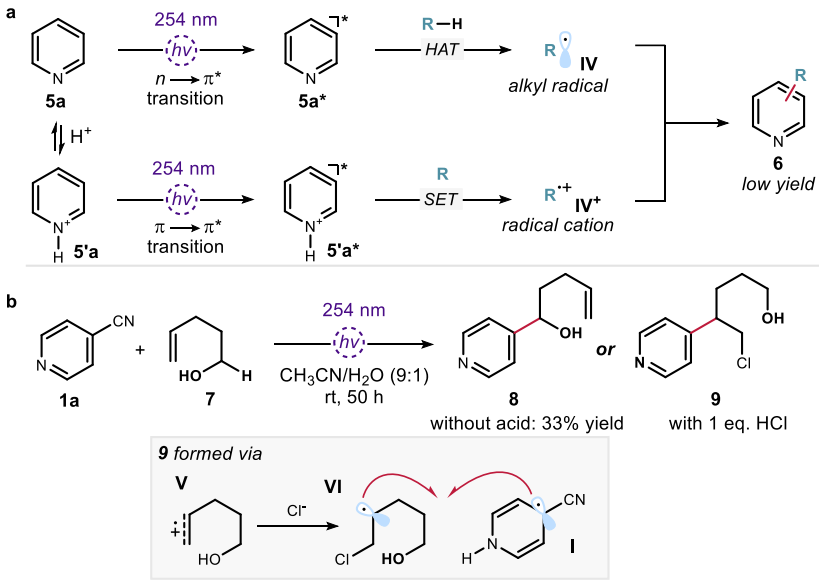

Figure 2.3. (a) Photoexcitation of pyridines and (b) cyanopyridine **1a** with UV light.

[3] a) Stermitz, F. R.; Seiber, R. P.; Nicodem, D. E. "Imine Photoalkylations. Papaverine, Phenanthridine, and a General Mechanism" *J. Org. Chem.* **1968**, *33*, 1136–1140; b) Stermitz, F. R.; Wei, C. C.; O'Donnel, C. M. "Photochemistry of N-Heterocycles. Photochemistry of Quinoline and Some Substituted Quinoline Derivatives" *J. Am. Chem. Soc.* **1970**, *92*, 2745–2752; c) Noyori, R.; Katô, M. "Photochemical Reaction of Benzopyridines with Alkanoic Acids. Novel Reductive Alkylation of Acridine, Quinoline, and Isoquinoline under Decarboxylation" *Tetrahedron,* **1969**, *25*, 1125–1136.

[4] a) Caronna, T.; Clerici, A.; Coggiola, D.; Morrocchi, S. "Photoreactions of 4-Cyanopyridine with Alkenols. Influence of the Medium on the Reaction Mechanism and Photoproducts Formation" *Tetrahedron Lett.* **1981**, *22*, 2115−2118; b) Bernardi, R.; Caronna, T.; Morrocchi, S.; Ursini, M. "Photochemically induced reactions of selected ketones with 4-cyanopyridine in neutral and acidic medium" *J. Heterocyclic Chem.*, **1996**, *33*, 1137–1142.

Photoexcitation of the protonated 4-cyanopyridinium resulted in an oxidant **1a'*** able to activate alkenol **7**. Subsequent attack to the radical cation **V** by chloride afforded the alkyl radical **VI**, which upon radical coupling with the persistent radical **I** afforded the final product **9**.

The unique properties of 4-cyanopyridines and their ability to get easily reduced to form persistent radical anions of type **I** found utility in photoredox catalysis (see section 1.3.1 in Chapter I). This was due to the high demand for the selective functionalization of pyridines under milder conditions. 4-Cyanopyridines **1** are powerful substrates broadly used for C4 selective functionalization.[5] The persistent radical species formed upon SET reduction allows the participation in radical coupling with various radical partners. The seminal work of MacMillan discussed in section 1.3.1 of Chapter I was followed by a report from the Inoue group (Scheme 2.1).[6] 4-Cyanopyridines **1** were used together with various alkyl partners containing benzylic C-H positions **10** in the presence of benzophenone (BP) as a photocatalyst. The generation of the radical **VII** relied on a hydrogen atom abstraction from benzylic positions by the diradical ^{3}BP, formed upon excitation of benzophenone using 100 W medium pressure mercury lamp. Proton-coupled electron transfer between the 4-cyanopyridine **1**, and BPH• was suggested to regenerate benzophenone and the stabilized carbon centered radical **I**. Finally radical coupling of **I** with **VII** followed by cyanide elimination afforded the final product **11**.

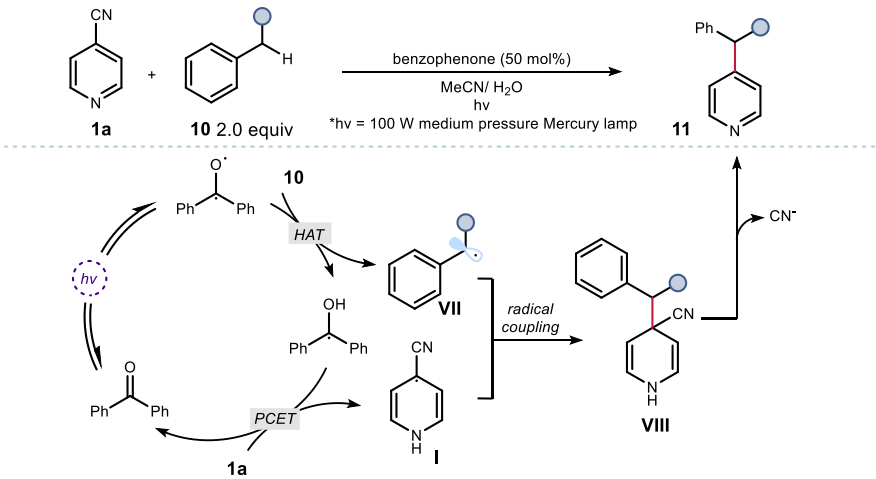

Scheme 2.1. 4-Cyanopyridine reactions with benzylic C-H bond-containing molecules under light irradiation.

[5] Tong, S.; Li, K.; Ouyang, X.; Song, R.; Li, J. "Recent Advances in the Radical-Mediated Decyanative Alkylation of Cyano(hetero)arene" *Green Synth. Catal.* **2021**, *2*, 145–155.

[6] Hoshikawa, T.; Inoue, M. "Photoinduced direct 4-pyridination of C(sp3)–H Bonds" *Chem. Sci.* **2013**, *4*, 3118−3123.

The MacMillan group had subsequently developed two additional methodologies using i) α-amino acids as precursors of α-amino radicals, and ii) aldehydes to generate 5π electrons intermediates (Scheme 2.2). In the former example, α-amino radicals **IX** were formed upon a SET oxidation by the Ir-based photocatalyst and subsequent decarboxylation (Scheme 2.2a).[7] In the latter study, a dual photoredox/organocatalysis system enabled the formation of the key 5π electrons intermediate **XI** (Scheme 2.2b).[8] The enamine **X**, formed upon condensation of the starting aldehyde **14** and the aminocatalyst **16**, underwent SET oxidation by the Ir photocatalyst. Concomitant deprotonation resulted in the intermediate **XI** prone to radical coupling with the cyanopyridinyl radical anion **I** to give β-(hetero)aryl aldehyde products **15**.

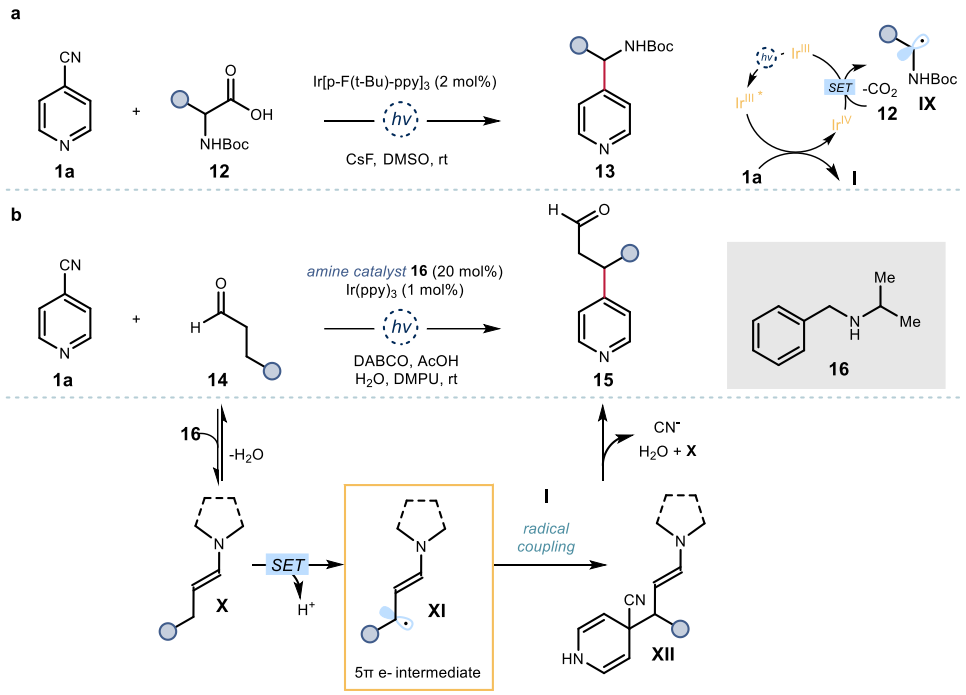

Scheme 2.2. 4-Cyanopyridine reactions with a) α-amino radicals and b) 5π-electrons intermediates.

MacMillan *et al.* also developed a reaction that allowed the formation of a new C−C bond between cyanopyridines and allylic C−H bonds (Scheme 2.3).[9] In order to achieve this transformation, the synergistic merger of visible-light photocatalysis with organocatalysis

[7] Zuo, Z. W.; MacMillan, D. W. C. "Decarboxylative Arylation of α-Amino Acids *via* Photoredox Catalysis: A One-Step Conversion of Biomass to Drug Pharmacophore" *J. Am. Chem. Soc.* **2014**, *136*, 5257−5260.
[8] Pirnot, M. T.; Rankic, D. A.; Martin, D. B. C.; MacMillan, D. W. C. "Photoredox Activation for the Direct β-Arylation of Ketones and Aldehydes" *Science* **2013**, *339*, 1593–1596.
[9] Cuthbertson, J. D.; MacMillan, D. W. C. "The direct arylation of allylic sp^3 C-H bonds *via* organic and photoredox catalysis" *Nature* **2015**, *519*, 74− 77.

was used. A thiol-based organocatalyst **19** enabled hydrogen atom abstraction from the C−H allylic bond of various alkenes **17**. Upon deprotonation by a base, the thiolate anion **19**$^-$ undergoes a SET oxidation by the iridium-based photocatalyst to form the thiyl radical **19•**. Then, a thermodynamically favored HAT process between the cyclic alkene (C-H, BDE 83.2 kcal/mol) and the thiyl radical **19•** (S-H, BDE 87 kcal/mol) took place.

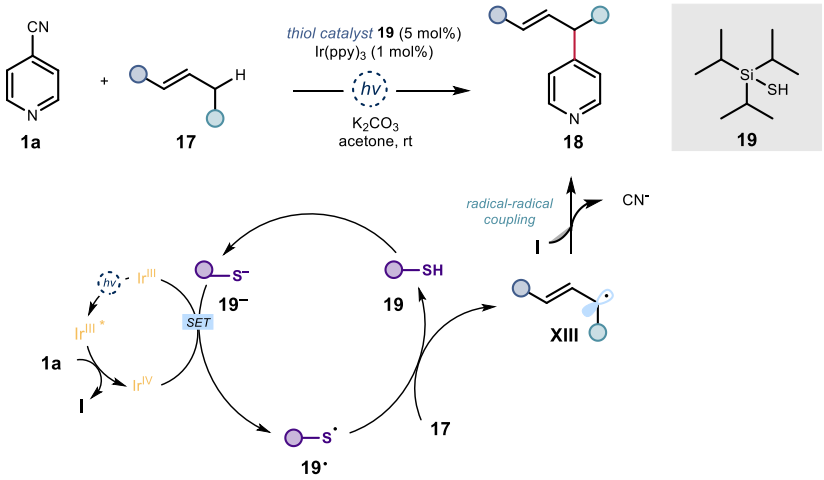

Scheme 2.3. 4-Cyanopyridines reaction with C-H allylic bonds.

Cyanopyridines **1** have also been used for the site-selective synthesis of vinylpyridines **21** with complete branched selectivity (Scheme 2.4).[10] The protocol used a sulfonate-assisted photoredox catalytic mechanism. The radical partner was generated upon addition of the sulfonyl radical into alkene **20**. The resulting benzylic radical **XIV** coupled with the cyanopyrine radical anion to generate the alkyl sulfone. A base-assisted E1 elimination of the sulfinate furnished the final product **21**.

[10] Zhu, S.; Qin, J.; Wang, F.; Li, H.; Chu, L. "Photoredox-catalyzed branch-selective pyridylation of alkenes for the expedient synthesis of triprolidine" *Nat. Commun.* **2019**, *10*, 749.

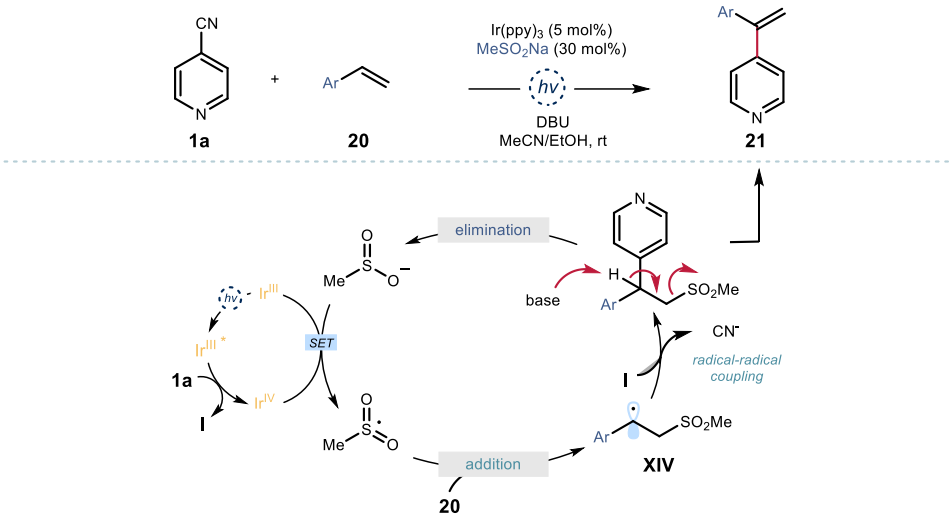

Scheme 2.4. 4-Cyanopyridines reaction with alkenes for their branch-selective pyridylation.

Finally, a noteworthy report is the one where the pyridine scaffold could be decorated with primary amines in a sterically hindered environment. Rovis and co-workers developed a photoredox catalytic protocol using *O*-benzoyl oximes **22** or iminium chloride salts **23** to form tertiary α-amino radicals **XVI**, which could couple with the pyridine radical intermediate **I** (Scheme 2.5).[11] Experimental and computational mechanistic studies suggested a concurrent tandem catalysis where the photocatalyst played a dual role. Initially, the iridium photocatalyst acted as a triplet sensitizer to activate the oxime and cause the N−O bond cleavage, wherein then it acted as a SET reductant to activate the cyanopyridines.

[11] Nicastri, M. C.; Lehnherr, D.; Lam, Y.-h.; DiRocco, D. A.; Rovis, T. "Synthesis of Sterically Hindered Primary Amines by Concurrent Tandem Photoredox Catalysis" *J. Am. Chem. Soc.* **2020**, *142*, 987−998.

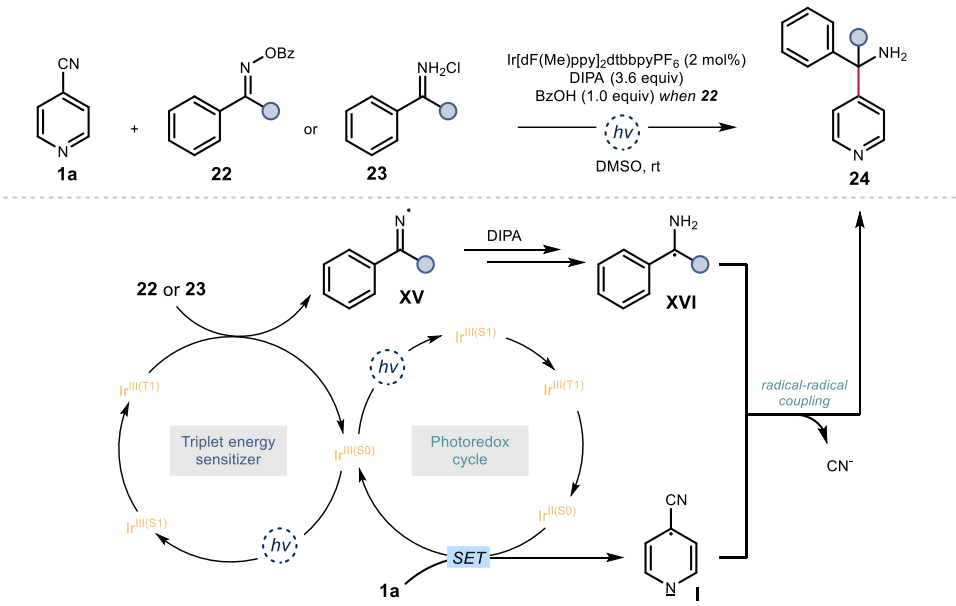

Scheme 2.5. Synthesis of sterically hindered amines from 4-cyanopyridines and *O*-benzoyl oximes or iminium chloride salts.

Overall, the persistent nature of pyridine radical anions **I** derived from 4-cyanopyridines **1** enabled various transformation with C4-selectivity. We were interested in developing a 4-selective benzylation of cyano-pyridines upon activation of *N*-fluoroamides. The following section details the methodologies available to activate N−X bonds.

2.1.2 Activation of N−X bonds for the remote functionalization of amides

Distal or remote functionalization refers to the installation of a functional group at a non-activated C(sp^3)-H bond away from a second, reference functional group. Typically, a 1,5-HAT (hydrogen atom transfer) is the key process to access alkyl radical intermediates at the remote δ position.[12] This process is used in a classical approach to synthesize pyrrolidines: the Hofmann-Löffler reaction (Figure 2.4). This transformation consists of three individual steps: a) homolytic cleavage of an N−X bond to form a nitrogen-centered radical, b) a subsequent 1,5-HAT process mastered by the N radical leading to a carbon centered radical,

[12] Kumar, G.; Pradhan, S.; Chatterjee, I. "N-Centered Radical Directed Remote C-H Bond Functionalization *via* Hydrogen Atom Transfer" *Chem. Asian J.* **2020**, *15*, 651−672.

and c) a halogen abstraction followed by intramolecular nucleophilic displacement.[13] An interrupted Hofmann-Löffler reaction happens when the last intertwined step c can be prevented. Specifically, the resulting alkyl radical can be used for further diversification, including the formation of new C−C and C−heteroatom bonds using radical traps/quenchers.

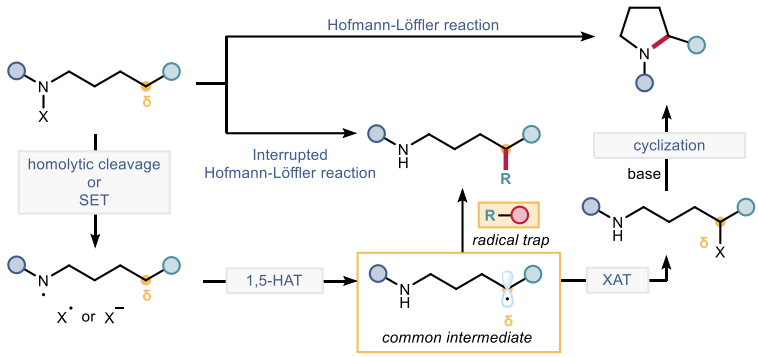

Figure 2.4. Hofmann-Löffler and interrupted Hofmann-Löffler reaction.

The first examples of interrupted Hofmann-Loffler reactions involved the halogenation at the remote δ positions of amine derivatives. In 1985, seminal work from Nikishin *et al*. has shown the potential of the amidyl radical **XVII** for the direct C-H functionalization.[14] A δ-chlorination process was developed using stoichiometric amounts of $CuCl_2$ and sodium persulfate (Scheme 2.6a). The reactivity was extended later by Corey and coworkers to include bromination reactions (Scheme 2.6b).[15] Specifically, the selective bromination of α-aminoacids **27** was achieved. Treatment of **27** with acetyl bromide and subsequent UV light irradiation led to the formation of the nitrogen centered radicals **XVIII** to eventually afford product **28**.

[13] a) Hofmann, A. W. *Ber. Dtsch. Chem. Ges.* **1883**, *16*, 558−560; b) Löffler, K. *Ber. Dtsch. Chem. Ges.* **1910**, *43*, 2035−2048; c) Corey, E. J.; Hertler, W. R. "A Study of the Formation of Haloamines and Cyclic Amines by the Free Radical Chain Decomposition of *N*-Haloammonium Ions (Hofmann-Löffler Reaction)" *J. Am. Chem. Soc.* **1960**, *82*, 1657-1668.

[14] Nikishin, G. I.; Troyansky, E. I.; Lazareva, M. I. "Regioselective One-Step γ-Chlorination of Alkanesulfonamides. Pre-ponderance of 1,5-H Migration from Sulfonyl Versus Amide Moiety in Sulfonylamidyl Radicals" *Tetrahedron Lett.* **1985**, *26*, 3743–3744.

[15] Reddy, B. V. S.; Reddy, L. R.; Corey, E. J. "Efficient Method for Selective Introduction of Substituents as C(5) of Isoleucine and Other α-Amino Acids" *Org. Lett.* **2006**, *8*, 2819−2821.

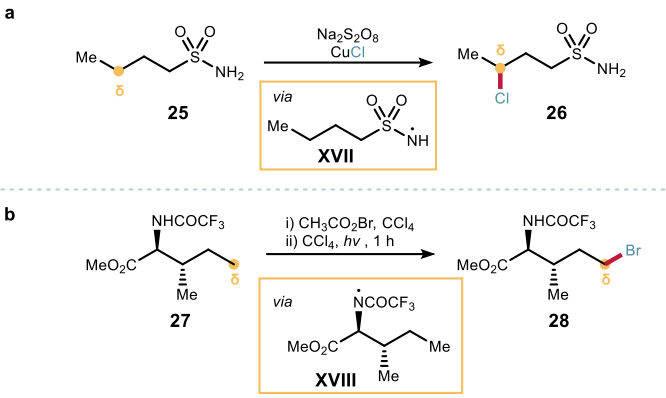

Scheme 2.6. Early examples of interrupted Hofmann-Loffler reactions: a) δ-chlorination of alkanesolfonamides; b) δ-bromination of isoleucine derivative.

In 2015, with the emergence of photoredox catalysis, Yu *et al.* reported a remote chlorination using an iridium-based photocatalyst to activate *N*-chlorosulfonamides **29** (Scheme 2.7).[16]

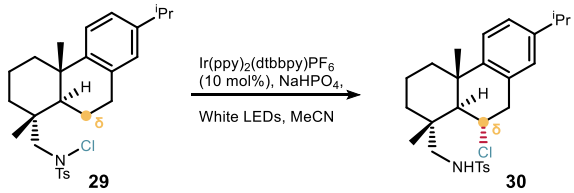

Scheme 2.7. Remote δ-chlorination of amines *via* iridium-catalyzed interrupted Hofmann-Löffler reaction.

Since iodine is a very good leaving group, developing an interrupted Hofmann-Löffler iodination protocol is particularly challenging. The Muñiz group developed an iodination of adamantane derivatives **30** which prevented the iodine displacement (Scheme 2.8 a).[17] The method used diiodogenated hydantoin (DIDMH) as the electrophilic halogen source. The Nagib group later demonstrated that iminyl radicals **XIX** can be used for interrupted Hofmann-Löffler deiodination to obtain product **33** using NaI as iodine source and $PhI(OAc)_2$ as oxidant (Scheme 2.8b).[18]

[16] Qin, Q.; Yu, S. "Visible-Light-Promoted Remote C(sp3)-H Amidation and Chlorination" *Org. Lett.* **2015**, *17*, 1894−1897.

[17] Del Castillo, E.; Martínez, M. D.; Bosnidou, A. E.; Duhamel, T.; O'Broin, C. Q.; Zhang, H.; Escudero-Adan, E. C.; Martínez-Belmonte, M.; Muñiz, K. "Multiple Halogenation of Aliphatic C−H Bonds within the Hofmann−Löffler Manifold" *Chem. - Eur. J.* **2018**, *24*, 17225−17229.

[18] Wappes, E. A.; Vanitcha, A.; Nagib, D. A. "*β* C-H Di-Halogenation *via* Iterative Hydrogen Atom Transfer" *Chem. Sci.* **2018**, *9* (19), 4500− 4504.

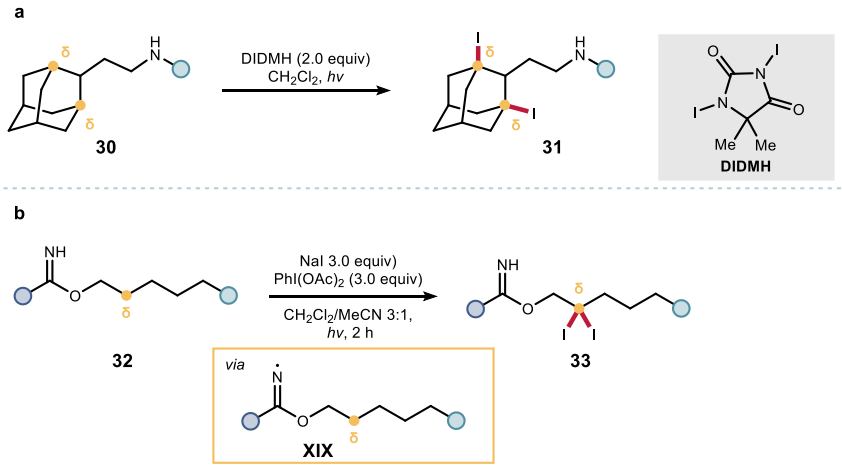

Scheme 2.8. Remote δ-iodination of amine derivatives a) on adamantane core and b) *via* activation of imines.

The halogen series suitable to interrupted Hofmann-Löffler reactions was completed by a methodology for C(sp^3)-H δ-fluorination reported in 2016 by Cook and coworkers. Specifically, they reported an intramolecular directed benzylic fluorination (Scheme 2.9).[19] The starting *N*-fluorobenzamides **2** played a dual role serving as both the fluorine source and the directing group. The transformation proceeded under iron (II) triflate catalysis *via* a radical pathway. The proposed mechanism involved the SET reduction of the N−F bond by iron (II) to form a nitrogen centered radical **II** and a Fe(III)F species. Upon 1,5-HAT, the resulting carbon-centered radical **III** abstracted a fluorine atom from the iron intermediate to form a new C−F bond and furnish product **34**.

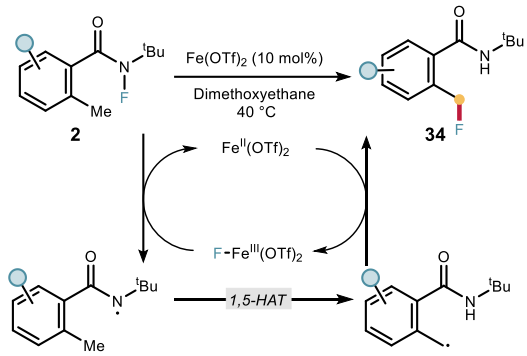

Scheme 2.9. Remote δ-fluorination under iron catalysis.

[19] Groendyke, B. J.; AbuSalim, D. I.; Cook, S. P. "Iron Catalyzed, Fluoroamide-Directed C-H Fluorination" *J. Am. Chem. Soc.* **2016**, *138*, 12771−12774.

The *N*-fluorobenzamides **2**, which were introduced by Cook, are the most stable compounds in the *N*-halogenated series. They are thermally stable and also resistant to degradation in air and on silica (Figure 2.5). This stability offers opportunities for reaction development using metal- and photoredox- catalysis. Recently, a number of new methodologies have been developed using *N*-fluorobenzamides **2** for the remote functionalization of amides using metal catalysis, including Cu[20] and Co,[21] to activate the N−F bond.

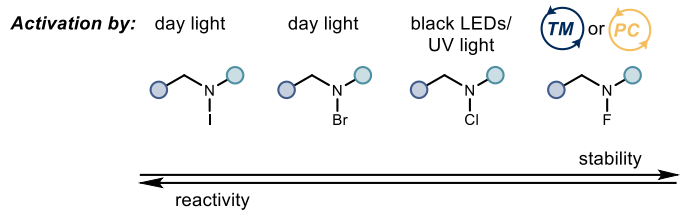

Figure 2.5. Comparison of N-X bond stability *vs* reactivity within the halogenated series of *N*-haloamides.

In 2020, Zhaoqing Xu and co-workers reported the activation of the N−F bond within *N*-fluorobenzamides **2** under metal-free conditions to form new C−C and C−N bonds (Scheme 2.10.).[22] An iridium-based photocatalyst was used for the reduction of the N−F bond in **2**, leading to nitrogen-centered radicals (NCRs) and, upon 1,5-HAT, to benzylic radicals. Radical coupling with alkyl radicals, generated from 4-alkyl-1,4-dihydropyridines **35** (Hantzsch ester analogues), delivered the final products **36**. The protocol was extended to other radicals starting from **35'** and **35''** to give products **37** and **38** respectively.

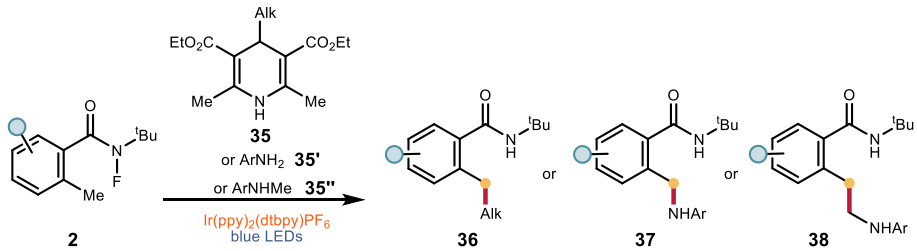

Scheme 2.10. First example of photocatalytic activation of N-F bond for the formation of a new C-C and C-N bond.

[20] Li, Z.; Wang, Q.; Zhu, J. "Copper-Catalyzed Arylation of Remote C(sp3)-H Bonds in Carboxamides and Sulfonamides*" Angew. Chem., Int. Ed.* **2018**, *57*, 13288−13292.

[21] Guo, P.; Li, Y.; Zhang, X.- G.; Han, J.-F.; Yu, Y.; Zhu, J.; Ye, K.-Y. "Redox Neutral Radical-Relay Cobalt Catalysis toward C−H Fluorination and Amination" *Org. Lett.* **2020**, *22*, 3601−3606.

[22] Guo, Q.; Peng, Q.; Chai, H.; Huo, Y.; Wang, S.; Xu, Z. "Visible-Light Promoted Regioselective Amination and Alkylation of Remote C(sp3)-H Bonds" *Nat. Commun.* **2020**, 11, 1463.

When I began my doctoral studies in 2019, there were limited methods for activating N−F bonds in *N*-fluorobenzamides **2**. Developing an efficient approach based on photoredox activation was one of the objectives set by my supervisor Kilian Muñiz, and this became the first scientific goal of my research.

2.1.3 Switchable chemodivergent synthesis in photocatalysis

Chemodivergent processes refer to chemical reactions where a single starting material can yield two or more different products, often through the use of different reaction conditions or catalysts (Figure 2.6). Chemoselective and chemodivergent synthesis therefore grants access to a wide chemical space, thus benefiting all facets of synthetic chemistry. Chemodivergent transformations are commonly achieved under transition metal-catalysis, where different catalysts or ligands determine different selectivity. The recent emergence of photocatalysis has also expanded the availability of new chemodivergent synthetic methods.[23] Switching the chemoselectivity of a process requires a number of factors including the chosen photocatalyst or other parameters including time, light source, temperature, additive, concentration, solvent, and stoichiometry.

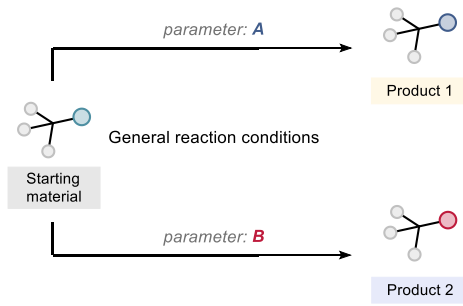

Figure 2.6. Chemodivergent reactions.

A recent example is the chemodivergent alkylation of heteroarenes **39** using DMSO as a switchable alkylating agent (Scheme 2.11).[24] Key for the chemoselective switch was the additive used to activate DMSO. When using phenylphosphonic dichloride, a methyl radical **XX** was formed that eventually reacted with heteroarene **39** to afford product **40**. On the other hand, using trimethylsilyl chloride led to a methylthiomethyl radical **XXI**, which added to 4-methylquinoline **39** to yield compound **41**.

[23] Sakakibara, Y.; Murakami, K. "Switchable Divergent Synthesis Using Photocatalysis" *ACS Catal.* **2022**, *12*, 1857−1878.
[24] Garza-Sanchez, R. A.; Patra, T.; Tlahuext-Aca, A.; StriethKalthoff, F.; Glorius, F. "DMSO as a Switchable Alkylating Agent in Heteroarene C−H Functionalization" *Chem. Eur. J.* **2018**, *24*, 10064− 10068.

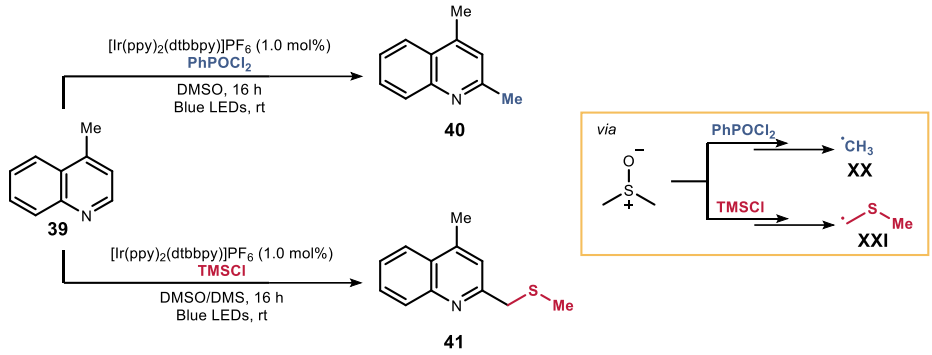

Scheme 2.11. Chemodivergent alkylation of heteroarenes using DMSO as switchable alkylating agent.

The development of new photocatalytic chemodivergent protocols would be beneficial, despite the complexity for designing such methods.

2.2 Target of the Project

The aim of the project was to develop a methodology for the C4 selective benzylation of 4-cyano pyridines based on radical patterns. Specifically, we sought to activate the N−F bond within *N*-fluorobenzamides **2** *via* SET reduction which, upon an 1,5-HAT, would form a benzyl radical. The classic chemistry of the radical anion, generated upon reduction of cyanopyridines, would then master a radical coupling step. The overall process would offer a C4 selective entry into benzylated pyridines containing a remote amide fragment.

Our original plan, detailed in Figure 2.7, was to use a photoredox catalyst (PC) to activate, *via* an SET reduction, the N−F bond in *N*-(*tert*-butyl)-*N*-fluoro-2-methylbenzamide (**2a**, E_{red} = -0.84 V vs SCE).[25] This process would first result in a nitrogen-centered radical **II**, and subsequently in a benzylic carbon-centered radical **III** bearing an amide group through a 1,5-HAT. To accomplish a radical coupling between radical **III** and cyanopyridine **1a** in an overall *ipso*-substitution manifold, it would also necessitate a SET reduction of **1a** (E_{red} = -1.60 V vs SCE),[13] resulting in the formation of the long-lived radical anion **I**. We surmised that the formation of both radical intermediates could be mastered by a single photoredox catalyst (PC) able to activate substrates **1** and **2** *via* two SET reduction steps. Efficient turnover of the photocatalyst PC, by means of reduction of the oxidized $PC^{+\cdot}$, would require a suitable donor quencher.

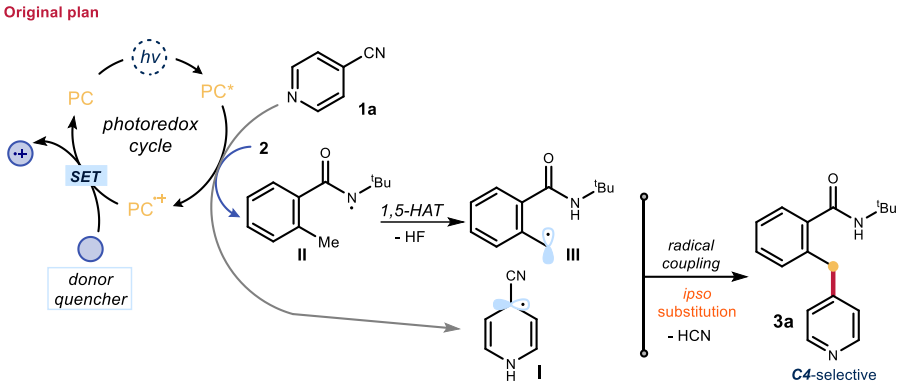

Figure 2.7. Original plan for the photoredox catalyzed amide distal benzylation of 4-cyanopyridine **1a**.

The quest for the optimal quencher brought us some surprises: we serendipitously found that using a *single photocatalyst* but *different quenchers* allowed us to select at will between mechanistically divergent processes (Figure 2.8). Specifically, we could regulate access to two reaction manifolds: an *ipso*-substitution path proceeding *via* radical coupling and a Minisci-type addition, enabling selective access to regioisomeric C4 or C2 benzylated pyridines, respectively.

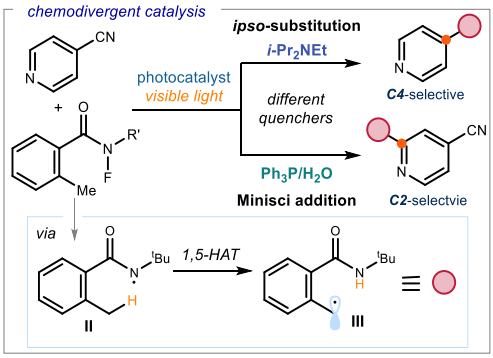

Figure 2.8. Designed and serendipitously discovered methodology for the chemodivergent benzylation of 4-cyanopyridines.

The next sections describe how we discovered these chemodivergent pathways and the mechanistic investigations which allowed us to understand the factors behind the ability of a single photocatalyst to switch chemoselectivity.

2.3 Results and Discussion

2.3.1 Discovery of the reaction and optimization

Our initial investigations were based on the original design plan detailed in Figure 2.7. 4-Cyanopyridine **1a** and *N*-(*tert*-butyl)-*N*-fluoro-2-methylbenzamide **2a** were chosen as model substrates. We then selected 1,3-dicyano-2,4,5,6-tetrakis(diphenylamino)-benzene **A** as the photocatalyst, since the redox potential of **A** ($E_{1/2}$(**A**$^{\bullet+}$/**A***) = -1.52 vs SCE)[25] indicated it as suitable for the activation of both substrates **1a** and **2a** *via* SET reduction.[26] Initial experiments were conducted using a blue LED emitting at 456 nm and acetonitrile (MeCN) as solvent. The last component of the model reaction was the donor additive, which should efficiently act as reductive quenchers of **A**. *N*,*N*-diisopropylethylamine (DIPEA) was chosen as it is a sacrificial electron donor (quencher) often used in photoredox catalytic processes. This initial test led to the formation of the desired C4-benzylated product **3a** in 50% yield (Table 2.1, entry 1). Switching solvent to 1,2-dichloromethane (DCE) improved the yield to 59% (entry 2), where other chlorinated solvents affected the reactivity. Various polar (protic and aprotic) and apolar solvents were screened but offered poor results. The initial encouraging results prompted us to pursue further optimization.

Table 2.1. Optimization studies: Screening of solvents.

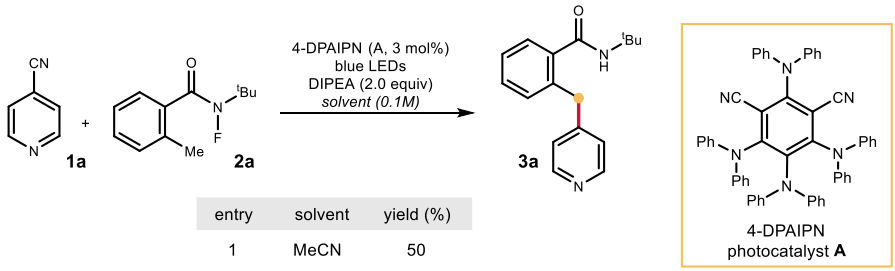

entry	solvent	yield (%)
1	MeCN	50
2	DCE	59
3	DCM	46
4	acetone	53
5	MeOH	n.d.
6	cyclohexane	n.d.

Reactions performed under argon on a 0.1 mmol scale at 40 °C for 16 h under illumination by a blue LED strip (λ_{max} = 465 nm, 14 W) using 2 equiv. of **1a** and of the additive. Yield determined by ^{1}H NMR analysis using 1,3,5-tromethoxybenzene as the internal standard.

[25] Garreau, M.; Le Vaillant, F.; Waser, J. "C-Terminal Bioconjugation of Peptides through Photoredox Catalyzed Decarboxylative Alkynylation" *Angew. Chem., Int. Ed.* **2019**, *58*, 8182−8186.

[26] The simplistic mechanistic picture detailed in Fig. 2.7, based on the SET reduction of **1a** and **2a** by photocatalyst **A**, served as our initial design plan.

Additional screening showed that 3.0 equivalents of the quencher donor (DIPEA) and 3.0 equivalents of 4-cyanopyridine were optimal. Hence, keeping those parameters consistent, we screened various photocatalysts (Table 2.2). Catalyst **A** (4-DPAIPN) was confirmed as the most successful one, delivering the target *ipso*-substitution C4-benzylated product **3a** in 75% yield (entry 1).

Table 2.2. Optimization studies: Screening of photocatalysts.

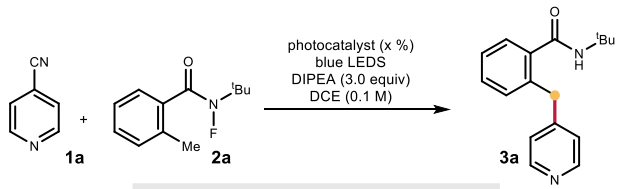

entry	photocatalyst	yield (%)
1	4-DPAIPN (1%)	75
2	$Ir(ppy)_3$ (1%)	59
3	$Ir(ppy)_2(dtbpy)PF_6$ (1%)	25
4	5CzBN (3%)	25
5	4CzIPN (3%)	20
6	3DPA2FPN (3%)	6

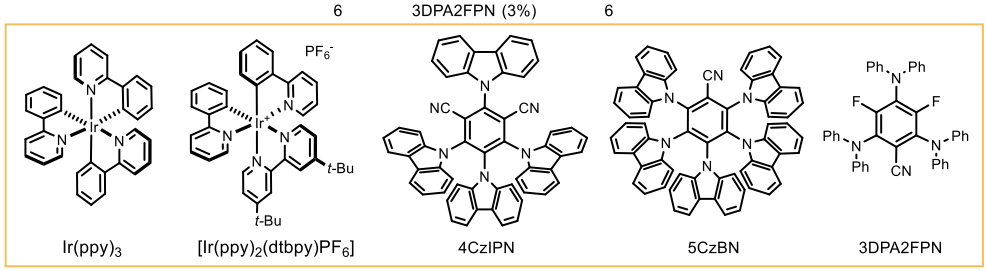

Reactions performed under argon on a 0.1 mmol scale at 40 °C for 16 h under illumination by a blue LED strip (λ_{max} = 465 nm, 14 W) using 3 equiv. of **1a** and of the additive. Yield determined by ^{1}H NMR analysis using 1,3,5-tromethoxybenzene as the internal standard.

With the optimum photocatalyst in hand, we screened various donor quenchers (Table 2.3.). When using tertiary amines, including DIPEA and pentamethyl piperidine (*N*-Me TMP), the *ipso*-benzylated product **3a** was formed in good yields (entries 1 and 2). The strained bicyclic amine DABCO completely inhibited the reactivity (entry 3). Much to our surprise, non-basic quenchers (entries 4-6) resulted in a complete switch of the reaction manifold: instead of the *ipso* C4 benzylated product **3a**, we observed the exclusive formation of the C2-benzylated pyridine **4a**. Specifically, the use of triphenylphosphine (PPh_3), Hantzsch ester (HE), and γ-terpinene all allowed for a different radical process to occur, leading to a C2-selective substitution by means of a Minisci-type pattern. We then optimized this C2-selective path and found that the addition of H_2O (5 equiv., entry 7) when using PPh_3 as the quencher, improved the yield of **4a** to 60%.

Table 2.3. Optimization studies: screening of donor quenchers and control experiments.

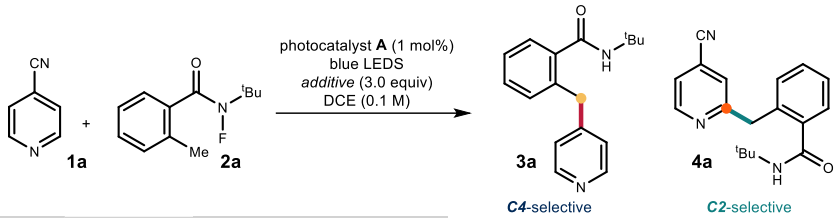

entry	additive	yield **3a** (%)	yield **4a** (%)
1	DIPEA	75	0
2	N-Me TMP	51	0
3	DABCO	0	0
4	Ph_3P	0	52
5	HE	0	45
6	γ-terpinene	0	10
7	Ph_3P/H_2O	0	60
8*	DIPEA	0	0
9*	Ph_3P	0	60

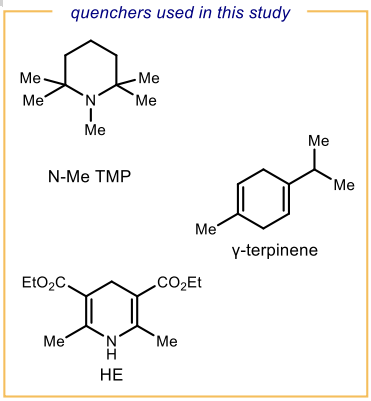

Reactions performed under argon on a 0.1 mmol scale at 40 °C for 16 h under illumination by a blue LED strip (λ_{max} = 465 nm, 14 W) using 3 equiv. of **1a** and of the additive. Yield determined by ^{1}H NMR analysis using 1,3,5-tromethoxybenzene as the internal standard. *For entries 8 and 9, reactions performed under air atmosphere.

Finally, control experiments for both processes leading to **3a** and **4a** showed that the donor quencher, the photocalatyst, light irradiation were all essential for reactivity. The two systems differed in their sensitivity to the presence of oxygen: the *ipso*-substitution reaction was completely suppressed under air atmosphere, wherein the C2-addition reaction remained unaffected (entries 8-9).

2.3.2 Investigation on the origin of chemodivergency

The intriguing possibility to switch the chemoselectivity of the process by simply changing the donor quencher led us to investigate the origin of this observation. We hypothesized that chemodivergency was due to a mechanistic switch: product **3a** would be formed by an *ipso*-substitution manifold while product **4a** though Minisci-type addition of the corresponding alkyl radical to the 4-cyanopyridine **1a**. Since it is known that Minisci reactions proceed under acidic conditions, which are essential for the activation of a heteroarene, we determined the pH of the two reaction systems (leading to **3a** and **4a**) using pH paper and a pH meter (Figure 2.9). The C2 selective system, mastered by PPh_3, had a pH of 3.1, confirming the acidic medium required for a Minisci-type pathway. In contrast, we measured a pH of 9.8 for the

DIPEA-based protocol, leading to the *ipso*-substitution product **3a**. The significant difference in acidity between the two reaction systems suggested that the pH might be the cause of the mechanistic switch and, therefore, the chemodivergence. The use of a basic quencher such as DIPEA facilitated the turnover of photocatalyst **A** while maintaining a basic pH by neutralizing the HCN and HF generated upon SET activation of substrates **1a** and **2a**, respectively. Switching to neutral quenchers (PPh_3, HE and γ-terpinene, entries 4-6 in Table 2.3) avoided the possibility of buffering the build-up of acidity in the reaction medium.

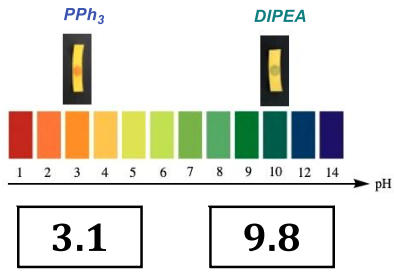

Figure 2.9. pH measurements of the two reactions using different donor quenchers (DIPEA and PPh_3).

In addition, the use of PPh_3 led to the formation of radical cation **IV** upon SET oxidation ($E_{1/2}$ = +0.98 V vs SCE) by the photocatalyst **A** (Figure 2.10). The radical cation **IV** is known to deliver the phosphoranyl radical **V** with the simultaneous liberation of protons upon addition of water.[27] The *in situ* formation of HF in combination with the release of protons from the distinct behavior of PPh_3 ensured the acidic conditions needed for a Minisci-type reaction to proceed, overriding a possible *ipso*-substitution reaction.

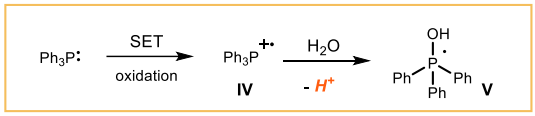

Figure 2.10. Rationale for the acidity increase in the PPh_3-based protocol.

To further corroborate the role of the acidic medium in the Minisci-type reactivity, we conducted a kinetic profile analysis. The following three processes were investigated: a) the reaction using DIPEA enabling the *ipso*-substitution affording **3a**; b) the reaction using PPh_3 leading to the Minisci product **4a**; c) and the same reaction with PPh_3 as in (b) but in the

[27] a) Pandey G.; Pooranchand D.; Bhalerao U. T. "Photoinduced single electron transfer activation of organophosphines: Nucleophilic trapping of phosphine radical cation" *Tetrahedron* **1991**, *47*, 1745–1752. b) Masuda, Y.; Tsuda, H.; Murakami, M. "Photoinduced Dearomatizing Three-Component Coupling of Arylphosphines, Alkenes, and Water" *Angew. Chem., Int. Ed.* **2021**, *60*, 3551−3555.

presence of trifluoroacetic acid (TFA) as acid (Figure 2.11). It was observed that the Minisci C2-selective path (in red) proceeded faster than the C4-selective process (in green; after 75 minutes the Minisci product **4a** was formed in 60% yield, while the *ipso*-substitution adduct **3a** in about 5% yield). The kinetic profile also showed an induction period for the Minisci reaction (in red), which was suppressed upon addition of TFA (5 mol%, in blue). This last observation suggested that the *in situ* acidic build-up should progress to a point where the pH is low enough to activate the Minisci pathway. Importantly, the Minisci reaction could not be promoted by simple addition of stoichiometric amounts of TFA and removal of PPh_3. This indicated the unique ability of the neutral quencher PPh_3 to switch on an effective photocatalytic pathway enabling the C2-selective process.

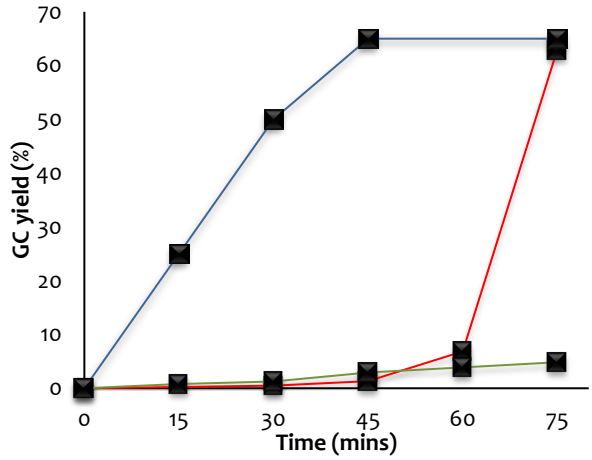

Figure 2.11. Kinetic profile analysis of a) *ipso*-substitution (green profile); b) Minisci reaction (red profile); c) Minisci reaction with 5 mol% of TFA (blue profile).

2.3.3 Scope of the reactions: Ipso-substitution and Minisci type reaction

Having rationalized the observed chemodivergency, we examined the synthetic applicability of our photocatalytic systems. We adopted the optimized conditions in entries 1 and 7 of Table 2.3. Both protocols required the same reaction conditions (substrates, photocatalyst **A**, and solvent), but differed in the additive used (DIPEA or PPh_3). We first evaluated the 2-alkyl *N*-fluorobenzamides **2** that could participate in the *ipso*-substitution and the Minisci processes with 4-cyanopyridine **1a** leading to C4 or C2 benzylated pyridines **3** and **4**, respectively (Figure 2.12). We first tested a methyl substituent at the benzylic position of **2**. This modification proved to be well-tolerated for both protocols leading to products **3b** and **4b**. Substitution at various positions of the aryl ring, including electron-donating groups and halides, was also tolerated well (adducts **c-j** in both protocols). Replacement of the phenyl

with a thiophenyl ring afforded the corresponding products **3k** and **4k**. Linear *N*-fluoramide could successfully participate in the *ipso*-substitution protocol to deliver product **3l**. On the other hand, the same linear substrate offered poor reactivity (<20 %) under Minisci conditions (a list of unsuccessful and moderately reactive substrates is reported in Figure 2.14 below).

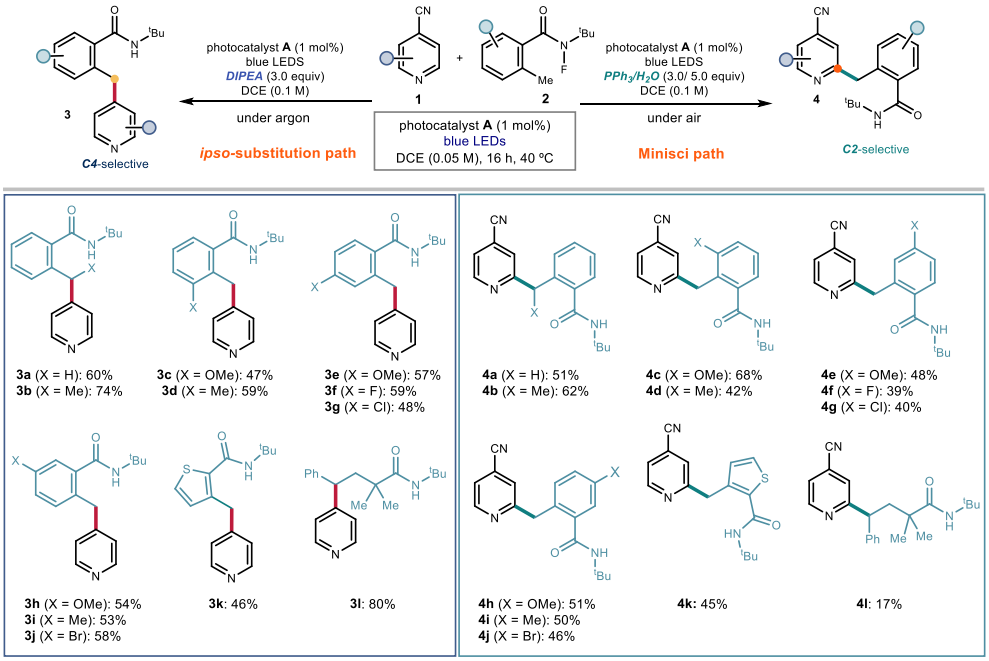

Figure 2.12. Scope of *N*-fluoroamides **2** suitable for the chemodivergent C4 and C2 radical benzylation of 4-cyanopyridines.

We then explored the applicability of the C4 and C2 selective protocols using various cyanopyridines **1** (Figure 2.13). 2-Alkyl- and 2-aryl- substituted cyanopyridines afforded the corresponding *ipso*-substitution **3m-r** and the Minisci products **4m-r** in good yields. For the *ipso*-substitution protocol, electron-rich groups installed at the C2 position, such as a pyrazole and a phenol ether, successfully delivered products **3s** and **3t**. 3-Substituted cyanopyridines bearing a phenyl or a chloro group led to the formation of *ipso*-substitution products **3u-v**. When those substrates were submitted to the C2-selective Minisci protocol, the chloro-substituted cyanopyridine gave the more crowded regioisomer **4s**, while the bulkier phenyl group led to adduct **4t**, likely for steric reasons.[28] A 2,3-fused cyclopentane substrate resulted in products **3w** and **4u** in moderate yields. The 2,3,5,6-tetrafluoro-4-cyanopyrine reacted

[28] O'Hara, F.; Blackmond, D. G.; Baran, P. S. "Radical-based regioselective C−H functionalization of electron-deficient heteroarenes: scope, tunability, and predictability" *J. Am. Chem. Soc.* **2013**, *135*, 12122−12134.

smoothly delivering the *ipso*-substituted product **3x**. The *ipso*-substitution methodology could also be applied to heteroarenes other than pyridines, such as 1-cyanoisoquinoline, which led to the formation of product **3y** in high yield. Moving to 4-substituted pyridines, substrates bearing electron-withdrawing groups other than nitrile (essential for the *ipso*-substitution reaction), could be applied under Minisci conditions, delivering the benzylated trifluoromethyl- and ethyl ester- substituted pyridines **4v** and **4w** in good yields. Finally, the Minisci-type protocol could be extended to the direct functionalization of a biorelevant compound, since *abiraterone acetate* (a medication used to treat prostate cancer) afforded adduct **4x** in satisfactory yield.

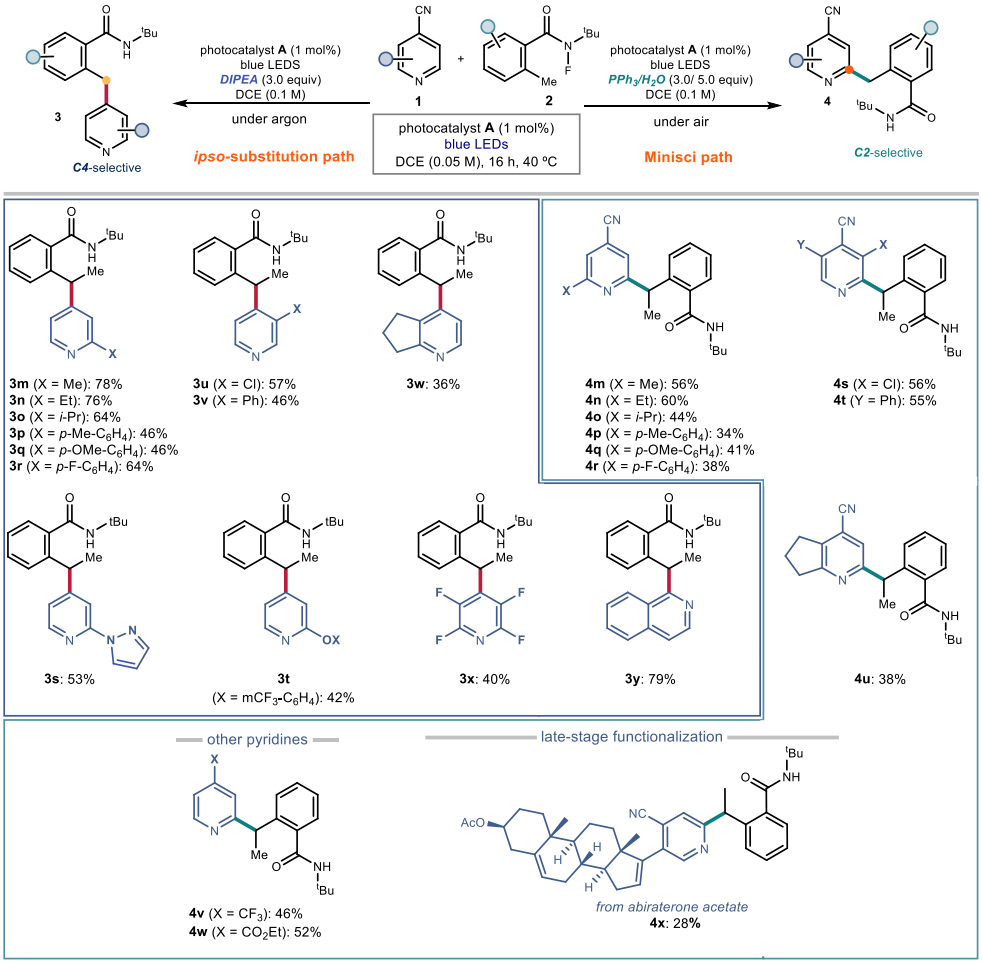

Figure 2.13. Scope of cyanopyridines **1** and other heteroarenes for the chemodivergent C4 and C2 radical benzylation.

We then sought to extend the application of our switchable protocols leading at will to C2 and C4-functionalized pyridines. For that purpose, we developed a sequential protocol (Scheme 2.12). Relying on the pH-regulated switchable methods, we first performed the Ph_3P-enabled Minisci process between 4-cyanopyridine **1a** and 2-ethyl *N*-fluorobenzamide **2b** to get **4b** with C2-selectivity. The Minisci-type addition product **4b** was first isolated and subsequently reacted with the linear *N*-fluoroamide **2c** using DIPEA to select the C4-selective *ipso*-substitution manifold. The overall sequence smoothly delivered the complex pyrdine **42**, demonstrating the potential of the switchable methodologies to grant access to complex pyridine-containing structures.

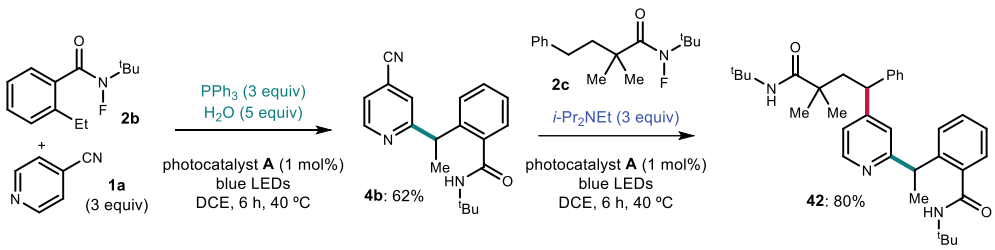

Scheme 2.12. Sequential procedure for the difunctionalization of 4-cyanopyridine **1a**.

We also investigated if the generality of our chemodivergent system could be expanded to include different radical precursors. Pyridinium salts are known to deliver radical species upon SET reduction and are commonly used in photoredox catalysis.[29] Thus, we tested the generality of our system using pyridinium salt **43** instead of *N*-fluoroamides **2** (Scheme 2.13). We were pleased to see that **43** was successfully activated towards benzyl radical formation in both systems by the photocatalyst **A** (E_{red} = -1.01V vs Ag/AgCl). The C4 and C2 benzylated pyridines **44** and **45** were obtained in satisfactory yields.

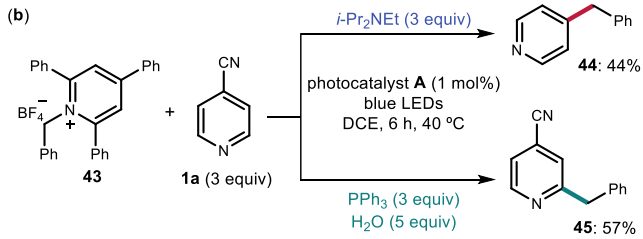

Scheme 2.13. *Ipso*-substitution (C4 selective) and Minisci-type reaction (C2 selective) for the benzylation of **1a** with *N*-benzyl pyridinium **6**.

[29] Ociepa, M.; Turkowska, J.; Gryko, D. "Redox-Activated Amines in C(sp^3)−C(sp) and C(sp^3)−C(sp^2) Bond Formation Enabled by Metal-Free Photoredox Catalysis" *ACS Catal.* **2018**, *8*, 11362−11367.

2.3.4 Limitations of the methodologies

The developed methodologies enabled the functionalization of a broad range of 4-cyanopyridines **1**, using various *N*-fluoroamides **2**. However, both protocols faced some limitations. Specifically, they could not be applied to 2-cyanopyridine and 3-cyanopiridine, as well as other cyanoheteroarenes (2-cyanopyrimidine, 2-cyanopyrazine, 2-cyanoquinoline) (Figure 2.14a). 1,4-Dicyanobenzene, a common substrate in *ipso*-substitution reactions *via* radical coupling mechanisms, proved unsuccessful under our conditions. On the other hand, 4-methylquinoline, which is often used in Minisci-type reaction, gave the desired product in only 18% yield under our Ph_3P-based conditions (Figure 2.14b). Figure 2.14c shows a series of *N*-fluoroamides that were either poorly reactive or failed in the reaction. The *N*-fluoroamide bearing an adamantyl substituent and a δ C-H benzylic position available reacted poorly under both protocols. Finally, linear *N*-fluoroamides and *N*-fluorosulfonamides both failed to deliver the corresponding products through the formation of secondary radicals at the δ position.

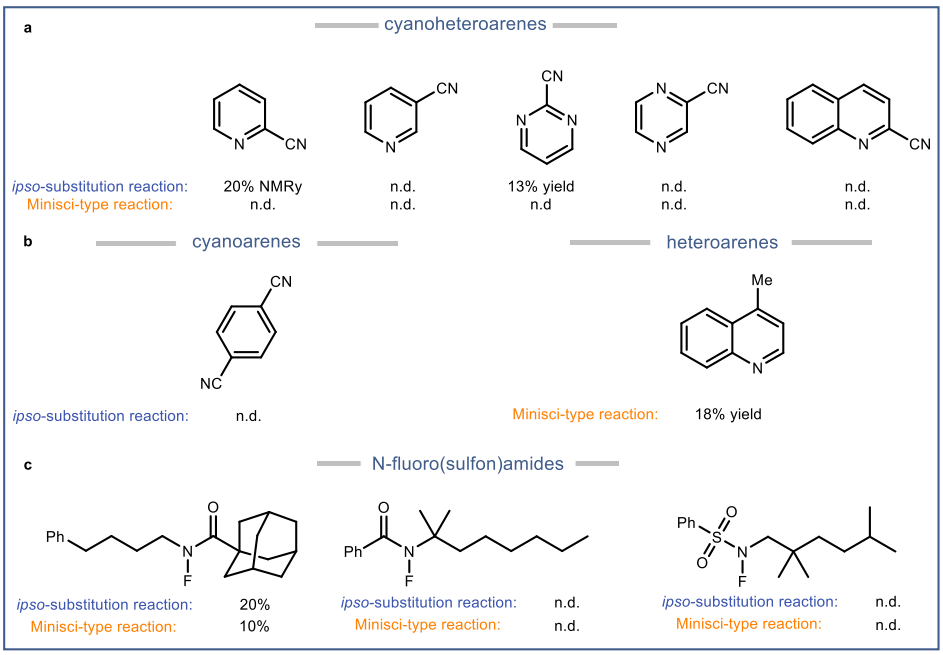

Figure 2.14. Limitation of the two methodologies.

2.3.5 Mechanistic investigation

The preliminary investigations had provided a solid rationale for the observed chemodivergency, but we wanted to gain further insights into the two mechanistic pathways.

To establish the interactions between the excited photocatalyst **A**, which enabled both pathways, and the substrates, we conducted Stern-Volmer quenching studies. This kind of experiments allows to quantify the dynamic quenching of the excited species by the observed decrease of its emission. We recorded the emission spectrum of the excited photocatalyst **A** (excitation at 527 nm) and we then proceeded to a series of Stern-Volmer quenching experiments (Figure 2.15). The progressive addition of a solution containing DIPEA indicated a quenching of the photocatalyst **A** excited state. Translating the collected data into a Stern-Volmer plot, we found a linear correlation between the concentration of DIPEA (the quencher) and the ratio I_0/I.[30] From the slope of the resulting line, we could estimate the Stern-Volmer constant (K_{SV}) to be 5.9 M^{-1}.

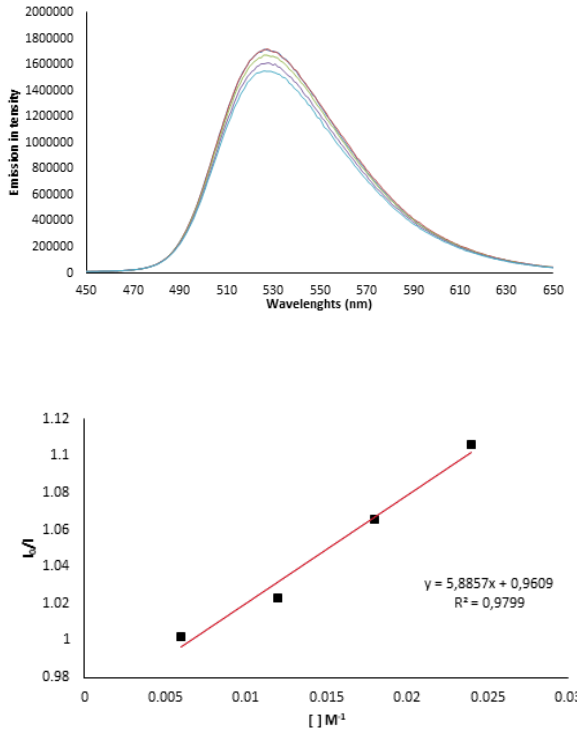

Figure 2.15. Quenching of photocatalyst **A** emission (4·10-6 M in 1,2-DCE) in the presence of increasing amounts of DIPEA (above) and the corresponding Stern-Volmer quenching plot (below).

The same experiment was performed between photocatalyst **A** and PPh_3 (used as an electron donor in the Minisci protocol, Figure 2.16). Progressive addition of PPh_3 led to a pronounced quenching. The Stern-Volmer constant was estimated to be 45.3 M^{-1}. Stern-Vomler quenching

[30] Lakowicz, J. R. Ed. *Principles of Fluorescence Spectroscopy*, Plenum Press, **1983**, 52–93.

experiments have been performed also with 4-cyanopyridine **1a** and *N*-fluoroamide **2a** resulting in K_{SV} = 4.4 M^{-1} and K_{SV} = 18.8 M^{-1} respectively (see experimental section for details). These results indicate that all components (DIPEA, PPh_3, **1a** and **2a**) can quench the excited state of **A**, therefore confirming the feasibility of an SET event taking place.

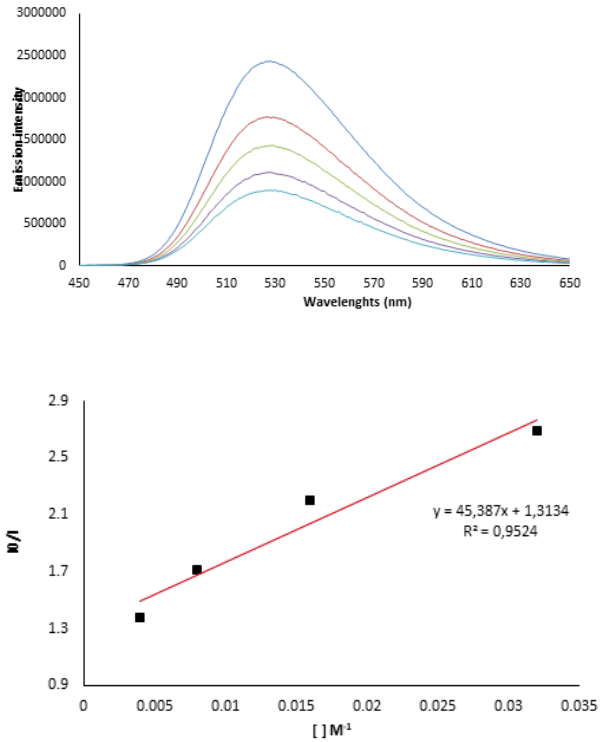

Figure 2.16. Quenching of photocatalyst **A** emission (4·10-6 M in 1,2-DCE) in the presence of increasing amounts of PPh_3 (above) and the corresponding Stern-Volmer quenching plot (below).

Overall, these studies have shown that the excited photocatalyst **A*** can interact with all the reaction components. We also investigated the possibility of other reaction intermediates to act as SET reductants. In the *ipso*-substitution protocol, an SET oxidation of DIPEA by the excited state of **A** would result in the formation of the corresponding radical cation **a** (Figure 2.17a). Deprotonation of this intermediate by a second molecule of DIPEA (3.0 equivalent were used in the reaction) could afford a α-amino radical **b**. α-Amino radicals have been previously reported to act as reductants. To gain evidence of whether a α-amino radical could reduce the *N*-fluoroamides **2**, we performed an experiment where α-amino radicals could be generated in the absence of the photocatalyst **A**. We used a protocol previously reported by Ritter *et al.* which made use of sodium persulfate to oxidize tertiary amines, delivering α-

amino radicals.[31] . Treatment of the *N*-fluoroamide **2b** with $Na_2S_2O_8$ in the presence of DIPEA resulted in 20% of the corresponding hydrodefluorinated product **2b'** (Figure 2.17b). This observation showed that a SET reduction of compounds **2** by the α-amino radical **b** was feasible.

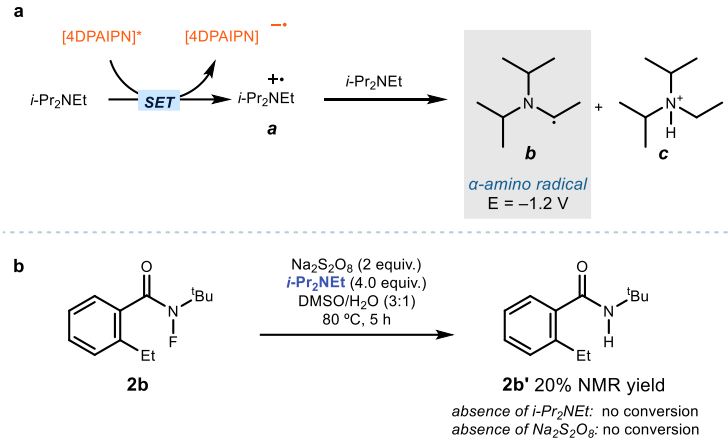

Figure 2.17. a) α-Amino radical formation under DIPEA-based protocol. b) Benzyl radical generation driven by the α-amino radical **b**.

The same experiment, in the presence of sodium persulfate and absence of photocatalyst **A** was then performed using PPh_3 (Minisci-reaction protocol, Figure 2.18b). This resulted in the formation of the defluorinated product **2b'**, suggesting that an intermediate derived from oxidation of PPh_3 could act as a SET reductant for substrate **2b**. As suggested previously in section 2.3.2, a phosphoranyl radical **f** could be formed under the Minisci reaction conditions, which is also related to the *in-situ* formation of acid (Figure 2.18a). Phosphoranyl radicals were recently reported to serve as strong SET reductants.[32] Overall, this experiment suggested the possibility for the phopshoranyl radical **f** resulting from oxidation of PPh_3 to activate the *N–F* fluoramide.

[31] Alvarez, E. M.; Karl, T.; Berger, F.; Torkowski, L.; Ritter, T. "LateStage Heteroarylation of Hetero (aryl) sulfonium Salts Activated by α-Amino Alkyl Radicals" *Angew. Chem., Int. Ed.* **2021**, *60*, 13609– 13613.

[32] Caiger, L.; Sinton, C.; Constantin, T.; Douglas, J. J.; Sheikh, N. S.; Juliá, F.; Leonori, D. "Radical Hydroxymethylation of Alkyl Iodides Using Formaldehyde as a C1 Synthon" *Chem. Sci.* **2021**, *12*, 10448– 10454.

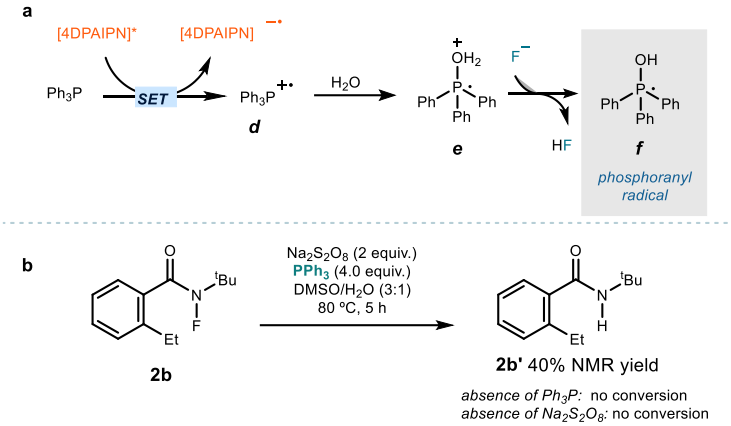

Figure 2.18. a) Phosphoranyl radical formation under PPh_3-based protocol. b) Proving the formation of phosphoranyl radical for examining its reducing ability toward *N*-fluoroamide **2b**.

To gain more insights about the destiny of PPh_3, an oxygen isotope experiment was performed (Figure 2.19). The general conditions used in the Minisci protocol were used, but replacing H_2O with labelled H_2O^{18}. We observed formation of the labelled Ph_3PO^{18}, which is congruent with the mechanistic proposal shown in Figure 2.18a.

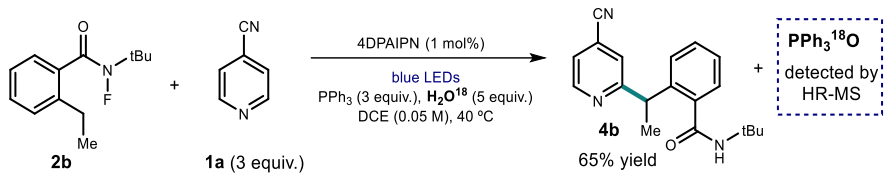

Figure 2.19. Detection of ^{18}O-labelled triphenylphosphine oxide.

To examine the nature of the radical *ipso*-substitution and Minisci processes, we measured the quantum yields. The quantum yield (Φ) of a photochemical reaction indicates the number of molecules reacted per quantum (single photon) of the absorbed light by the chromophore. Φ can be expressed with the following ratio: Φ = molecules of product number/ number of photons absorbed.

For the *ipso*-substitution reaction, we measured a value Φ = 0.01.[33] The obtained value, which is lower than 1, suggested that a radical chain mechanism is unlikely. Unfortunately, the

[33] A value of <1 does not completely exclude a radical chain mechanism, since the measured quantum yield does not account for non-productive energy-wasting processes that quench the excited state of the key photoactive species and affect the efficiency of the photo-initiation for a possible chain process. For a review detailing the key aspects of mechanistic studies in photocatalysis, see: Buzzetti, L., Crisenza, G. E. M., Melchiorre, P. "Mechanistic Studies in Photocatalysis" *Angew. Chem. Int. Ed.* **2019**, *58*, 3730-3747.

quantum yield for the Minisci reaction protocol could not be measured. This was due to insoluble solid formation during the reaction causing light scattering which in turn prevented the precise measurement of the quantum yield. In addition, the induction time observed during the process (see reaction profile in section 2.3.2) further complicated the experiment for determining the Φ value.

2.3.6 Mechanistic proposal

Overall, our investigations led us to propose the following mechanisms. The proposal for the *ipso*-substitution process mastered by DIPEA is shown in Figure 2.20. The excited state of the photoredox catalyst **A** (4-DPAIPN) was generated upon visible-light irradiation. The resulted **A*** was reduced *via* SET by DIPEA (see Stern-Volmer quenching studies). This step resulted in the highly reducing catalyst PC^{n-1} ($E^{1/2}$ (**PC**/**PC**$^{-}$) = -1.65 vs SCE)[25] which then activated 4-cyanopyridine **1a** (E^{ox} (**1a**/**1a**$^{\bullet-}$) = -1.60 V vs SCE)[11] by SET reduction, delivering the radical anion **I**. On the other side of the photocatalytic cycle, a radical cation derived from DIPEA was generated, which is known to undergo rapid deprotonation forming the α-amino radical **b**. As supported by our mechanistic experiments, as well as from literature reports, intermediate **b** might act as SET reductant.[34] In the context of this so-called reductant up-conversion process,[35] the α-amino radical **b** ($E^{ox}(Bu_3N^{+}/Bu_3N)$ = -1.2 V vs SCE)[34] performed a thermodynamically favorable SET reduction of the N−F bond within *N*-(*tert*-butyl)-*N*-fluoro-2-methylbenzamide **2a** (E^{ox}(**2a**/**2a**$^{\bullet-}$) = -0.84 V vs SCE).[22] Alternatively, cleavage of the N−F bond of **2a** could be achieved *via* an atom transfer mechanism (XAT), again from α-amino radical **b**.[32] The resulting nitrogen-centered radical underwent a 1,5-HAT for the formation of the benzylic radical **III**. A final radical coupling step between **III** and **I**, followed by extrusion of the cyano group, delivered the desired product **3**.

[34] Alvarez, E. M.; Karl, T.; Berger, F.; Torkowski, L.; Ritter, T. "LateStage Heteroarylation of Hetero (aryl) sulfonium Salts Activated by α-Amino Alkyl Radicals" *Angew. Chem., Int. Ed.* **2021**, *60*, 13609− 13613.
[35] Syroeshkin, M. A.; Kuriakose, F.; Saverina, E. A.; Timofeeva, V. A.; Egorov, M. P.; Alabugin, I. V. "Upconversion of Reductants" *Angew. Chem., Int. Ed.* **2019**, *58*, 5532−5550.

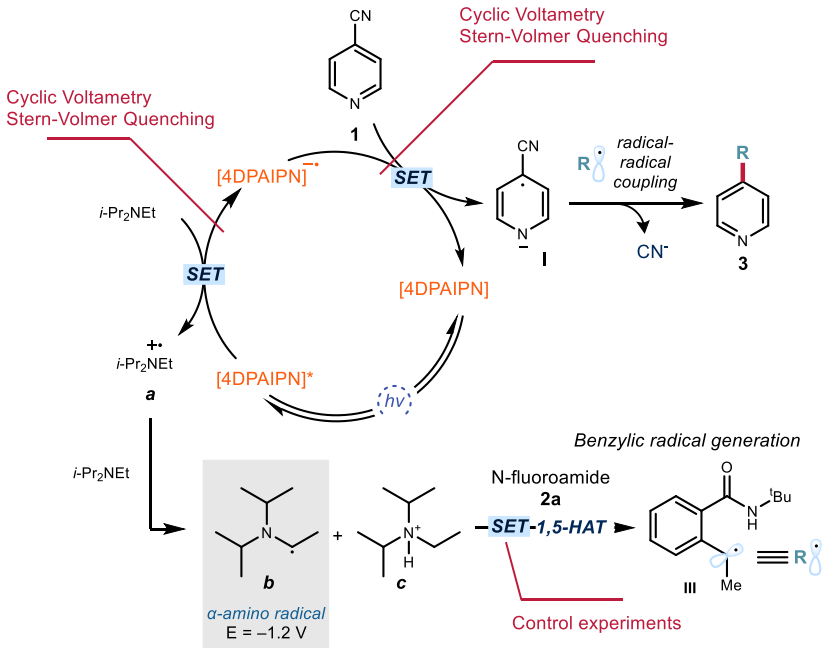

Figure 2.20. Proposed mechanism for DIPEA-based *ipso*-substitution reaction.

A plausible mechanism for the Minisci-type reaction is depicted in Figure 2.21. Similarly to the *ipso*-substitution reaction, a reductive quenching of the excited photocatalyst **A*** is triggered by triphenylphosphine (see Stern-Volmer quenching studies) generating the reducing photocatalyst PC^{n-1} ($E^{1/2}$ (**PC**/**PC**$^{-}$) = -1.65 vs SCE)[25] and the phosphorus-based radical cation **d**.[32] A nucleophilic attack by water on to the electron deficient **d**, followed by deprotonation, afforded the phosphoranyl radical **f**. Intermediate **f** triggered SET reduction of *N*-fluoroamide **2a** delivering the benzylic radical **III**, upon a 1,5-HAT. This SET process is supported by the redox potentials of similar phopshoranyl radicals (e.g., E_{ox} ($Ph_3POMe^{+}/Ph_3POMe^{\cdot}$) = -1.63 vs SCE).[32] *In situ* acid formation led to a low pH, thus facilitating the Minisci-type addition of **III** into cyano-pyridine **1a**, delivering **V**. Subsequent deprotonation and oxidation of intermediate **V** by another molecule of **2a** (or by traces of oxygen, since the reaction is performed under air) led to the C2-alkylated product **4a**. An alternative radical chain process through the oxidation of **V** by **2a** could not be excluded due to the difficulties of measuring the quantum yield of the overall process.

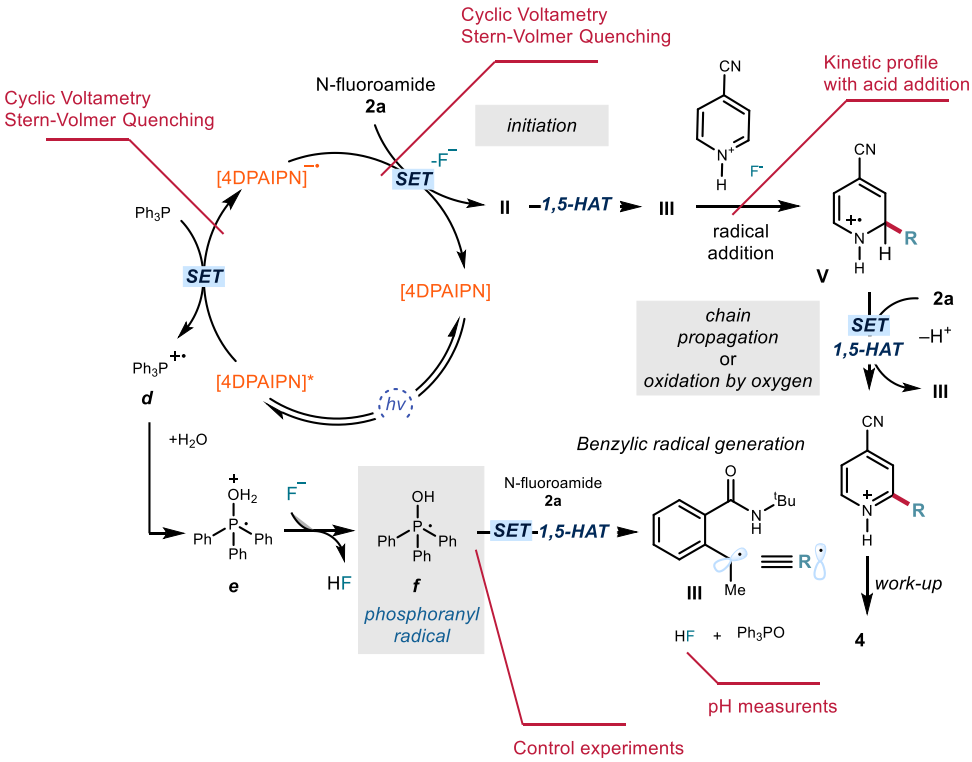

Figure 2.21. Proposed mechanism for PPh_3-based Minisci reaction.

2.4 Conclusions

In conclusion, we have developed a photocatalytic strategy that allows switchable control of the chemoselectivity in the radical benzylation of 4-cyanopyridines. According to our initial plan, we developed an *ipso*-substitution path affording C4 benzylated pyridines **3**. A serendipitous discovery allowed us to also develop a Minisci-type reaction yielding products **4** with C2 selectivity. After conducting mechanistic investigations, we were able to provide an explanation for the observed switch in chemoselectivity, which was primarily attributed to the difference in acidity (pH) between the two reaction media. By selecting a specific photocatalyst quencher, the two complementary reaction pathways, which employ identical reaction conditions, substrates, and photocatalyst, could be selectively triggered.

2.5 Experimental Section

General Information The ^{1}H NMR, ^{19}F NMR, ^{13}C NMR spectra and UPC[2] traces are available in the literature[1] and are not reported in the present dissertation.

The NMR spectra were recorded at 300 MHz, 400 MHz and 500 MHz for ^{1}H and 75, 100 or 125 MHz for ^{13}C. The chemical shift (δ) for ^{1}H and ^{13}C are given in ppm relative to residual signals of the solvents ($CHCl_3$ @ 7.26 ppm ^{1}H NMR and 77.16 ppm ^{13}C NMR, and tetramethylsilane @ 0 ppm). Coupling constants are given in hertz (Hz). The following abbreviations are used to indicate the multiplicity: s, singlet; d, doublet; q, quartet; m, multiplet; bs, broad signal; app, apparent.

High resolution mass spectra (HRMS) were obtained from the ICIQ HRMS unit on MicroTOF Focus and Maxis Impact (Bruker Daltonics) with electrospray ionization. (ESI).

UV-vis measurements were carried out on a Shimadzu UV-2401PC spectrophotometer equipped with photomultiplier detector, double beam optics and D_2 and W light sources or an Agilent Cary60 spectrophotometer. Emission spectra of light sources were recorded on Ocean Optics USB4000 fiber optic spectrometer.

Yields refer to isolated materials of >95% purity, as determined by ^{1}H NMR.

The authors are indebted to the team of the Research Support Area at ICIQ, particularly to the NMR and the High-Resolution Mass Spectrometry Units.

General Procedures. All reactions were set up under an argon atmosphere (unless indicated otherwise) in oven-dried glassware. Synthesis grade solvents were used as purchased, anhydrous solvents were taken from a commercial SPS solvent dispenser. Chromatographic purification of products was accomplished using flash chromatography (FC) on silica gel (35-70 mesh). For thin layer chromatography (TLC) analysis throughout this work, Merck pre-coated TLC plates (silica gel 60 GF_{254}, 0.25 mm) were employed, using UV light as the visualizing agent and an acidic mixture of vanillin or basic aqueous potassium permanganate ($KMnO_4$) stain solutions, and heat as developing agents. Organic solutions were concentrated under reduced pressure on a Büchi rotatory evaporator.

Materials. Most of the starting materials used in this study are commercial and were purchased at the highest purity available from Sigma-Aldrich, Fluka, Alfa Aesar, Fluorochem, and used as received, without further purifications.

Substrate Synthesis

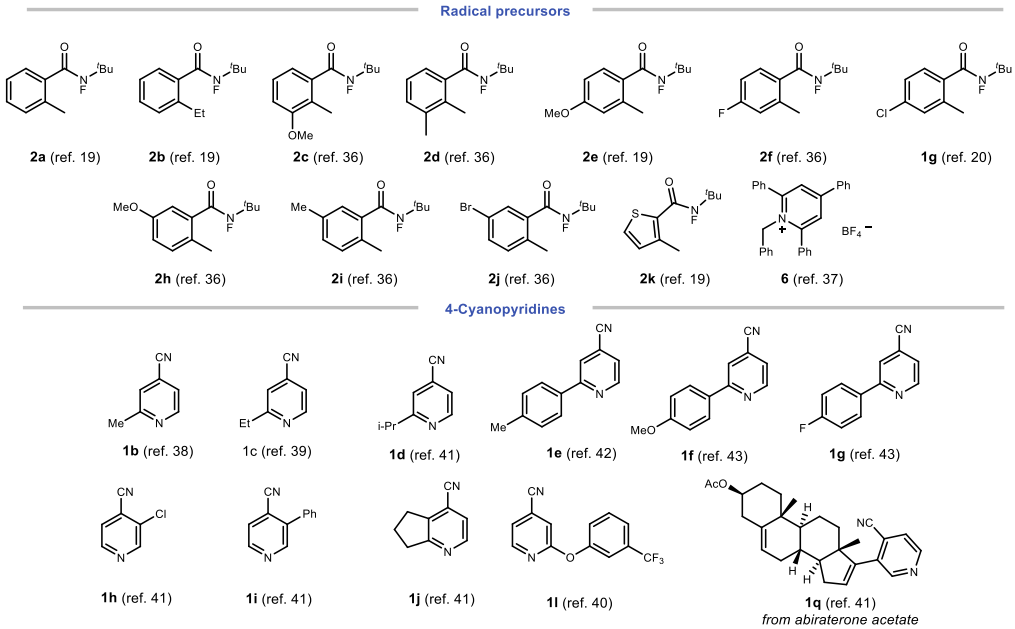

Figure 2.22. Starting materials synthesized according to literature precedents and corresponding references.[19, 20, 36, 37, 38, 39, 40, 41, 42, 43]

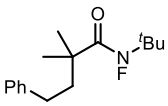

2l

***N*-(*tert*-butyl)-N-fluoro-2,2-dimethyl-4-phenylbutanamide** (**2l**): To a round-bottom flask with a stirrer bar was added 2,2-dimethyl-4-phenylbutanoic acid (5 mmol, 961 mg, 1.0 equiv.) and CH_2Cl_2 (17 mL, 0.3 M). *N*,*N*-Dimethylformamide (DMF; 0.05 equiv.) was added at room

[36] Liu, H.-C.; Li, Y.; Gong, X.-P.; Niu, Z. J.; Wang, Y.-Z.; Li, M.; Shi, W.-Y.; Zhang, Z.; Liang, Y.-M. "Cu-Catalyzed Direct C−H Alkylation of Polyflfluoroarenes *via* Remote C(sp^3)−H Functionalization in Carboxamides" *Org. Lett.* **2021**, *23*, 2693–2698.
[37] Wu, J.; He, L.; Noble, A.; Aggarwal, V. K. "Photoinduced Deaminative Borylation of Alkylamines" *J. Am. Chem. Soc.* **2018**, *140*, 10700−10704.
[38] Van Gool, M.; Alonso De Diego, S. A.; Delgado, O.; Trabanco, A. A.; Jourdan, F.; Macdonald, G. J.; Somers M.; Ver Donck, L. "1,3,5-Trisubstituted Pyrazoles as Potent Negative Allosteric Modulators of the mGlu2/3 Receptors" *ChemMedChem* **2017**, *12*, 905–912.
[39] Yamaguchi, K.; Yajima, K.; Mizuno, N. "Facile synthesis of nitriles *via* manganese oxide promoted oxidative dehydrosulfurization of primary thioamides" *Chem. Commun.* **2012**, *48*, 11247–11249.
[40] Rowbottom, M. W.; Bain, G.; Calderon, I.; Lasof T. *et. al.* "Identification of 4-(Aminomethyl)-6-(trifluoromethyl)-2-(phenoxy)pyridine Derivatives as Potent, Selective, and Orally Efficacious Inhibitors of the Copper-Dependent Amine Oxidase, Lysyl Oxidase-Like 2 (LOXL2)" *J. Med. Chem.* **2017**, *60*, 4403–4423.
[41] Elbert, B. L.; Farley, A. J. M.; Gorman, T. W.; Johnson, T. C.; Genicot, C.; Lallemand, B.; Pasau, P.; Flasz, J.; Castro, J. L.; MacCoss, M.; Paton, R. S.; Schofield, C. J.; Smith, M. D.; Willis, M. C.; Dixon, D. J. "C−H Cyanation of 6-Ring N-Containing Heteroaromatics" *Chem. Eur. J.* **2017**, *23*, 14733−14737.
[42] Cuthbertson, J. D.; MacMillan, D. W. C. "The direct arylation of allylic sp^3 C-H bonds *via* organic and photoredox catalysis" *Nature* **2015**, *519*, 74− 77.
[43] Huang, Y.; Guan, D.; Wang, L. "Direct Arylation of Substituted Pyridines with Arylboronic Acids Catalyzed by Iron(II) Oxalate" *Chin. J. Chem.* **2014**, *32*, 1294–1298.

temperature. Oxalyl chloride (1.5 equiv.) was added dropwise. The reaction was stirred at room temperature until effervescence subsided (45 min). The volatile components were then removed by rotary evaporation. The crude reaction product was dissolved in CH_2Cl_2 (0.3 M) and stirred. *tert*-Butylamine (1.5 equiv.) and triethylamine (2.0 equiv.) were added sequentially at room temperature, and the reaction was stirred for 3 hours. The reaction was quenched with aqueous HCl (1 M) and diluted with CH_2Cl_2 (0.1 M) and water (0.1 M) before being transferred to a separatory funnel. The organic layer was removed, and the aqueous layer was then extracted with CH_2Cl_2 (3 x 0.1 M). The combined organic layers were washed with saturated aqueous $NaHCO_3$ and then brine. The organic layer was dried with MgSO4, filtered, and concentrated by rotary evaporation. The crude amide was used for the next step without further purification. To the crude residue was added anhydrous THF (0.13 M), and the solution stirred at 0 °C for 15 min. *n*-Butyllithium (1.1 equiv, 2.5 M in hexanes) was added dropwise. The reaction was maintained at 0 ºC for 1.5 h, then *N*-fluorodibenzenesulfonimide (1.5 equiv, 0.6 M in THF) was added dropwise as solution in THF (0.6 M). The reaction was left overnight in the ice bath and allowed to warm to room temperature. After 12 h, the reaction was quenched with aqueous HCl (1 M) and transferred to a separatory funnel. The crude mixture was diluted with $CHCl_3$ (0.1 M) and water (0.1 M). The organic layer was removed, and the aqueous layer was extracted with $CHCl_3$ (3 x 0.1 M). The combined organic layers were washed with saturated aqueous $NaHCO_3$ and then brine, dried over $MgSO_4$, filtered, and concentrated by rotary evaporation. The crude residue was purified by flash column chromatography (SiO_2: hexanes/EtOAc 95:5) to give the product as a yellowish oil (633 mg, 60% yield).

^{1}H NMR (400 MHz, CDCl3) δ 7.32 – 7.28 (m, 2H), 7.22 – 7.18 (m, 3H), 2.63 – 2.59 (m, 2H),

1.94 – 1.89 (m, 2H), 1.49 (d, J = 2.1 Hz, 9H), 1.30 (d, J = 2.2 Hz, 6H).

^{13}C{^{1}H} NMR (101 MHz, CDCl3) δ 181.8 (d, J = 3.3 Hz), 142.5, 128.4, 128.3, 125.8, 64.4 (d, J = 10.2 Hz), 45.1 (d, J = 3.2 Hz), 41.6 (d, J = 7.8 Hz), 31.5, 27.2 (d, J = 6.6 Hz), 25.2 (d, J = 5.4

Hz).

^{19}F NMR (376 MHz, CDCl3) δ -78.8 (s).

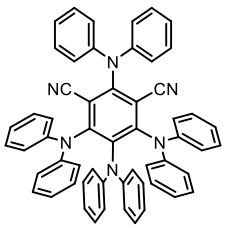

4DPAIPN

4DPAIPN (photocatalyst **A**)**:** Following a modified procedure of a reported protocol,[11] sodium hydride (60% suspension in mineral oil, 1.92 g, 48 mmol, 12 equiv.) was added slowly to a stirred solution of diphenylamine (4.06 g, 24.0 mmol, 6 equiv.) in anhydrous DMF (40 mL). The resulting suspension was heated to 60 °C under argon for 1.5–2 h. Then, 2,4,5,6-tetrafluoroisophthalonitrile (0.80 g, 4.0 mmol, 1.0 equiv.) was added and the resulting reaction mixture was stirred at 50 °C for 4 h, and then at room temperature overnight. Water (10 mL) was added and the mixture was diluted with 160 mL H_2O, extracted with CH_2Cl_2 (3 x 80 mL) and dried over Na_2SO_4. The solution was concentrated *in vacuo* and the residue was

suspensended in hexane/EtOAc (2:1, 150 mL). The precipitate was filtered and washed with THF (30 mL) to remove excess diphenylamine, affording the title compound as a yellow-orange crystalline solid (1.42 g, 1.78 mmol, 45% yield) with characterization data in accordance with the literature.[25]

^{1}H NMR (400 MHz, $CDCl_3$) δ 7.32 – 7.22 (m, 4H), 7.12 – 7.05 (m, 12H), 7.07 – 6.98 (m, 2H), 6.96 – 6.84 (m, 8H), 6.73 – 6.63 (m, 10H), 6.56 (d, J = 7.4 Hz, 4H).

^{13}C{^{1}H} NMR (101 MHz, $CDCl_3$) δ 154.2, 151.7, 145.5, 144.6, 143.1, 140.3, 129.4, 128.6, 127.5, 124.2, 123.9, 122.9, 122.6, 122.6, 121.1, 113.1, 113.0.

Experimental Procedures

Experimental set-up

- ***Set-up 1:*** *3D printed reactor with blue LED strip*

For reactions performed using a blue LED strip as the light source, a 3D-printed photoreactor was used, consisting of a 9 cm diameter crystallizing dish with a 3D printed support of 6 positions, and a hole of 22 mm in the middle to allow ventilation (Figure S2, left). A commercial 1-meter LED strip was wrapped around the crystallizing dish, while a fan was used to cool down the reactor (the reaction temperature was measured to be 35–40 ºC). Each of the positions could be used to fit a standard 16 mm diameter vial with a Teflon screw cap. Experiments at 465 nm were conducted using a 1 m strip, 14.4 W "LEDXON MODULAR 9009083 LED, SINGLE 5050" purchased from Farnell, catalog number 9009083. The emission spectrum of these LEDs is shown in Figure S2, right panel.

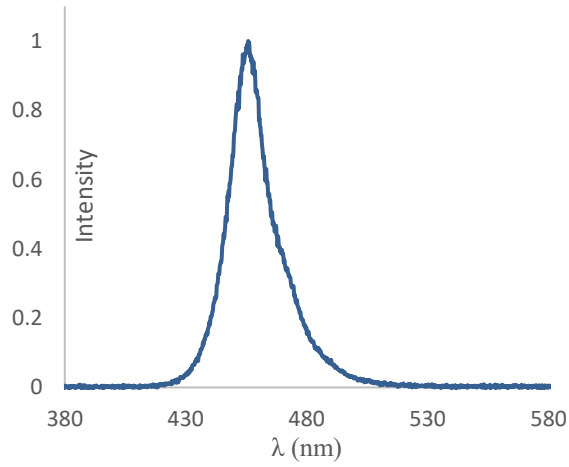

Figure 2.23. Blue LED photoreactor used for reactions where temperature control was not needed (*left*). Emission spectrum of the 465 nm LED strip used in this reactor (*right*).

- ***Set-up 2:*** *HP single LED*

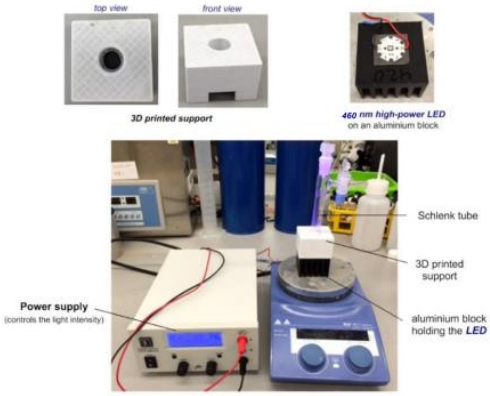

Figure 2.24. Detailed set-up and illumination system. The light source for illuminating the reaction vessel consisted in a 460 nm high-power single LED (LZ1-00DB00) purchased from OSA OPTO.

General procedure (A): Ipso substitution

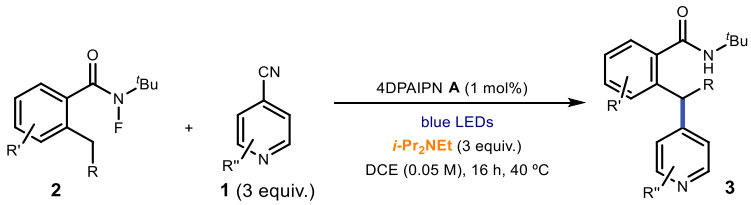

*Reactions performed using **set-up 1** in Figure S2*. In an oven dried vial with a Teflon septum screw cap, 2-alkyl *N*-fluorobenzamide **2** (0.1 mmol, 1 equiv.) was added and dissolved in 1,2-DCE (2 mL, synthesis grade solvent). Cyano-pyridine **1** (0.3 mmol, 3 equiv.), 4DPAIPN (photocatalyst **A**, 0.8 mg, 0.01 mmol, 0.01 equiv.), and DIPEA (52 µL, 0.3 mmol, 3 equiv.) were then added. The resulting yellow mixture was degassed with argon sparging for 60 seconds. The vial was irradiated under stirring for 16 hours, unless otherwise specified. Volatiles were evaporated and the residue purified by column chromatography on silica gel to afford the corresponding product in the stated yield with >95% purity according to ^{1}H-NMR analysis. The exact conditions for chromatography are reported for each compound.

Characterization of ipso substitution products

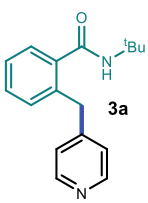

***N*-(*tert*-butyl)-2-(pyridin-4-ylmethyl)benzamide (3a):** Synthesized according to General Procedure A using *N*-(*tert*-butyl)-*N*-fluoro-2-methylbenzamide **2a** (21.0 mg, 0.1 mmol, 1 equiv.) and isonicotinonitrile **1a** (31.2 mg, 0.3 mmol, 3 equiv.). The crude mixture was purified by flash column chromatography on silica gel (hexanes/EtOAc 1:1) to afford **3a** (16 mg, 60%% yield) as an off-white solid.

^{1}H NMR (500 MHz, $CDCl_3$) δ 8.50 – 8.39 (m, 2H), 7.35 (td, J = 7.5, 1.1 Hz, 2H), 7.29 – 7.26 (m, 1H), 7.22 – 7.18 (m, 1H), 7.11 – 7.07 (m, 2H), 5.47 (s, 1H), 4.20 (s, 2H), 1.32 (s, 9H).

$^{13}C\{^{1}H\}$ NMR (126 MHz, $CDCl_3$) δ 169.2, 150.2, 149.8, 137.9, 137.0, 131.4, 130.1, 127.3, 127.0, 124.4, 52.0, 38.3, 28.7.

HRMS: (ESI^+) calculated for $C_{17}H_{21}N_2O$ ($M+H^+$): 269.1648, found 269.1642.

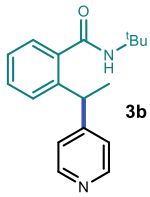

***N*-(*tert*-butyl)-2-(1-(pyridin-4-yl)ethyl)benzamide (3b):** Synthesized according to General Procedure A using *N*-(*tert*-butyl)-2-ethyl-*N*-fluorobenzamide **2b** (22.5 mg, 0.1 mmol, 1 equiv.) and isonicotinonitrile **1a** (31.0 mg, 0.3 mmol, 3 equiv.). The crude mixture was purified by flash column chromatography on silica gel (hexanes/EtOAc from 7:3 to 1:1) to afford **3b** (21 mg, 74% yield) as an off-white solid.

^{1}H NMR (500 MHz, $CDCl_3$) δ 8.49 – 8.44 (m, 2H), 7.37 (td, J = 7.6, 1.5 Hz, 1H), 7.31 (dt, J = 7.6, 1.0 Hz, 1H), 7.29 – 7.20 (m, 2H), 7.14 – 7.12 (m, 2H), 5.41 (brs, 1H), 4.78 (q, J = 7.2 Hz, 1H), 1.63 (d, J = 7.2 Hz, 3H), 1.4 (s, 9H).

$^{13}C\{^{1}H\}$ NMR (126 MHz, $CDCl_3$) δ 169.6, 155.3, 150.0, 142.2, 137.9, 130.0, 128.0, 127.0, 126.7, 123.3, 52.0, 39.6, 28.8, 21.5.

HRMS: (ESI^+) calculated for $C_{18}H_{23}N_2O$ ($M+H^+$): 283.1805, found 283.1794.

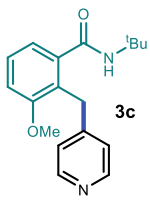

***N*-(*tert*-butyl)-*N*-fluoro-3-methoxy-2-(pyridin-4-ylmethyl)benzamide (3c):** Synthesized according to General Procedure A using *N*-(*tert*-butyl)-*N*-fluoro-3-methoxy-2-methylbenzamide **2c** (22.0 mg, 0.1 mmol, 1 equiv.) and isonicotinonitrile **1a** (31.0 mg, 0.3 mmol, 3 equiv.). The crude mixture was purified by flash column chromatography on silica gel (hexanes/EtOAc from 8:2 to 1:1) to afford **3c** (15 mg, 47% yield) as an off-white solid.

^{1}H NMR (300 MHz, $CDCl_3$) δ 8.42 (d, J = 4.9 Hz, 2H), 7.31 – 7.22 (m, 1H), 7.12 (d, J = 5.3 Hz, 2H), , 6.98 (dd, J = 7.6, 1.2 Hz, 1H), 6.93 (dd, J = 8.3, 1.1 Hz, 1H), 5.41 (s, 1H), 4.17 (s, 2H), 3.78 (s, 3H), 1.32 (s, 9H).

$^{13}C\{^{1}H\}$ NMR (75 MHz, $CDCl_3$) δ 169.2, 158.1, 150.6, 149.5, 139.7, 128.29, 125.1, 124.2, 119.2, 112.0, 55.8, 52.0, 31.7, 29.0.

HRMS: (ESI^+) calculated for $C_{18}H_{23}N_2O_2$ ($M+H^+$): 299.1754, found 299.1746.

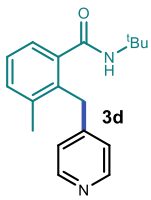

***N*-(*tert*-butyl)-3-methyl-2-(pyridin-4-ylmethyl)benzamide (3d):** Synthesized according to General Procedure A using *N*-(*tert*-butyl)-*N*-fluoro-2,3-dimethylbenzamide **2d** (20.0 mg, 0.1 mmol, 1 equiv.) and isonicotinonitrile **1a** (31.0 mg, 0.3 mmol, 3 equiv.). The crude mixture was purified by flash column chromatography on silica gel (hexanes/EtOAc from 8:2 to 1:1) to afford **3d** (16.5 mg, 59% yield) as an off-white solid.

^{1}H NMR (400 MHz, $CDCl_3$) δ 8.47 (s, 2H), 7.29 – 7.21 (m, 3H), 7.06 (d, J = 5.3 Hz, 2H), 5.47 (s, 1H), 4.21 (s, 2H), 2.20 (s, 3H), 1.32 (s, 9H).

$^{13}C\{^{1}H\}$ NMR (75 MHz, $CDCl_3$) δ 169.2, 158.1, 150.6, 149.5, 139.7, 128.29, 125.1, 124.2, 119.2, 112.0, 55.8, 52.0, 31.7, 29.0.

HRMS: (ESI^+) calculated for $C_{18}H_{23}N_2O$ ($M+H^+$): 283.1805, found 283.1805.

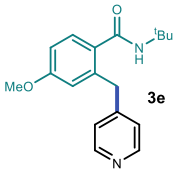

***N*-(*tert*-butyl)-4-methoxy-2-(pyridin-4-ylmethyl)benzamide (3e):** Synthesized according to General Procedure A using *N*-(*tert*-butyl)-*N*-fluoro-4-methoxy-2-methylbenzamide **2e** (22.0 mg, 0.1 mmol, 1 equiv.) and isonicotinonitrile **1a** (31.0 mg, 0.3 mmol, 3 equiv.). The crude mixture was purified by flash column chromatography on silica gel (hexanes/EtOAc from 8:2 to 1:1) to afford **3e** (17 mg, 57% yield) as an off-yellow solid.

^{1}H NMR (400 MHz, $CDCl_3$) δ 8.52 – 8.48 (m, 2H), 7.45 (d, *J* = 5.5 Hz, 2H), 7.37 (d, *J* = 8.5 Hz, 1H), 6.81 (dd, *J* = 8.5, 2.6 Hz, 1H), 6.74 (d, *J* = 2.6 Hz, 1H), 5.52 (s, 1H), 4.33 (s, 2H), 3.82 (s, 3H), 1.33 (s, 9H).

$^{13}C\{^{1}H\}$ NMR (101 MHz, $CDCl_3$) δ 168.2, 162.5, 161.4, 140.0, 137.2, 129.4, 129.3, 127.3, 118.1, 112.6, 77.5, 77.2, 76.8, 55.7, 52.0, 40.1, 28.9.

HRMS: (ESI^+) calculated for $C_{18}H_{23}N_2O_2$ ($M+H^+$): 299.1754, found 299.1750.

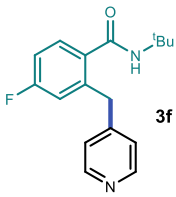

***N*-(*tert*-butyl)-4-fluoro-2-(pyridin-4-ylmethyl)benzamide (3f):** Synthesized according to General Procedure A using *N*-(*tert*-butyl)-*N*,4-difluoro-2-methylbenzamide **2f** (22.0 mg, 0.1 mmol, 1 equiv.) and isonicotinonitrile **1a** (31.0 mg, 0.3 mmol, 3 equiv.). The crude mixture was purified by flash column chromatography on silica gel (hexanes/EtOAc 7:3) to afford **3f** (17 mg, 59% yield) as an off-white solid.

^{1}H NMR (400 MHz, $CDCl_3$) δ 8.54 – 8.43 (m, 2H), 7.36 (dd, *J* = 8.4, 5.7 Hz, 1H), 7.10 (ddd, *J* = 4.5, 1.6, 0.8 Hz, 2H), 6.95 (td, *J* = 8.3, 2.6 Hz, 1H), 6.90 (dd, *J* = 9.5, 2.6 Hz, 1H), 5.44 (s, 1H), 4.19 (s, 2H), 1.33 (s, 9H).

$^{13}C\{^{1}H\}$ NMR (101 MHz, $CDCl_3$) δ 168.2, 163.2 (d, *J* = 250.3 Hz, C), 149.8, 149.2, 140.0 (d, *J* = 7.6 Hz), 133.93 (d, *J* = 3.3 Hz, C), 129.1 (d, *J* = 8.7 Hz, C), 124.2, 118.1 (d, *J* = 21.8 Hz, CH), 113.7 (d, *J* = 21.4 Hz, CH), 51.9, 38.1, 28.6.

^{19}F NMR (376 MHz, $CDCl_3$) δ -110.3.

HRMS: (ESI^+) calculated for $C_{17}H_{20}FN_2O$ ($M+H^+$): 287.1554, found 287.1548.

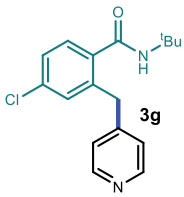

***N*-(*tert*-butyl)-4-chloro-2-(pyridin-4-ylmethyl)benzamide (3g):** Synthesized according to General Procedure A *N*-(*tert*-butyl)-4-chloro-*N*-fluoro-2-methylbenzamide **2g** (24.0 mg, 0.1 mmol, 1 equiv.) and isonicotinonitrile **1a** (31.0 mg, 0.3 mmol, 3 equiv.). The crude mixture was purified by flash column chromatography on silica gel (hexanes/EtOAc 8:2 to 1:1) to afford **3g** (14.5 mg, 48% yield) as an off-white solid.

^{1}H NMR (400 MHz, $CDCl_3$) δ 8.54 – 8.42 (m, 2H), 7.31 (d, *J* = 8.1 Hz, 1H), 7.26 – 7.23 (m, 1H), 7.19 (d, *J* = 2.1 Hz, 1H), 7.13 (d, *J* = 5.4 Hz, 2H), 5.48 (br s, 1H), 4.18 (s, 2H), 1.31 (s, 9H).

^{13}C{^{1}H} NMR (101 MHz, $CDCl_3$) δ 168.2, 149.9, 149.4, 139.1, 136.2, 136.0, 131.3, 128.7, 127.3, 124.6, 52.1, 38.2, 28.8.

HRMS: (ESI$^+$) calculated for $C_{17}H_{20}ClN_2O$ (M+H$^+$): 303.1259, found 303.1254.

***N*-(*tert*-butyl)-*N*-fluoro-5-methoxy-2-(pyridin-4-ylmethyl)benzamide (3h):** Synthesized according to General Procedure A using *N*-(*tert*-butyl)-*N*-fluoro-5-methoxy-2-methylbenzamide **2h** (24.0 mg, 0.1 mmol, 1 equiv.) and isonicotinonitrile **1a** (31.0 mg, 0.3 mmol, 3 equiv.). The crude mixture was purified by flash column chromatography on silica gel (hexanes/EtOAc from 8:2 to 1:1) to afford **3h** (17 mg, 54% yield) as an white solid.

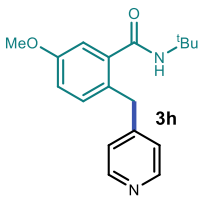

^{1}H NMR (500 MHz, $CDCl_3$) δ 8.50 – 8.36 (m, 2H), 7.11 (d, J = 7.8 Hz, 1H), 7.08 (d, J = 6.0, 2H), 6.91 – 6.87 (m, 2H), 5.42 (s, 1H), 4.11 (s, 2H), 3.82 (s, 3H), 1.30 (s, 9H).

^{13}C{^{1}H} NMR (126 MHz, $CDCl_3$) δ 168.9, 158.4, 150.7, 150.0, 139.0, 132.5, 128.57, 124.3, 115.1, 113.3, 55.6, 52.0, 37.6, 28.7.

HRMS: (ESI$^+$) calculated for $C_{18}H_{23}N_2O_2$ (M+H$^+$): 299.1754, found 299.1747.

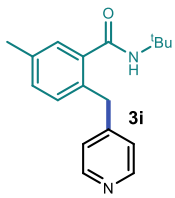

***N*-(*tert*-butyl)-5-methyl-2-(pyridin-4-ylmethyl)benzamide (3h):** Synthesized according to General Procedure A using *N*-(*tert*-butyl)-*N*-fluoro-2,5-dimethylbenzamide **2i** (22.5 mg, 0.1 mmol, 1 equiv.) and isonicotinonitrile **1a** (31.0 mg, 0.3 mmol, 3 equiv.). The crude mixture was purified by flash column chromatography on silica gel (hexanes/EtOAc 7:3) to afford **3i** (16 mg, 53% yield) as an off-white solid.

^{1}H NMR (400 MHz, $CDCl_3$) δ 8.45 (s, 2H), 7.19 – 7.14 (m, 2H), 7.09 (q, *J* = 4.9, 3.8 Hz, 3H), 5.42 (s, 1H), 4.15 (s, 2H), 2.34 (s, 3H), 1.32 (s, 9H).

^{13}C{^{1}H} NMR (101 MHz, $CDCl_3$) δ 169.4, 150.5, 149.8, 137.8, 136.8, 133.8, 131.3, 130.7, 128.0, 124.4, 51.9, 38.0, 29.0, 21.0.

HRMS: (ESI$^+$) calculated for $C_{18}H_{23}N_2O$ (M+H$^+$): 283.1805, found 283.1796.

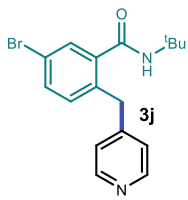

5-Bromo-*N*-(*tert*-butyl)-2-(pyridin-4-ylmethyl)benzamide (3i): Synthesized according to General Procedure A using 5-bromo-*N*-(*tert*-butyl)-*N*-fluoro-2-methylbenzamide **2j** (29.0 mg, 0.1 mmol, 1 equiv.) and isonicotinonitrile **1a** (31.0 mg, 0.3 mmol, 3 equiv.). The crude mixture was purified by flash column chromatography on silica gel (hexanes/EtOAc 7:3) to afford **3j** (20 mg, 58% yield) as an off-white solid.

^{1}H NMR (400 MHz, $CDCl_3$) δ 8.51 (d, *J* = 5.1 Hz, 2H), 7.54 – 7.49 (m, 2H), 7.29 (d, *J* = 5.1 Hz, 2H), 7.12 – 7.08 (m, 1H), 5.54 (s, 1H), 4.21 (s, 2H), 1.33 (s, 9H).

^{13}C{^{1}H} NMR (101 MHz, $CDCl_3$) δ 167.5, 150.2, 149.4, 139.6, 135.9, 133.1, 133.0, 130.3, 124.5, 120.8, 52.2, 37.9, 28.7.

HRMS: (ESI$^+$) calculated for $C_{17}H_{20}BrN_2O$ (M+H$^+$): 347.0754, found 347.0748.

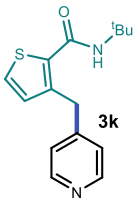

***N*-(*tert*-butyl)-3-(pyridin-4-ylmethyl)thiophene-2-carboxamide (3k):** Synthesized according to General Procedure A using *N*-(*tert*-butyl)-*N*-fluoro-3-methylthiophene-2-carboxamide **2k** (21.5 mg, 0.1 mmol, 1 equiv.) and isonicotinonitrile **1a** (31.0 mg, 0.3 mmol, 3 equiv.). The crude mixture was purified by flash column chromatography on silica gel (hexanes/EtOAc 7:3) to afford **3k** (12.6 mg, 46% yield) as a yellow oil.

^{1}H NMR (400 MHz, $CDCl_3$) δ 8.57 (d, *J* = 5.9 Hz, 2H), 7.74 (d, *J* = 5.9 Hz, 2H), 7.34 (d, *J* = 5.1 Hz, 1H), 6.92 (d, *J* = 5.1 Hz, 1H), 5.67 (s, 1H), 4.58 (s, 2H), 1.41 (s, 9H).

^{13}C{^{1}H} NMR (101 MHz, $CDCl_3$) δ 161.7, 142.6, 140.3, 133.0, 131.0, 127.9, 126.7, 52.5, 35.2, 29.0.

HRMS: (ESI$^+$) calculated for $C_{15}H_{19}N_2OS$ (M+H$^+$): 275.1213, found 275.1212.

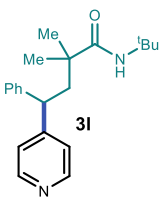

***N*-(*tert*-butyl)-2,2-dimethyl-4-phenyl-4-(pyridin-4-yl)butanamide (3l):** Synthesized according to General Procedure A using *N*-(*tert*-butyl)-2,2-dimethyl-4-phenylbutanamide **2l** (25.0 mg, 0.1 mmol, 1 equiv.) and isonicotinonitrile **1a** (31.0 mg, 0.3 mmol, 3 equiv.). The crude mixture was purified by flash column chromatography on silica gel (hexanes/EtOAc 1:1) to afford **3l** (26 mg, 80% yield) as an white solid.

^{1}H NMR (400 MHz, $CDCl_3$) δ 8.48 (d, J = 5.7 Hz, 2H), 7.34 – 7.25 (m, 3H), 7.24 – 7.18 (m, 3H), 5.33 (s, 1H), 4.00 (t, J = 6.6 Hz, 1H), 2.44 (dd, J = 14.2, 6.2 Hz, 1H), 2.34 (dd, J = 14.2, 7.1 Hz, 1H), 1.31 (s, 9H), 1.08 (s, 3H), 1.02 (s, 3H).

^{13}C{^{1}H} NMR (126 MHz, $CDCl_3$) δ 176.1, 154.8, 150.0, 144.0, 128.9, 128.1, 126.9, 123.3, 51.1, 48.32, 46.1, 43.2, 28.8, 27.2, 26.3.

HRMS: (ESI$^+$) calculated for $C_{21}H_{29}N_2O$ (M+H$^+$): 325.2274, found 325.2276.

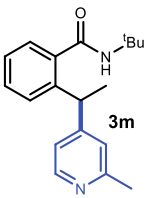

***N*-(*tert*-butyl)-2-(1-(2-methylpyridin-4-yl)ethyl)benzamide (3m):** Synthesized according to General Procedure A using *N*-(*tert*-butyl)-2-ethyl-*N*-fluorobenzamide **2b** (22.5 mg, 0.1 mmol, 1 equiv.) and 2-methylisonicotinonitrile **1b** (50.5 mg, 0.3 mmol, 3 equiv.). The crude mixture was purified by flash column chromatography on silica gel (hexanes/EtOAc from 7:3 to 1:1) to afford **3m** (23 mg, 78% yield) as a white solid.

^{1}H NMR (300 MHz, $CDCl_3$) δ 8.34 (d, J = 5.5 Hz, 1H), 7.42 – 7.33 (m, 1H), 7.33 – 7.26 (m, 2H), 7.26 – 7.18 (m, 1H), 7.01 (d, J = 1.7 Hz, 1H), 6.91 (dd, J = 5.2, 1.7 Hz, 1H), 5.39 (s, 1H), 4.73 (q, J = 7.2 Hz, 1H), 2.49 (s, 3H), 1.60 (d, J = 7.2 Hz, 3H), 1.35 (s, 9H).

$^{13}C\{^{1}H\}$ NMR (75 MHz, $CDCl_3$) δ 169.6 158.4, 155.5, 149.2, 142.3, 137.9, 130.0, 127.9, 127.0, 126.6, 122.9, 120.3, 51.9, 39.6, 28.8, 24.6, 21.5.

HRMS: (ESI^+) calculated for $C_{19}H_{25}N_2O$ ($M+H^+$): 297.1961, found 297.1961.

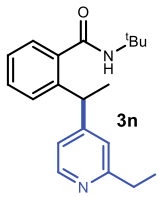

***N*-(*tert*-butyl)-2-(1-(2-ethylpyridin-4-yl)ethyl)benzamide (3n):** Synthesized according to General Procedure A using *N*-(*tert*-butyl)-2-ethyl-*N*-fluorobenzamide **2b** (22.5 mg, 0.1 mmol, 1 equiv.) and 2-ethylisonicotinonitrile **1c** (39.5 mg, 0.3 mmol, 3 equiv.). The crude mixture was purified by flash column chromatography on silica gel (hexanes/EtOAc from 6:1 to 3:2) to afford **3n** (23 mg, 76% yield) as a yellow solid.

^{1}H NMR (400 MHz, $CDCl_3$) δ 8.38 (d, *J* = 5.2 Hz, 1H), 7.37 (td, *J* = 7.5, 1.6 Hz, 1H), 7.32 – 7.27 (m, 2H), 7.26 – 7.21 (m, 1H), 7.04 (s, 1H), 6.94 (dd, *J* = 5.4, 1.7 Hz, 1H), 5.40 (s, 1H), 4.76 (q, *J* = 7.2 Hz, 1H), 2.78 (q, *J* = 7.6 Hz, 2H), 1.61 (d, *J* = 7.2 Hz, 3H), 1.34 (s, 9H), 1.27 (t, *J* = 7.6 Hz, 3H).

$^{13}C\{^{1}H\}$ NMR (101 MHz, $CDCl_3$) δ 169.6, 163.3, 156.3, 148.7, 142.1, 137.9, 130.0, 128.0, 127.0, 126.7, 121.9, 120.7, 51.9, 39.8, 31.2, 28.8, 21.6, 14.0.

HRMS: (ESI^+) calculated for $C_{20}H_{27}N_2O$ ($M+H^+$): 311.2118, found 311,2114.

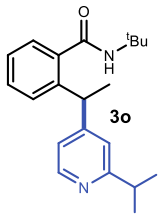

***N*-(*tert*-butyl)-*N*-fluoro-2-(1-(2-isopropylpyridin-4-yl)ethyl)benzamide (3o):** Synthesized according to General Procedure A using *N*-(*tert*-butyl)-2-ethyl-*N*-fluorobenzamide **2b** (22.5 mg, 0.1 mmol, 1 equiv.) and 2-isopropylisonicotinonitrile **1d** (44.0 mg, 0.3 mmol, 3 equiv.). The crude mixture was purified by flash column chromatography on silica gel (hexanes/EtOAc 8:2) to afford **3o** (22 mg, 64% yield) as a whit gum.

^{1}H NMR (500 MHz, $CDCl_3$) δ 8.41 (d, J = 5.2 Hz, 1H), 7.39 (td, J = 7.5, 1.5 Hz, 1H), 7.34 (dd, J = 7.6, 1.6 Hz, 1H), 7.31 – 7.29 (m, 1H), 7.26 (td, J = 7.4, 1.3 Hz, 1H), 7.08 – 7.00 (m, 1H), 6.92 (dd, J = 5.1, 1.8 Hz, 1H), 5.39 (s, 1H), 4.77 (q, J = 7.2 Hz, 1H), 3.02 (hept, J = 6.9 Hz, 1H), 1.64 (d, J = 7.2 Hz, 3H), 1.35 (s, 9H), 1.29 (d, 6H).

$^{13}C\{^{1}H\}$ NMR (126 MHz, $CDCl_3$) δ 169.7, 167.4, 155.8, 149.1, 142.1, 138.0, 130.0, 128.0, 127.0, 126.63 120.6, 120.3, 51.9, 39.8, 36.4, 28.8, 22.8, 22.7, 21.7.

HRMS: (ESI^+) calculated for $C_{21}H_{29}N_2O$ ($M+H^+$): 325.2274, found 325.2277.

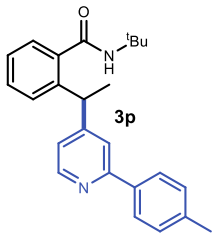

***N*-(*tert*-butyl)-2-(1-(2-(p-tolyl)pyridin-4-yl)ethyl)benzamide (3p):** Synthesized according to General Procedure A using *N*-(*tert*-butyl)-2-ethyl-*N*-fluorobenzamide **2b** (22.5 mg, 0.1 mmol, 1 equiv.) and 2-(p-tolyl)isonicotinonitrile **1e** (58.0 mg, 0.3 mmol, 3 equiv.). The crude mixture was purified by flash column chromatography on silica gel (hexanes/EtOAc 8:2) to afford **3p** (17 mg, 46% yield) as a white solid.

^{1}H NMR (300 MHz, $CDCl_3$) δ 8.53 (d, J = 5.1, 1H), 7.89 – 7.77 (m, 2H), 7.58 – 7.53 (m, 1H), 7.43 – 7.28 (m, 3H), 7.26 – 7.20 (m, 3H), 7.03 (dd, J = 5.1, 1.7 Hz, 1H), 5.40 (s, 1H), 4.85 (q, J = 7.2 Hz, 1H), 2.39 (s, 3H), 1.67 (d, J = 7.2 Hz, 3H), 1.32 (s, 9H).

^{13}C{^{1}H} NMR (75 MHz, $CDCl_3$) δ 169.7, 157.7, 156.0, 149.7, 142.1, 139.0, 138.0, 136.9, 130.0, 129.5, 128.0, 127.0, 127.0, 126.7, 121.5, 120.0, 52.0, 39.9, 28.8, 21.6, 21.4.

HRMS: (ESI$^+$) calculated for $C_{25}H_{29}N_2O$ (M+H$^+$): 373.2274, found 373.2273.

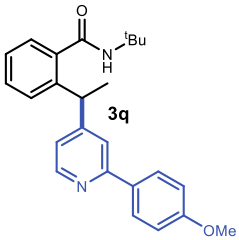

***N*-(*tert*-butyl)-2-(1-(2-(4-methoxyphenyl)pyridin-4-yl)ethyl)benzamide (3q):** Synthesized according to General Procedure A using *N*-(*tert*-butyl)-2-ethyl-*N*-fluorobenzamide **2b** (22.5 mg, 0.1 mmol, 1 equiv.) and 2-(4-methoxyphenyl)isonicotinonitrile **1f** (59.5 mg, 0.3 mmol, 3 equiv.). The crude mixture was purified by flash column chromatography on silica gel (hexanes/EtOAc from 86:14 to 1:1) to afford **3q** (18 mg, 46% yield) as a white solid.

^{1}H NMR (400 MHz, $CDCl_3$) δ 8.51 (d, *J* = 5.2 Hz, 1H), 7.92 – 7.86 (m, 2H), 7.53 (s, 1H), 7.37 (td, *J* = 7.1, 1.4 Hz, 1H), 7.34 – 7.29 (m, 2H), 7.23 (td, *J* = 7.5, 1.4 Hz, 1H), 7.01 (dd, *J* = 5.1, 1.6 Hz, 1H), 6.99 – 6.94 (m, 2H), 5.41 (br s, 1H), 4.85 (q, *J* = 7.2 Hz, 1H), 3.85 (s, 3H), 1.67 (d, *J* = 7.2 Hz, 3H), 1.33 (s, 10H).

^{13}C{^{1}H} NMR (101 MHz, $CDCl_3$) δ 169.7, 160.6, 157.2, 156.3, 149.4, 142.1, 138.0, 130.1, 128.4, 128.0, 127.1, 126.7, 121.1, 119.7, 114.2, 55.5, 52.0, 39.9, 28.8, 21.6.

HRMS: (ESI$^+$) calculated for $C_{25}H_{29}N_2O_2$ (M+H$^+$): 389.2224, found 389.2212.

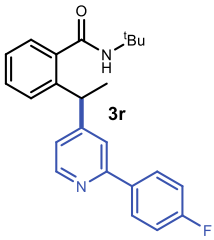

***N*-(*tert*-butyl)-2-(1-(2-(4-fluorophenyl)pyridin-4-yl)ethyl)benzamide (3r):** Synthesized according to General Procedure A using *N*-(*tert*-butyl)-2-ethyl-*N*-fluorobenzamide **2b** (22.5 mg, 0.1 mmol, 1 equiv.) and 2-(4-fluorophenyl)isonicotinonitrile **1g** (59.5 mg, 0.3 mmol, 1.5 equiv.). The crude mixture was purified by flash column chromatography on silica gel (hexanes/EtOAc from 86:14 to 1:1) to afford **3r** (24 mg, 64% yield) as a white solid.

^{1}H NMR (500 MHz, $CDCl_3$) δ 8.53 (d, J = 5.2 Hz, 1H), 7.96 – 7.86 (m, 2H), 7.55 – 7.53 (m, 1H), 7.41 – 7.35 (m, 1H), 7.35 – 7.29 (m, 2H), 7.24 (m, 1H), 7.18 – 7.10 (m, 2H), 7.09 – 7.02 (m, 1H), 5.42 (s, 1H), 4.87 (q, J = 7.2 Hz, 1H), 1.67 (d, J = 7.2 Hz, 3H), 1.34 (s, 9H).

^{13}C{^{1}H} NMR (101 MHz, $CDCl_3$) δ 169.5, 163.5 (d, *J* = 248.3 Hz, C), 156.5, 156.1, 149.6, 142.1, 137.8, 135.7 (d, *J* = 3.1 Hz, C), 130.0, 128.8 (d, *J* = 8.4 Hz, CH), 127.8, 126.9, 126.6, 121.5, 119.9, 115.6 (d, *J* = 21.6 Hz, CH), 51.8, 39.7, 28.7, 21.4.

^{19}F NMR (376 MHz, $CDCl_3$) δ -113.4.

HRMS: (ESI$^+$) calculated for $C_{24}H_{26}FN_2O$ (M+H$^+$): 377.2024, found 377.2022.

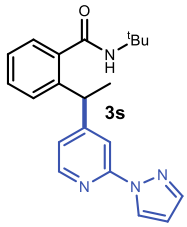

2-(1-(2-(1*H*-pyrazol-1-yl)pyridin-4-yl)ethyl)-*N*-(*tert*-butyl)benzamide (3s): Synthesized according to General Procedure A using *N*-(*tert*-butyl)-2-ethyl-*N*-fluorobenzamide **2b** (22.5 mg, 0.1 mmol, 1 equiv.) and 2-(1*H*-pyrazol-1-yl)isonicotinonitrile **1k** (51.0 mg, 0.3 mmol, 3 equiv.). The crude mixture was purified by flash column chromatography on silica gel (hexanes/EtOAc from 86:14 to 1:1) to afford **3s** (18 mg, 53% yield) as a off-white solid.

^{1}H NMR (400 MHz, $CDCl_3$) δ 8.53 (d, *J* = 2.6 Hz, 1H), 8.26 (d, *J* = 5.2 Hz, 1H), 7.86 (s, 1H), 7.70 (s, 1H), 7.36 (td, *J* = 7.5, 1.6 Hz, 1H), 7.30 (td, *J* = 8.0, 1.4 Hz, 2H), 7.23 (td, *J* = 7.3, 1.4 Hz, 1H), 7.09 (dd, *J* = 5.3, 1.6 Hz, 1H), 6.44 (t, *J* = 2.2 Hz, 1H), 5.54 (s, 1H), 4.84 (q, *J* = 7.2 Hz, 1H), 1.69 (d, *J* = 7.2 Hz, 3H), 1.38 (s, 9H).

^{13}C{^{1}H} NMR (101 MHz, $CDCl_3$) δ 169.7, 158.4, 142.1, 137.8, 130.2, 128.1, 127.0, 126.7, 52.0, 40.0, 28.8, 21.3.

HRMS: (ESI$^+$) calculated for $C_{21}H_{25}N_4O$ (M+H+): 349.2023, found 349.2017.

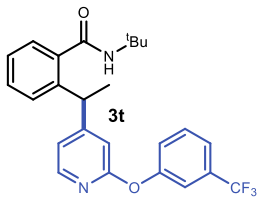

***N*-(*tert*-butyl)-2-(1-(2-(3-(trifluoromethyl)phenoxy)pyridin-4-yl)ethyl)benzamide (3t):** Synthesized according to General Procedure A using *N*-(*tert*-butyl)-2-ethyl-N-fluorobenzamide **2b** (22.5 mg, 0.1 mmol, 1 equiv.) and 2-(3-(trifluoromethyl)phenoxy)isonicotinonitrile **1l** (79.0 mg, 0.3 mmol, 3.0 equiv.). The crude mixture was purified by flash column chromatography on silica gel (hexanes/EtOAc from 86:14 to 1:1) to afford **3t** (18.5 mg, 42% yield) as a off-white solid.

^{1}H NMR (400 MHz, $CDCl_3$) δ 8.04 (d, *J* = 5.3 Hz, 1H), 7.49 (t, *J* = 7.9 Hz, 1H), 7.45 – 7.35 (m, 3H), 7.31 (ddd, *J* = 11.0, 7.8, 1.4 Hz, 3H), 7.25 (td, *J* = 7.4, 1.3 Hz, 2H), 6.92 (dd, *J* = 5.4, 1.5 Hz, 1H), 6.85 (s, 1H), 5.48 (s, 1H), 4.81 (q, *J* = 7.2 Hz, 1H), 1.65 (d, *J* = 7.2 Hz, 3H), 1.39 (s, 9H).

^{13}C{^{1}H} NMR (101 MHz, $CDCl_3$) δ 169.6, 163.3, 160.0, 154.4, 147.2, 141.9, 137.8, 132.3, 132.0, 130.2, 128.0, 127.0, 126.8, 124.6, 121.3 (q, $^{3}J_{F\text{-}C}$ = 3.8 Hz), 119.4, 118.2 (q, $^{3}J_{F\text{-}C}$ = 3.8 Hz), 111.0, 52.0, 39.7, 28.9, 21.4.

^{19}F NMR (376 MHz, $CDCl_3$) δ -62.76.

HRMS: (ESI$^+$) calculated for $C_{25}H_{26}N_2O_2$ (M+H$^+$):443.1941, found 443.1953.

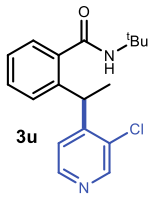

***N*-(*tert*-butyl)-2-(1-(3-chloropyridin-4-yl)ethyl)benzamide (3u:** Synthesized according to General Procedure A using *N*-(*tert*-butyl)-2-ethyl-*N*-fluorobenzamide **2b** (22.5 mg, 0.1 mmol, 1 equiv.) and 3-chloroisonicotinonitrile **1h** (41.5 mg, 0.3 mmol, 3 equiv.). The crude mixture was purified by flash column chromatography on silica gel (hexanes/EtOAc 84:16) to afford **3u** (18 mg, 57% yield) as a white solid.

^{1}H NMR (300 MHz, $CDCl_3$) δ 8.49 (s, 1H), 8.41 (d, J = 5.0 Hz, 1H), 7.40 – 7.30 (m, 2H), 7.25 – 7.23 (m, 1H), 7.17 – 7.08 (m, 2H), 5.44 (s, 1H), 5.03 (q, J = 7.0 Hz, 1H), 1.64 (d, J = 7.1 Hz, 3H), 1.36 (s, 9H).

^{13}C{^{1}H} NMR (75 MHz, $CDCl_3$) δ 169.4, 152.5, 149.7, 148.0, 140.9, 138.1, 132.4, 130.0, 128.0, 127.1, 127.0, 123.2, 52.0, 38.0, 29.0, 20.6.

HRMS: (ESI$^+$) calculated for $C_{18}H_{22}ClN_2O$ (M+H$^+$): 317.1415, found 317.1415.

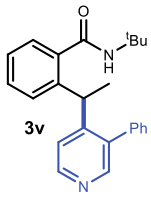

***N*-(*tert*-butyl)-2-(1-(3-phenylpyridin-4-yl)ethyl)benzamide (3v):** Synthesized according to General Procedure A using *N*-(*tert*-butyl)-2-ethyl-*N*-fluorobenzamide **2b** (22.5 mg, 0.1 mmol, 1 equiv.) and 3-phenylisonicotinonitrile **1i** (54.0 mg, 0.3 mmol, 3 equiv.). The crude mixture was purified by flash column chromatography on silica gel (hexanes/EtOAc 84:16) to afford **3v** (16.5 mg, 46% yield) as a off-white solid.

^{1}H NMR (400 MHz, $CDCl_3$) δ 8.52 (d, *J* = 5.1 Hz, 1H), 8.31 (s, 1H), 7.35 – 7.27 (m, 4H), 7.22 – 7.20 (m, 2H), 7.17 (d, *J* = 5.2 Hz, 1H), 7.15 – 7.12 (m, 2H), 7.06 (d, *J* = 7.8 Hz, 1H), 4.99 (s, 1H), 4.74 (q, *J* = 7.1 Hz, 1H), 1.50 (d, *J* = 7.1 Hz, 3H), 1.25 (s, 9H).

^{13}C{^{1}H} NMR (101 MHz, $CDCl_3$) δ 169.4, 153.0, 150.5, 148.7, 142.8, 138.2, 137.8, 129.9, 129.5, 128.5, 128.4, 127.6, 127.2, 126.5, 122.2, 51.6, 38.1, 28.7, 21.1.

HRMS: (ESI$^+$) calculated for $C_{24}H_{27}N_2O$ (M+H$^+$): 359.2118, found 359.2124.

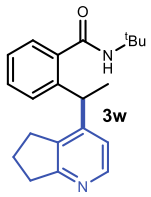

***N*-(*tert*-butyl)-2-(1-(6,7-dihydro-5*H*-cyclopenta[*b*]pyridin-4-yl)ethyl)-*N*-fluorobenzamide (3w):** Synthesized according to General Procedure A using *N*-(*tert*-butyl)-2-ethyl-*N*-fluorobenzamide **2b** (22.5 mg, 0.1 mmol, 1 equiv.) and 6,7-dihydro-5*H*-cyclopenta[*b*]pyridine-4-carbonitrile **1j** (59.5 mg, 0.3 mmol, 3.0 equiv.). The crude mixture was purified by flash column chromatography on silica gel (hexanes/EtOAc from 86:14 to 1:1) to afford **3w** (12.5 mg, 36% yield) as a white wax.

^{1}H NMR (300 MHz, $CDCl_3$) δ 8.28 (d, *J* = 5.3 Hz, 1H), 7.38 – 7.29 (m, 2H), 7.27 – 7.14 (m, 2H), 6.80 (d, *J* = 5.3 Hz, 1H), 5.38 (s, 1H), 4.84 (q, *J* = 7.1 Hz, 1H), 3.01 – 2.64 (m, 4H), 2.13 – 1.98 (m, 2H), 1.59 (d, *J* = 7.1 Hz, 3H), 1.33 (s, 9H).

^{13}C{^{1}H} NMR (75 MHz, $CDCl_3$) δ 169.6, 165.5, 147.9, 142.0, 138.0, 130.0, 129.2, 127.9, 127.2, 127.0, 126.5, 119.1, 51.8, 37.7, 34.4, 29.3, 28.7, 22.5, 20.7.

HRMS: (ESI$^+$) calculated for $C_{21}H_{27}N_2O$ (M+H$^+$):323.2118, found 323.2114.

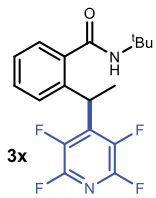

***N*-(*tert*-butyl)-2-(1-(perfluoropyridin-4-yl)ethyl)benzamide (3x):** Synthesized according to General Procedure A using *N*-(*tert*-butyl)-2-ethyl-*N*-fluorobenzamide **2b** (22.5 mg, 0.1 mmol, 1 equiv.) and 2,3,5,6-tetrafluoroisonicotinonitrile **1m** (53.0 mg, 0.3 mmol, 3 equiv.). The crude

mixture was purified by flash column chromatography on silica gel (hexanes/CH_2Cl_2/EtOAc 80:16:4) to afford **3x** (14 mg, 40% yield) as a yellow solid.

^{1}H NMR (300 MHz, $CDCl_3$) δ 7.56 – 7.38 (m, 2H), 7.36 – 7.27 (m, 2H), 5.56 (s, 1H), 5.24 (t, J = 7.3 Hz, 1H), 1.78 (d, J = 7.3 Hz, 3H), 1.39 (s, 9H).

^{13}C{^{1}H} NMR (101 MHz, $CDCl_3$) δ 169.1, 139.3, 137.3, 130.4, 128.1, 127.4, 127.1, 52.1, 33.0, 28.8, 19.5.

^{19}F NMR (376 MHz, $CDCl_3$) δ -91.3 – -92.5 (m, 2F), -142.1 – -143.50 (m, 2F).

HRMS: (ESI$^+$) calculated for $C_{18}H_{18}F_4N_2NaO$ (M+Na$^+$): 377.1247, found 377.1242.

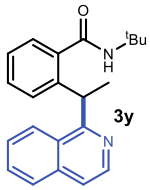

***N*-(*tert*-butyl)-2-(1-(isoquinolin-1-yl)ethyl)benzamide (3y):** Synthesized according to General Procedure A using *N*-(*tert*-butyl)-2-ethyl-*N*-fluorobenzamide **2b** (22.5 mg, 0.1 mmol, 1 equiv.) and isoquinoline-1-carbonitrile **1n** (46.5 mg, 0.3 mmol, 3.0 equiv.). The crude mixture was purified by flash column chromatography on silica gel (hexanes/CH_2Cl_2/EtOAc 50:48:2) to afford **3y** (25 mg, 79% yield) as a yellowish solid.

^{1}H NMR (500 MHz, $CDCl_3$) δ 8.53 (d, J = 5.7 Hz, 1H), 8.44 (d, J = 8.6, 1H), 7.83 – 7.72 (m, 1H), 7.64 – 7.56 (m, 1H), 7.54 (dt, J = 7.3, 1.5 Hz, 2H), 7.37 – 7.30 (m, 1H), 7.21 – 7.09 (m, 3H), 5.78 (q, J = 6.9 Hz, 1H), 5.74 (s, 1H), 1.79 (d, J = 7.0 Hz, 3H), 1.42 (s, 9H).

^{13}C{^{1}H} NMR (126 MHz, $CDCl_3$) δ 170.3, 163.6, 143.7, 141.6, 136.9, 136.5, 129.9, 129.8, 128.4, 127.5, 127.3, 127.2, 126.7, 126.2, 126.1, 119.8, 52.0, 38.8, 28.9, 21.8.

HRMS: (ESI$^+$) calculated for $C_{22}H_{25}N_2O$ (M+H$^+$): 333.1961, found 333.1951.

General procedure (B): Minisci reaction

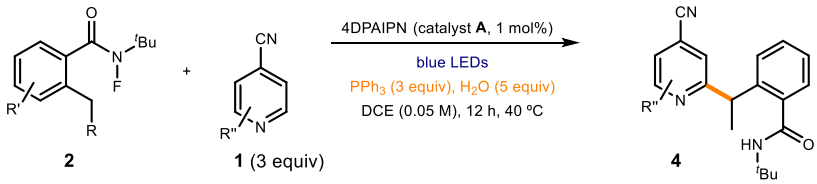

*Reactions performed using **set-up 1** in Figure S2.* In an oven dried vial with a Teflon septum screw cap, 2-alkyl *N*-fluorobenzamide **2** (0.1 mmol, 1 equiv.) was added and dissolved in 1,2-DCE (2 mL, synthesis grade solvent). Cyanopyridine **1** (0.3 mmol, 3 equiv.), 4DPAIPN catalyst **A** (0.8 mg, 0.01 mmol, 0.01 equiv.), and PPh_3 (79 mg, 0.3 mmol, 3 equiv.) were added. Finally, water is added (9 uL, 0.5 mmol, 5 equiv.). The resulting yellow mixture was irradiated under stirring for 12 hours. The mixture was transferred to an extraction funnel, saturated aqueous $NaHCO_3$ was added and the organic layer was extracted with EtOAc. The organic layer was washed with brine twice. The combined organic layers were dried over anhydrous $MgSO_4$, filtered, and concentrated to dryness. The residue purified by column chromatography on silica gel to afford the corresponding product in the stated yield with

>95% purity according to ^{1}H-NMR analysis. The exact conditions for chromatography are reported for each compound.

Characterization of Minisci products

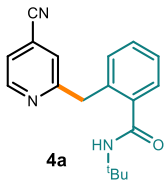

***N*-(*tert*-butyl)-2-((4-cyanopyridin-2-yl)methyl)benzamide (4a):** Synthesized according to General Procedure B using using *N*-(*tert*-butyl)-*N*-fluoro-2-methylbenzamide **2a** (21.0 mg, 0.1 mmol, 1 equiv.) and isonicotinonitrile **1a** (31.0 mg, 0.3 mmol, 3.0 equiv.). The crude mixture was purified by flash column chromatography on silica gel (hexanes/CH_2Cl_2/acetone 50:48:2) to afford **4a** (15 mg, 51% yield) as a white solid.

^{1}H NMR (500 MHz, CDCl3) δ 8.66 (dd, J = 5.0, 0.9 Hz, 1H), 7.58 (brs, 1H), 7.56 – 7.51 (dd, J = 7.3, 1.6 Hz, 1H), 7.39 (dd, J = 5.0, 1.5 Hz, 1H), 7.36 – 7.28 (m, 2H), 7.21 – 7.17 (m, 2H), 4.38 (s, 2H), 1.44 (s, 9H).

^{13}C{^{1}H} NMR (126 MHz, $CDCl_3$) δ 169.0, 162.8, 150.1, 138.3, 135.3, 131.0, 130.1, 128.3, 127.4, 125.2, 123.1, 121.4, 116.6, 52.0, 41.3, 28.9.

HRMS: (ESI$^+$) calculated for $C_{18}H_{19}N_3NaO$ (M+Na$^+$): 316.1420, found 316.1420.

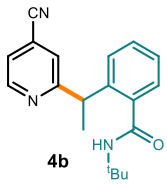

***N*-(*tert*-butyl)-2-(1-(4-cyanopyridin-2-yl)ethyl)benzamide (4b):** Synthesized according to General Procedure B using using *N*-(*tert*-butyl)-2-ethyl-*N*-fluorobenzamide **2b** (22.5 mg, 0.1 mmol, 1 equiv.) and isonicotinonitrile **1a** (31.0 mg, 0.3 mmol, 3.0 equiv.). The crude mixture was purified by flash column chromatography on silica gel (hexanes/CH_2Cl_2/acetone 50:48:2) to afford **4b** (19.0 mg, 62% yield) as a white solid.

^{1}H NMR (500 MHz, $CDCl_3$) δ 8.65 (dd, J = 5.0, 0.9 Hz, 1H), 7.60 – 7.58 (m, 1H), 7.42 (dd, J = 7.6, 1.5 Hz, 1H), 7.36 – 7.29 (m, 2H), 7.25 – 7.20 (m, 2H), 6.85 (s, 1H), 4.91 (q, J = 7.2 Hz, 1H), 1.72 (d, J = 7.2 Hz, 3H), 1.45 (s, 9H).

^{13}C{^{1}H} NMR (75 MHz, $CDCl_3$) δ 169.4, 166.6, 150.0, 141.3, 138.0, 130.1, 128.0, 127.0, 123.5, 123.0, 121.19, 117.0, 52.0, 42.0, 29.0, 20.1.

HRMS: (ESI$^+$) calculated for $C_{19}H_{21}N_3NaO$ (M+Na$^+$): 330.1577, found 330.1573.

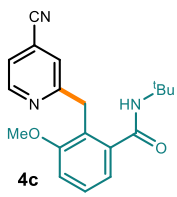

***N*-(*tert*-butyl)-2-((4-cyanopyridin-2-yl)methyl)-3-methoxybenzamide (4c):** Synthesized according to General Procedure B using using *N*-(*tert*-butyl)-*N*-fluoro-3-methoxy-2-methylbenzamide **2c** (24.0 mg, 0.1 mmol, 1 equiv.) and isonicotinonitrile **1a** (31.0 mg, 0.3 mmol, 3.0 equiv.). The crude mixture was purified by flash column chromatography on silica gel (hexanes/EtOAc 93:7 to 85:15) to afford **4c** (22 mg, 68% yield) as a off-white solid.

^{1}H NMR (400 MHz, $CDCl_3$) δ 8.56 (dd, *J* = 5.0, 0.9 Hz, 1H), 8.30 (s, 1H), 7.62 (t, *J* = 1.2 Hz, 1H), 7.35 (dd, *J* = 5.1, 1.5 Hz, 1H), 7.27 (t, *J* = 7.9 Hz, 1H), 7.19 (dd, *J* = 7.7, 1.2 Hz, 1H), 6.82 (dd, *J* = 8.1, 1.2 Hz, 1H), 4.25 (s, 2H), 3.73 (s, 3H), 1.42 (s, 9H).

^{13}C{^{1}H} NMR (101 MHz, $CDCl_3$) δ 168.7, 162.5, 157.4, 149.1, 140.4, 128.6, 126.2, 123.3, 123.0, 121.1, 120.7, 116.7, 111.3, 55.7, 52.0, 35.8, 28.9.

HRMS: (ESI$^+$) calculated for $C_{19}H_{21}N_3NaO_2$ (M+Na$^+$): 346.1526, found 346.1533.

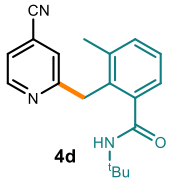

4d

***N*-(*tert*-butyl)-2-((4-cyanopyridin-2-yl)methyl)-3-methylbenzamide (4d):** Synthesized according to General Procedure B using using *N*-(*tert*-butyl)-*N*-fluoro-2,3-dimethylbenzamide **2d** (22.5 mg, 0.1 mmol, 1 equiv.) and isonicotinonitrile **1a** (31.0 mg, 0.3 mmol, 3.0 equiv.). The crude mixture was purified by flash column chromatography on silica gel (hexanes/EtOAc 93:7 to 85:15) to afford **4d** (13 mg, 42% yield) as a white solid.

^{1}H NMR (400 MHz, $CDCl_3$) δ 8.64 (d, *J* = 4.9 Hz, 1H), 7.49 (s, 1H), 7.36 (dt, *J* = 5.5, 1.6 Hz, 2H), 7.25 – 7.15 (m, 2H), 6.99 (s, 1H), 4.34 (s, 2H), 2.14 (s, 3H), 1.37 (s, 9H).

^{13}C{^{1}H} NMR (101 MHz, $CDCl_3$) δ 169.8, 162.1, 149.8, 139.8, 137.9, 133.0, 131.9, 127.6, 125.6, 125.5, 123.0, 121.4, 116.6, 51.9, 38.9, 28.9, 28.9, 20.3.

HRMS: (ESI$^+$) calculated for $C_{19}H_{22}N_3O$ (M+H$^+$): 308.1757, found 308.1749.

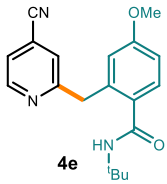

4e

***N*-(*tert*-butyl)-2-((4-cyanopyridin-2-yl)methyl)-4-methoxybenzamide (4e):** Synthesized according to General Procedure B using using *N*-(*tert*-butyl)-N-fluoro-4-methoxy-2-methylbenzamide **2e** (24.0 mg, 0.1 mmol, 1 equiv.) and isonicotinonitrile **1a** (31.0 mg, 0.3 mmol, 3.0 equiv.). The crude mixture was purified by flash column chromatography on silica gel (hexanes/EtOAc 93:7 to 75:25) to afford **4e** (15.5 mg, 48% yield) as a off-white solid.

^{1}H NMR (400 MHz, $CDCl_3$) δ 8.64 (d, *J* = 5.0 Hz, 1H), 7.58 (s, 1H), 7.47 (d, *J* = 8.5 Hz, 1H), 7.37 (dd, *J* = 5.1, 1.5 Hz, 1H), 7.05 (s, 1H), 6.79 (dd, *J* = 8.6, 2.6 Hz, 1H), 6.70 (d, *J* = 2.6 Hz, 1H), 4.36 (s, 2H), 3.77 (s, 3H), 1.40 (s, 9H).

^{13}C{^{1}H} NMR (101 MHz, $CDCl_3$) δ 168.8, 162.7, 160.7, 149.8, 137.4, 130.8, 130.0, 125.5, 123.2, 121.6, 116.6, 116.4, 112.4, 55.5, 51.9, 41.4, 29.0.

HRMS: (ESI$^+$) calculated for $C_{19}H_{22}N_3O_2$ (M+H$^+$): 324.1707, found 324.1712.

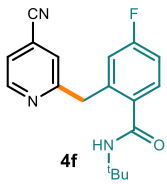

4f

***N*-(*tert*-butyl)-2-((4-cyanopyridin-2-yl)methyl)-4-fluorobenzamide (4f):** Synthesized according to General Procedure B using using *N*-(*tert*-butyl)-*N*,4-difluoro-2-methylbenzamide **2f** (22.5 mg, 0.1 mmol, 1 equiv.) and isonicotinonitrile **1a** (31.0 mg, 0.3 mmol, 3.0 equiv.). The crude mixture was purified by flash column chromatography on silica gel (hexanes/EtOAc 93:7 to 87:13) to afford **4f** (12 mg, 39% yield) as a white solid.

^{1}H NMR (400 MHz, $CDCl_3$) δ 8.65 (d, *J* = 5.0 Hz, 1H), 7.59 (s, 1H), 7.51 (dd, *J* = 8.6, 5.8 Hz, 1H), 7.39 (dt, *J* = 5.4, 2.6 Hz, 1H), 7.23 (s, 1H), 6.96 (td, *J* = 8.3, 2.6 Hz, 1H), 6.87 (dd, *J* = 9.5, 2.6 Hz, 1H), 4.34 (s, 2H), 1.41 (s, 9H).

^{13}C{^{1}H} NMR (101 MHz, $CDCl_3$) δ 168.0, 163.1 (d, *J* = 255.5 Hz), 150.0, 137.9, 137.9 (d, *J* = 7.7 Hz), 134.4, 130.4 (d, *J* = 8.7 Hz), 125.2, 123.3, 121.5, 117.4, 117.2, 116.3, 114.3 (d, *J* = 21.1 Hz), 52.0, 41.0, 28.8.

^{19}F NMR (376 MHz, $CDCl_3$) δ -110.25.

HRMS: (ESI^+) calculated for $C_{18}H_{19}FN_3O$ ($M+H^+$): 312.1507, found 312.1512.

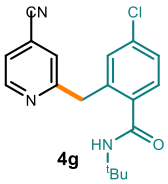

4g

***N*-(*tert*-butyl)-4-chloro-2-((4-cyanopyridin-2-yl)methyl)benzamide (4g):** Synthesized according to General Procedure B using *N*-(*tert*-butyl)-4-chloro-*N*-fluoro-2-methylbenzamide **2g** (24.5 mg, 0.1 mmol, 1 equiv.) and isonicotinonitrile **1a** (31.0 mg, 0.3 mmol, 3.0 equiv.). The crude mixture was purified by flash column chromatography on silica gel (hexanes/EtOAc 93:7 to 85:15) to afford **4g** (13 mg, 40% yield) as a white solid.

^{1}H NMR (400 MHz, $CDCl_3$) δ 8.64 (d, *J* = 5.1 Hz, 1H), 7.59 (s, 1H), 7.46 (d, *J* = 8.3 Hz, 1H), 7.40 (dd, *J* = 5.0, 1.5 Hz, 1H), 7.36 (s, 1H), 7.25 (m, 2H), 7.16 (d, *J* = 2.1 Hz, 1H), 4.31 (s, 2H), 1.40 (s, 9H).

^{13}C{^{1}H} NMR (101 MHz, $CDCl_3$) δ 168.0, 161.9, 150.1, 137.1, 136.8, 135.8, 130.7, 129.9, 127.6, 125.7, 123.6, 121.7, 116.4, 52.2, 41.0, 28.9.

HRMS: (ESI^+) calculated for $C_{18}H_{19}ClN_3O$ ($M+H^+$): 328.1211, found 328.1208.

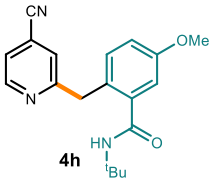

4h

***N*-(*tert*-butyl)-2-((4-cyanopyridin-2-yl)methyl)-5-methoxybenzamide (4h):** Synthesized according to General Procedure B using using *N*-(*tert*-butyl)-*N*-fluoro-5-methoxy-2-methylbenzamide **2h** (24.0 mg, 0.1 mmol, 1 equiv.) and isonicotinonitrile **1a** (31.0 mg, 0.3 mmol, 3.0 equiv.). The crude mixture was purified by flash column chromatography on silica gel (hexanes/EtOAc 93:7 to 85:15) to afford **4h** (16.5 mg, 51% yield) as a white solid. ^{1}H NMR (400 MHz, $CDCl_3$) δ 8.63 (d, *J* = 5.0 Hz, 1H), 7.56 (s, 1H), 7.42 (s, 1H), 7.37 (dd, *J* = 5.1, 1.5 Hz, 1H), 7.07 (d, *J* = 8.5 Hz, 1H), 7.04 (d, *J* = 2.8 Hz, 1H), 6.86 (dd, *J* = 8.5, 2.8 Hz, 1H), 4.28 (s, 2H), 3.81 (s, 3H), 1.41 (s, 9H).

^{13}C{^{1}H} NMR (101 MHz, $CDCl_3$) δ 168.7, 163.0, 158.6, 149.7, 139.4, 132.0, 127.0, 125.3, 123.2, 121.7, 116.5, 116.4, 113.1, 55.6, 52.0, 40.4, 28.9.

HRMS: (ESI^+) calculated for $C_{19}H_{21}N_3NaO_2$ ($M+Na^+$): 346.1526, found 346.1522.

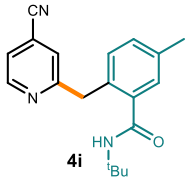

***N*-(*tert*-butyl)-2-((4-cyanopyridin-2-yl)methyl)-5-methylbenzamide (4i):** Synthesized according to General Procedure B using using *N*-(*tert*-butyl)-*N*-fluoro-2,5-dimethylbenzamide **2i** (22.5 mg, 0.1 mmol, 1 equiv.) and isonicotinonitrile **1a** (31.0 mg, 0.3 mmol, 3.0 equiv.). The crude mixture was purified by flash column chromatography on silica gel (hexanes/EtOAc 93:7 to 85:15) to afford **4i** (15 mg, 50% yield) as a off-white solid.

^{1}H NMR (400 MHz, $CDCl_3$) δ 8.63 (d, *J* = 5.1 Hz, 1H), 7.55 (s, 1H), 7.36 (dd, *J* = 5.0, 1.5 Hz, 1H), 7.32 (d, *J* = 1.9 Hz, 1H), 7.19 (s, 1H), 7.13 (ddd, *J* = 7.8, 2.0, 0.8 Hz, 1H), 7.06 (d, *J* = 7.8 Hz, 1H), 4.31 (s, 2H), 2.33 (s, 3H), 1.41 (s, 9H).

^{13}C{^{1}H} NMR (101 MHz, $CDCl_3$) δ 169.1, 163.0, 149.6, 138.2, 137.3, 132.1, 130.9, 130.9, 128.8, 125.4, 123.2, 121.7, 116.5, 52.0, 40.8, 28.9, 21.1.

HRMS: (ESI$^+$) calculated for $C_{19}H_{22}N_3O$ (M+H$^+$): 308.1757, found 308.1759.

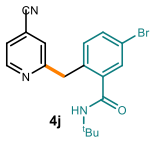

5-bromo-*N*-(*tert*-butyl)-2-((4-cyanopyridin-2-yl)methyl)benzamide (4j): Synthesized according to General Procedure B using using 5-bromo-*N*-(*tert*-butyl)-*N*-fluoro-2-methylbenzamide **2j** (29.0 mg, 0.1 mmol, 1 equiv.) and isonicotinonitrile **1a** (31.0 mg, 0.3 mmol, 3.0 equiv.). The crude mixture was purified by flash column chromatography on silica gel (hexanes/AcOEt 93:7 to 85:15) and (toluene/EtOAc 9:4 for further purification from dibenzylated side-product) to afford **4j** (17 mg, 46% yield) as a white solid.

^{1}H NMR (400 MHz, $CDCl_3$) δ 8.63 (d, *J* = 5.0 Hz, 1H), 7.64 (d, *J* = 2.2 Hz, 1H), 7.58 (s, 1H), 7.43 (dd, *J* = 8.2, 2.2 Hz, 1H), 7.40 (dd, *J* = 5.1, 1.5 Hz, 1H), 7.23 (br s, 1H), 7.06 (d, *J* = 8.2 Hz, 1H), 4.30 (s, 2H), 1.41 (s, 9H).

^{13}C{^{1}H} NMR (101 MHz, $CDCl_3$) δ 167.4, 162.0, 149.9, 140.0, 134.1, 133.1, 132.6, 131.3, 125.5, 123.5, 121.8, 121.2, 116.3, 52.3, 40.7, 28.9.

HRMS: (ESI$^+$) calculated for $C_{18}H_{19}BrN_3O$ (M+H$^+$): 372.0706, found 372.0704.

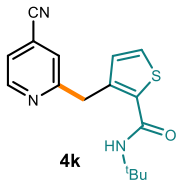

***N*-(*tert*-butyl)-3-((4-cyanopyridin-2-yl)methyl)thiophene-2-carboxamide (4k):** Synthesized according to General Procedure B using using *N*-(*tert*-butyl)-*N*-fluoro-3-methylthiophene-2-carboxamide **2k** (21.5 mg, 0.1 mmol, 1 equiv.) and isonicotinonitrile **1a** (31.0 mg, 0.3 mmol, 3.0 equiv.). The crude mixture was purified by flash column chromatography on silica gel gel (hexanes/EtOAc 93:7 to 85:15) to afford **4k** (13 mg, 45% yield) as a yellowish wax.

^{1}H NMR (400 MHz, $CDCl_3$) δ 8.66 (d, *J* = 5.1 Hz, 1H), 8.08 (s, 1H), 7.63 (s, 1H), 7.42 (dd, *J* = 5.1, 1.5 Hz, 1H), 7.28 (d, *J* = 5.1 Hz, 1H), 6.89 (d, *J* = 5.1 Hz, 1H), 4.40 (s, 2H), 1.48 (s, 9H).

^{13}C{^{1}H} NMR (101 MHz, $CDCl_3$) δ 162.1, 161.5, 149.3, 137.3, 137.1, 129.9, 127.5, 125.4, 123.7, 122.3, 116.3, 52.3, 37.3, 29.1.

HRMS: (ESI$^+$) calculated for $C_{16}H_{18}N_3OS$ (M+H$^+$): 300.1165, found 300.1152.

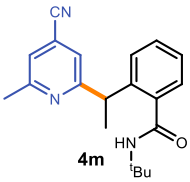

***N*-(*tert*-butyl)-2-(1-(4-cyano-6-methylpyridin-2-yl)ethyl)benzamide (4m):** Synthesized according to General Procedure B using using *N*-(*tert*-butyl)-2-ethyl-*N*-fluorobenzamide **2b** (22.5 mg, 0.1 mmol, 1 equiv.) and 2-methylisonicotinonitrile **1b** (35.5 mg, 0.3 mmol, 3.0 equiv.). The crude mixture was purified by flash column chromatography on silica gel (hexanes/EtOAc form 95:5 to 80:20) to afford **4m** (18 mg, 56% yield) as a white solid.

^{1}H NMR (500 MHz, $CDCl_z$) δ 7.49 – 7.45 (m, 1H), 7.40 (brs, 1H), 7.32 (td, J = 7.6, 1.5 Hz, 1H), 7.24 (td, J = 7.5, 1.3 Hz, 1H), 7.21 (brs, 1H), 7.18 (dd, J = 7.8, 1.3 Hz, 1H), 7.08 (s, 1H), 4.86 (q, J = 7.1 Hz, 1H), 2.56 (s, 3H), 1.71 (d, J = 7.1 Hz, 3H), 1.49 (s, 9H).

^{13}C{^{1}H} NMR (126 MHz, $CDCl_3$) δ 169.4, 166.0, 159.4, 141.3, 138.0, 130.0, 128.0, 127.6, 126.7, 122.6, 121.3, 119.7, 117.1, 52.1, 42.0, 29.0, 24.6, 20.1.

HRMS: (ESI$^+$) calculated for$C_{20}H_{24}N_3O$ (M+H$^+$): 322.1914, found 322.1915.

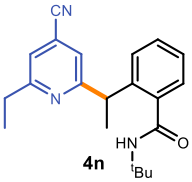

***N*-(*tert*-butyl)-2-(1-(4-cyano-6-ethylpyridin-2-yl)ethyl)benzamide (4n):** Synthesized according to General Procedure B using using *N*-(*tert*-butyl)-2-ethyl-*N*-fluorobenzamide **2a** (22.5 mg, 0.1 mmol, 1 equiv.) and 2-ethylisonicotinonitrile **1c** (40.0 mg, 0.3 mmol, 3.0 equiv.). The crude mixture was purified by flash column chromatography on silica gel (hexanes/EtOAc form 95:5 to 80:20) to afford **4n** (20 mg, 60% yield) as a yellow oil.

^{1}H NMR (400 MHz, $CDCl_3$) δ 7.44 – 7.38 (m, 1H), 7.35 (d, *J* = 0.7 Hz, 1H), 7.33 – 7.27 (m, 1H), 7.24 – 7.18 (m, 3H), 6.70 (s, 1H), 4.85 (q, *J* = 7.1 Hz, 1H), 2.82 (q, *J* = 7.6 Hz, 2H), 1.69 (d, *J* = 7.1 Hz, 3H), 1.45 (s, 9H), 1.25 (t, *J* = 7.6 Hz, 3H).

^{13}C{^{1}H} NMR (101 MHz, $CDCl_3$) δ 169.5, 165.8, 164.3, 141.5, 137.9, 129.9, 127.8, 127.6, 126.7, 121.3, 120.4, 117.2, 52.1, 42.0, 31.2, 29.0, 20.4, 13.5.

HRMS: (ESI$^+$) calculated for$C_{21}H_{26}N_3O$ (M+H$^+$): 336.2070, found 336.2062.

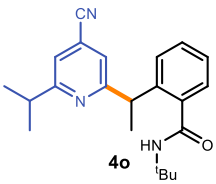

***N*-(*tert*-butyl)-2-(1-(4-cyano-6-isopropylpyridin-2-yl)ethyl)-*N*-fluorobenzamide (4o):** Synthesized according to General Procedure B using using *N*-(*tert*-butyl)-2-ethyl-*N*-fluorobenzamide **2a** (22.5 mg, 0.1 mmol, 1 equiv.) and 2-isopropylisonicotinonitrile **1d** (44.0 mg, 0.3 mmol, 3.0 equiv.). The crude mixture was purified by flash column chromatography on silica gel (hexanes/EtOAc 8:2) to afford **4o** (16 mg, 44% yield) as a yellowish wax.

^{1}H NMR (300 MHz, $CDCl_3$) δ 7.42 – 7.35 (m, 1H), 7.30 (dd, *J* = 4.1, 1.3 Hz, 3H), 7.25 – 7.15 (m, 2H), 6.25 (s, 1H), 4.84 (q, *J* = 7.1 Hz, 1H), 3.05 (p, *J* = 6.9 Hz, 1H), 1.45 (s, 9H), 1.26 (d, *J* = 2.0 Hz, 6H).

$^{13}C\{^{1}H\}$ NMR (75 MHz, $CDCl_3$) δ 169.5, 168.1, 165.4, 141.8, 137.6, 130.0, 128.0, 127.1, 126.5, 1., 120.8, 119.5, 117.2, 52.0, 42.0, 36.2, 29.0, 22.3, 22.2, 20.6.

HRMS: (ESI^+) calculated for $C_{22}H_{28}N_3O$ ($M+H^+$): 350.2227, found 350.2226.

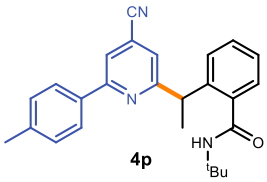

4p

***N*-(*tert*-butyl)-2-(1-(4-cyano-6-(p-tolyl)pyridin-2-yl)ethyl)benzamide (4e):** Synthesized according to General Procedure B using using *N*-(*tert*-butyl)-2-ethyl-*N*-fluorobenzamide **2a** (22.5 mg, 0.1 mmol, 1 equiv.) and 3-chloroisonicotinonitrile **1e** (41.5 mg, 0.3 mmol, 3.0 equiv.) and 10 mol% of the photocatalyst. The crude mixture was purified by flash column chromatography on silica gel (hexanes/EtOAc 86:14) to afford **4e** (13 mg, 34% yield) as an yellowish solid.

^{1}H NMR (400 MHz, $CDCl_3$) δ 7.80 (d, J = 8.2 Hz, 2H), 7.71 (d, J = 1.2 Hz, 1H), 7.46 – 7.40 (m, 2H), 7.33 (d, J = 4.0 Hz, 2H), 7.28 (d, J = 8.1 Hz, 2H), 7.25 – 7.21 (m, 1H), 6.53 (s, 1H), 4.93 (q, J = 7.1 Hz, 1H), 2.41 (s, 3H), 1.77 (d, J = 7.1 Hz, 3H), 1.36 (s, 9H).

$^{13}C\{^{1}H\}$ NMR (101 MHz, $CDCl_3$) δ 169.6, 166.0, 157.8, 142.0, 140.5, 137.8, 135.0, 130.0, 129.8, 128.1, 127.4, 127.1, 126.7, 121.6, 121.5, 119.3, 117.2, 52.0, 42.1, 29.0, 21.5, 20.4.

HRMS: (ESI^+) calculated for $C_{26}H_{27}N_3NaO$ ($M+Na^+$): 420.2046, found 420.2047.

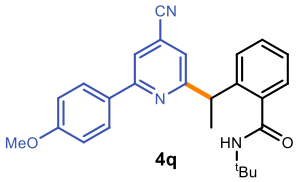

4q

***N*-(*tert*-butyl)-2-(1-(4-cyano-6-(4-methoxyphenyl)pyridin-2-yl)ethyl)benzamide (4q):** Synthesized according to General Procedure B using *N*-(*tert*-butyl)-2-ethyl-*N*-fluorobenzamide **2a** (22.5 mg, 0.1 mmol, 1 equiv.) and 2-(4-methoxyphenyl)isonicotinonitrile **1f** (63.0 mg, 0.3 mmol, 3.0 equiv.). The crude mixture was purified by flash column chromatography on silica gel (hexanes/EtOAc 93:7 to 85:15) to afford **4q** (17 mg, 41% yield) as an yellowish solid.

^{1}H NMR (400 MHz, $CDCl_3$) δ 7.89 – 7.83 (m, 2H), 7.67 (d, *J* = 1.2 Hz, 1H), 7.43 (dt, *J* = 7.6, 1.1 Hz, 1H), 7.41 – 7.39 (m, 1H), 7.34 – 7.30 (m, 2H), 7.23 (ddd, *J* = 7.6, 5.3, 3.4 Hz, 1H), 7.02 – 6.96 (m, 2H), 6.58 (s, 1H), 4.92 (q, *J* = 7.1 Hz, 1H), 3.87 (s, 3H), 1.77 (d, *J* = 7.1 Hz, 3H), 1.36 (s, 9H).

$^{13}C\{^{1}H\}$ NMR (101 MHz, $CDCl_3$) δ 169.6, 165.9, 161.5, 157.5, 141.9, 137.9, 130.2, 130.0, 128.6, 128.0, 127.4, 126.7, 121.6, 120.9, 118.9, 117.3, 114.5, 55.6, 52.0, 42.1, 28.9, 20.4.

HRMS: (ESI^+) calculated for $C_{26}H_{28}N_3O$ ($M+H^+$): 414.2176, found 414.2185.

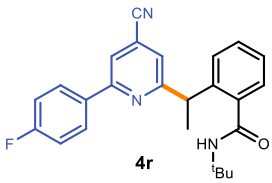

4r

***N*-(*tert*-butyl)-2-(1-(4-cyano-6-(4-fluorophenyl)pyridin-2-yl)ethyl)benzamide (4r):** Synthesized according to General Procedure B using using *N*-(*tert*-butyl)-2-ethyl-*N*-fluorobenzamide **2a** (22.5 mg, 0.1 mmol, 1 equiv.) and 2-(4-fluorophenyl)isonicotinonitrile **1g** (59.5 mg, 0.3 mmol, 3.0

equiv.) The crude mixture was purified by flash column chromatography on silica gel (hexanes/EtOAc 93:7 to 85:15) to afford **4r** (15 mg, 38% yield) as an yellowish solid.

^{1}H NMR (400 MHz, $CDCl_3$) δ 7.96 – 7.91 (m, 2H), 7.69 (d, *J* = 1.2 Hz, 1H), 7.46 (d, *J* = 1.2 Hz, 1H), 7.40 (dt, *J* = 7.5, 1.0 Hz, 1H), 7.36 – 7.33 (m, 2H), 7.25 – 7.21 (m, 1H), 7.20 – 7.14 (m, 2H), 6.29 (s, 1H), 4.95 (q, *J* = 7.1 Hz, 1H), 1.77 (d, *J* = 7.1 Hz, 3H), 1.39 (s, 9H).

^{13}C{^{1}H} NMR (101 MHz, $CDCl_3$) δ 169.6, 166.2, 164.2 (d, *J* = 250.7 Hz), 156.7, 141.8, 137.8, 133.8, 130.1, 129.1 (d, *J* = 8.5 Hz), 128.1, 127.3, 126.8, 122.2, 121.8, 119.2, 117.1, 116.2 (d, *J* = 21.8 Hz), 52.1, 42.2, 28.9, 20.5.

^{19}F NMR (376 MHz, $CDCl_3$) δ -111.00.

HRMS: (ESI$^+$) calculated for $C_{25}H_{25}FN_3O$ (M+H$^+$): 402.1976, found 402.1967.

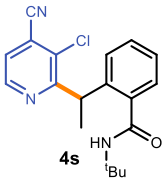

***N*-(*tert*-butyl)-2-(1-(3-chloro-4-cyanopyridin-2-yl)ethyl)benzamide (4s):** Synthesized according to General Procedure B using using *N*-(*tert*-butyl)-2-ethyl-*N*-fluorobenzamide **2a** (22.5 mg, 0.1 mmol, 1 equiv.) and 2-(p-tolyl)isonicotinonitrile **1h** (58.5 mg, 0.3 mmol, 3.0 equiv.). The crude mixture was purified by flash column chromatography on silica gel (hexanes/acetone 92:8) to afford **4s** (19 mg, 56% yield) as a white solid.

^{1}H NMR (500 MHz, $CDCl_3$) δ 8.65 (d, J = 4.9 Hz, 1H), 7.41 (d, J = 4.9 Hz, 1H), 7.34 (dd, J = 7.5, 1.5 Hz, 1H), 7.30 (td, J = 7.6, 1.5 Hz, 1H), 7.22 (td, J = 7.5, 1.3 Hz, 1H), 7.19 (dd, J = 7.8, 1.3 Hz, 1H), 5.66 (s, 1H), 5.31 (q, J = 6.9 Hz, 1H), 1.71 (d, J = 6.9 Hz, 4H), 1.45 (s, 9H).

^{13}C{^{1}H} NMR (126 MHz, $CDCl_3$) δ 169.5, 163.7, 147.3, 141.3, 137.5, 132.5, 130.1, 128.4, 126.8, 126.7, 124.4, 121.7, 114.4, 52.0, 40.0, 29.0, 21.0.

HRMS: (ESI$^+$) calculated for $C_{19}H_{20}ClN_3NaO$ (M+Na$^+$): 364.1187, found 364.1188.

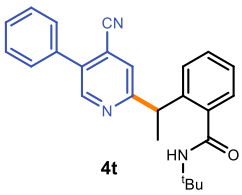

***N*-(*tert*-butyl)-2-(1-(4-cyano-5-phenylpyridin-2-yl)ethyl)benzamide (4t):** Synthesized according to General Procedure B using using *N*-(*tert*-butyl)-2-ethyl-*N*-fluorobenzamide **2a** (22.5 mg, 0.1 mmol, 1 equiv.) and 3-phenylisonicotinonitrile **1i** (54.0 mg, 0.3 mmol, 3.0 equiv.). The crude mixture was purified by flash column chromatography on silica gel (hexanes/acetone 92:8) to afford **4t** (21 mg, 55% yield) as a white solid.

^{1}H NMR (400 MHz, $CDCl_3$) δ 8.69 (s, 1H), 7.68 (s, 1H), 7.54 – 7.43 (m, 7H), 7.35 (ddd, *J* = 8.5, 7.2, 1.5 Hz, 1H), 7.29 – 7.26 (m, 1H), 7.24 (dd, *J* = 7.4, 1.4 Hz, 1H), 6.98 (s, 1H), 4.94 (q, *J* = 7.2 Hz, 1H), 1.76 (d, *J* = 7.1 Hz, 3H), 1.47 (s, 9H).

^{13}C{^{1}H} NMR (101 MHz, $CDCl_3$) δ 169.4, 164.6, 150.0, 141.3, 138.0, 136.4, 134.5, 130.1, 129.5, 129.3, 128.9, 127.9, 127.8, 126.9, 124.1, 119.6, 116.7, 52.1, 41.7, 29.0, 20.1.

HRMS: (ESI$^+$) calculated for $C_{25}H_{26}N_3O$ (M+H$^+$): 384.2070, found 384.2054.

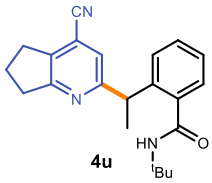

***N*-(*tert*-butyl)-2-(1-(4-cyano-6,7-dihydro-5*H*-cyclopenta[*b*]pyridin-2-yl)ethyl)benzamide (4u):** Synthesized according to General Procedure B using using *N*-(*tert*-butyl)-2-ethyl-*N*-fluorobenzamide **2a** (22.5 mg, 0.1 mmol, 1 equiv.) and 6,7-dihydro-5*H*-cyclopenta[*b*]pyridine-4-carbonitrile **1j** (43.5 mg, 0.3 mmol, 3.0 equiv.). The crude mixture was purified by flash column chromatography on silica gel (hexanes/EtOAc 93:7 to 87:13) to afford **4u** (13 mg, 38% yield) as a yellow oil.

^{1}H NMR (400 MHz, $CDCl_3$) δ 7.51 (s, 1H), 7.48 – 7.45 (m, 1H), 7.32 (d, *J* = 0.8 Hz, 1H), 7.29 (td, *J* = 7.6, 1.7 Hz, 1H), 7.21 (td, *J* = 7.5, 1.4 Hz, 1H), 7.14 (dd, *J* = 7.8, 1.3 Hz, 1H), 4.83 (q, *J* = 7.2 Hz, 1H), 3.07 (t, *J* = 7.5 Hz, 2H), 3.01 (t, *J* = 7.8 Hz, 2H), 2.23 – 2.11 (m, 2H), 1.68 (d, *J* = 7.2 Hz, 3H), 1.47 (s, 9H).

^{13}C{^{1}H} NMR (101 MHz, $CDCl_3$) δ 169.4, 167.0, 164.2, 141.3, 138.1, 137.9, 129.9, 128.2, 127.4, 126.8, 119.3, 116.2, 52.1, 41.5, 34.3, 30.0, 29.0, 22.7, 20.2.

HRMS: (ESI$^+$) calculated for $C_{22}H_{26}N_3O$ (M+H$^+$): 348.2070, found 348.2073.

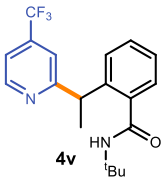

***N*-(*tert*-butyl)-2-(1-(4-(trifluoromethyl)pyridin-2-yl)ethyl)benzamide (4v):** Synthesized according to General Procedure B using using *N*-(*tert*-butyl)-2-ethyl-*N*-fluorobenzamide **2a** (22.5 mg, 0.1 mmol, 1 equiv.) and 4-(trifluoromethyl)pyridine **1o** (44.0 mg, 0.3 mmol, 3.0 equiv.). The crude mixture was purified by flash column chromatography on silica gel (hexanes/EtOAc 93:7 to 85:15) to afford **4v** (16 mg, 46% yield) as an off-yellow solid.

^{1}H NMR (400 MHz, $CDCl_3$) δ 8.65 (d, J = 5.1 Hz, 1H), 7.59 (s, 1H), 7.45 (dd, J = 7.7, 1.5 Hz, 1H), 7.35 (d, J = 5.2 Hz, 1H),7.32 (br s, 1H), 7.30 (td, J = 7.6, 1.6 Hz, 1H), 7.23 (dd, J = 7.5, 1.4 Hz, 1H), 7.19 (dd, J = 8.0, 1.2 Hz, 1H), 4.94 (q, J = 7.2 Hz, 1H), 1.74 (d, J = 7.1 Hz, 3H), 1.44 (s, 9H).

^{13}C{^{1}H} NMR (101 MHz, $CDCl_3$) δ 169.4, 166.5, 149.8, 141.3, 138.2, 129.9, 128.0, 127.6, 126.8, 117.3, 116.9, 52.0, 42.0, 28.9, 20.1.

^{19}F NMR (376 MHz, $CDCl_3$) δ -64.8.

HRMS: (ESI$^+$) calculated for $C_{19}H_{22}F_3N_2O$ (M+H$^+$): 351.1679, found 351.1672.

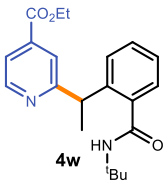

Ethyl-2-(1-(2-(*tert*-butylcarbamoyl)phenyl)ethyl)isonicotinate (5w): Synthesized according to General Procedure B using using *N*-(*tert*-butyl)-2-ethyl-*N*-fluorobenzamide **2a** (22.5 mg, 0.1 mmol, 1 equiv.) and ethyl isonicotinate **1p** (45.5 mg, 0.3 mmol, 3.0 equiv.). The crude mixture was purified by flash column chromatography on silica gel (hexanes/EtOAc 93:7 to 85:15) to afford **4w** (18.5 mg, 52% yield) as off-yellow solid.

^{1}H NMR (400 MHz, $CDCl_3$) δ 8.59 (d, *J* = 5.0 Hz, 1H), 7.97 (s, 1H), 7.81 (s, 1H), 7.70 (d, *J* = 5.1 Hz, 1H), 7.47 (dd, *J* = 7.5, 1.6 Hz, 1H), 7.27 (td, *J* = 7.5, 1.6 Hz, 2H), 7.20 (td, *J* = 7.5, 1.4 Hz, 1H), 7.16 (dd, *J* = 7.7, 1.4 Hz, 1H).

$^{13}C\{^{1}H\}$ NMR (101 MHz, $CDCl_3$) δ 169.5, 166.0; 165.2, 149.2, 141.4, 138.3, 129.8, 128.2, 127.5, 126.7, 121.0, 120.1, 62.1, 52.0, 41.8, 28.9, 19.9, 14.4.

HRMS: (ESI$^+$) calculated for $C_{21}H_{27}N_2O_3$ ($M+H^+$): 355.2016, found 355.2008.

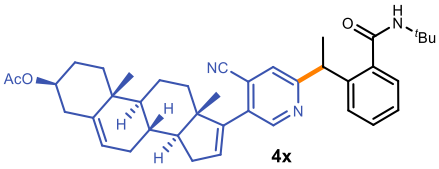

(3*S*,8*R*,9*S*,10*R*,13*S*,14*S*)-17-(6-((*S*)-1-(2-(*tert*-butylcarbamoyl)phenyl)ethyl)-4-cyanopyridin-3-yl)-10,13-dimethyl-2,3,4,7,8,9,10,11,12,13,14,15-dodecahydro-1*H*-cyclopenta[*a*]phenanthren-3-yl acetate (4x): Synthesized according to General Procedure B using using *N*-(*tert*-butyl)-2-ethyl-*N*-fluorobenzamide **2a** (22.5 mg, 0.1 mmol, 1 equiv.) and (3*S*,8*R*,9*S*,10*R*,13*S*,14*S*)-17-(4-cyanopyridin-3-yl)-10,13-dimethyl-2,3,4,7,8,9,10,11,12,13,14,15-dodecahydro-1*H*-cyclopenta[*a*]phenanthren-3-yl acetate **1q** (125 mg, 0.3 mmol, 3.0 equiv.). The crude mixture was purified by flash column chromatography on silica gel (toluene/EtOAc 97:3) to afford **4x** (17 mg, 28% yield) as a white solid.

^{1}H NMR (400 MHz, $CDCl_3$) δ 8.54 (s, 1H), 7.59 (s, 1H), 7.45 – 7.41 (m, 1H), 7.34 (ddd, *J* = 8.6, 7.0, 1.5 Hz, 1H), 7.26 – 7.21 (m, 1H), 6.94 (d, *J* = 22.4 Hz, 1H), 6.15 (ddd, *J* = 5.0, 3.3, 1.7 Hz, 1H), 5.41 (d, *J* = 5.1 Hz, 1H), 4.88 (q, *J* = 7.1 Hz, 1H), 4.61 (tt, *J* = 10.7, 5.2 Hz, 1H), 2.42 – 2.30 (m, 3H), 2.20 – 2.12 (m, 1H), 2.12 – 2.05 (m, 1H), 2.03 (s, 3H), 1.90 – 1.81 (m, 2H), 1.78 – 1.50 (m, 8H), 1.73 (d, *J* = 7.2 Hz, 3H), 1.45 (s, 9H), 1.19 – 1.11 (m, *J* = 13.9, 13.1, 4.2 Hz, 2H), 1.06 (s, 3H), 1.00 (d, *J* = 1.5 Hz, 3H).

$^{13}C\{^{1}H\}$ NMR (101 MHz, $CDCl_3$) δ 170.7, 169.4, 163.3, 147.9, 147.9, 147.7, 140.9, 140.1, 138.0, 138.0, 135.7, 135.6, 133.3, 130.1, 127.9, 127.8, 127.1, 124.7, 122.3, 121.4, 116.9, 73.9, 57.2, 52.1, 50.3, 49.4, 41.5, 38.2, 37.1, 36.9, 35.2, 32.7, 31.6, 30.7, 29.0, 27.9, 21.6, 20.8, 20.1, 19.4, 16.8, 16.7.

HRMS: (ESI$^+$) calculated for $C_{40}H_{50}N_3O_3$ ($M+H^+$): 620.3847, found 620.3840.

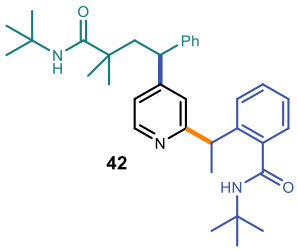

***N*-(*tert*-butyl)-2-(1-(4-(4-(*tert*-butylamino)-3,3-dimethyl-4-oxo-1-phenylbutyl)pyridin-2-yl)ethyl)benzamide (4y):** Synthesized according to General Procedure B using using *N*-(*tert*-butyl)-*N*-fluoro-2,2-dimethyl-4-phenylbutanamide **2e** (26.5 mg, 0.1 mmol, 1 equiv.) and *N*-(*tert*-butyl)-2-(1-(4-cyanopyridin-2-yl)ethyl)benzamide **4b** (92.0 mg, 0.3 mmol, 3.0 equiv.). The crude mixture was purified by flash column chromatography on silica gel (hexanes/EtOAc 8:2) to afford **5** (42 mg, 80% yield) as a white solid.

^{1}H NMR (500 MHz, $CDCl_3$) δ 8.53 (d, J = 53.5 Hz, 1H), 8.24 (t, J = 5.3 Hz, 1H), 7.49 (ddd, J = 7.5, 5.8, 1.6 Hz, 1H), 7.31 – 7.24 (m, 5H), 7.23 – 7.13 (m, 3H), 7.09 – 6.99 (m, 2H), 5.32 (s, 1H), 4.73 (q, J = 7.2 Hz, 1H), 3.99 (td, J = 6.6, 3.1 Hz, 1H), 2.47 – 2.25 (m, 2H), 1.66 (d, J = 7.2 Hz, 3H), 1.41 (d, J = 5.4 Hz, 9H), 1.27 (d, J = 3.6 Hz, 9H), 1.06 (brs, 3H), 1.00 (d, J = 12.7 Hz, 3H).

$^{13}C\{^{1}H\}$ NMR (126 MHz, $CDCl_3$) δ 176.0, 176.0, 169.4, 169.3, 164.7, 164.6, 156.0, 155.8, 148.5, 148.5, 143.8, 143.8, 141.7, 138.3, 138.3, 129.4, 128.8, 128.3, 128.3, 128.0, 127.9, 127.2, 127.1, 126.8, 126.3, 121.0, 120.7, 119.6, 119.2, 51.7, 51.6, 51.0, 51.0, 48.5, 48.5, 46.0, 45.9, 43.1, 41.5, 41.5, 28.7, 28.7, 27.1, 27.1, 26.2, 26.0.

HRMS: (ESI$^+$) calculated for $C_{34}H_{46}N_3O_2$ ($M+H^+$): 528.3585, found 528.3569.

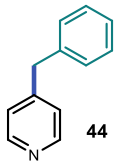

44

4-benzylpyridine (44): Synthesized according to General Procedure A using 1-benzyl-2,4,6-triphenylpyridin-1-ium tetrafluoroborate **43** (48.5 mg, 0.1 mmol, 1 equiv.) and isonicotinonitrile **1a** (31.0 mg, 0.3 mmol, 3 equiv.). The crude mixture was purified by flash column chromatography on silica gel (hexanes/EtOAc 8:2) to afford **44** (7.5 mg, 44% yield) as an off-white solid, with characterization data in accordance with the literature.[12]

^{1}H NMR (300 MHz, $CDCl_3$) δ 8.52 – 8.44 (m, 2H), 7.36 – 7.28 (m, 2H), 7.25 (d, *J* = 2.3 Hz, 1H), 7.21 – 7.15 (m, 2H), 7.13 – 7.06 (m, 2H), 3.97 (s, 2H).

$^{13}C\{^{1}H\}$ NMR (75 MHz, $CDCl_3$) δ 150.2, 150.0, 139.0, 129.2, 128.9, 126.8, 124.3, 41.4.

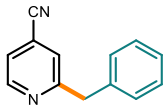

45

2-benzylisonicotinonitrile (45): Synthesized according to General Procedure B using 1-benzyl-2,4,6-triphenylpyridin-1-ium tetrafluoroborate **43** (48.5 mg, 0.1 mmol, 1 equiv.) and isonicotinonitrile **1a** (31.0 mg, 0.3 mmol, 3 equiv.). The crude mixture was purified by flash column chromatography on silica gel (hexanes/EtOAc 8:2) to afford **45** (11 mg, 57% yield) as an off-yellow solid with characterization data in accordance with the literature.[13]

^{1}H NMR (400 MHz, $CDCl_3$) δ 8.70 (dd, *J* = 5.0, 0.9 Hz, 1H), 7.35 – 7.20 (m, 7H), 4.19 (s, 2H).

$^{13}C\{^{1}H\}$ NMR (101 MHz, $CDCl_3$) δ 163.0, 150.5, 138.0, 129.3, 129.1, 127.2, 124.8, 122.8, 121.0, 116.7, 44.7.

pH Measurements

We measured the pH of the reaction mixture upon complete conversion of the both DIPEA- and PPh_3-enabled processes. Upon reaction completion, 4 mL of H_2O was added. The aqueous phase of the biphasic mixture was transferred to a clean vial. The pH was measured using a Mettler Toledo FG2-Kit FiveGo™ Portable pH Meter (Figure 2.25). A sample for crude pH measurement was taken using standard pH universal indicator paper.

*Ipso-substitution process of **1a** and **2a** to afford **3a** enabled by DIPEA*

conditions as in entry 1 of Figure 2b in the main manuscript

pH = 9.8

*Minisci reaction of **1a** and **2a** to afford **3a** enabled by PPh3 - water*

conditions as in entry 7 of Figure 2b in the main manuscript

pH = 3.1

These measurements indicate that the C2-selective reaction operates under a typical Minisci mechanistic regime, whereby protonation of the *N*-heterocycle leads to radical addition at the C2 position. In contrast, the basicity of the aqueous solution derived from the reaction with DIPEA indicates that any protons generated during the process are quenched by the excess of DIPEA. This implies that protonation of the pyridine substrate is not feasible, and therefore a Minisci pathway is unavailable.

Figure 2.25. pH measurements.

Quantum yield determination

Ipso-substitution

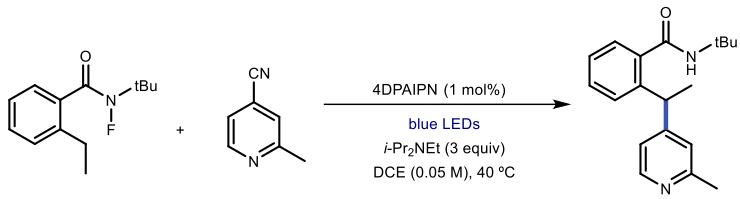

2b **1b** (3 equiv.) **3m**

A ferrioxalate actinometer solution was prepared by following the Hammond variation of the Hatchard and Parker procedure outlined in the Handbook of Photochemistry.[20] The ferrioxalate actinometer solution measures the decomposition of ferric ions to ferrous ions, which are complexed by 1,10-phenanthroline and monitored by UV/Vis absorbance at 510 nm. The moles of iron-phenanthroline complex formed are related to moles of photons absorbed. The following solutions were prepared and stored in a dark laboratory (red light):

1. Potassium ferrioxalate solution: 294.8 mg of potassium ferrioxalate (commercially available from Alfa Aesar) and 139 µL of sulfuric acid (96%) were added to a 50 mL volumetric flask, and filled to the mark with water (HPLC grade).

2. Phenanthroline solution: 0.2% by weight of 1,10-phenanthroline in water (100 mg in 50 mL volumetric flask).

3. Buffer solution: 2.47 g of NaOAc and 0.5 mL of sulfuric acid (96%) were added to a 50 mL volumetric flask and filled to the mark with water (HPLC grade).

The actinometry measurements were done as follows:

1. 1 mL of the actinometer solution was added to a Schlenk tube (diameter = 12 mm). The Schlenk tube was placed in a single HP LED 1.5 cm (***set-up 2***, Figure S3) away from the light source (760uA). The solution was irradiated at 460 nm. This procedure was repeated 4 times, quenching the solutions after different time intervals: 5 sec, 10 sec, 20 sec, and 40 sec.
2. Then 1 mL of the model reaction following general procedure A with **1b** (0.10 mmol) and **2b** as substrates was placed in a Schlenk tube, degassed *via* argon bubbling, placed in the irradiation set up and irradiated for 15 minutes. This procedure was performed a total of four times with different irradiation times (15 min, 30 min, 45 min, and 60 min).
3. After irradiation, the actinometer solutions were removed and placed in a 10 mL volumetric flask containing 0.5 mL of 1,10-phenanthroline solution and 2 mL of buffer solution. These flasks were filled to the mark with water (HPLC grade).
4. The UV-Vis spectra of the complexed actinometer samples were recorded for each time interval. The absorbance of the complexed actinometer solution was monitored at 510 nm.

The moles of Fe^{2+} formed for each sample is determined using Beers' Law (Eq. 1) :

$$\text{Mols of Fe(II)} = V_1 \times V_3 \times \Delta A(510\text{ nm})/10^3 \times V_2 \times l \times \varepsilon(510\ nm) \text{ (Eq. 1)}$$

where V_1 is the irradiated volume (1 mL), V_2 is the aliquot of the irradiated solution taken for the determination of the ferrous ions (1 mL), V_3 is the final volume after complexation with phenanthroline (10 mL), l is the optical path-length of the irradiation cell (1 cm), ΔA(510 nm) is the optical difference in absorbance between the irradiated solution and the one stored in the dark, ε(510 nm) is the extinction coefficient the complex $Fe(phen)_3^{2+}$ at 510 nm (11100 L mol^{-1} cm^1). The moles of Fe2+ formed (x) are plotted as a function of time (t). The slope of this line was correlated to the moles of incident photons by unit of time (q0 n,p) by the use of the following Equation 2:

$$\Phi(\lambda) = dx/dt\ qn,p\ 0\ [1-10-A(\lambda)\ ] \text{ (Eq. 2)}$$

where dx/dt is the rate of change of a measurable quantity (spectral or any other property), the quantum yield (Φ) for Fe^{2+} at 458 nm is 1.1,[21] $[1\text{-}10^{-A(\lambda)}]$ is the ratio of absorbed photons by the solution, and A(λ) is the absorbance of the actinometer at the wavelength used to carry out the experiments (460 nm). The absorbance at 460 nm A(460) was measured using a Shimadzu 2401PC UV-Vis spectrophotometer in a 10 mm path quartz cuvette, obtaining an absorbance of 0.182. $q^0_{n,p}$, which is the photon flux, was determined to be $4{,}14*10^{-08}$.

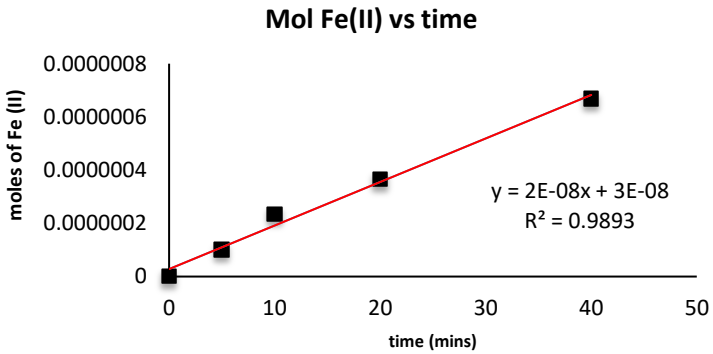

Figure 2.26. Plot of mols of Fe^{2+} formed vs irradiation time. Slope of the line correlates to the moles of incident photons by unit of time.

The moles of product **3m** formed for the model reaction were determined by GC measurement (FID detector) using 1,3,5-trimethoxybenzene as internal standard. The moles of product per unit of time are related to the number of photons absorbed.

The photons absorbed are correlated to the number of incident photons by the use of Equation 1. According to this, if we plot the moles of product (**3m**) versus the moles of incident photons (q0 n,p·dt), the slope is equal to: $\Phi\cdot(1\text{-}10^{-A(460\ nm)})$, where Φ is the quantum yield to be determined and A(460 nm) is the absorption of the reaction under study. A(460 nm) was measured using a Shimadzu 2401PC UV-Vis spectrophotometer in 10 mm path quartz. An absorbance of 1.52 was determined for the model reaction mixture (1:4 dilution). The quantum yield (Φ) of the photochemical transformation was measured to be 0.01.

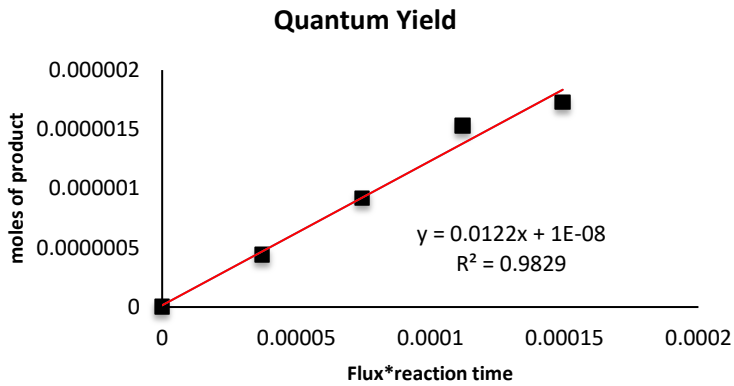

Figure 2.27. Plot of mols of incident photons vs mols of product formed. Slope of the line correlates to quantum yield of the photochemical transformation.

Minisci reaction

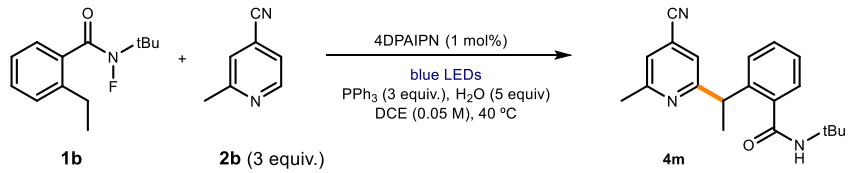

While the reaction mixture for the *ipso* substitution remains homogenous during irradiation, the Minisci reaction mixture becomes heterogenous and blurry upon irradiation. Light scattering prevented a precise quantum yield determination. In addition, the induction time observed in the kinetic studies reported in section I below further complicated our efforts to precisely measure the quantum yield of the C2-selectvie process.

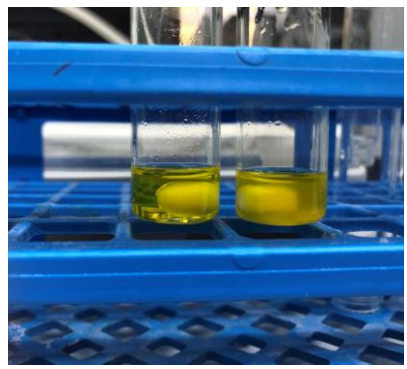

Figure 2.28. Reaction mixture before and after 20 mins under irradiation.

Kinetic profile analyses

The kinetic profile of both the *ipso*-substitution and the Minisci reaction have been followed for 75 minutes. The two reactions have been conducted under inert conditions using the illumination ***set-up 2*** in Figure S3. Product yield was determined by GC-FID analysis upon calibration with trimethoxybenzene as the internal standard. The three processes in Figure S14 has been analyzed: a) the DIPEA-enabled *ipso*-substitution; b) the PPh_3-enabled Minisci reaction; c) and the same PPh_3-enabled Minisci reaction adding TFA.

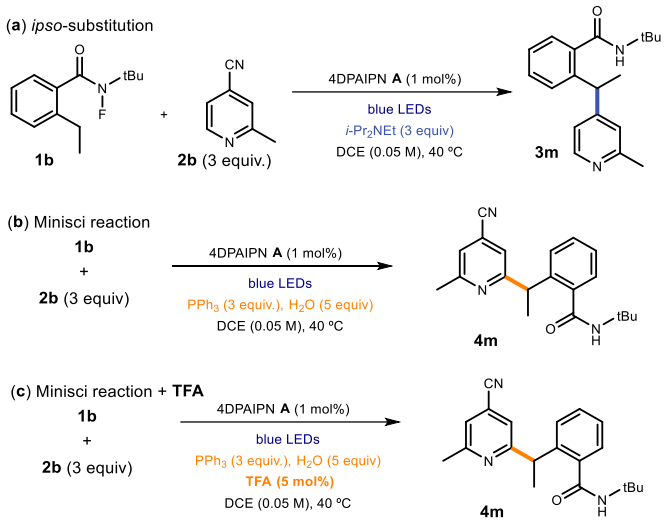

Figure 2.29. The three processes analysed in our kinetic investigations.

As shown in Figure **S15**, the PPh_3-enabled Minisci reaction (reaction b, red line) exhibits an induction period with low product **4m** formation. After about 45 minutes, the reaction rate rapidly increases, reaching 62% yield after 75 minutes. The induction time is not observed when the Minisci reaction is performed in the presence of a catalytic amount of trifluoroacetic acid (TFA, reaction c, blue line). In contrast, the *ipso*-substitution reaction exhibits a slow but steady kinetic rate profile, delivering 5% of product after 75 minutes (reaction a, green line).

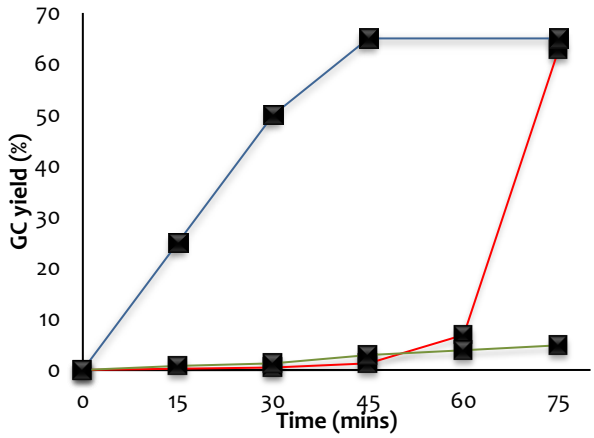

Figure 2.30. *Ipso*-substitution: green profile; *Minisci reaction*: red profile; Minisci reaction with 5 mol% of TFA: blue profile.

Stern Volmer quenching studies

Stern-Volmer quenching studies with DIPEA

Stern-Volmer fluorescence quenching experiments were conducted with a Fluorolog Horiba Jobin Yvon spectrofluorimeter equipped with a photomultiplier detector, a double monochromator, and a 350W xenon light source. 2.5 mL of 1,2-DCE, thoroughly degassed by freeze pump thaw, were placed in a 10 x10 mm light path quartz fluorescence cuvette equipped with Silicone/PTFE 3.2 mm septum under an argon atmosphere. Then, 10 µL of a $1 \cdot 10^{-3}$ M solution of photocatalyst in 1,2-DCE was added to give a final concentration of 4-DPAIPN of $4 \cdot 10^{-6}$ M.

A 0.43M solution of DIPEA and 15 µL of this stock solution were added to the solution of photocatalyst. Between each addition the fluorescence spectra was measured. The emission intensity was recorded at 527 nm. After each addition, an absorption spectrum and an emission spectrum of the solution were recorded. The excitation wavelength was fixed at 390 nm (incident light slit regulated to 2 mm); the emission light was acquired from 410 nm to 650 nm (emission light slit regulated to 2 mm).

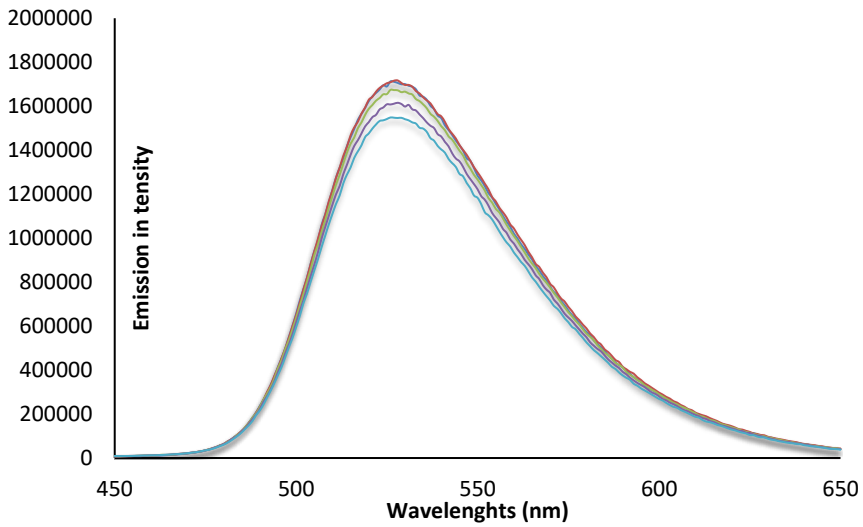

Figure 2.31. Quenching of the photocatalyst emission ($4 \cdot 10^{-6}$ M in 1,2-DCE) in the presence of increasing amounts of DIPEA.

The Stern-Volmer plot, reported in Figure S17, shows a linear correlation between the amounts of DIPEA and the ratio I_0/I. On the basis of the following Equation (Eq. 1), it is possible to calculate the Stern-Volmer constant K_{SV}.[22]

$$I_0/I = 1 + K_{SV}*[Q] \qquad \text{(Eq. 1)}$$

We calculated a Stern-Volmer quenching constant of 5.9 M^{-1} .

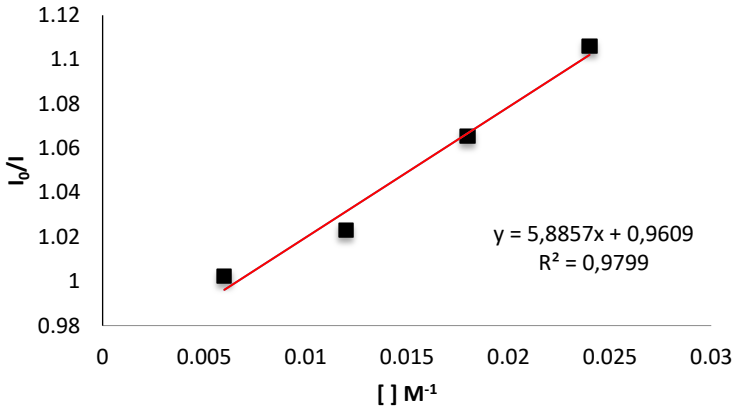

Figure 2.32. Stern-Volmer quenching plot using DIPEA as a quencher.

Stern-Volmer quenching studies with PPh_3

A 2M solution of PPh_3 was added *via* Hamilton syringe in portions 5 µL, 10 µL, 20 µL, 40 µL and between each addition the fluorescence spectra was measured. The emission intensity was recorded at 527 nm. After each addition, an absorption spectrum and an emission spectrum of the solution were recorded. The excitation wavelength was fixed at 390 nm (incident light slit regulated to 2 mm); the emission light was acquired from 410 nm to 650 nm (emission light slit regulated to 2 mm).

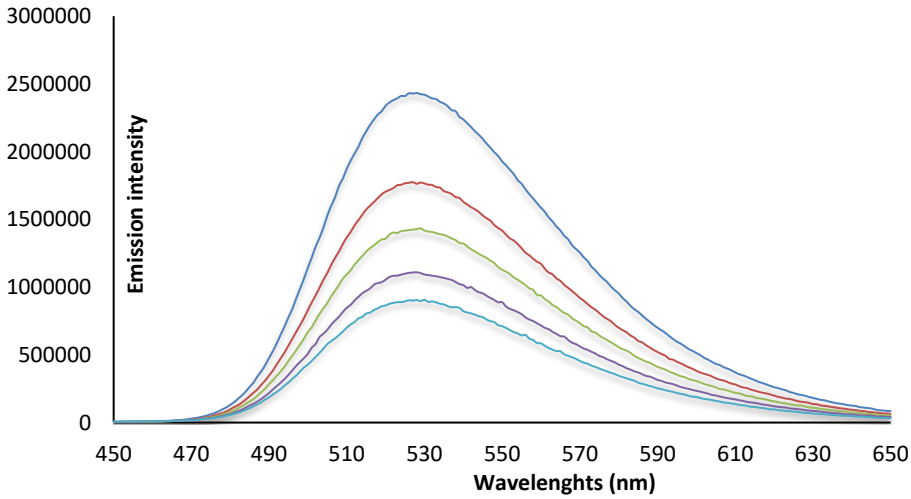

Figure 3.33. Quenching of the photocatalyst emission ($4 \cdot 10^{-6}$ M in 1,2-DCE) in the presence of increasing amounts of PPh_3.

The Stern-Volmer plot, reported in Figure **S19**, shows a linear correlation between the amounts of PPh_3 and the ratio I_0/I. On the basis of the following Equation (Eq. 1), it is possible to calculate the Stern-Volmer constant K_{SV}.[22]

$$I_0/I = 1 + K_{SV}*[Q] \qquad \text{(Eq. 1)}$$

We calculated a Stern-Volmer quenching constant of 45.3 M^{-1} .

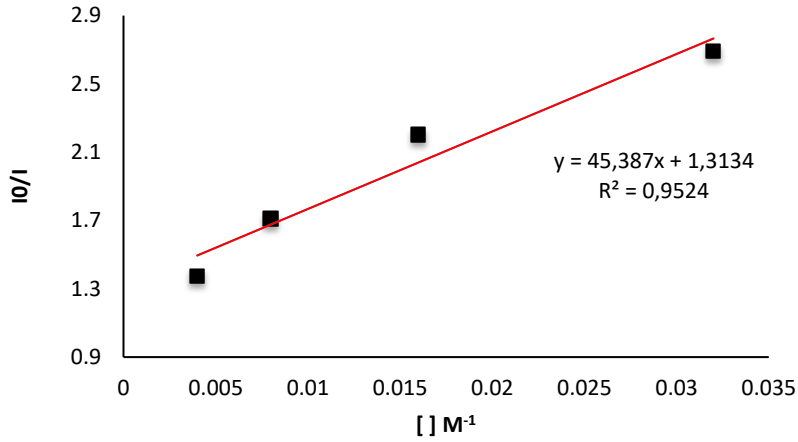

Figure 2.34. Stern-Volmer quenching plot using PPh_3 as a quencher.

*Stern-Volmer quenching studies with **2a** model*

A 0.43 M solution of *N*-fluorobenzamide **2a** and 15 µL of this stock solution were added to the solution of photocatalyst. Between each addition the fluorescence spectra was measured. The emission intensity was recorded at 527 nm. After each addition, an absorption spectrum and an emission spectrum of the solution were recorded. The excitation wavelength was fixed at 390 nm (incident light slit regulated to 2 mm); the emission light was acquired from 410 nm to 650 nm (emission light slit regulated to 2 mm).

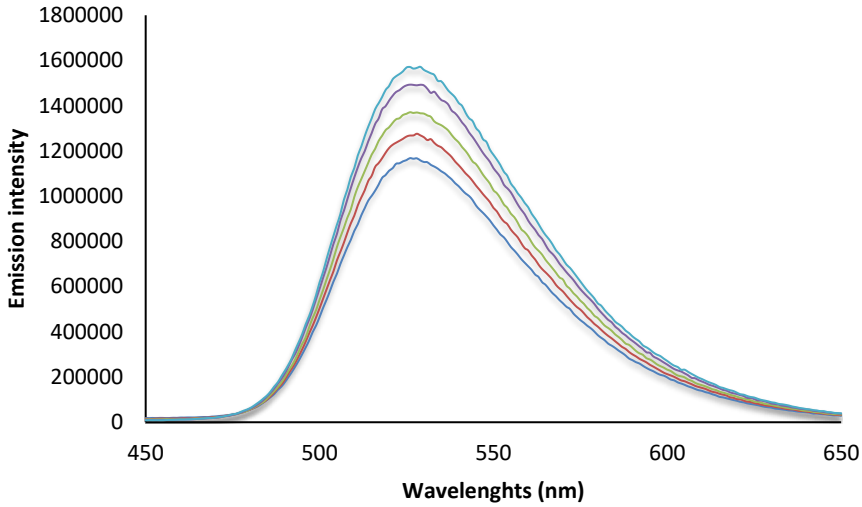

Figure 2.35. Quenching of the photocatalyst emission ($4 \cdot 10^{-6}$ M in 1,2-DCE) in the presence of increasing amounts of N-fluorobenzamide **2a**.

The Stern-Volmer plot, reported in Figure S21, shows a linear correlation between the amounts of NF and the ratio I_0/I. On the basis of the following Equation (Eq. 1) , it is possible to calculate the Stern-Volmer constant K_{SV}.[22]

$$I_0/I = 1 + K_{SV}*[Q] \qquad \text{(Eq. 1)}$$

We calculated a Stern-Volmer quenching constant of 18.8 M^{-1} .

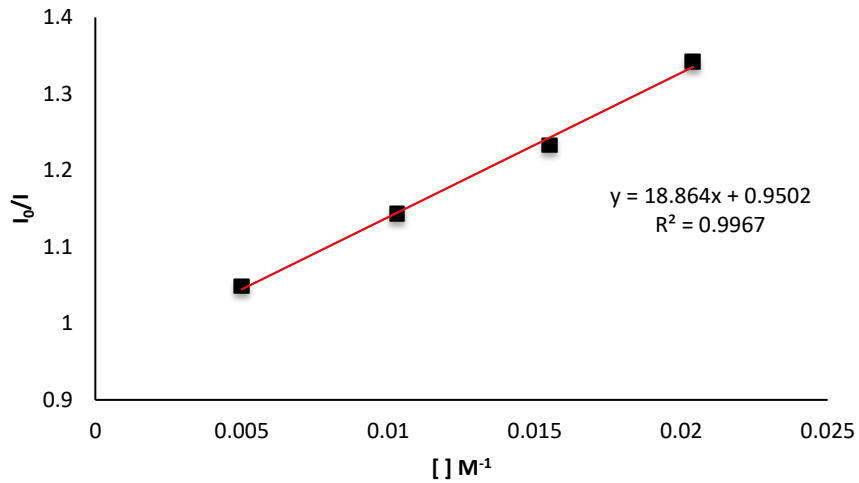

Figure 2.36. Stern-Volmer quenching plot using N-fluorobenzamide **2a** as a quencher.

Stern-Volmer quenching studies with 4-cyanopyridine ***1a***

A 1.22 M solution of 4-cyanopyridine **1a** and 10 μL of this stock solution were added to the solution of photocatalyst. Between each addition the fluorescence spectra was measured. The emission intensity was recorded at 527 nm. After each addition, an absorption spectrum and an emission spectrum of the solution were recorded. The excitation wavelength was fixed at 390 nm (incident light slit regulated to 2 mm); the emission light was acquired from 410 nm to 650 nm (emission light slit regulated to 2 mm).

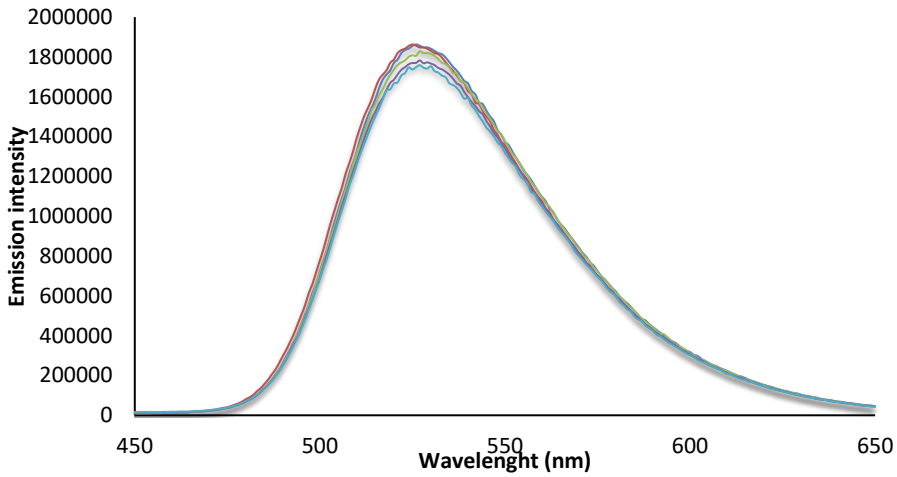

Figure 2.37. Quenching of the photocatalyst emission ($4 \cdot 10^{-6}$ M in 1,2-DCE) in the presence of increasing amounts of 4-cyanopyridine **1a**.

The Stern-Volmer plot, reported in Figure S23, shows a linear correlation between the amounts of NF and the ratio I_0/I. On the basis of the following Equation (eq. 1), it is possible to calculate the Stern-Volmer constant K_{SV}.[22]

$$I_0/I = 1 + K_{SV}*[Q] \qquad \text{(eq. 1)}$$

We calculated a Stern-Volmer quenching constant of 4.4 M^{-1} .

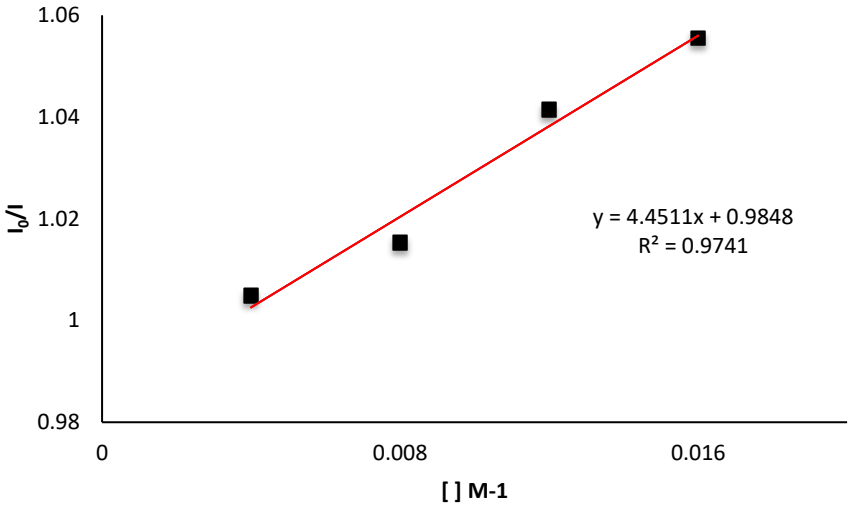

Figure 2.38. Stern-Volmer quenching plot using 4-cyanopyridine **1a** as a quencher.

Chapter III

Photochemical Organocatalytic Functionalization of Pyridines *via* Pyridinyl Radicals

Target

The direct site-selective functionalization of pyridines *via* a new mechanism based on pyridinyl radical intermediates.

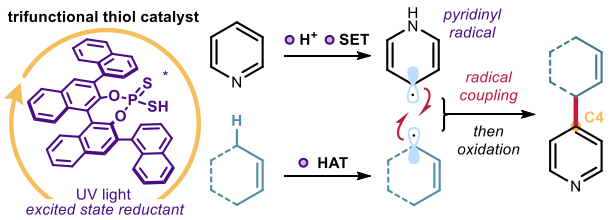

Tool

Exploiting the wide spectrum of catalytic properties of a thiol organocatalyst, which can perform three distinct activating roles: protonation of pyridine; single-electron reduction to afford a pyridinyl radical; and hydrogen atom abstraction for the generation of allylic radicals from simple alkenes, suitable for radical coupling.[1]

3.1 Introduction and Target of the Project

The success of pyridine-containing molecules in pharmaceuticals, agrochemicals, and materials has led to a continued need to improve and optimize current methodologies for their preparation. The modification of the pyridyl ring has gained significant attention, as it offers rapid access to more complex pyridine scaffolds that would be difficult to access otherwise. This late-stage functionalization approach grants access to libraries of pyridine-containing analogues for medicinal chemistry applications.

In the domain of radical chemistry, the main strategy to functionalize pyridines is the Minisci-type reaction, already discussed in Chapter I. A typical Minisci protocol involves acid activation of a pyridine (or other heteroarenes) to form a pyridinium ion **I** (Figure 3.1), which is then susceptible to addition of nucleophilic radicals **II**. However, the similar LUMO energies at more than one carbon of the activated pyridinium ion **I** often result in a mixture of products (mainly C4 and C2 alkylated pyridines, with a preference for the latter). Although

[1] The project discussed in this chapter has been conducted in collaboration with Emilien Le Saux, Igor A. Dmitriev, and Dr. Will C. Hartley. I was involved in the investigation of the reaction scope and in the mechanistic elucidation. This study has been published: Le Saux, E.; Georgiou, E.; Dmitriev, I. A.; Hartley, W. C.; Melchiorre, P. "Photochemical Organocatalytic Functionalization of Pyridines *via* Pyridinyl Radicals" *J. Am. Chem. Soc.* **2023**, *145,* 47–52.

the Minisci reaction remains a powerful approach, the lack of regioselectivity makes the purification of the products often challenging. This strategy is therefore unattractive for industrial applications and challenging for medicinal chemistry.

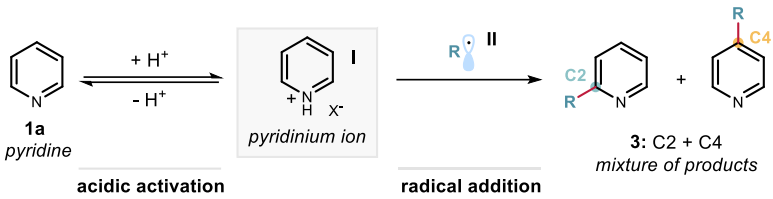

Figure 3.1. The Minisci reaction and the associated regioselectivity challenge.

This limitation in regioselectivity prompted us to look into new radical-based strategies that allow the site-selective functionalization of native pyridines. Specifically, the target of this project was to exploit the underexplored reactivity of pyridinyl radical intermediates **III** for the functionalization of pyridines **1** and other azaarenes using C-H substrates **2** (Figure 3.2).

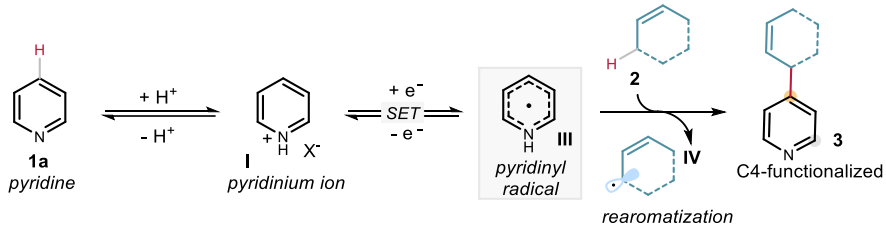

Figure 3.2. Pyridinyl radical-mediated C-H functionalization of pyridines.

This Chapter details how this design plan for a new radical functionalization of pyridines was developed. The process exploits the reactivity of pyridinyl radicals **III**, formed upon protonation of the native pyridine and sequential single-electron transfer (SET) reduction of the pyridium ion **I**. The final product is formed by radical coupling between the pyridinyl intermediate **III** and an allylic radical **IV**, generated from allylic C–H bonds, followed by rearomatization. Products **3** are obtained with good to complete regioselectivity, leading to the less common alkylation at the C4 carbon. This protocol for pyridine functionalization resulted in a regioselective outcome that deviated from the classical Minisci chemistry, as the major product formed was the C4-adduct instead of the typically preferred C2 isomer. The net process couples two unsubstituted substrates *via* activation of the corresponding C−H bonds on each reaction partner.

The following sections discuss the classical pathways available for the direct functionalization of pyridines, along with their limitations, and the scientific background pertinent to the development of our method.

3.1.1 Direct C-H functionalization of pyridines with C4 selectivity

Regioselective functionalization of pyridines and other azaarenes is highly desirable. Control over the reactivity of a specific position of the pyridine ring is however challenging. Classic methodologies result in a mixture of regioisomers. Selectivity is gained at the expense of additional steps to direct the reactivity toward a specific C−H bond. Achieving C4 functionalization generally requires three steps. First, pyridine **1a** is activated by reacting the nitrogen with an electrophile to form a pyridinium salt **6**, which results in the electrophilic activation of the ring system (Figure 3.3). Then, upon addition of the nucleophile, a dihydropyridine intermediate **7** is formed. A final oxidation step leads to the rearomatized pyridine product **3**.

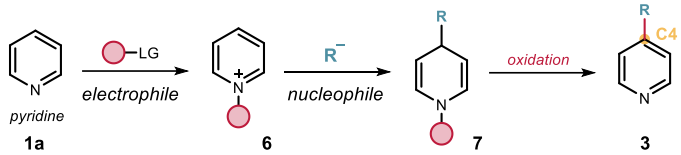

Figure 3.3. Stepwise C4-selective functionalization of pyridines.

Using this approach, Comins *et al.* reported the C4-selective functionalization of *(S)*-nicotine **4** using organocuprate reagents (Scheme 3.1).[2] *(S)*-Nicotine **4** was activated through reaction with pivaloyl chloride **5** to form the corresponding *N*-acyl pyridinium salt **6a**. Addition of the preformed cuprates (*via* a reaction of Grignard reagents with copper bromide) took place at the C4 position of the pyridinium salt **6a**, resulting in the dihydropyridine adduct **7a**. Treatment with elemental sulfur afforded the desired product **8** through rearomatization.

[2] Comins, D. L.; King, L. S.; Smith, E. D.; Fevier, F. C. "Synthesis of C-4 Substituted Nicotine Derivatives *via* an *N*-Acylpyridinium Salt of (*S*)-Nicotine" *Org. Lett.* **2005**, *7*, 5059−5062.

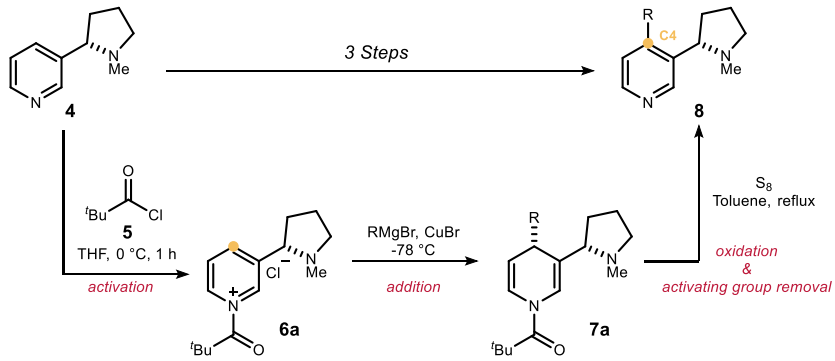

Scheme 3.1. 3-step-strategy for the C4-functionalization of *(S)*-nicotine with organocuprates.

C4-Selective perfluoroalkylation has been achieved by Kanai *et al.* (Scheme 3.2.).[3] Pyridine **1** was first activated by coordination to a bulky borane Lewis acid with the pyridine nitrogen, which also sterically shielded the C2 and C3 positions. In the meantime, a mixture of *tetra*butylammuniun difluorotriphenylsilicate (TBAT) and trimethyl(trifluoromethyl)silane (Me_3SiCF_3) generated a trifluoromethyl anion *in situ*. Its selective attack at the C4 position of the activated salt **9** resulted in a dihydropyridine intermediate **10**, which was oxidized upon treatment with *bis*(trifluoroacetoxy)iodobenzene ($PhI(CO_2CF_3)_2$) to afford the trifluoromethylated pyridine **11**. The major regioisomers obtained were C4-perfluoroalkylated pyridines, although a mixture with C2 and C6-adducts was also formed.

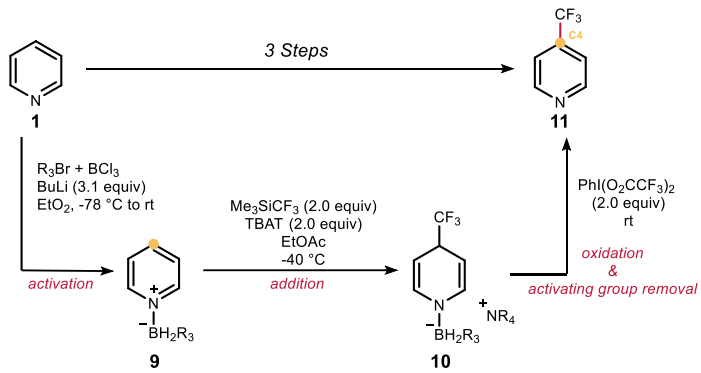

Scheme 3.2. 3-step-strategy for the C4-selective perfluoroalkylation using perfluorosilane reagents.

More recently, another method to obtain C4 functionalized pyridines was reported using silylium catalysis (Scheme 3.3).[4] In this study, a silyl ion acted as the active intermediate upon

[3] Nagase, M.; Kuninobu, Y.; Kanai, M. "4-Position-Selective C–H Perfluoroalkylation and Perfluoroarylation of Six-Membered Heteroaromatic Compounds" *J. Am. Chem. Soc.* **2016**, *138*, 6103−6106.
[4] Obradors, C.; List, B. "Azine activation *via* silylium catalysis" *J. Am. Chem. Soc.* **2021**, *143*, 6817−6822.

in situ formation from a Brønsted acid precatalyst (^{Ph}PADI), which triggered protodesilylation of a silyl ketene acetal **12**. The key for efficiency was the acidity of ^{Ph}PADI. The transformation was performed in a one pot (two-step) process, since oxidation of the *N*-silyldihydropyridine intermediate **13** by DDQ was required to restore aromaticity.

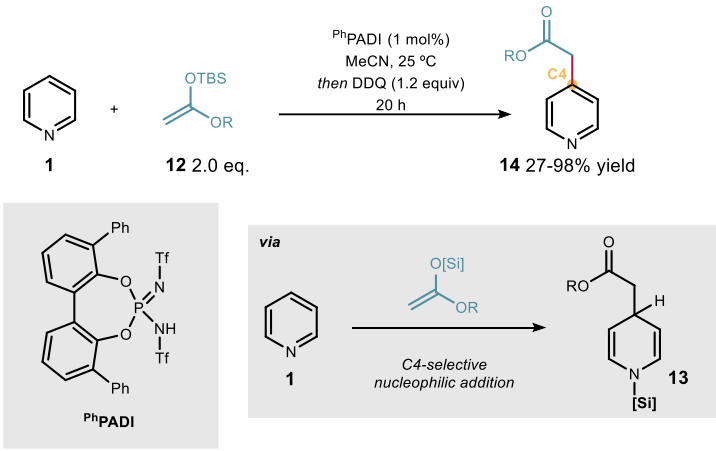

Scheme 3.3. C4-functionalization with silyl ketene acetals under silyl catalysis.

One-step protocols for the C4-selective functionalization of pyridines were achieved under nickel/Lewis acid catalysis. T.-G. Ong *et al.* developed a bimetallic nickel/aluminum method for the alkenylation of pyridines and quinolines through C-H activation (Scheme 3.4a).[5] Triethylaluminium acted as a Lewis acid, coordinating the Lewis-basic nitrogen of the pyridine moiety. An amino-linked *N*-heterocyclic carbene (NHC) ligand **L1** was used to form a η^2,η^1 -pyridine Ni(0)-Al(III) complex in presence of Ni(cod)$_2$ and the pyridine substrate **1**. The proposed mechanism followed an oxidative addition, insertion of the alkyne moiety **15** and a final reductive elimination sequence to deliver the final product **16** with C4:C3 selectivity in a 3.3:1 ratio. Nakao *et al.* improved the selectivity in a similar transformation (Scheme 3.4b).[6] Specifically, the C4-alkylation of pyridines **1** with alkenes **17** was achieved using a bulkier Lewis acid. Methylaluminum *bis*(2,6-di-*tert*-butyl-4-methylphenoxide (MAD) coordinated the pyridine nitrogen and shielded the 2- and 3-positions, hampering reactivity. Therefore, the C-H activation happened at the 4-position of the pyridine using a NHC nickel catalyst formed from Ni(cod)$_2$ and the IPr **L2** ligand. Subsequent migratory

[5] Tsai, C.-C.; Shih, W.-C.; Fang, C.-H.; Li, C.-Y.; Ong, T.-G.; Yap, G. P. A. "Bimetallic Nickel Aluminun Mediated Para-Selective Alkenylation of Pyridine: Direct Observation of η2,η1-Pyridine Ni(0)−Al(III) Intermediates Prior to C−H Bond Activation" *J. Am. Chem. Soc.* **2010**, *132*, 11887−11889.

[6] Nakao, Y.; Yamada, Y.; Kashihara, N.; Jiyama, T. "Selective C-4 Alkylation of Pyridine by Nickel/Lewis Acid Catalysis" *J. Am. Chem. Soc.* **2010**, *132*, 13666−13668.

insertion across an alkene **17**, followed by reductive elimination, delivered the alkylated pyridines **18** with exclusive C4-selectivity, although as mixtures of branched and linear isomers.

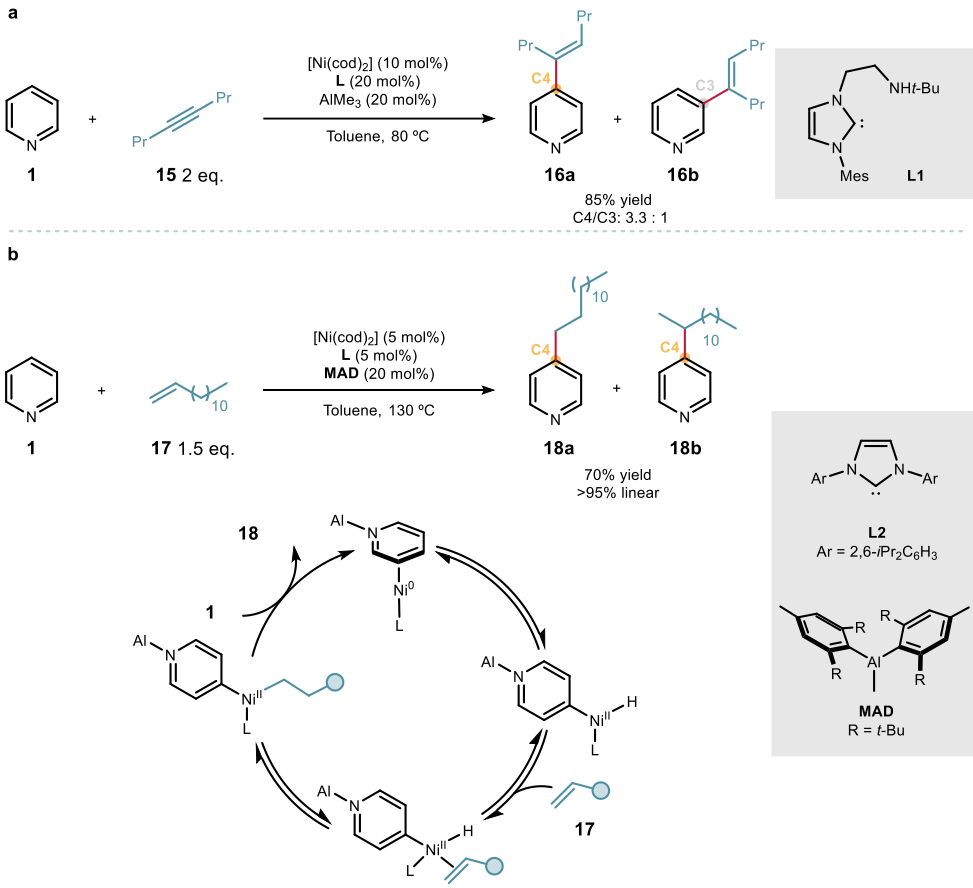

Scheme 3.4. Nickel/Lewis acid dual catalysis for the C4-selective alkenylation and alkylation of pyridines.

Another transition-metal catalyzed protocol for the C4-alkylation of pyridines using alkenes was reported by Kanai and co-workers.[7] The method relied on a catalytic nucleophilic addition-rearomatization sequence under cobalt catalysis (Scheme 3.5). Reaction of cobalt(II) bromide ($CoBr_2$) and lithium triethylborohydride ($LiBEt_3H$) resulted in the formation of a cobalt-hydride [Co-H] (**V**). A subsequent hydrometallation step between the substituted alkene **19** with [Co-H] afforded a reactive alkyl-cobalt species (**VI**). Nucleophilic addition to pyridine **1** and rearomatization by release of [Co-H] (without oxidation) afforded

[7] Anduo, T.; Saga, Y.; Komai, H.; Matsunaga, S.; Kanai, M. "Cobalt-Catalyzed C4-Selective Direct Alkylation of Pyridines" *Angew. Chem. Int. Ed.* **2013**, *52*, 3213−3216.

alkylpyridine **20** with high C4 selectivity. Although this methodology showed high selectivity towards the 4-position, its applicability was restricted to mono-substituted pyridines as the only tolerated substrates. In addition, and in analogy to the previous report from Nakao *et al.*, a mixture of branched and linear products was obtained.

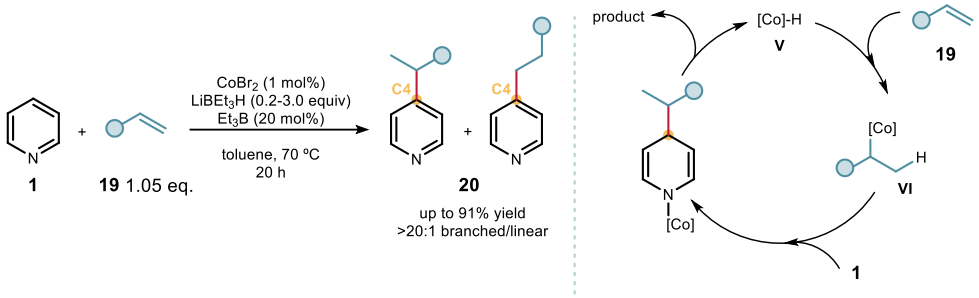

Scheme 3.5. C-4-alkylation of pyridines through cobalt-hydride [Co-H] catalysis.

Within the radical domain, a Minisci-type reaction was developed by Baran *et al.* to achieve selective C4 functionalization of pyridines.[8] The reported methodology relied on the installation of maleate-derived groups on the pyridine moiety **1** to sterically guide the reaction at the C4 position. The two-step synthesis of *N*-succinate pyridinium salts **22** offered several advantages, including the easy installation and removal of the directing group from fumarate **21**, high stability of the adduct, and complete C4 regioselectivity (Scheme 3.6.). The *N*-succinate pyridinium salt **22** was submitted to classic Minisci conditions. Specifically, various carboxylic acids served as radical precursors, using silver nitrate as catalyst and peroxydisulfate as the terminal oxidant. However, the traditional acid activation of the pyridine used in Minisci-type reactions was avoided. Subsequent deprotection with DBU resulted exclusively in C4-alkylated pyridines **24** in good yields. The regioselectivity of the method is attributed to the succinate group, which acted as a blocking group and shielded the C2 position.

[8] Choi, J.; Laudadio, G.; Godineau, E.; Baran, P. S. "Practical and Regioselective Synthesis of C-4-Alkylated Pyridines" *J. Am. Chem. Soc.* **2021**, *143*, 11927−11933.

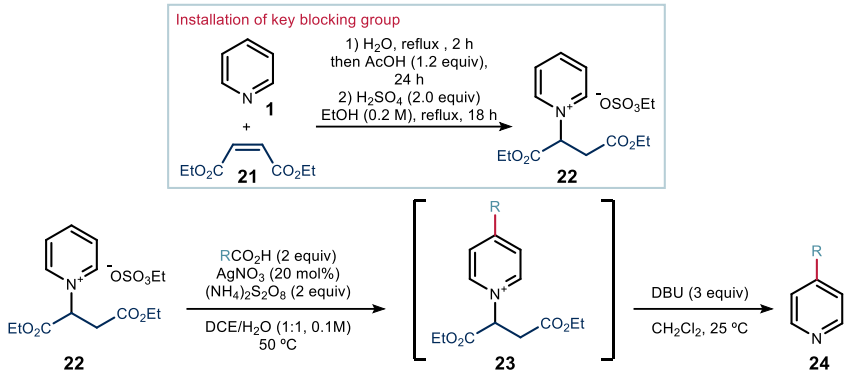

Scheme 3.6. C-4-alkylation of pyridines *via* Minisci-type addition on maleate-derived pyridinium salts.

3.1.2 N-Pyridinium salts for C-4 selective C-H functionalization of pyridines under visible-light irradiation

In recent years, the scientific community has shifted its efforts towards developing milder and more benign conditions that allow C4-selective C-H functionalization of pyridines. The use of *N*-pyridinium salts **25** in the presence of visible-light-activated photoredox catalysts allowed this issue to be addressed (Figure 3.4).[9] *N*-Pyridinium salts **25** exhibit enhanced reactivity compared to their parent pyridine analogues and have the ability to improve selectivity towards a specific position in Minisci alkylations. This is attributed to the bulky *N*-activating group which impedes the C2- and C6-positions, thereby promoting greater C4-regioselectivity.

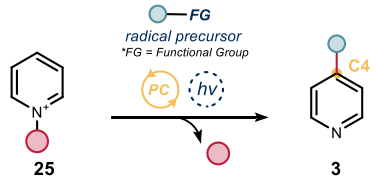

Figure 3.4. Photochemical activation of *N*-pyridinium salts for C-4-selective functionalization of pyridines.

[9] Kim, M.; Koo, Y.; Hong, S. "*N*-Functionalized Pyridinium Salts: A New Chapter for Site-Selective Pyridine C-H Functionalization *via* Radical-Based Processes under Visible Light Irradiation" *Acc. Chem. Res.* **2022**, *55*, 3043−3056.

In 2019, Hong *et al.* reported a photochemical method using *N*-aminopyridinium salts as bifunctional reagents for the difunctionalization of alkenes (Scheme 3.7).[10] Specifically, an aminopyridilation reaction of alkenes was achieved using *N*-(methyltosyl)aminopyridinium **25a** serving as both the amine and pyridine source. SET reduction of **25a** by the excited Eosin Y led to the cleavage of the N−N bond to form a nitrogen-centered radical **VII** (Scheme 3.7a). A favorable addition of the amino radical **VII** to electron rich alkenes **26** resulted in formation of an alkyl radical **VIII**. Radical addition of **VIII** to the electron deficient aminopyridinium **25a** in a Minisci-type fashion, followed by deprotonation, generated the C4-pyridine radical intermediate **X**. Finally, homolytic cleavage of the N−N bond afforded the desired C4-functionalized pyridine product **27** with simultaneous extrusion of the same amino radical **VII**, which could start a new catalytic cycle and propagate a radical chain mechanism.

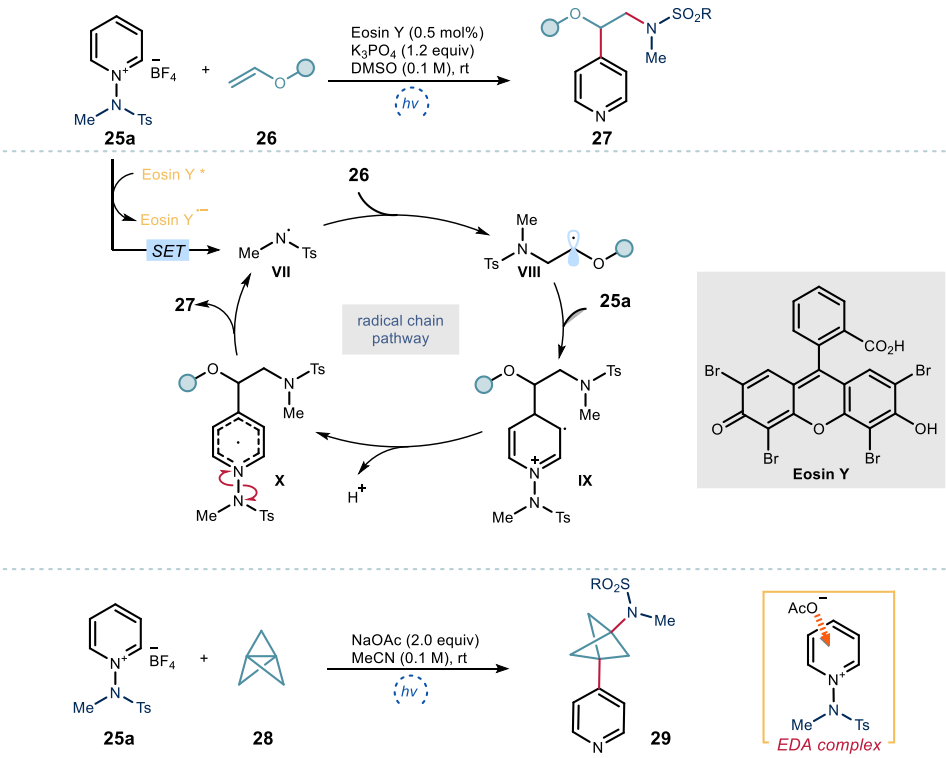

Scheme 3.7. Photochemical activation of *N*-aminopyridinium salts for aminopyridilation reactions.

[10] Moon, Y.; Park, B.; Kim, I.; Kang, G.; Shin, S.; Kang, D.; Baik, M.-H.; Hong, S. "Visible Light Induced Alkene Aminopyridylation Using N-Aminopyridinium Salts as Bifunctional Reagents" *Nat.Commun.* **2019**, *10*, 4117.

In a similar fashion, *N*-(methyltosyl)aminopyridinium **25a** was used as a bifunctional reagent to promote the synthesis of 1,3-aminopyridylated bicyclo[1.1.1]pentane (BCP) **29** upon ring-opening of propellanes **28** (Scheme 3.7b).[11] In this case, the activation of the aminopyridium **25a** was achieved through the formation of an electron donor-acceptor (EDA) complex with acetate, which triggered an intra-complex SET.

Photochemical EDA activation with aminopyridinium ions as the accepting substrates was also used to generate radicals from alkyl bromides and dihydropyridines. A protocol used an EDA complex formed between the aminopyridinium **25a** and the bromine anion (Scheme 3.8).[12] Alkyl radicals were then generated in the presence of super stoichiometric amounts of supersilane [$(TMS)_3SiH$], which acted as a halogen atom transfer (XAT) reagent to activate the alkyl bromide **30**.

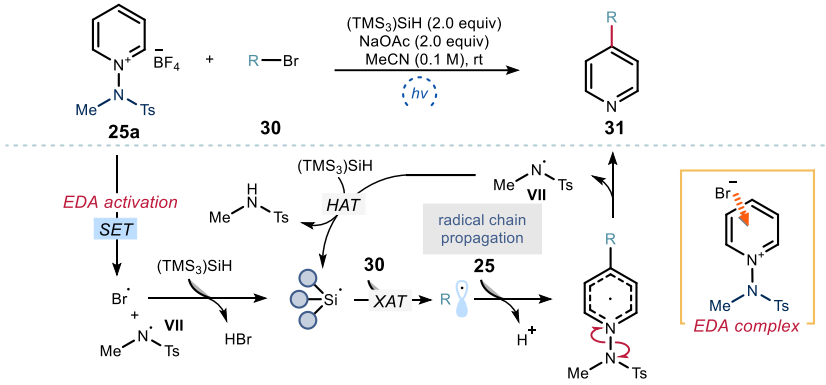

Scheme 3.8. EDA activation of *N*-aminopyridinium salts for C4-alkylatition of pyridines using alkylbromides.

In a second protocol, an EDA complex was formed between the aminopyridium ions **25a** and the dihydropyridine **30'** (Scheme 3.9).[13] An intra-complex SET triggered the alkyl radical formation upon C−C bond cleavage within the oxidized form of the dihydropyridine.

[11] Shin, S.; Lee, S.; Choi, W.; Kim, N.; Hong, S. "Visible-Light-Induced 1,3-Aminopyridylation of [1.1.1]Propellane with *N*-Aminopyridinium Salts" *Angew. Chem., Int. Ed.* **2021**, *60*, 7873−7879.
[12] Jung, S.; Shin, S.; Park, S.; Hong, S. "Visible-Light-Driven C4-Selective Alkylation of Pyridinium Derivatives with Alkyl Bromides" *J. Am. Chem. Soc.* **2020**, *142*, 11370−11375.
[13] Kim, I.; Park, S.; Hong, S. "Functionalization of Pyridinium Derivatives with 1,4-Dihydropyridines Enabled by Photoinduced Charge Transfer" *Org. Lett.* **2020**, *22*, 8730−8734.

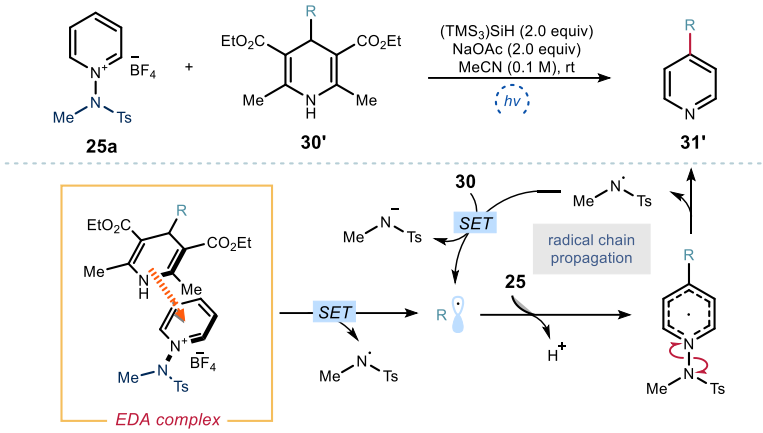

Scheme 3.9. EDA activation of *N*-aminopyridinium salts for C-4-alkylatition of pyridines using 1,4-DHPs.

In 2021, another methodology was developed for the C4-alkylation of pyridines, using unactivated alkanes **32** and an excited anthraquinone (AQ) catalyst (Scheme 3.10). [14] Under visible-light irradiation, AQ reached a triplet-excited state, which was able to abstract a hydrogen atom from various C−H bonds, affording alkyl radicals **XI**. The amidyl radical **VII**, generated upon radical addition to the pyridine substrate **25** and N−N bond cleavage, had a key role for the success of the transformation, since it acted as a reverse hydrogen atom transfer (RHAT) reagent, which regenerated the AQ catalyst. Moreover, the amidyl **VII** radical contributed to the radical chain propagation *via* direct HAT. This C4-alkylation of pyridines offered an important advance with respect to previous methods since the net process involved the formation of a C−C bond from two C−H bonds.

[14] Lee, W.; Jung, S.; Kim, M.; Hong, S. "Site-Selective Direct C-H Pyridylation of Unactivated Alkanes by Triplet Excited Anthraquinone" *J. Am. Chem. Soc.* **2021**, *143*, 3003−30.

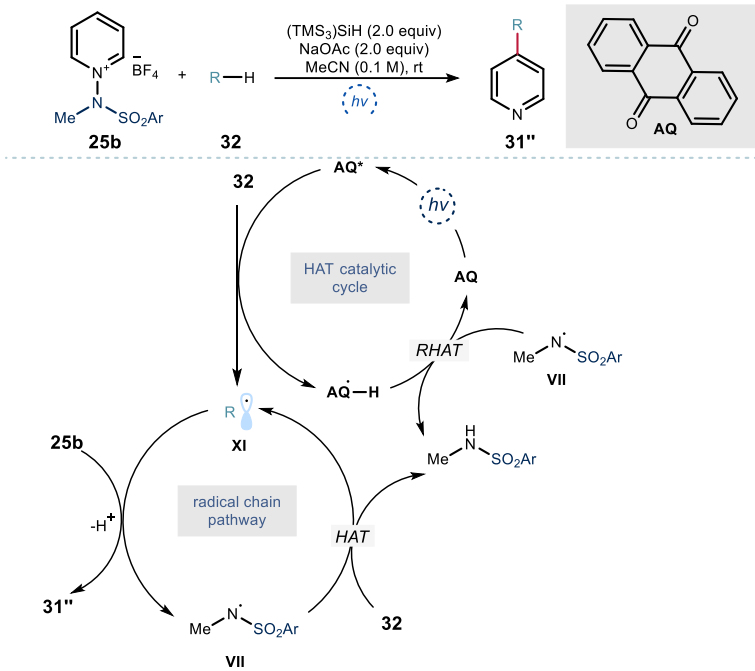

Scheme 3.10. *N*-Aminopyridinium salts for C-4-alkylatition of pyridines using unactivated hydrocarbons.

The approach of using *N*-aminopyridinium salts allowed for precise control over the C4 position in non-classical Minisci reactions, making it a promising strategy for the late-stage functionalization of bioactive molecules. However, one limitation is the requirement for prefunctionalization of the pyridine nitrogen, which involves multiple synthetic steps. Three steps are required for the blocking group installation: *i*) *N*-amination using hydroxylamine-*O*-sulfonic acid; *ii*) tosylation; and *iii*) methylation with Meerwein's salt (Scheme 3.11).

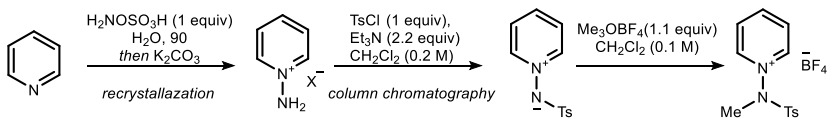

Scheme 3.11. Synthesis of the pyridine surrogates: *N*-aminopyridinium salts.

3.1.3 Pyridine radical intermediates

A complementary strategy for achieving site-selectivity in the functionalization of pyridines uses prefunctionalized pyridines to enable *ipso*-substitution reactions (approach discussed in Chapters I & II). Specifically, 4-cyanopyridines **33a** and 4-triphenyl phosphonium salts **33b** were shown to undergo SET reduction to generate pyridinyl radical anions **XII** (Figure 3.5). The functional groups installed at the C4 position guaranteed the regioselective outcome of

the transformation by performing two useful actions: *i*) stabilization of the radical anion resulting from SET reduction; and *ii*) acting as leaving groups.

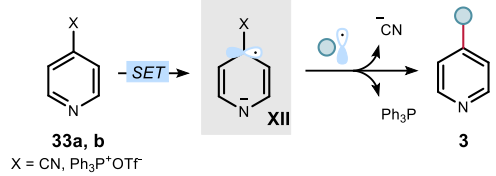

Figure 3.5. Pyridine radical intermediates for C4-functionalization.

Pyridinyl radicals are neutral open-shell species generated through SET reduction of pyridinium ions. There is a correspondent reactivity in nature: nicotinamide adenine dinucleotide cofactor (NADH/NAD$^+$) radicals (NAD$^\bullet$) have been reported as intermediates in certain biological processes, serving as SET donors (Figure 3.6a).[15] Titration calorimetry and electrochemistry studies revealed that the spin density of NAD$^\bullet$ was higher at the C4 position.[16] Outside of biological systems, pyridinyl radicals have been generated by a variety of methods including the use of sodium metal, electrochemical reduction, and photochemical reduction.[17] In 1973, pyridinyl radical intermediates were detected by electron paramagnetic resonance (EPR) spectroscopy, which allowed to define the hyperfine coupling constants and the electronic distribution within the pyridine core (Figure 3.6b).[18] Those experimental results showed a greater spin density at the C4 position in analogy to NAD$^\bullet$. From a reactivity standpoint, dimerization reactions were found to take place upon electrolysis of pyridinium salts, which afforded a mixture of dihydropyridine products (Figure 3.6c).[19] It was observed that the major dimeric product resulted from the coupling of the C4 localized radicals, unless this path was prevented by steric hindrance.

[15] (a) Carlson, B. W.; Miller, L. L. "Oxidation of NADH by Ferrocenium Salts, Rate-Limiting One-Electron Transfer" *J. Am. Chem. Soc.* **1983**, *105*, 7453−7454; (b) Powell, M. F.; Wu, J. C.; Bruice, T. C. "Ferricyanide Oxidation of Dihydropyridines and Analogues" *J. Am. Chem. Soc.* **1984**, *106,* 3850−3856.

[16] Zhu, X.-Q.; Li, H.-R.; Li, Q.; Ai, T.; Lu, J.-Y.; Yang, Y.; Cheng, J.-P. "Determination of the C4-H Bond Dissociation Energies of NADH Models and Their Radical Cations in Acetonitrile" *Chem. Eur. J.* **2003**, *9*, 871−880.

[17] Kosower, E. M. "Stable Pyridinyl Radicals" *Top. Curr. Chem.* **1983**, *112*, 117−162.

[18] a) Fessenden, R. W.; Neta, P. "ESR Spectra of Radicals Produced by Reduction of Pyridine and Pyrazine" Chem. Phys. Lett. **1973**, 18, 14−17. b) Alberti, A.; Guerra, M.; Pedulli, G. F. "Effect of Temperature and Isotopic Substitution on the NH Proton Hyperfine Splitting In 1-Hydropyridinyl Radicals" *J. Magn. Reson.* **1979**, *34*, 233−236. c) Itoh, M.; Nagakura, S. "The Electron Spin Resonance and Electronic Spectra Of 4-Substituted Pyridinyl Radicals" *Bull. Chem. Soc. Jpn.* **1966**, *39*, 369−375.

[19] Carelli, V.; Liberatore, F.; Casini, A.; Tortorella, S.; Scipione, L.; Di Rienzo, B. "On the regio- and stereoselectivity of pyridinyl radical dimerization" *New J. Chem.* **1998**, *22*, 999−1004. For a review: Patrick S. Mariano. "The photochemistry of iminium salts and related heteroaromatic systems" *Tetrahedron* **1983**, *39*, 3845-3879.

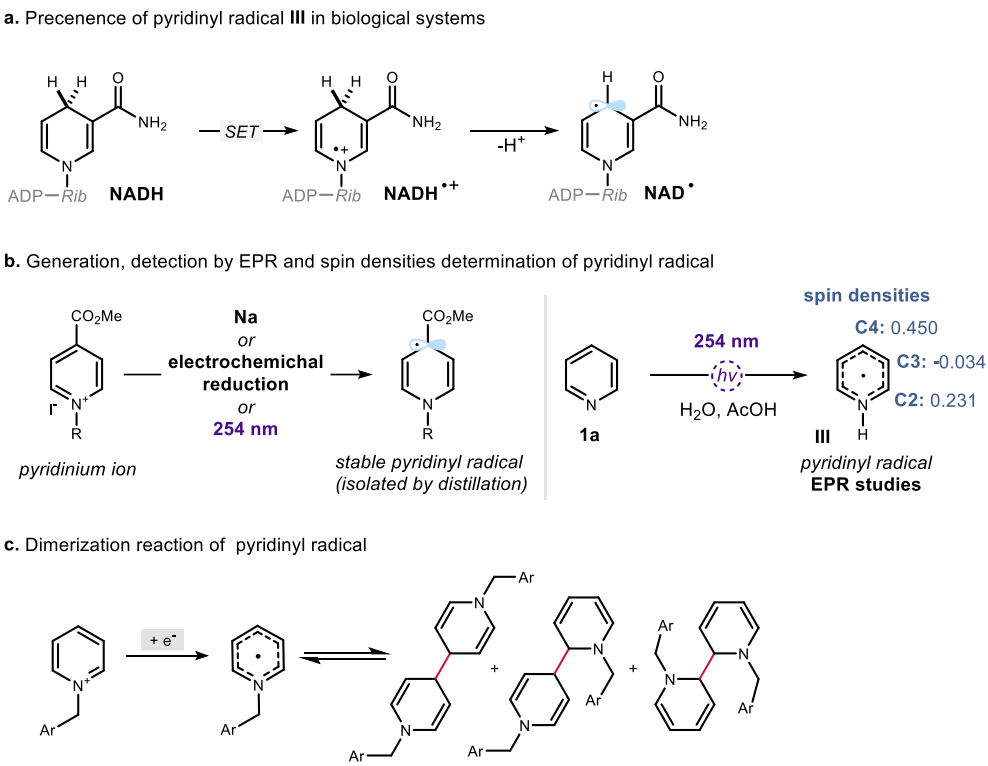

Figure 3.6. Pyridinyl radicals **III** **a.** in biological systems, **b.** their generation and detection, and **c.** dimerization reactions.

It is surprising that, to date, the reactivity of pyridinyl radicals has only been exploited as a one-electron shuttle for the catalytic reduction of carbon dioxide and has not been used further in synthetic applications.

3.2 Target of the Project

In order to sustain the continued success of pyridine-containing molecules in pharmaceuticals, agrochemicals, materials, and other sectors of the chemical industry, new methodologies must be developed to overcome current limitations. Previous sections have provided an overview of recent developments and their contributions towards this goal. However, an even more desirable scenario would involve achieving high regioselectivity under mild conditions without the need for pre-functionalization of the pyridine substrates. We wondered if pyridinyl radicals could be used to achieve this target and functionalize unactivated pyridines with high selectivity.

One of our groups' main research lines is to develop new methodologies based on the photo-activation of electron donor-acceptor (EDA) complexes[20] and the direct photoexcitation of organic catalysts and intermediates, which can be useful to elicit redox pathways and generate radicals.[21] In 2022, our group introduced dithiophosphoric acids (DTPAs, **A**) as catalytic donors for EDA complex photochemistry (Figure 3.7).[22] Upon photoinduced intra-complex SET, a thiyl radical was formed, which acted as a hydrogen atom transfer (HAT) abstractor to activate allylic C−H bonds.[23] Radical coupling of the two radicals, generated *via* sequential SET and HAT mastered by the catalyst, led to the direct benzylation of allylic C−H bonds (products **35**).

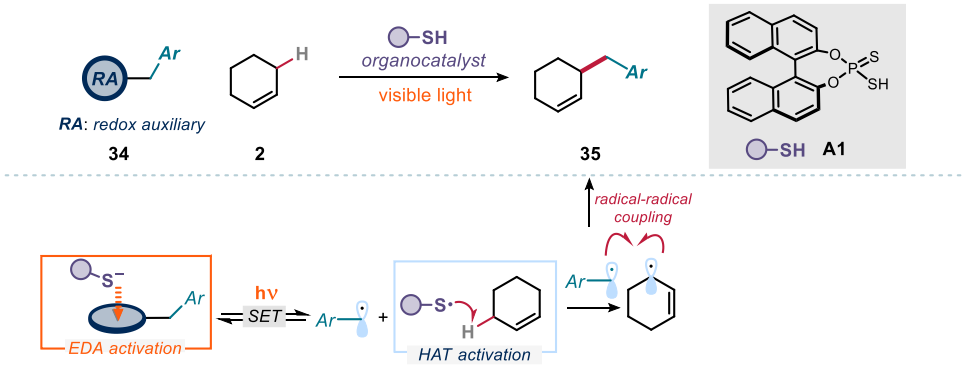

Figure 3.7. Dithiophosporic acid **A1** as electron donor in EDA complex and application in the benzylation of allylic C−H bonds.

The radical allylation of heretoarenes is another challenging transformation with only one reported precedent example in the literature.[24] The methodology made use of semiconductor quantum dots under visible light irradiation to generate allylic radicals **IV** from alkenes **2** through a SET oxidation/deprotonation step (Scheme 3.12). The proposed catalytic cycle was

[20] Crisenza, G. E. M.; Mazzarella, D.; Melchiorre, P. "Synthetic Methods Driven by the Photoactivity of Electron Donor−Acceptor Complexes" *J. Am. Chem. Soc.* **2020**, *142*, 5461−5476.
[21] a) Silvi, M., Arceo, E., Jurberg, I. D., Cassani, C., Melchiorre, P. "Enantioselective Organocatalytic Alkylation of Aldehydes and Enals Driven by the Direct Photoexcitation of Enamines" *J. Am. Chem. Soc.* **2015**, *137*, 6120; b) Silvi, M.; Verrier, C.; Rey, Y. P.; Buzzetti, L; Melchiorre, P. "Visible-light Excitation of Iminium Ions Enables the Enantioselective Catalytic β-Alkylation of Enals" *Nat. Chem.*, **2017**, *9*, 868; c) Silvi, M., Melchiorre, P., "Enhancing the Potential of Enantioselective Organocatalysis with Light", *Nature* **2018**, *554*, 41.
[22] Le Saux, E.; Zanini, M.; Melchiorre, P. "Photochemical Organocatalytic Benzylation of Allylic C-H Bonds" *J. Am. Chem. Soc.* **2022**, *144*, 1113−1118.
[23] Cuthbertson, J. D.; MacMillan, D. W. C. "The Direct Arylation of Allylic sp^3 C-H Bonds *via* Organic and Photoredox Catalysis" *Nature* **2015**, *519*, 74−77.
[24] Huang, C.; Qiao, J.; Ci, R.-N.; Wang, X.-Z.; Wang, Y.; Wang, J.H.; Chen, B.; Tung, C.-H.; Wu, L.-Z. "Quantum Dots Enable Direct Alkylation and Arylation of Allylic C(sp^3)-H Bonds with Hydrogen Evolution by Solar Energy" *Chem* **2021**, *7*, 1244−1257.

closed with reduction of the protons with simultaneous liberation of hydrogen gas. The formation of the new C−C bond, presumably by addition of the allylic radical into the heteroarenes **1**, was not detailed by the authors. The reaction scope of this transformation included isoquinolines, with only a few examples of pyridine substrates.

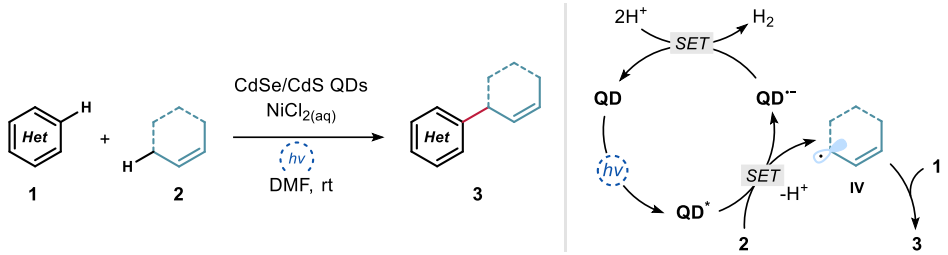

Scheme 3.12. Quantum dots-enabled allylation of heteroarenes.

The target of my project was to develop a new methodology for the selective functionalization of pyridines, which would circumvent the need of pre-installed functionalities exploiting the properties of a thiol catalyst.

Specifically, we sought that the dithiophorsphoric catalyst **A1**, upon protonation of pyridine, would form a photoactive ion pair (Figure 3.8). Photoexcitation would trigger an intra-complex SET event to generate a pyridinyl radical intermediate **III** along with a sulfur centered radical **A•** from the catalyst. A subsequent HAT abstraction of weak C−H bonds in substrates **2a** from the thiyl radical **A•** would result in carbon-centered radicals. A radical coupling between the two formed radicals would furnish a new C−C bond. The reported literature discussed in section 3.1.3 on the spin density of pyridinyl radicals suggested that the radical coupling step could selectively occur at the C4-position.

Eventually, our design plan turned out not to be feasible; in particular the formation of the supposed EDA complex was not possible. Yet, the following section details how we could successfully develop the target transformation.

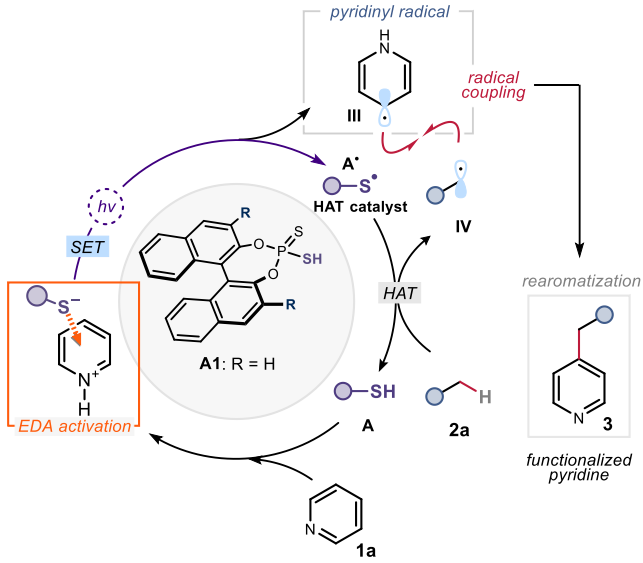

Figure 3.8. Envisioned catalytic cycle with a dithiophosporic acid mastering three catalytic tasks.

3.3 Results and Discussion

3.3.1 Discovery of the reaction and optimization of the reaction conditions

Based on our initial design, we started our investigation by choosing simple pyridine **1a** and cyclohexene **2a** as the model substrates using dithiophosphoric acid (DTPA) **A1** as the catalyst (20 mol%) and acetone as the solvent. Irradiation with blue light (λ = 455 nm), usually sufficient to excite EDA complexes, gave no product (Table 3.1). We continued our investigations by screening different light sources. Irradiation at λ = 365 nm eventually afforded the desired product **3a** in 17% yield. Noteworthy, the regioisomeric ratio of the obtained mixture was 8:1 in favor of the C4-functionalized pyridine product. Encouraged by this interesting result, we sought to get more insights on the observed reactivity by understanding which was the operating photoactive species.

Table 3.1. Reaction discovery.

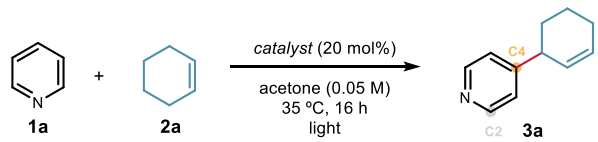

entry	catalyst	light	additive	yield (%)	**3a** (*C4:C2*)
1	**A1**	455 nm	-	n.d.	n.d.
2	**A1**	365 nm	-	17	8:1

Reaction performed on a 0.2 mmol scale using 10 equiv. of **2a** under light irradiation. Yield of **3a** determined by ^{1}H NMR analysis of the crude reaction mixtures using trichloroethylene as the internal standard.

We recorded the absorption spectra of the individual reaction components, of a mixture of catalyst **A1** in the presence of $NaHPO_4$ (to obtain the deprotonated thiolate form **A1**$^-$, purple line), and of a 1:1 mixture of **A1** and pyridine **1a** (green line, Figure 3.9). The spectrum of the **A1** + **1a** mixture displayed the same absorption as **A1**$^-$, thus excluding the formation of an EDA complex. However, these studies also revealed the ability of the deprotonated dithiophosphoric acid (thiolate **A1**$^-$) to absorb in the near-UV region. This observation led us to reconsider our initial reaction design, since thiolate **A1**$^-$ could directly absorb light, leading to a highly reducing excited state [**A**$^-$]* which could be responsible for the SET activation of the pyridinium ion **I**, generated upon protonation of **1a** from the catalyst.

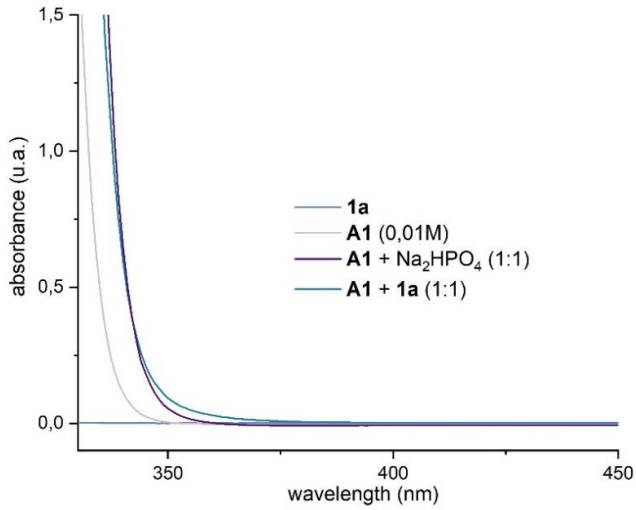

Figure 3.9. Optical absorption spectra of the individual substrates and their combinations.

In the revised catalytic cycle (Figure 3.10.), the excited photocatalyst [**A**$^-$]* would trigger an SET reduction of the pyridinium ion **I** resulting in the formation of pyridinyl radical intermediate **III** and the sulfur-centered radical **A**$^\bullet$. Subsequent HAT from cyclohexene **2** would afford an allylic radical **IV**. Radical coupling of **III** and **IV**, followed by a rearomatization step, would yield the desired product **3**.

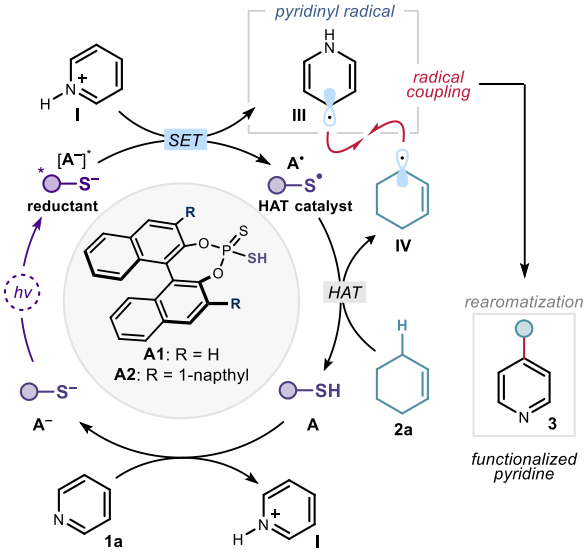

Figure 3.10. Revised catalytic cycle involving the direct photoexcitation of dithiophosphoric acid anion **A**$^-$.

With this new mechanistic picture in mind, we sought to optimize the reaction conditions. The screening of various solvents proved unsuccessful, with a 17% yield of the product **3a** in acetone remaining the best result. Our efforts then focused on the addition of various acidic and basic additives. The addition of acetic acid and trifluoroacetic acid was detrimental, leading to a loss of reactivity (entry 1 and 2, Table 3.2). Basic additives resulted in an improvement of the yield of product **3a**. The inorganic base K_3PO_4 and the organic base diisopropylethylamine (DIPEA) gave no reaction (entries 3,4), while the addition of 2,4,6-collidine led to an improved yield of 41% (entry 5). The bulkier 2,6-di-*tert*butyl-4-methyl-pyridine resulted in a slightly decreased yield of 35% (entry 6).

Table 3.2. Screening of acidic and basic additives.

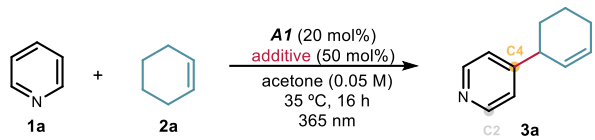

entry	additive	yield (%)
1	AcOH	0
2	TFA	0
3	K_3PO_4	0
4	DIPEA	0
5	2,4,6-collidine	41
6	2,6-^{t}Bu-4-Me-pyridine	35

Reaction performed on a 0.2 mmol scale using 10 equiv. of **2a** under irradiation with a 365 nm EvoluChem LED spotlight. Yield of **3a** determined by ^{1}H NMR analysis of the crude reaction mixtures using trichloroethylene as the internal standard.

We continued the optimization by screening various (di)thiophosphoric acids (Figure 3.11). A series of (di)thiophosphoric acids were synthesized and subjected to the reaction conditions. First, 1,1-diaryl-substituted thiophosphoric acids were screened (**A2**-**A6**): catalyst **A2** (aryl = naphthyl) offered the best result, since **3a** was formed in 67% yield mad with 6:1 C-4/C-2 selectivity. Replacing the aryl group to a trifluoromethyl group at the C1 position of the catalyst (**A7**) led to a significant decrease in yield. Additional attempts to further improve the yield with thiophosphoric acid **A8** and thiophosphoramide **A9** were unsuccessful. Interestingly, **3a** could be obtained as the only positional isomer upon purification by column chromatography. The protocol in the presence of catalyst **A2** was equally efficient at an increased scale of 1.0 mmol, giving **3a** in 68% yield (81.2 mg, 51% of the isolated product).

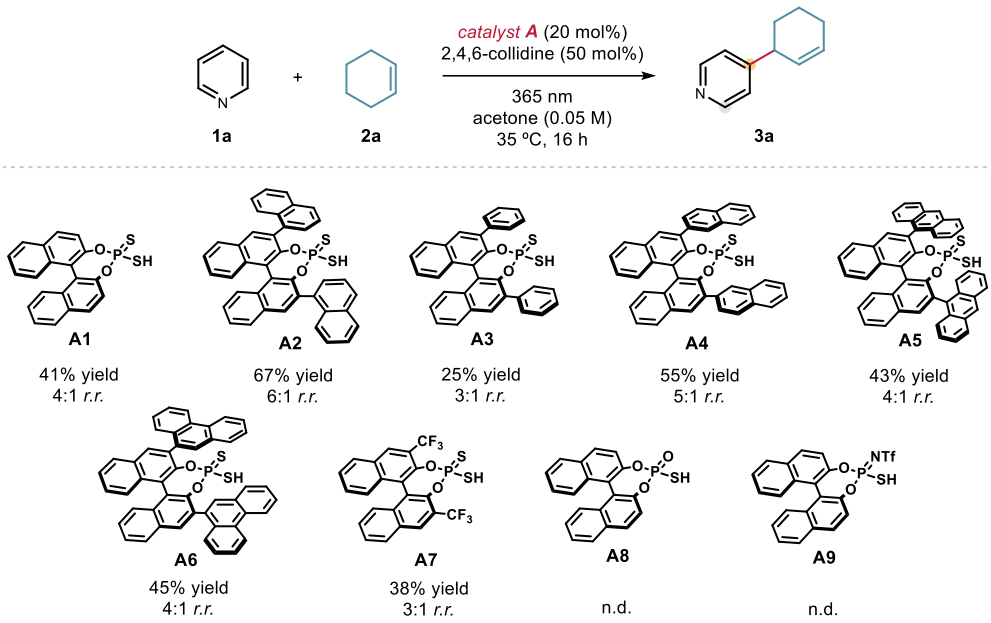

Figure 3.11. Screening of catalysts for the C-4 allylation of pyridine **1a**. Yields and regioisomeric ratios were determined by ^{1}H NMR analysis of the crude mixtures. r.r. refers to the C4/C2 ratio in **3a**. n.d.: not detected. Catalysts **A1–9** were synthesized as described in the experimental section.

Alternatively to the direct photoexcitation method, the reaction could proceed with high efficiency (**3a** formed in 79% yield, 4:1 regioisomeric ratio of C4:C2) under blue light irradiation using $[Ir(dtbbpy)(ppy)_2]PF_6$ as an exogenous photocatalyst (Table 3.3, entry 5). This result was obtained upon screening of various photoredox catalysts in the presence of catalyst **A2** under visible light irradiation (blue LEDs). Finally, control experiments showed that the catalyst and light irradiation were required for the reaction in order to proceed.

Although the inclusion of a photoredox catalyst led to a higher yield, we considered the approach based on the direct excitation of the dithiophosphoric acid catalyst **A2** (UV light irradiation) to be conceptually more interesting. Thus, the optimized conditions (Figure 3.11) with catalyst **A2** under UV light irradiation (no photoredox catalyst) were used for investigating the reaction scope.

Table 3.3. Screening of photoredox catalysts.

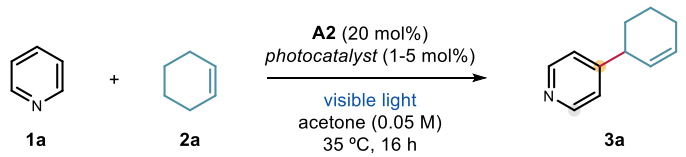

entry	photocatalyst	yield **3a** (%)[a]	C4:C2[a]
1	4CzIPN	51	2:1
2	$Ir(ppy)_3$	*n.d.*	-
3	Mes-Acr$^+$BF$_4^-$	*n.d.*	-
4	$(Ir[dF(CF_3)ppy]_2(dtbbpy))PF_6$	23	4:1
5	**$(Ir(ppy)_2dtbbpy)PF_6$**	**79 (65)**	**4:1 (> 20:1)**
6[b]	$(Ir(ppy)_2dtbbpy)PF_6$	*n.d.*	-

Reaction performed on a 0.2 mmol scale using 10 equiv. of **2a** under irradiation with a 455 nm 14 W LEDs strip. [a]Yields and ratios of regioisomers of **3a** were determined by ^{1}H NMR analysis of the crude reaction mixtures using trichloroethylene as the internal standard. Yields and regioisomeric ratio of isolated **3a** are reported in parentheses. [b]No **A2**. *n.d.:* not detected.

3.3.2 Mechanistic investigation

We first performed further investigations to obtain more insights into the reaction mechanism. We initially focused on the electrochemical characterization of pyridine **1a** *via* cyclic voltammetry (CV, Figure 3.12) which revealed no reduction wave upon application of potentials up to -2.5 V vs. Ag^+/Ag in MeCN.

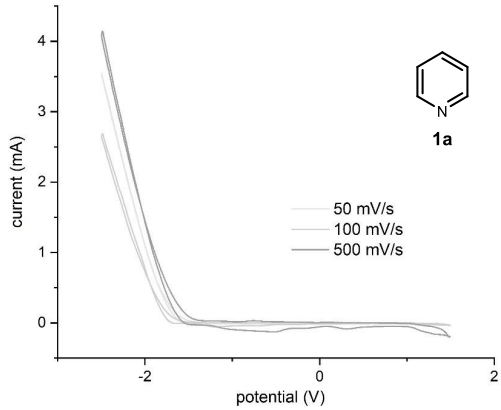

Figure 3.12. Cyclic voltammogram for pyridine **1a** [0.025M] in [0.1 M] $TBAPF_6$ in CH_3CN. Measurement started by reduction from 0 to -2.5 V and finishing at 0 V. Platinum disk working electrode, Ag/AgCl (NaCl 3 M) reference electrode, Pt wire auxiliary electrode. No reduction wave was observed.

The pyridine trifluoromethyl acetate salt **1a·TFA** showed a completely different electrochemical profile (Figure 3.13). A reversible reduction wave was obtained by the CV measurement of **1a·TFA**, with a reduction taking place at about -0.6 V. This observation indicated an easy reduction of the protonated pyridine. In addition, the acquired well-shaped reversible spectrum was indicative of a certain kinetic stability of the resulting pyridinyl radical **III**.[25]

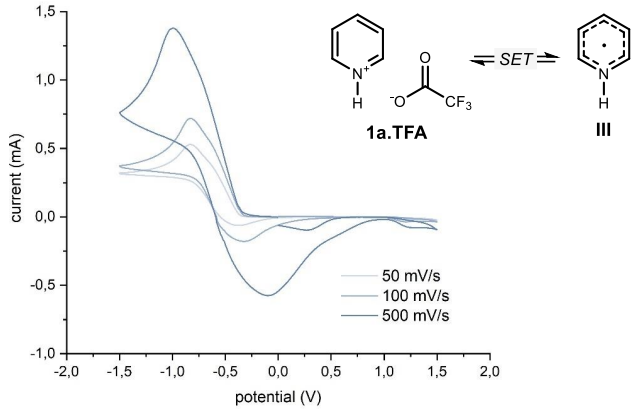

Figure 3.13. Cyclic voltammogram for **1a·TFA** [0.025M] in [0.1 M] $TBAPF_6$ in CH_3CN. Measurement started by reduction from 0 to -1.5 V and finishing at 0 V. Platinum disk working electrode, Ag/AgCl (NaCl 3 M) reference electrode, Pt wire auxiliary electrode. One reversible reduction wave observed at -0.6 V.

In order to understand the electronic properties of the key pyridinyl radical **III**, we conducted calculations at the uB3LYP/6-31G+(d) level, which showed greater spin density at C4 (0.561) than C2 (0.302, Figure 3.14). These results are in good agreement with the spin densities reported in the literature derived from an experimental method, specifically from the EPR hyperfine coupling constants of **III**.[26] Moreover, according to natural bond orbital (NBO) analysis, the singly occupied molecular orbital (SOMO) is preferentially localized at the C4 position. These computed data support the observed experimental results where product **3a** was obtained with high C4 selectivity.

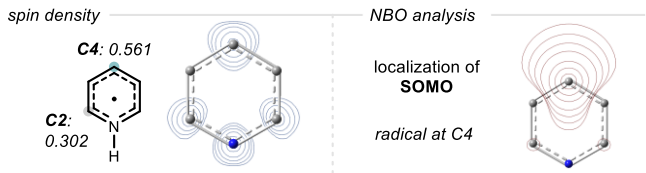

Figure 3.14. Spin densities and NBO analysis on the pyridinyl radical **III**.

[25] Elgrishi, N.; Rountree, K. J.; McCarthy, B. D.; Rountree, E. S.; Eisenhart, T. T.; Dempsey, J. L. "A Practical Beginner's Guide to Cyclic Voltammetry" *J. Chem. Educ.* **2018**, *95*, 197–206.
[26] Fessenden, R. W.; Neta, P. "ESR Spectra of Radicals Produced by Reduction of Pyridine and Pyrazine" Chem. Phys. Lett. **1973**, *18*, 14−17.

We then focused on the photochemical processes. Particularly, we wanted to confirm whether the excited thiolate catalyst $\mathbf{A}^-$ could reduce the pyridinium ion **I** *via* SET. This redox path would lead to the pyridinyl radical **III**. Initially, the emission spectrum of the triethylammonium salt of catalyst **A** (source of $\mathbf{A}^-$) was recorded at 350 nm, and it exhibited an emission centered at 382 nm (Figure 3.16). This supported our hypothesis that the deprotonated catalyst **A2** could reach an electronically excited state. Combining the information acquired from the cyclic voltammetry (CV) studies on **A2** and the absorption spectra of catalyst **A2**, we applied the Rehm−Weller formalism (equation 1) to estimate the redox potential of the excited state $[\mathbf{A2}^-]^*$.[27] $E(\mathbf{A2}^\bullet/\mathbf{A2}^-)$ = 1.12 V was determined by CV analysis, while λ_{tail} was found to be at 370 nm by UV-vis spectroscopy. Overall, these data led to an estimated excited-state energy $E_{00}(\mathbf{[A2}^-\mathbf{]}^*/\mathbf{A2}^-)$ of 3.350 V.

Using these data, the following potential was calculated for the excited anion of **A2** using Equation 1:

Equation 1: $E^*(A2^\bullet/[A2^-]^*) = E(A2^\bullet/A2^-) - E00([A2^-]^*/A2^-)$

$$E^*(\mathbf{A2}^\bullet/\mathbf{[A2}^-\mathbf{]}^*) = 1.12 - 3.35 = \mathbf{-2.23\ V}\ (\text{vs AgCl/Ag})$$

The estimated redox potential of −2.23 V vs Ag+/Ag in CH_3CN meant that the deprotonated catalyst **A2** in the excited state is a strong reductant and a SET event with pyridinium ion **I** is exergonic ($E_{1/2}$ **(I/III)** = -0.6 V).

Additional supporting data about an interaction between pyridine **1** and catalyst **A2** were gained through Stern-Volmer quenching studies. A series of quenching experiments on the emission of $[\mathbf{A2}^-]^*$ (initial emission spectrum shown in Figure 3.15) highlighted a pronounced quenching through progressive addition of a solution of **1a·HCl** pyridinium chloride salt (Figure 3.16, see experimental section for Stern-Volmer plot and Stern-Volmer quenching constant calculation).

[27] Farid, S.; Dinnocenzo, J. P.; Merkel, P. B.; Young, R. H.; Shukla, D.; Guirado, G. Reexamination of the Rehm−Weller Data Set Reveals Electron Transfer Quenching that Follows a Sandros− Boltzmann Dependence on Free Energy. *J. Am. Chem. Soc.* **2011**, *133*, 11580−11587.

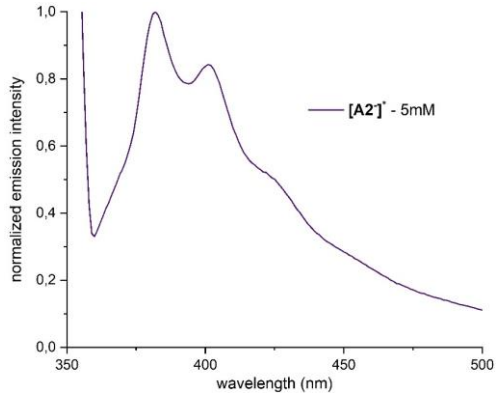

Figure 3.15. Normalized emission of [**A2**-]* upon 350 nm irradiation in acetone.

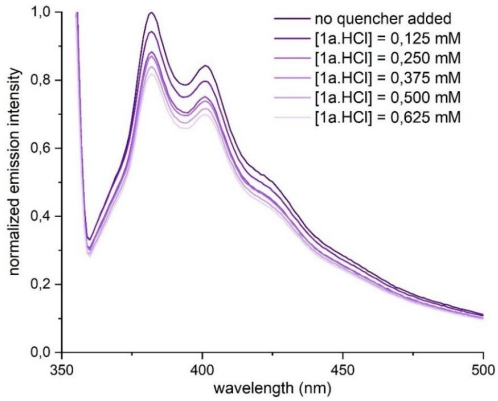

Figure 3.16. Quenching of the emission of [**A2**-]* (5 mM in acetone) in the presence of increasing amounts of **1a**·HCl.

Finally, transient absorption spectroscopy (TAS) was performed to detect the formation of [**A2**⁻]* at 625 nm and to identify its half-life time at ½ τ_0 **= 5 µs** (Figure 3.17).

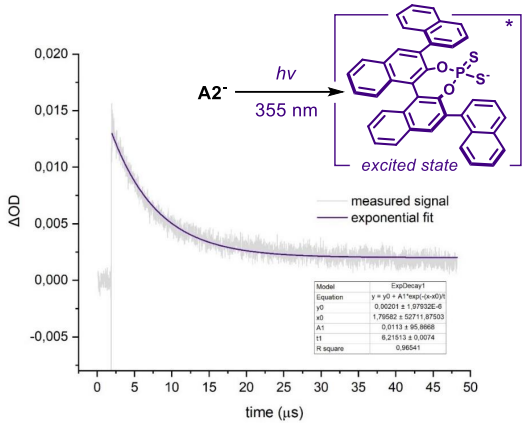

Figure 3.17. Absorption at 625 nm of the transient excited state of **A2**$^{-}$ generated upon 355 nm laser excitation. [**A2**] = 0.01 M in acetone. A first order exponential fit (purple line) was applied to the signal to facilitate the lifetime measurement. ΔOD: optical density variation.

An experimental proof for the formation of the suggested pyridinyl radical intermediate **III** was finally obtained by recording an EPR spectrum. Two different spectra were obtained in the absence and presence of light irradiation (for 15 minutes) of a solution containing pyridine **1a** and the catalyst **A2** in methanol (Figure 3.18). In the dark, the spectrum remained silent with no peak, whereas upon light irradiation a new high intensity signal appeared, which corresponded to a g value of 2.00324, characteristic of the pyridinyl radical **III**.[27]

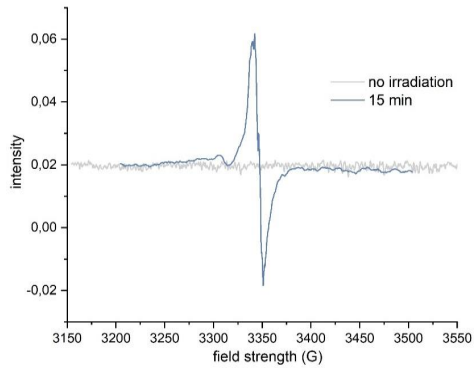

Figure 3.18. Measured EPR spectra of a 5:1 mixture of **1a** and catalyst **A2** in methanol in the dark and after 15 min of irradiation (365 nm).

We then performed radical clock experiments to ascertain whether a radical was generated and where it was located (Figure 3.19). We synthesized both C2 and C4 cyclopropyl pyridines **36a** and **36b** and submitted them under standard reaction conditions. In both cases, a ring opening of the cyclopropyl ring took place leading to products **37a** and **37b** in 51% and 45%, respectively. The observed product distribution is consistent with the formation of the pyridinyl radical **XIII**, which triggered the ring opening to form a highly stabilized benzylic

radical **XIV**, which finally underwent radical coupling with the allylic radical **IV**. Products derived from radical addition (Minisci-type addition) into the pyridine core were not observed.

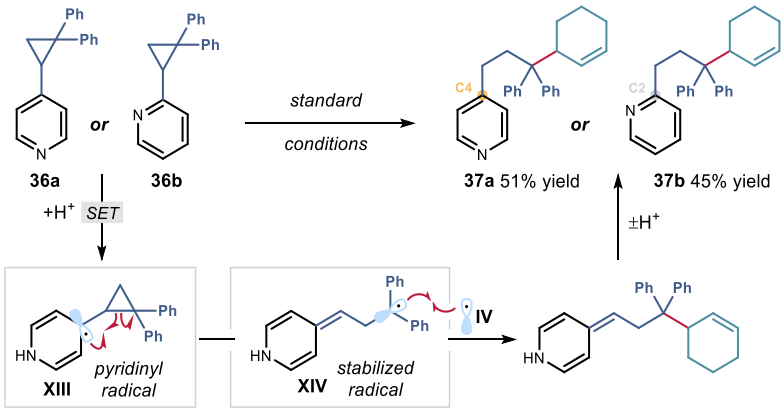

Figure 3.19. Radical clock experiments to probe the formation of the key pyridinyl radical.

3.3.3 Mechanistic proposal

Overall, our studies allowed us to gain a more comprehensive mechanistic picture of our reaction. However, few queries remained unanswered, including: a) what is the role of 2,4,6-collidine in the reaction? and b) how rearomatization does take place after radical coupling? 2,4,6-Collidine is slightly more basic than the other present pyridines (the starting material and the product). We assumed that a dynamic equilibrium between these partially protonated bases may take place and therefore allowed the reaction to proceed. To get more insights on the role of 2,4,6-collidine, we acquired additional cyclic voltammograms and performed other quenching experiments (see experimental section) using 2,4,6-collidine. The obtained results showed that collidine and pyridine behaved and interacted in a similar way with catalyst **A2**. Specifically, the collidinium ion **XV** showed the same reversible reduction wave at -0.6 V as observed for pyridine (Figure 3.20).

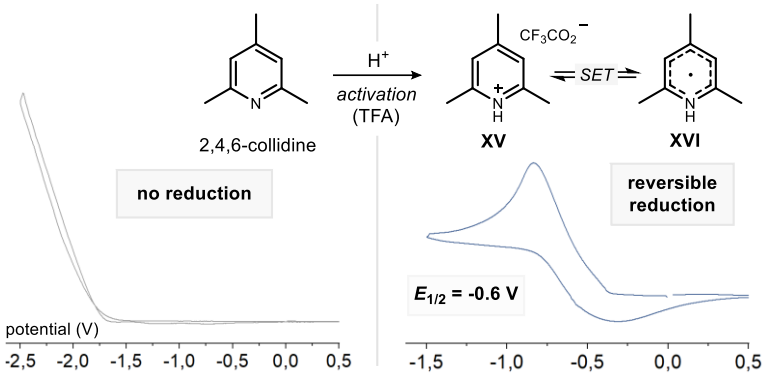

Figure 3.20. Electrochemical studies using collidine and the pre-formed collidinium ion **XV**. AgCl/Ag reference electrode in CH_3CN.

In addition, the collidinium ion **XV** quenched the excited state of catalyst **A2** to generate a collidinyl radical **XVI** with a lower rate when compared to the pyridinium ion (K_{SV} = 283.4 M^{-1} for **XV** against K_{SV} = 346.4 M^{-1} for **III**). Although the reduction of 2,4,6-collidine is possible, the radical coupling of **XVI** with an allylic radical **IV** is likely hampered by steric effects caused by the methyl groups at C2 and C4 positions. In addition, the methyl group would prevent an aromatization step, which further avoided any by-product formation. We concluded that 2,4,6-collidine may have the role of an electron reservoir and redox mediator in the reaction (Figure 3.21). A similar behavior, in which pyridines behave as electron shuttles or redox mediators was proposed previously.[28]

[28] Bieszczad, B.; Perego, L. A.; Melchiorre, P. "Photochemical C-H Hydroxyalkylation of Quinolines and Isoquinolines" *Angew. Chem. Int. Ed.* **2019**, *58*, 16878-16883.

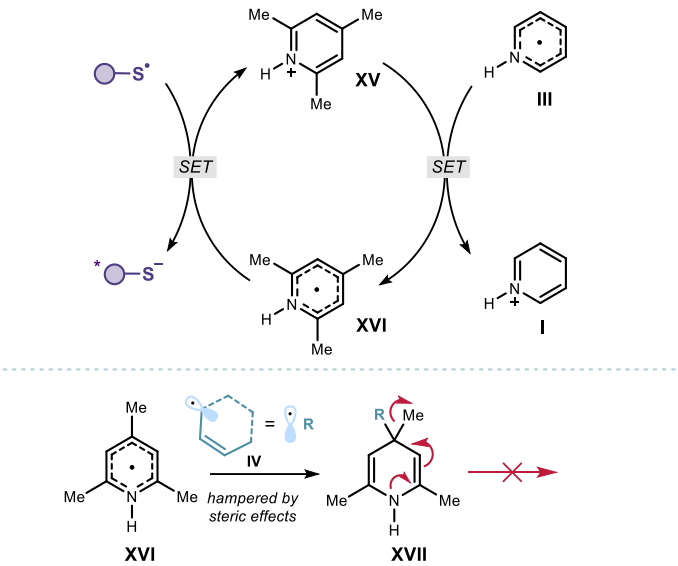

Figure 3.21. Possible role of collidine as redox mediator.

The formal product formed upon radical coupling of pyridinyl radical **III** and allylic radical **IV** is the dihydropyridine **XVIII** (Figure 3.22a). This product/intermediate was never observed or isolated during our investigations. Instead, the aromatic compound **3** was the only detectable product of the reaction. To understand how the aromatization step occurred, we performed a series of experiments based on an early observation made during reaction development. Specifically, we observed that isopropanol was formed as a by-product (as detected by ^{1}H NMR analysis of the crude reaction mixture). Isopropanol could be formed upon reduction of acetone, which was the reaction solvent. This would imply that acetone could act as an oxidant. The active participation of acetone in the mechanism would also explain why acetone performed as the best solvent during optimization, with other solvents offering inferior results. A possible scenario involves the SET reduction of protonated acetone **XIX** (formed under the action of the acidic catalyst) to form ketyl radical **XX**, while the direct reduction of acetone by the excited catalyst [**A2**$^{-}$]* would be thermodynamically unfavorable (for cyclohexanone, E_{ox} = -2.33 V vs. SCE).[29] In a similar fashion as with the reduction of pyridinium ion **I**, a thiyl radical would emerge from this SET event and abstract a hydrogen atom from the C4 position of the dihydropyridine intermediate **XVIII** (BDE (S-H) = 83.3

[29] Roth, H. G.; Romero, N. A.; Nicewicz, D. A. "Experimental and Calculated Electrochemical Potentials of Common Organic Molecules for Applications to Single-Electron Redox Chemistry" *Synlett*, **2016**, *27*, 714–723.

kcal mol^{-1} for **A1**,[22] while for NADH analogues BDE (C4-H) ~ 69 kcal mol^{-1}).[30] Those processes would eventually lead to isopropanol and the aromatized product **3** (Figure 3.22b).

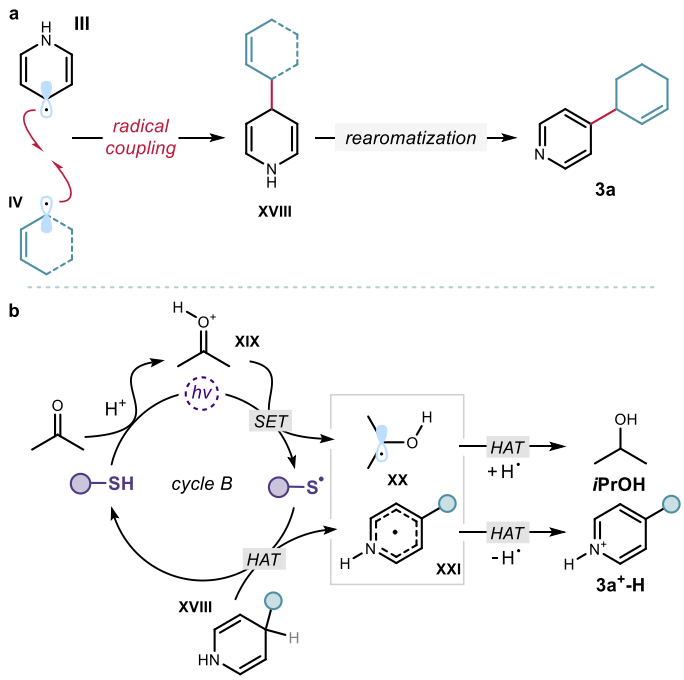

Figure 3.22. Proposed secondary catalytic cycle for the reduction of acetone to isopropanol and oxidation of **VII**.

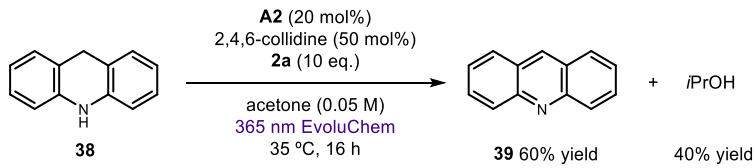

Scheme 3.13. Oxidation of 9,10-dihydroacridine and reduction of acetone under the reaction conditions.

This scenario was validated through two additional experiments. First, a stable dihydropyridine derivative (9,10-dihydroacridine **38**) was chosen to mimic dihydropyridine intermediate **XVIII**. 9,10-Dihydroacridine **38** was submitted to our standard reaction

[30] (a) Stout, D. M.; Meyers, A. I. "Recent Advances in the Chemistry of Dihydropyridines" *Chem. Rev.* **1982**, *82*, 223–243; (b) Lavilla, R. "Recent Developments in the Chemistry of Dihydropyridines" *J. Chem. Soc., Perkin Trans. 1*, **2002**, 1141–1156.

conditions (Scheme 3.13) leading to the formation of acridine **39** (aromatized product) in 60% yield along with isopropanol in 40% yield. Importantly, when the same experiment was conducted in the absence of light or catalyst, no conversion was observed.

The second experiment aimed to validate the proposed SET reduction between the excited catalyst and acetone (Scheme 3.14). We performed a reaction in the absence of the pyridine substrates and 2,4,6-collidine. The observable products were the dimer **40**, formed in 7%, and iPrOH, formed in 17%. This experiment hinted at the ability of the excited catalyst **A2**$^{-}$ to reduce acetone and form the thiyl radical prone to HAT activation of allylic C−H bonds in **2a**.

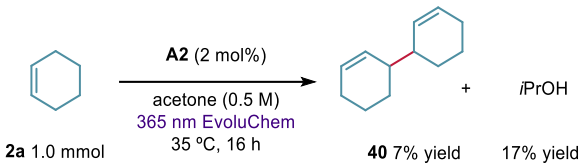

Scheme 3.14. Reduction of acetone to isopropanol by [**A2**$^{-}$]*.

Gathering all the information collected in our mechanistic investigation allowed us to propose the full mechanistic picture, as depicted in Figure 3.23.

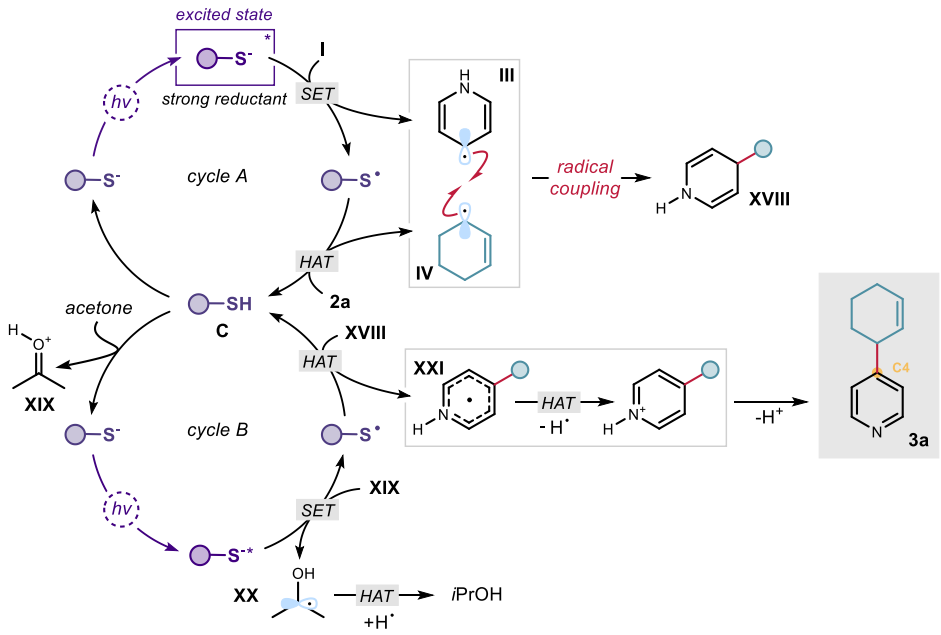

Figure 3.23. Mechanistic proposal.

3.3.4 Scope of the reaction

Having the optimized conditions in hand and the reaction mechanism investigated in depth, we continued with the exploration of the reaction scope. A wide range of pyridines, azaarenes and allylic C-H partners were subjected to this newly developed methodology. Noteworthy, Minisci-type addition of allylic radicals to heteroarenes is extremely difficult and such examples are rare.[25] Our strategy, based on the radical coupling of allylic radicals with pyridinyl radicals **I**, could fill the existing synthetic gap.

We started by testing 2-substituted pyridines under the optimized conditions, which gave exclusively the corresponding C4-allylated products **3b** and **3c** in good yields (Figure 3.24). 2-Halogenated pyridines failed to deliver the corresponding allylation products, since they suffered from dehalogenation side reactivity (for a list of unsuccessful substrates, see the section below). Halogens at the C3-pyridine position were more tolerated, and they afforded C4 functionalized pyridines **3d** and **3e** with high regioselectivity. C2-allylated regioisomers were observed, albeit as minor products. Pyridines bearing electron-withdrawing groups at the C3 position, such as trifluoromethyl and cyano, were tolerated well, delivering the C4-allylated products **3f** and **3g** in good yields. Pyridine-3-acetonitrile yielded exclusively the C4-product **3h**. When a bulkier group was introduced at the C3 position of the starting pyridine, such as a *para*-cyanobenzene, a complete switch of regioselectivity was observed from C4- to C6-allylated product (**3i**).

Nicotinic acid and many of its derivatives are known as dietary supplements and their action as lipid-controlling drugs.[31] In our reaction scope, we tested the reactivity of niacin (vitamin B3) and nicotinate esters, nicotinamides, and 3,5-difunctionalized derivatives. The outcome of those reactions was positive, since all these substrates delivered selectively products **3j-s** in good yields with a positional preference for C6 functionalization. Notably, various functionalities could be tolerated in the pyridine moiety such as a double bond, an unprotected secondary amine (**3r**), and a ketone (**3s**). Various amino acid nicotinamides were also tested and proved suitable substrates, affording products **3t-w** in good yields. Again, the presence of non-protected functional groups within the substrates did not inhibit the reactivity, highlighting the method's potential for the functionalization of complex pyridines.

The observed selectivities towards C4 in some cases and C6 in others suggested a combination of factors that dictated the regiochemical outcome of the reaction. It appears that the greater spin density at C4 through the pyridinyl radical intermediate **I**, that explains the C4 selectivity for simply functionalized pyridines, is overridden when pyridines are bearing bulky substituents in close proximity of the 4-position (3-substitution).[19] Further studies on

[31] Carlson, L. A. "Nicotinic Acid: The Broad-Spectrum Lipid Drug. A 50th Anniversary Review" *J. Intern. Med.* **2005**, *258*, 94−114.

the steric and electronic factors of the system are needed to better understand the regioselective outcome of the methodology.

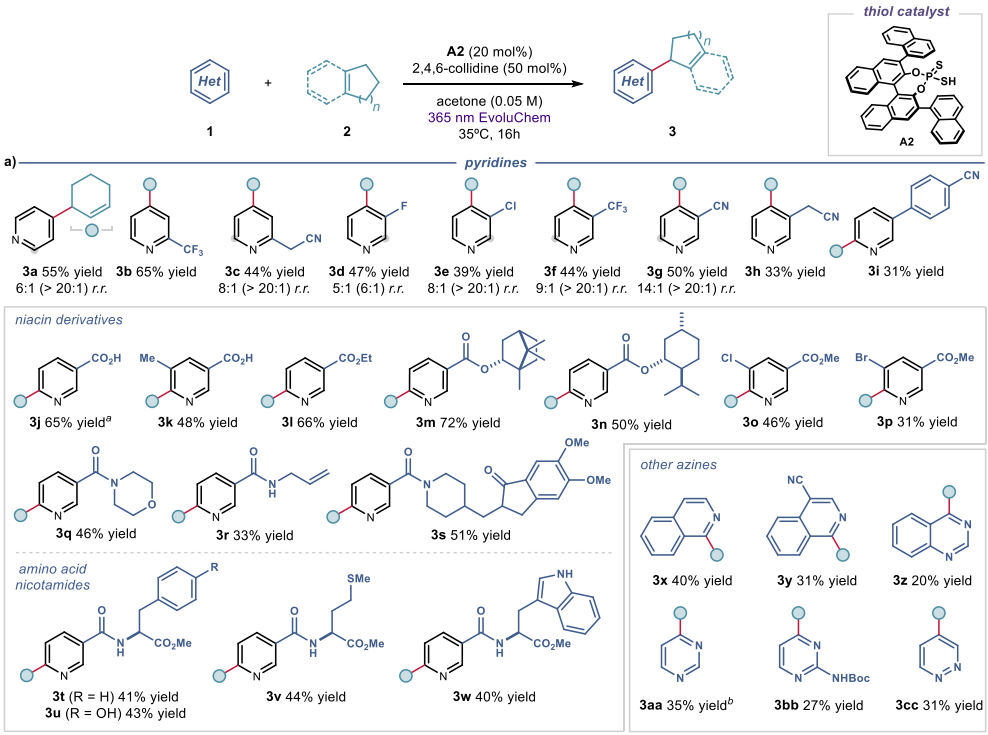

Figure 3.24. Photochemical organocatalytic allylation of pyridines and other azaarenes. Reactions were performed on a 0.2 mmol scale using 10 equiv of **2**. Yields refer to isolated products **3** after purification. Products **3** were obtained as single regioisomers (>20:1 *r.r.*), unless otherwise stated. When more than one regioisomer was observed, the minor site of functionalization is highlighted by a gray circle. In these cases, the regioisomeric ratio (*r.r.*) of the crude mixture is specified, and the *r.r.* after isolation is reported in parentheses. When applicable, *d.r.* was ~1:1. a. Yield determined by ^{1}H NMR analysis.

The reaction scope could be extended to other azaarenes, such as *iso*quinolines (products **3x** and **3y**), pyrimidines (**3z-bb**), and pyridazine (**3cc**), which afforded the desired allylated products in a regioselective fashion and modest yields. We then turned our attention towards the direct functionalization of pyridine-containing pharmaceuticals.[32] Late-stage functionalization of three niacin derivatives, i.e. *Nicoboxil* (rubefacient), *Etofibrate* (hypolipidemic agent), and *Picamilon* (dietary supplement), was possible, delivering C6-functionalized pyridines in good yields (**3dd-ff**). On the other hand, *Bisacodyl* (stimulant laxative drug), and a C2-substitutent pyridine and pyrimidine-based *Voriconazole* (antifungal) both afforded the C4-allylated products in synthetically useful yields (products **3gg** and **3hh**, respectively).

[32] Börgel, J.; Ritter, T. "Late-Stage Functionalization" *Chem.* **2020**, *6*, 1877−1887.

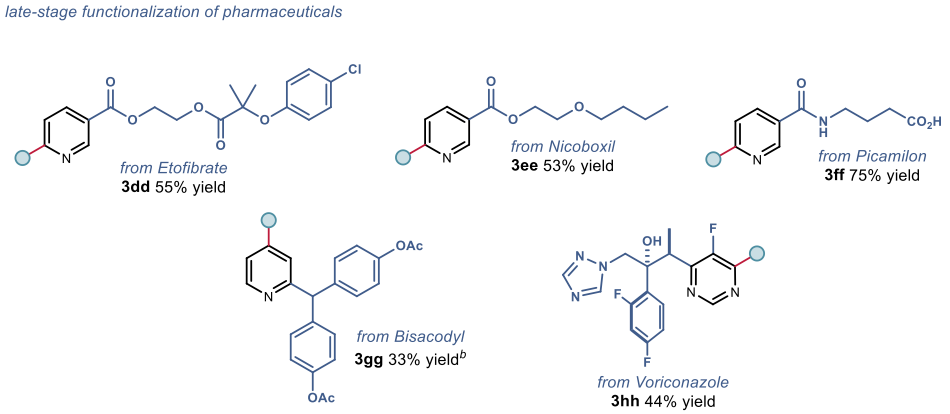

Figure 3.25 Late-stage C-H allylation of pyridine-containing biorelevant molecules. Reactions were performed on a 0.2 mmol scale using 10 equiv. of **2**. Yields refer to isolated products **3** after purification. Products **3** were obtained as single regioisomers (>20:1 *r.r.*), unless otherwise stated. When more than one regioisomer was observed, the minor site of functionalization is highlighted by a gray circle. In these cases, the regioisomeric ratio (*r.r.*) of the crude mixture is specified, and the *r.r.* after isolation is reported in parentheses. When applicable, *d.r.* was ~1:1. [a]Yield determined by ^{1}H NMR analysis. [b][Ir(dtbbpy)(ppy)$_2$]PF$_6$ under 455 nm light irradiation was used in place of collidine and 365 nm light irradiation of the standard conditions.

Finally, we evaluated C(sp^3)-H substrates that could serve as radical precursors, using 2-CF$_3$ pyridine as the model substrate (Figure 3.26). 5-, 6- and 8-Membered cyclic alkenes with different substitution patterns delivered selectively the desired C4-functionalized products in good yields. The non-cyclic tetramethylethylene was also a suitable radical precursor, affording the C4 adduct (**3nn**). Oxygen and nitrogen heterocycles, such as dihydropyran and a protected piperidine, could also decorate the pyridine scaffold at the C4 position in good yields (**3oo** and **3pp**, respectively). Evaluation of C(sp^3)-H benzylic radical precursors led to positive results, with tetrahydronaphtalene and acenaphthylene able to deliver products **3qq** and **3rr** in good yields.

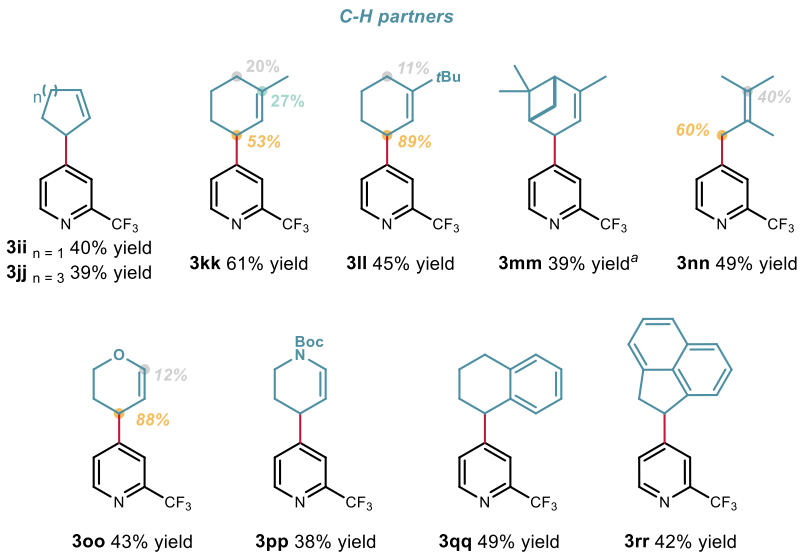

Figure 3.26. Evaluation of the C-H partners in the photochemical organocatalytic C4-functionalization of pyridines. Reactions were performed on a 0.2 mmol scale using 10 equiv of **2**. Yields refer to isolated products **3** after purification. Products **3** were obtained as single regioisomers (>20:1 *r.r.*), unless otherwise stated. When more than one regioisomer was observed, the minor site of functionalization is highlighted by a gray circle. In these cases, the regioisomeric ratio (*r.r.*) of the crude mixture is specified, and the *r.r.* after isolation is reported in parentheses. When applicable, *d.r.* was ~1:1. [a]Yield determined by ^{1}H NMR analysis.

Overall, all pyridine substrates resulted in C4-functionalized products, except of nicotinic acid derivatives that afforded the C6-products. This reactivity is consonant with the greater spin density at the C4 position. For the nicotinic acid derivatives though, the difference between the C4- and C6-spin densities is not as large as for other pyridines (see Experimental section for calculations). On the other hand, the C3-cyano pyridine derivative bearing a strongly electron-withdrawing group gave the C4-regioisomer. This observation is explained by the difference in size of these two groups (cyano vs amides/esters). The cyano group is less sterically encumbered than the methyl ester (steric factors: *A*(CN) = 0.17 against *A*(CO_2Me) = 1.23). The other azines investigated during the scope investigation (isoquinoline, pyridimidine and pyridazine), gave products consistent with the calculated spin densities. The observed site-selectivity appears to be governed by an interplay between electronics and sterics.

3.3.5 Limitation of the methodology

A broad scope of pyridines, azaerenes, and C-H partners were tested under our reaction conditions. Unfortunately, some limitations were noticed and some pyridines and azaarenes failed to deliver the desired product (Figure 3.27). The unsuccessful pyridine/heteroarene substrates are generally electron-rich systems, which were likely unable to effectively undergo the required SET reduction. In addition, some of the halogenated pyridines suffered from dehalogenation side-reactions.

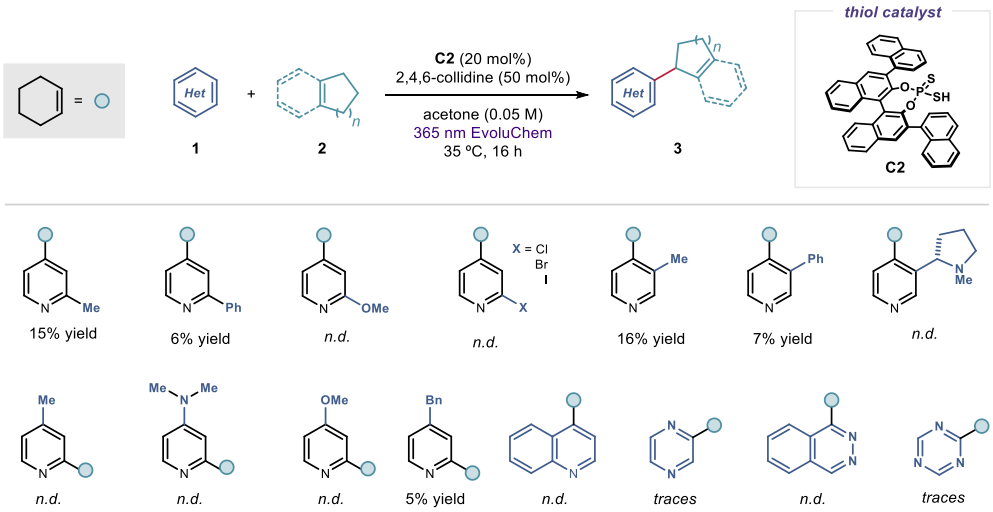

Figure 3.27. Moderately successful and unsuccessful pyridine and azaarenes in the C-H allylation reaction. Yields and ratios determined by ^{1}H NMR analysis of the crude mixtures. *n.d.*: not detected.

We have also explored a wide range of C-H radical precursors. Our methodology was limited to cyclic alkenes and could not be expanded to linear alkenes with available C-H allylic positions. Other C−H bonds next to heteroatoms, such α-oxo- and α-amino- compounds as well as aldehydic C−H bonds, proved poorly reactive.

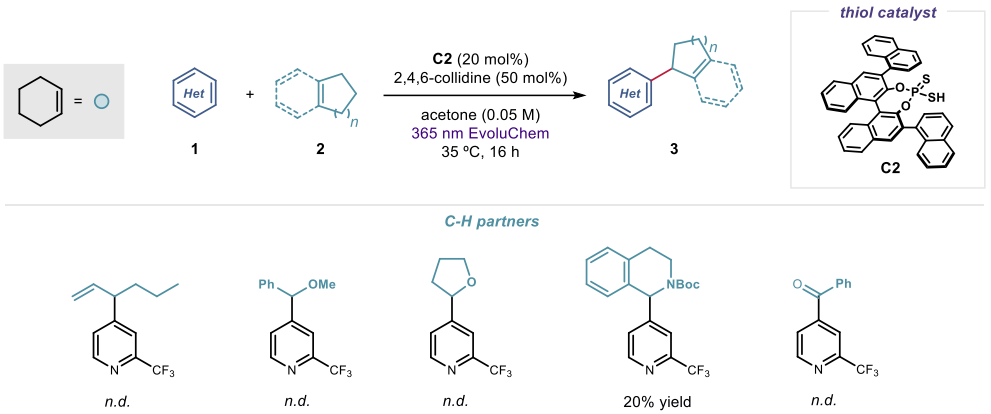

Figure 3.27. Moderately successful and unsuccessful C-H partners in the C-H functionalization reaction of azaarenes. Yields and ratios determined by ^{1}H NMR analysis of the crude mixtures. *n.d.*: not detected.

3.4 Conclusions

In this chapter, we described a new strategy for the selective functionalization of pyridines and other azaarenes. Importantly, our approach avoids the previous need for pre-functionalization of the pyridine core for directing the reaction towards a specific position. The method relies on the unique reactivity of pyridinyl radical intermediates that were previously neglected by synthetic chemists, due to the harsh conditions required for their formation. In our approach, pyridinyl radical intermediates are readily generated upon SET reduction of pyridinium ions. The multifunctional dithiophosphoric acid catalyst plays a key role in the process, acting initially as a Brønsted acid. Upon photoexcitation, it acts as a strong electron reductant and finally as a hydrogen atom transfer (HAT) abstractor of allylic C−H bonds. We envisage that the herein described reactivity could provide further opportunities for developing new pyridine functionalization strategies.

3.5 Experimental Section

General Information. The ^{1}H NMR, ^{19}F NMR, ^{13}C NMR spectra and UPC^{2} traces are available in the literature[1] and are not reported in the present dissertation. The NMR spectra were recorded at 300 MHz, 400 MHz and 500 MHz for 1H or at 75 MHz, 101 MHz and 126 MHz for 13C, 376 MHz for 19F, 162 MHz for 31P, respectively. The chemical shifts (δ) for 1H and 13C{1H} are given in ppm relative to residual signals of the solvents (CHCl3 @ 7.26 ppm 1H NMR, 77.00 ppm 13C NMR). Coupling constants are given in Hz. The following abbreviations are used to indicate the multiplicity: s, singlet; d, doublet; t, triplet; q, quartet; m, multiplet; br s, broad signal.

High-resolution mass spectra (HRMS) were obtained from the ICIQ High-Resolution Mass Spectrometry Unit on MicroTOF Focus and Maxis Impact (Bruker Daltonics) with electrospray ionization or atmospheric pressure chemical ionization. UV-vis measurements were carried out on a Shimadzu UV-2401PC spectrophotometer equipped with photomultiplier detector, double beam optics and D2 and W light sources.
The authors are indebted to the team of the Research Support Area at ICIQ, particularly to the NMR, and the High-Resolution Mass Spectrometry Units.

General Procedures. All reactions were set up under an argon atmosphere in oven-dried glassware using standard Schlenk techniques, unless otherwise stated. Synthesis grade solvents were used as purchased. Anhydrous solvents were taken from a commercial SPS solvent dispenser. Chromatographic purification of products was accomplished using flash column chromatography (FC) on silica gel (230-400 mesh). For thin layer chromatography (TLC) analysis throughout this work, Merck precoated TLC plates (silica gel 60 GF254, 0.25 mm) were used, using UV light as the visualizing agent and either phosphomolybdic acid in EtOH, dinitrophenylhydrazine in EtOH/H_2O, *p*-anisaldehyde or basic aqueous potassium permanganate (KMnO4), and heat as developing agents. Organic solutions were concentrated under reduced pressure on a Büchi rotary evaporator (in vacuo at 40 ºC, ~5 mbar).

Determination of Diastereomeric Ratio. The diastereomeric ratio was determined by 1H NMR analysis of the crude reaction mixture through integration of diagnostic signals, or by UPC2 analysis on chiral stationary phase using a Waters Acquity instrument. The exact conditions for the analyses are specified within the characterization section.

Materials: Commercial grade reagents and solvents were purchased at the highest commercial quality from Sigma Aldrich, Fluka, Acros Organics, Fluorochem, or Alfa Aesar and used as received, unless otherwise stated. Catalysts **A8** and **A9** were prepared according to a reported procedure.[33]

Dithiphorphoric Acid Catalysts and Substrate Synthesis

Synthesis of Binols

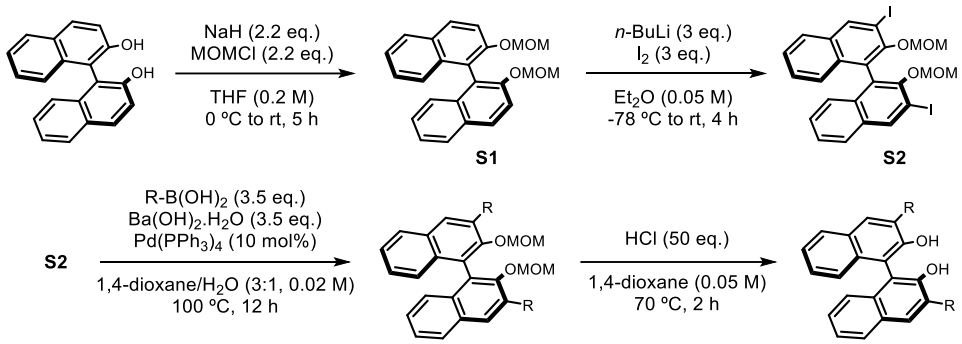

Scheme 3.14. Synthetic route for the preparation of 3,3'-substiuted (*S*)-binol derivatives.

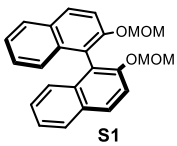

(*S*)-2,2'-bis(methoxymethoxy)-1,1'-binaphthalene (S1) NaH (1.8 g, 2.2 equiv., 60% in mineral oil) was suspended in dry THF (90 mL) at 0 ºC under an atmosphere of argon. A solution of (*S*)-2,2'-dihydroxy- 1,1'-binaphthyl (5.73 g, 20.0 mmol) in THF (30 mL) was added dropwise and the mixture stirred at 0 ºC for 1 h and then at room temperature for 30 min. After the mixture was cooled-down to 0 ºC, chloromethyl methyl ether (3.33 mL, 2.2 equiv.) was slowly added and the reaction mixture was warmed-up to room temperature and stirred for 5 h. Saturated NH_4Cl (50 mL) was added to the flask, then the solvent was removed in vacuo. The residue was extracted with CH_2Cl_2 (50 mL x 3). The organic layers were combined, washed with brine (50 mL), dried over $MgSO_4$, filtered and concentrated. The crude product was triturated with cold hexanes, filtered and dried under high vacuum to afford **S1** as a white solid (6.82 g, 91% yield).

[33] Kato, S.; Saga, Y.; Kojima, M.; Fuse, H.; Matsunaga, S.; Fukatsu, A.; Kondo, M.; Masaoka, S.; Kanai, M. "Hybrid Catalysis Enabling Room-Temperature Hydrogen Gas Release from N-Heterocycles and Tetrahydronaphthalenes" *J. Am. Chem. Soc.* **2017**, *139*, 2204.

^{1}H NMR (400 MHz, $CDCl_3$) δ 7.97 (d, *J* = 8.7 Hz, 2H), 7.89 (d, *J* = 8.1 Hz, 2H), 7.60 (d, *J* = 9.0 Hz, 2H), 7.36 (ddd, *J* = 8.1, 6.6, 1.3 Hz, 2H), 7.24 (ddd, *J* = 8.1, 6.7, 1.3 Hz, 2H), 7.18 (d, *J* = 8.5 Hz, 2H), 5.10 (d, *J* = 6.8 Hz, 2H), 5.00 (d, *J* = 6.8 Hz, 2H), 3.17 (s, 6H).
^{13}C NMR (126 MHz, $CDCl_3$) δ 152.7, 134.0, 129.9, 129.4, 127.9, 126.3, 125.6, 124.1, 121.3, 117.3, 95.2, 55.8, 29.7.

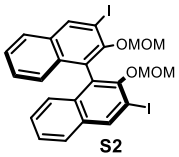

S2

(*S*)-3,3'-diiodo-2,2'-bis(methoxymethoxy)-1,1'-binaphthalene (S2) To a solution of MOM protected (*S*)-binol **S1** (6.82 g, 18.2 mmol) in dry Et_2O (350 mL, 0.05 M), was added *n*-BuLi (2.5 M in hexanes, 21.9 mL, 3 equiv.) at 0 ºC. The resulting mixture was warmed-up to room temperature and stirred for 3h. It was then cooled-down to -78 ºC and I_2 (13.9 g, 3 equiv.) was added portionwise. The reaction mixture was allowed to warm-up to room temperature overnight. Saturated NH_4Cl (100 mL) was then added and the biphasic mixture diluted with water (100 mL) and EtOAc (100 mL). The aqueous layer was extracted with EtOAc (100 mL x 2), and the combined organic layers washed with water (100 mL x 2), 10% $Na_2S_2O_3$ (100 mL x 2), brine, dried over $MgSO_4$, filtered and concentrated under reduced pressure. The crude product was purified by column chromatography (SiO_2, 5:95 EtOAc/hexanes) to afford **S2** as an off-white foamy solid (6.9 g, 60% yield).

^{1}H NMR (500 MHz, $CDCl_3$) δ 8.56 (s, 2H), 7.80 (d, *J* = 7.8 Hz, 2H), 7.45 (ddd, *J* = 8.1, 6.7, 1.2 Hz, 2H), 7.32 (ddd, *J* = 8.2, 6.8, 1.3 Hz, 2H), 7.19 (d, *J* = 8.5 Hz, 2H), 4.83 (d, *J* = 5.7 Hz, 2H), 4.71 (d, *J* = 5.7 Hz, 2H), 2.62 (s, 6H).

The remaining steps for the synthesis of substituted binols are illustrated with the preparation of the 1-naphthyl-subsituted one.

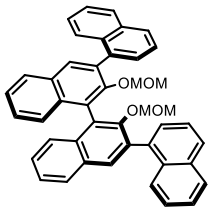

(*S*)-3,3'-bis(1-naphtyl)-2,2'-bis(methoxymethoxy)-1,1'-binaphthalene To **S2** (4.0 g, 6.39 mmol), $Ba(OH)_2.8H_2O$ (7.1 g, 3.5 equiv.), and $Pd(PPh_3)_4$ (738 mg, 0.1 equiv.) was added 1,4-dioxane/H_2O (320 mL, 0.02 M, 3:1 mixture) at room temperature, under an atmosphere of argon. Naphthalene-1-boronic acid (3.85 g, 3.5 equiv.) was then added in one portion, and the mixture stirred at 100ºC for 12h. 1,4-dioxane was then removed under reduced pressure, and the residue extracted with CH_2Cl_2 (100 mL x 3), the combined organic layers washed with brine, dried over $MgSO_4$, filtered and concentrated under reduced pressure. The crude product was purified by column chromatography (SiO_2, 5:95 EtOAc/hexanes) to afford the product as a white solid (3.85 g, 96% yield).

NMR analysis of this compound is complicated by the presence of multiple conformers due to slow rotation around the 3,3′-biaryl bonds and the unsymmetrical nature of the 1-naphthyl substituent.

^{1}H NMR (400 MHz, $CDCl_3$) δ 8.05 – 7.35 (m, 24H), 4.53 – 4.18 (m, 4H), 2.20 – 2.12 (m, 6H).

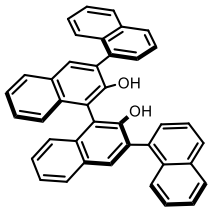

(*S*)-3,3'-bis(1-naphthyl)-2,2'-dihydroxy-1,1'-binaphtalene To (*S*)-3,3'-bis(1-naphtyl)-2,2'-bis(methoxymethoxy)-1,1'-binaphthalene (3.85 g, 6.2 mmol) dissolved in 1,4-dioxane (20 mL, 0.3 M) was added concentrated HCl (10 mL). The resulting mixture was stirred at 70 ºC for 2 h. The solvent was then removed under reduced pressure, the residue dissolved in CH_2Cl_2 (100 mL) and the organic layer washed with water (100 mL), saturated $NaHCO_3$ (100 mL), brine, dried over $MgSO_4$, filtered and concentrated under reduced pressure. After drying under high-vacuum for several hours, the product was obtained as a light-yellow solid (3.4 g, quant. yield) that was used in the next step without further purification.

NMR analysis of this compound is complicated by the presence of multiple conformers due to slow rotation around the 3,3′-biaryl bonds and the unsymmetrical nature of the 1-naphthyl substituent.

^{1}H NMR (400 MHz, CDCl3) δ 8.07 – 8.02 (m, 2H), 8.02 – 7.91 (m, 6H), 7.89 – 7.83 (m, 1H), 7.78 – 7.59 (m, 5H), 7.59 – 7.35 (m, 10H), 5.30 – 5.16 (m, 2H).

Synthesis of Catalysts A1-7

GP1 – General Procedure for the Synthesis of Binol-derived Dithiophosphoric Acids

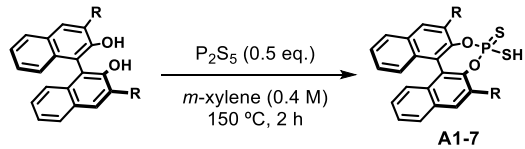

Scheme 3.15. Synthesis of dithiophosphoric acid catalysts.

A flame dried flask was charged with the appropriate (*S*)-binol derivative (1.0 equiv), P_2S_5 (0.5 equiv), and anhydrous *m*-xylene (0.2 M). The flask was equipped with a condenser and placed in an aluminum heating block preheated to 150 ºC. The progress of the reaction was monitored by disappearance of the phenolic protons, as inferred by ^{1}H NMR analysis of the crude mixture. After 2 h, the reaction was completed, and the mixture was cooled to ambient temperature. The solvent was evaporated in vacuo. The crude product was dissolved in a minimum amount of CH_2Cl_2 and treated with hexanes. The resulting fine precipitate was then collected by filtration and the operation repeated until no more precipitate was formed. The pure dithiophosphoric acids **C1-7** were obtained after washing the precipitates with cold hexanes.

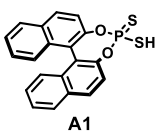

(11bS)-4-mercaptodinaphtho[2,1-d:1',2'-f][1,3,2]dioxaphosphepine 4-sulfide (A1) Prepared according to GP1 using (S)-1,1'-bi-2-naphtol (2.23 g, 5.86 mmol). **C1** (2.23 g, 5.86 mmol, 73% yield) was obtained as a white

powder which displayed spectroscopic data consistent with those reported previously.[34]

^{1}H NMR (400 MHz, $CDCl_3$) δ 8.13 – 8.07 (m, 2H), 8.00 (dd, *J* = 8.1, 1.2 Hz, 2H), 7.60 (dd, *J* = 8.8, 1.4 Hz, 2H), 7.54 (ddt, *J* = 8.0, 6.8, 1.1 Hz, 2H), 7.48 – 7.42 (m, 2H), 7.36 (ddd, *J* = 8.4, 6.7, 1.3 Hz, 2H).

^{13}C NMR (75 MHz, $CDCl_3$) δ 147.2, 132.4, 132.0, 131.1, 128.6, 127.2, 126.9, 126.1, 122.6, 121.1.

^{31}P NMR (162 MHz, $CDCl_3$) δ 100.24.

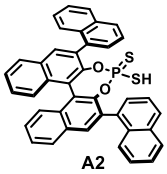

A2

(11bS)-4-mercapto-2,6-di(naphthalen-1-yl)dinaphtho[2,1-d:1',2'-f][1,3,2]dioxaphosphepine 4-sulfide (A2) Prepared according to GP1 using (1′S)-[1,3′:1′,1″:3″,1‴-Quaternaphthalene]-2′,2″-diol (1.25 g, 2.32 mmol). **C2** (1.17 g, 1.85 mmol, 80% yield) was obtained as a white powder which displayed spectroscopic data consistent with those reported previously.[35]

NMR analysis of this compound is complicated by the presence of multiple conformers due to slow rotation around the 3,3′-biaryl bonds and the unsymmetrical nature of the 1-naphthyl substituent.

^{1}H NMR (400 MHz, $CDCl_3$) δ 8.24 – 7.31 (m, 24H).

^{31}P NMR (162 MHz, $CDCl_3$) δ 96.3, 96.2, 96.1.

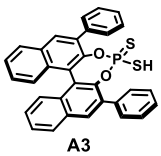

A3

(11bS)-4-mercapto-2,6-diphenyldinaphtho[2,1-d:1',2'-f][1,3,2]dioxaphosphepine 4-sulfide (A3) Prepared according to GP1 using (1S)-3,3′-Diphenyl[1,1′-binaphthalene]-2,2′-diol (317 mg, 0.72 mmol). **C3** (256 mg, 0.48 mmol, 67% yield) was obtained as a white powder which displayed spectroscopic data consistent with those reported previously.[2]

^{1}H NMR (500 MHz, CDCl3) δ 8.14 (s, 2H), 8.06 – 8.02 (m, 2H), 7.75 – 7.71 (m, 4H), 7.58 (dt, J = 7.0, 1.0 Hz, 2H), 7.52 – 7.42 (m, 8H), 7.38 (ddd, J = 8.5, 6.8, 1.3 Hz, 3H).

^{13}C NMR (101 MHz, CDCl3) δ 137.2, 131.4, 130.2, 129.6, 128.9, 128.6, 128.3, 127.8, 127.1, 126.7, 126.3.

^{31}P NMR (202 MHz, CDCl3) δ 96.2.

[34] Le Saux, E.; Zanini, M.; Melchiorre, P. Photochemical Organocatalytic Benzylation of Allylic C-H Bonds. *J. Am. Chem. Soc.* **2022**, *144*, 1113–1118.

[35] Shapiro, N. D.; Rauniyar, V.; Hamilton, G. L.; Wu, J.; Toste, F. D. Asymmetric Additions to Dienes Catalyzed by a Dithiophosphoric Acid. *Nature* **2011**, *470*, 245–249.

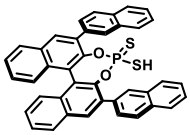

A4

(11bS)-4-mercapto-2,6-di(naphthalen-2-yl)dinaphtho[2,1-d:1',2'-f][1,3,2]dioxaphosphepine 4-sulfide (A4) Prepared according to GP1 using (1′S)-[2,3′:1′,1″:3″,2‴-Quaternaphthalene]-2′,2″-diol (590 mg, 1.1 mmol). **C4** (564 mg, 0.89 mmol, 81% yield) was obtained as a white powder.

^{1}H NMR (400 MHz, $CDCl_3$) δ 8.24 – 8.18 (m, 4H), 8.06 (d, *J* = 8.2 Hz, 2H), 7.97 – 7.82 (m, 8H), 7.61 – 7.55 (m, 2H), 7.54 – 7.48 (m, 6H), 7.44 – 7.35 (m, 2H).

^{13}C NMR (126 MHz, $CDCl_3$) δ 134.7, 133.3, 132.8, 132.0, 131.7, 129.3, 128.6, 128.4, 128.0, 127.8, 127.7, 127.1, 126.8, 126.4, 126.3, 126.2.

^{31}P NMR (162 MHz, $CDCl_3$) δ 96.3.

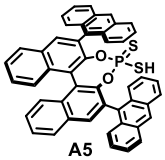

A5

(11bS)-2,6-di(anthracen-9-yl)-4-mercaptodinaphtho[2,1-d:1',2'-f][1,3,2]dioxaphosphepine 4-sulfide (A5) Prepared according to GP1 using (1S)-3,3′-Di-9-anthracenyl[1,1′-binaphthalene]-2,2′-diol (585 mg, 0.92 mmol). **C5** (543 mg, 0.74 mmol, 81% yield) was obtained as a white powder.

^{1}H NMR (400 MHz, $CDCl_3$) δ 8.54 – 8.49 (m, 2H), 8.17 (s, 2H), 8.08 – 7.95 (m, 8H), 7.74 – 7.61 (m, 6H), 7.57 – 7.50 (m, 2H), 7.46 – 7.37 (m, 4H), 7.36 – 7.26 (m, 4H).

^{13}C NMR (126 MHz, $CDCl_3$) δ 134.7, 131.6, 131.0, 131.0, 130.9, 130.3, 128.7, 128.6, 128.4, 128.1, 127.5, 127.2, 126.5, 126.3, 126.2, 125.1, 125.1, 125.0.

^{31}P NMR (122 MHz, $CDCl_3$) δ 93.2.

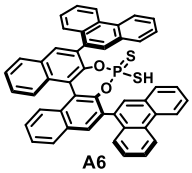

A6

(11bS)-4-mercapto-2,6-di(phenanthren-9-yl)dinaphtho[2,1-d:1',2'-f][1,3,2]dioxaphosphepine 4-sulfide (A6) Prepared according to GP1 using (1S)-3,3′-Di-9-phenanthrenyl[1,1′-binaphthalene]-2,2′-diol (540 mg, 0.85 mmol). **C6** (460 mg, 0.63 mmol, 74% yield) was obtained as a white powder.

^{1}H NMR (500 MHz, $CDCl_3$) δ 8.84 – 8.71 (m, 4H), 8.25 – 8.02 (m, 5H), 8.00 – 7.89 (m, 3H), 7.75 – 7.58 (m, 12H), 7.58 – 7.43 (m, 4H).

^{31}P NMR (202 MHz, $CDCl_3$) δ 96.5.

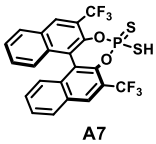

A7

(11bS)-4-mercapto-2,6-bis(trifluoromethyl)dinaphtho[2,1-d:1',2'-f][1,3,2]dioxaphosphepine 4-sulfide (A7) Prepared according to GP1 using (1R)-3,3′-Bis(trifluoromethyl)[1,1′-binaphthalene]-2,2′-diol (470 mg, 1.1 mmol). **C7** (487 mg, 0.94 mmol, 85% yield) was obtained as a white powder

^{1}H NMR (500 MHz, $CDCl_3$) δ 8.46 (s, 2H), 8.09 (d, *J* = 8.2 Hz, 2H), 7.63 (t, *J* = 7.6 Hz, 2H), 7.43 (t, *J* = 8.4 Hz, 1H), 7.16 (d, *J* = 8.6 Hz, 2H).

^{13}C NMR (126 MHz, $CDCl_3$) δ 143.1, 143.0, 133.9, 130.3, 130.3, 130.1, 129.5, 129.3, 127.4, 126.9, 123.6, 123.6, 121.8, 121.4.

^{19}F NMR (471 MHz, $CDCl_3$) δ -59.1.

^{31}P NMR (202 MHz, $CDCl_3$) δ 97.7.

Synthesis of Pyridines 1

Synthesis of 4-(pyridin-3-yl)benzonitrile 1i

Pyridine **1i** was prepared following a reported procedure (Scheme S3).[36]

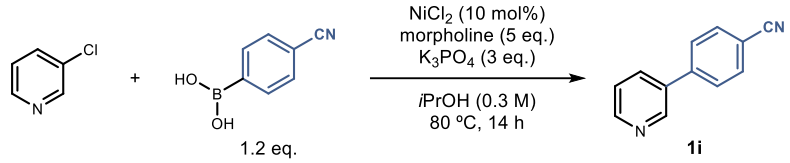

Scheme 3.16. Synthesis of pyridine 1i.

To a mixture of 3-chloropyridine (95 µL, 1 mmol), K_3PO_4 (637 mg, 3 equiv.), $NiCl_2$ (13 mg, 0.1 equiv.), and (4-cyanophenyl)boronic acid (176 mg, 1.2 equiv.) was added morpholine (431 µL, 5 equiv.) followed by 2-propanol (3 mL, 0.3 M). The mixture was stirred at 80 °C under nitrogen. After 14 h, the mixture was diluted with ethyl acetate and H_2O. The organic layer was separated and the aqueous layer was extracted with ethyl acetate. The combined organic layers were washed with brine, dried over MgSO4, filtered, and concentrated under reduced pressure. The crude mixture was purified by column chromatography (SiO_2, 20:80 EtOAc/hexanes) to afford **1i** as a white solid (63 mg, 35% yield) which displayed spectroscopic data consistent with those reported previously.

^{1}H NMR (300 MHz, $CDCl_3$) δ 8.86 (s, 1H), 8.68 (d, *J* = 4.9 Hz, 1H), 7.92 (ddd, *J* = 8.0, 2.4, 1.6 Hz, 1H), 7.82 – 7.76 (m, 2H), 7.73 – 7.67 (m, 2H), 7.45 (dd, *J* = 7.9, 4.8 Hz, 1H).

^{13}C NMR (101 MHz, $CDCl_3$) δ 149.7, 148.1, 142.2, 134.6, 134.4, 132.8, 127.7, 123.7, 118.4, 111.8.

Synthesis of Nicotinamides and Nicotinates

GP2 – General Procedure for the Synthesis of Nicotinamides and Nicotinates from Nicotinoyl Chloride

A suspension of nicotinic acid (1 equiv.) in thionyl chloride (3 equiv.) was stirred at 70 ºC for 1h. The mixture was cooled-down to room temperature and concentrated under reduced pressure to afford the crude nicotinoyl chloride hydrochloride **S3** as a white solid which was used in the next step without further purification.

To an ice-cold suspension of **S3** (1 equiv) in dichloromethane (0.2 M) was added the amine or alcohol (1.1 equiv.) in portions, followed by dropwise addition of triethylamine (3 equiv.). The reaction was allowed to warm-up to room temperature over 12 h. The mixture was washed with water, brine, dried over magnesium sulfate, filtered and concentrated under reduced pressure. Purification by column chromatography afforded the pure nicotinamides.

[36] Abe, T.; Mino, T.; Watanabe, K.; Sakamoto, M. Suzuki–Miyaura Coupling of Aryl Chlorides with Arylboronic Acids Using the Morpholine–NiCl2 Catalyst System. *Eur. J. Org. Chem.* **2014**, *31*, 6983–6991.

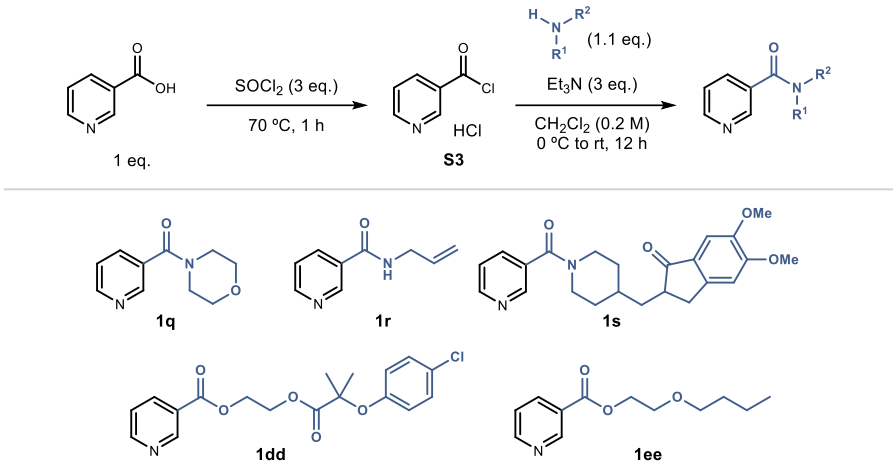

Figure 3.28. Synthesis of nicotinamides and nicotinic esters from nicotinoyl hydrochloride.

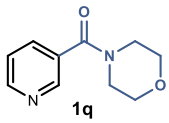

morpholino(pyridin-3-yl)methanone (1q)

Prepared according to GP2 using nicotinic acid (985 mg, 8.0 mmol), and morpholine (769 µL, 1.1 equiv.). Purification by column chromatography (SiO_2, 1:2:97 Et_3N/MeOH/CH_2Cl_2) afforded product **1q** as a colorless oil (1.1 g, 68% yield) which displayed spectroscopic data consistent with those reported previously.[37]

^{1}H NMR (300 MHz, $CDCl_3$) δ 8.70 – 8.65 (m, 2H), 7.76 (dt, *J* = 7.8, 2.0 Hz, 1H), 7.37 (ddd, *J* = 7.8, 4.9, 0.9 Hz, 1H), 3.89 – 3.39 (m, 8H).

^{13}C NMR (101 MHz, $CDCl_3$) δ 167.8, 151.0, 148.0, 135.1, 131.2, 123.5, 66.8, 46.3, 30.9, 8.6.

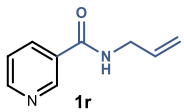

***N*-allyl-nicotinamide (1r)**

Prepared according GP2 using nicotinic acid (616 mg, 5 mmol) and allylamine (636 µL, 1.7 equiv.). Purification by column chromatography (SiO_2, 30:70 EtOAc/hexanes) afforded product **1r** as a colorless oil (581 mg, 72% yield) which displayed spectroscopic data consistent with those reported previously.[38]

^{1}H NMR (400 MHz, $CDCl_3$) δ 8.98 (d, *J* = 1.4 Hz, 1H), 8.66 (dd, *J* = 4.9, 1.7 Hz, 1H), 8.12 (dt, *J* = 7.9, 2.0 Hz, 1H), 7.35 (ddd, *J* = 7.9, 4.9, 0.9 Hz, 1H), 6.90 (br s, 1H), 5.90 (ddt, *J* =

[37] Deguest, G.; Devineau, A.; Bischoff, L.; Fruit, C.; Marsais, F. One-Pot Synthesis of 2,3-Dihydro-pyrrolopyridinones Using in Situ Generated Formimines. *Org. Lett.* **2006**, *25*, 5889–5892.

[38] Azizi, M. S.; Edder, Y.; Karim, A.; Sauthier, M. Nickel(0)-Catalyzed N-Allylation of Amides and p-Toluenesulfonamide with Allylic Alcohols under Neat and Neutral Conditions. *Eur. J. Org. Chem.* **2016**, *22*, 3796–3803.

17.2, 10.2, 5.7 Hz, 1H), 5.23 (dq, *J* = 17.1, 1.6 Hz, 1H), 5.16 (dq, *J* = 10.3, 1.4 Hz, 1H), 4.06 (tt, *J* = 5.7, 1.6 Hz, 2H).

^{13}C NMR (101 MHz, $CDCl_3$) δ 165.6, 152.2, 148.0, 135.4, 133.9, 130.3, 123.6, 117.0, 42.6.

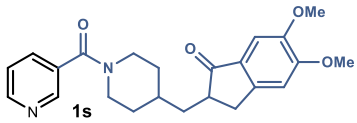

5,6-dimethoxy-2-((1-nicotinoylpiperidin-4-yl)methyl)-2,3-dihydro-1H-inden-1-one (1s)

Prepared according to GP2 using nicotinic acid (369 mg, 3.0 mmol), and 5,6-dimethoxy-2-(piperidin-4-ylmethyl)-2,3-dihydro-1H-inden-1-one (955 mg, 1.1 equiv.). Purification by column chromatography (SiO_2, 1:1:98 Et_3N/MeOH/CH_2Cl_2) afforded product **1s** as a white solid (794 mg, 67% yield).

^{1}H NMR (400 MHz, $CDCl_3$) δ 8.67 (s, 2H), 7.76 (dt, *J* = 7.8, 1.9 Hz, 1H), 7.37 (dd, *J* = 7.8, 4.9 Hz, 1H), 7.17 (s, 1H), 6.86 (s, 1H), 4.88 – 4.62 (m, 1H), 3.97 (s, 3H), 3.91 (s, 3H), 3.83 – 3.63 (m, 1H), 3.28 (dd, *J* = 17.3, 8.0 Hz, 1H), 3.17 – 2.99 (m, 1H), 2.92 – 2.78 (m, 1H), 2.79 – 2.65 (m, 2H), 2.02 – 1.84 (m, 3H), 1.81 – 1.69 (m, 2H), 1.49 – 1.34 (m, 2H).
^{13}C NMR (126 MHz, $CDCl_3$) δ 207.2, 167.6, 155.6, 150.6, 149.6, 148.6, 147.8, 134.9, 132.1, 129.2, 123.5, 107.3, 104.4, 68.5, 56.3, 56.1, 48.1, 45.0, 42.6, 38.6, 34.5, 33.4.

HRMS (ESI$^+$) Calculated for $C_{23}H_{26}N_2NaO_4$ $[M+Na]^+$: 417.1785 found: 417.1786.

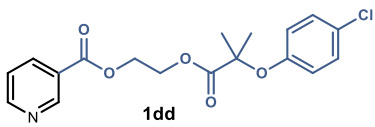

Etofibrate (1dd)

Prepared according to GP2 using nicotinic acid (222 mg, 1.8 mmol), and 2-hydroxyethyl 2-(4-chlorophenoxy)-2-methylpropanoate (512 mg, 1.1 equiv.). Purification by column chromatography (SiO_2, 1:10:89 Et_3N/EtOAc/hexanes) afforded product **1dd** as a yellow oil (473 mg, 72% yield).

^{1}H NMR (300 MHz, $CDCl_3$) δ 9.17 (dd, *J* = 2.2, 0.9 Hz, 1H), 8.81 (dd, *J* = 4.9, 1.7 Hz, 1H), 8.15 (ddd, *J* = 8.0, 2.2, 1.8 Hz, 1H), 7.40 (ddd, *J* = 8.0, 4.9, 0.9 Hz, 1H), 7.17 – 7.08 (m, 2H), 6.83 – 6.74 (m, 2H), 4.56 (m, 4H), 1.62 (s, 6H).
^{13}C NMR (126 MHz, $CDCl_3$) δ 173.9, 164.9, 153.9, 153.7, 150.9, 137.1, 129.1, 127.2, 125.5, 123.4, 120.2, 79.3, 63.0, 62.8, 25.3.

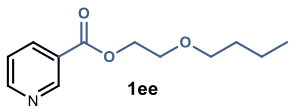

Nicoboxil (1ee) Prepared according to GP2 using nicotinic acid (222 mg, 1.8 mmol), and 2-butoxyethanol (260 µL, 1.1 equiv.). Purification by column chromatography (SiO_2, 1:10:89 Et_3N/EtOAc/hexanes) afforded product **1ee** as a yellow oil (199.4 mg, 50% yield).

^{1}H NMR (300 MHz, $CDCl_3$) δ 9.27 (d, *J* = 1.8 Hz, 1H), 8.80 (dd, *J* = 4.9, 1.8 Hz, 1H), 8.34 (dt, *J* = 8.0, 2.0 Hz, 1H), 7.42 (dd, *J* = 8.0, 4.9 Hz, 1H), 4.55 – 4.50 (m, 2H), 3.83 – 3.77 (m, 2H), 3.54 (t, *J* = 6.6 Hz, 2H), 1.66 – 1.55 (m, 2H), 1.48 – 1.34 (m, 2H), 0.94 (t, *J* = 7.3 Hz, 3H).

^{13}C NMR (101 MHz, $CDCl_3$) δ 165.3, 153.4, 151.0, 137.2, 126.1, 123.3, 71.3, 68.4, 64.6, 31.7, 19.3, 13.9.

HRMS (ESI^+) Calculated for $C_{12}H_{18}NO_3$ $[M+H]^+$: 224.1281 found: 224.1279.

Synthesis of Nicotinates 1m-n

***GP3* – General Procedure for the Synthesis of Nicotinates Using DCC**

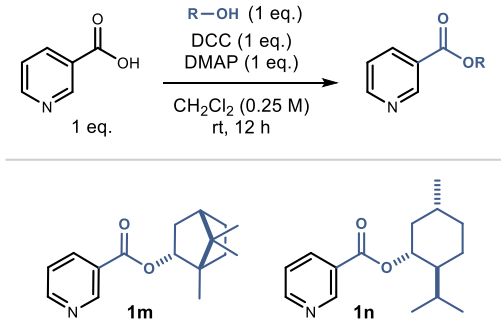

Figure 3.29. Synthesis of nicotinates 1m-n.

To a mixture of nicotinic acid (1.0 equiv.) and alcohol (1.0 equiv.) in dichloromethane (0.25 M) were added DCC (2.06 g, 10 mmol, 1.0 equiv.), followed by DMAP (1.22 g, 10 mmol, 1.0 equiv.) The resulting mixture was stirred at room temperature for 12 hours. The solution was concentrated under reduced pressure. Purification by column chromatography afforded the pure nicotinates.

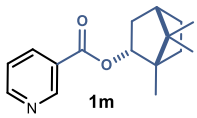

(1*R*,2*S*,4*R*)-1,7,7-trimethylbicyclo[2.2.1]heptan-2-yl nicotinate (1m) Prepared according to GP3 using nicotinic acid (1.23 g, 10.0 mmol), and L-borneol (1.54 g, 1.0 equiv.). Purification by column chromatography (SiO_2, 80:20 hexanes/EtOAc) afforded product **1m** as a colorless oil (1.27 g, 78% yield) which displayed spectroscopic data consistent with those reported previously.[39]

^{1}H NMR (400 MHz, CDCl3) δ 9.26 (d, J = 2.2 Hz, 1H), 8.78 (dd, J = 4.8, 1.8 Hz, 1H), 8.31 (dt, J = 8.0, 4.8 Hz, 1H), 7.50 – 7.35 (m, 1H), 5.15 (ddd, J = 10.0, 3.4, 2.2 Hz, 1H), 2.59 – 2.39 (m, 1H), 2.03 – 2.17 (m, 1H), 1.87 – 1.73 (m, 2H), 1.49 – 1.38 (m, 1H), 1.36 – 1.28 (m, 1H), 1.14 (dd, J = 13.8, 3.6 Hz, 1H), 0.98 (s, 3H), 0.93 (d, J = 1.2 Hz, 6H).

^{13}C NMR (100 MHz, CDCl3) δ 165.6, 153.4, 151.0, 137.1, 126.8, 123.4, 81.3, 49.2, 48.0, 45.0, 37.0, 28.2, 27.5, 19.8, 19.0, 13.7.

[39] Saito, R.; Naruse, S.; Takano, K.; Fukuda, K.; Katoh, A.; Inoue, Y. Unusual Temperature Dependence of Enantioselectivity in Asymmetric Reductions by Chiral NADH Models. *Org. Lett.* **2006**, 10, 2067–2070.

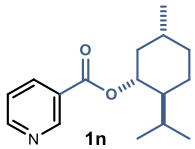

(1*R*,2*S*,5*R*)-2-Isopropyl-5-methylcyclohexyl nicotinate (1n).

Prepared according to GP3 using nicotinic acid (1.23 g, 10.0 mmol), and L-menthol (1.56 g, 1.0 equiv.). Purification by column chromatography (SiO_2, 80:20 hexanes/EtOAc) afforded product **1n** as a colorless oil (0.95 g, 73% yield) which displayed spectroscopic data consistent with those reported previously.[40]

^{1}H NMR (400 MHz, CDCl3) δ 9.20 (d, J = 2.0 Hz, 1H), 8.74 (dd, J = 5.0, 1.8 Hz, 1H), 8.27 (dt, J = 8.0, 2.0 Hz, 1H), 7.37 (dd, J = 7.9, 4.9 Hz, 1H), 4.94 (td, J = 10.8, 4.4 Hz, 1H), 2.14 – 2.07 (m, 1H), 1.99 – 1.86 (m, 1H), 1.80 – 1.67 (m, 2H), 1.65 – 1.30 (m, 3H), 1.16 – 1.03 (m, 2H), 0.94 – 0.89 (m, 6H), 0.80 – 0.74 (m, 3H).

^{13}C NMR (100 MHz, CDCl3) δ 164.9, 153.3, 151.0, 137.1, 126.7, 123.3, 75.6, 47.2, 41.0, 34.3, 31.5, 26.6, 23.6, 22.1, 20.8.

Synthesis of Amino Acid-deriving Nicotinamides 1t-w

GP4 – General Procedure for the Synthesis of Amino Acid-derived Nicotinamides

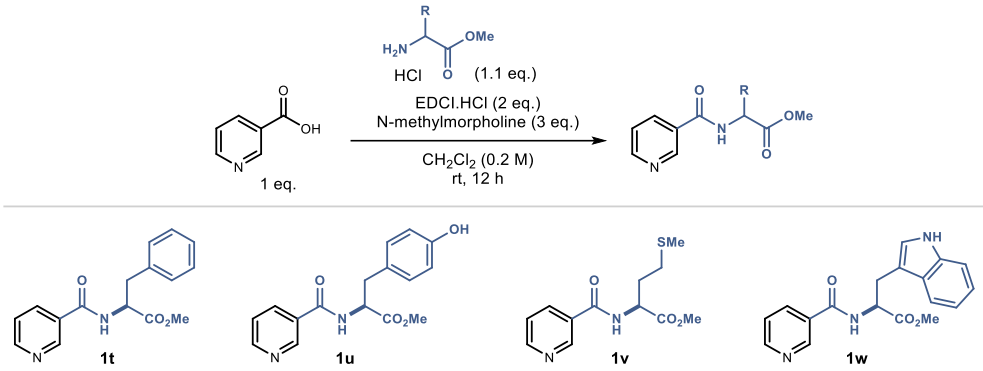

Figure 3.30. Synthesis of amino acids-derived nicotinamides 1t-w.

To a suspension of nicotinic acid (1 equiv.) in dichloromethane (0.2 M) was added EDCI hydrochloride (2 equiv.), followed by N-methylmorpholine (3 equiv.) and the hydrochloride salt of the amino acid methyl ester (1.1 equiv.). The reaction mixture was stirred at room temperature overnight. The mixture was diluted with dichloromethane, washed with water, brine, dried over magnesium sulfate, filtered and concentrated under reduced pressure. Purification by column chromatography afforded the pure nicotinamides.

[40] Zhang, T.; Luan, Y-X.; Lam, N. Y. S.; Li, J-F.; Li, Y.; Ye, M.; Yu, J-Q. A Directive Ni Catalyst Overrides Conventional Site Selectivity in Pyridine C–H Alkenylation. *Nat. Chem.* **2021**, *13*, 1207–1213.

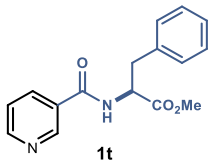

1t

methyl nicotinoyl-*L*-phenylalaninate (1t)

Prepared according to GP4 using nicotinic acid (1.38 g, 11.2 mmol), and methyl L-phenylalaninate (2.00 g, 1.0 equiv. Purification by column chromatography (SiO_2, 20:80 hexanes/EtOAc to 100% EtOAc) afforded product **1t** as a yellow oil (2.41 g, 76% yield) which displayed spectroscopic data consistent with those reported previously.[39]

^{1}H NMR (400 MHz, $CDCl_3$) δ 8.92 (d, *J* = 1.9 Hz, 1H), 8.74 (dd, *J* = 4.9, 1.7 Hz, 1H), 8.06 (dt, *J* = 7.9, 2.1 Hz, 1H), 7.39 (ddd, *J* = 7.9, 4.8, 0.9 Hz, 1H), 7.35 – 7.25 (m, 3H), 7.16 – 7.09 (m, 2H), 6.61 (d, *J* = 7.5 Hz, 1H), 5.09 (dt, *J* = 7.6, 5.6 Hz, 1H), 3.79 (s, 3H), 3.27 (qd, *J* = 13.9, 5.6 Hz, 2H).
^{13}C NMR (101 MHz, $CDCl_3$) δ 171.9, 165.1, 152.5, 148.0, 135.7, 135.4, 129.4, 128.9, 127.5, 123.7, 53.7, 52.7, 38.0.

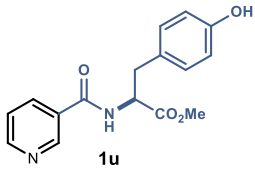

1u

methyl nicotinoyl-L-tyrosinate (1u)

Prepared according to GP4 using nicotinic acid (616 mg, 5.0 mmol), and methyl *L*-tyrosinate (976 mg, 1.0 equiv.). Purification by column chromatography (SiO_2, 20:80 EtOAc /hexanes to 100% EtOAc) afforded product **1u** as a white solid (852 mg, 57% yield) which displayed spectroscopic data consistent with those reported previously.[41]

^{1}H NMR (400 MHz, $CDCl_3$) δ 8.91 (s, 1H), 8.74 (d, *J* = 4.9 Hz, 1H), 8.09 (dt, *J* = 7.9, 2.0 Hz, 1H), 7.41 (dd, *J* = 8.0, 4.8 Hz, 1H), 7.02 – 6.95 (m, 2H), 6.80 – 6.73 (m, 2H), 6.60 (d, *J* = 7.6 Hz, 1H), 5.05 (dt, *J* = 7.7, 5.6 Hz, 1H), 3.79 (s, 3H), 3.20 (qd, *J* = 14.1, 5.6 Hz, 2H).
^{13}C NMR (101 MHz, MeOD) δ 173.5, 167.9, 157.5, 152.8, 149.2, 137.1, 131.7, 131.2, 128.9, 125.1, 116.3, 56.2, 52.8, 37.4.

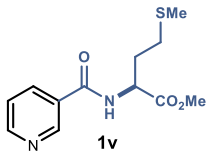

1v

methyl nicotinoyl-L-methioninate (1v)

Prepared according to GP4 using nicotinic acid (616 mg, 5.0 mmol), and methyl L-methioninate (816 mg, 1.0 equiv.). Purification by column chromatography (SiO_2, 20:80 EtOAc /hexanes to 100% EtOAc) afforded product **1v** as a colorless oil (593 mg, 44% yield).

^{1}H NMR (400 MHz, $CDCl_3$) δ 9.07 – 9.01 (m, 1H), 8.74 (dd, *J* = 5.0, 1.7 Hz, 1H), 8.14 (dt, *J* = 7.9, 2.0 Hz, 1H), 7.40 (ddd, *J* = 8.0, 4.8, 0.9 Hz, 1H), 7.19 (d, *J* = 7.7 Hz, 1H), 4.93 (td, *J* = 7.3, 5.0 Hz, 1H), 3.80 (s, 3H), 2.60 (t, *J* = 7.2 Hz, 2H), 2.29 (dtd, *J* = 14.7, 7.4, 5.1 Hz, 1H), 2.21 – 2.09 (m, 1H), 1.86 (s, 3H).
^{13}C NMR (101 MHz, $CDCl_3$) δ 172.4, 165.4, 152.7, 148.3, 135.4, 129.6, 123.7, 52.9, 52.4, 31.4, 30.3, 15.7.

[41] Yamaguchi, T.; Matsumura, Y.; Ishii, T.; Tokuoka, Y.; Kurita, K. Synthesis of Nicotinamide Derivatives Having a Hydroxy Substituted Benzene Ring and the Influence of Their Structures on the Apoptosis-Inducing Activity Against Leukemia Cells. *Drug Dev. Res.* **2011**, *72*, 289–297.

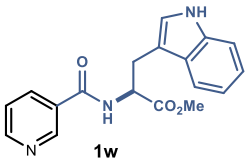

1w

methyl nicotinoyl-L-tryptophanate (1w)

Prepared according to GP4 using nicotinic acid (616 mg, 5.0 mmol), and methyl L-tryptophanate (1.09 g, 1.0 equiv.). Purification by column chromatography (SiO_2, 100% EtOAc) afforded product **1w** as a yellow oil (1.26 g, 78% yield) which displayed spectroscopic data consistent with those reported previously.[42]

^{1}H NMR (400 MHz, $CDCl_3$) δ 8.84 (d, *J* = 1.5 Hz, 1H), 8.68 (dd, *J* = 4.8, 1.7 Hz, 1H), 8.32 (s, 1H), 7.99 (dt, *J* = 7.9, 2.0 Hz, 1H), 7.53 (dd, *J* = 7.9, 1.1 Hz, 1H), 7.35 (dt, *J* = 8.2, 0.9 Hz, 1H), 7.32 (ddd, *J* = 7.9, 4.9, 0.9 Hz, 1H), 7.18 (ddd, *J* = 8.2, 7.0, 1.2 Hz, 1H), 7.08 (ddd, *J* = 8.0, 7.0, 1.0 Hz, 1H), 6.75 (d, *J* = 7.7 Hz, 1H), 5.14 (dt, *J* = 7.7, 5.2 Hz, 1H), 3.75 (s, 3H), 3.52 – 3.40 (m, 2H).
^{13}C NMR (101 MHz, $CDCl_3$) δ 172.3, 165.2, 152.4, 148.2, 136.3, 135.3, 129.8, 127.7, 123.6, 123.0, 122.6, 120.0, 118.6, 111.6, 109.9, 53.7, 52.7, 27.6.

Synthesis of the Radical Clock Substrates

The substrates for the radical clock experiments **36a** and **36b** were synthesized from the corresponding vinyl pyridines *via* cyclopropanation with diphenyldiazomethane (Scheme 3.17).

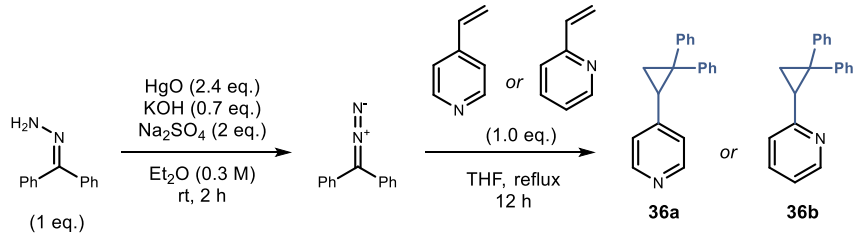

Scheme 3.17. Synthesis of 4-(2,2-diphenylcyclopropyl)pyridines.

Diphenyldiazomethane To benzophenone hydrazone (2.50 g, 12.7 mmol), anhydrous sodium sulfate (3.62 g, 2 equiv.), yellow mercuric oxide (II) (6.62 g, 2.4 equiv.) and potassium hydroxide (500 mg, 0.7 equiv., in 1 mL EtOH), was added 40 ml of diethyl ether. The suspension was stirred at room temperature for 2 hours. The reaction mixture was filtered, and the filtrate concentrated under reduced pressure. The resulting dark red oil was dissolved in hexanes at 50°C and filtered again. The solvent was evaporated under reduced pressure to obtain a dark red oil that was left to freeze overnight. Dark red crystals (2.47 g, quantitative yield) of diphenyldiazomethane formed when warmed-up to room temperature.

[42] Lu, J.; Yin, L.; Liu, T.; Wang, Y. Synthesis of Pseudopeptides Based L-Tryptophan as a Potential Antimicrobial Agent. *Bioorg. Med. Chem. Lett.* **2007**, *17*, 1601–1607.

GP4 – General Procedure for the Synthesis of (2,2-diphenylcyclopropyl)pyridines

Diphenyldiazomethane (1.17 g, 6.0 mmol) and vinylpyridine (1 equiv.) were dissolved in THF (10 mL, 0.6 M). The solution was stirred under reflux overnight. After cooling down to room temperature, the dark solution was diluted with hexanes and filtered to remove the precipitate. The filtrate was concentrated under reduced pressure and the crude mixture purified by column chromatography to afford the pure (2,2-diphenylcyclopropyl)pyridines.

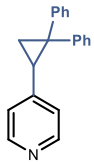

36a

4-(2,2-diphenylcyclopropyl)pyridine (36a) Prepared according to GP4 using 4-vinylpyridine (643 µL, 6.0 mmol). Purification by column chromatography (SiO_2, 1:40:59 Et_3N/EtOAc/hexanes) afforded **36a** as a light-yellow wax (1.1 g, 65% yield).

^{1}H NMR (400 MHz, $CDCl_3$) δ 8.29 (d, *J* = 6.2 Hz, 2H), 7.31 (d, *J* = 4.3 Hz, 4H), 7.25 – 7.10 (m, 6H), 6.74 (d, *J* = 6.2 Hz, 2H), 2.81 (dd, *J* = 8.8, 6.4 Hz, 1H), 2.05 (dd, *J* = 6.4, 5.5 Hz, 1H), 1.93 (dd, *J* = 8.8, 5.5 Hz, 1H).

^{13}C NMR (101 MHz, $CDCl_3$) δ 148.9, 148.5, 146.0, 139.2, 131.0, 128.5, 128.3, 127.3, 126.8, 126.3, 123.0, 40.8, 31.4, 21.5.

HRMS (ESI$^+$) Calculated for $C_{20}H_{18}N$ $[M+H]^+$: 272.1434 found: 272.1434.

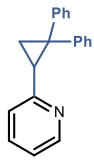

36b

2-(2,2-diphenylcyclopropyl)pyridine (36b) Prepared according to GP4 using 2-vinylpyridine (645 µL, 6.0 mmol). Purification by column chromatography (SiO_2, 1:40:59 Et_3N/EtOAc/hexanes) afforded **36b** as a light-yellow wax (1.0 g, 63% yield).

^{1}H NMR (400 MHz, $CDCl_3$) δ 8.35 (ddd, *J* = 4.9, 1.9, 0.9 Hz, 1H), 7.41 – 7.34 (m, 3H), 7.32 – 7.26 (m, 2H), 7.22 – 7.16 (m, 1H), 7.16 – 7.06 (m, 5H), 6.95 (ddd, *J* = 7.5, 4.9, 1.2 Hz, 1H), 6.80 (dt, *J* = 7.9, 1.1 Hz, 1H), 3.13 (dd, *J* = 8.7, 6.5 Hz, 1H), 2.34 (dd, *J* = 6.5, 5.1 Hz, 1H), 1.85 (dd, *J* = 8.7, 5.1 Hz, 1H).

^{13}C NMR (101 MHz, $CDCl_3$) δ 158.4, 148.6, 146.5, 140.2, 135.3, 131.0, 128.3, 127.9, 127.5, 126.2, 126.0, 122.3, 120.6, 40.2, 33.8, 20.3.

HRMS (ESI$^+$) Calculated for $C_{20}H_{18}N$ $[M+H]^+$: 272.1434 found: 272.1433.

Synthesis of tert-butyl pyrimidin-2-ylcarbamate 1bb

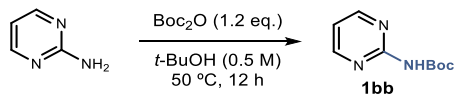

Scheme 3.18. Synthesis of *N*-Boc-2-aminopyrimidine 1bb.

2-Aminopyrimidine (475 mg, 5.0 mmol) and di-tert-butyl carbonate (1.31 g, 1.2 equiv.) were dissolved in tert-butyl alcohol (10 mL, 0.5 M). The reaction was stirred at 50ºC overnight.

The solvent was then removed under reduced pressure and the residue dissolved in ethyl acetate. The organic layer was washed three times with brine and dried over MgSO4, and the solvent was removed to afford **1bb** as a white solid (486 mg, 50% yield) which displayed spectroscopic data consistent with those reported previously.[43]

^{1}H NMR (300 MHz, $CDCl_3$) δ 8.62 (d, *J* = 4.9 Hz, 2H), 7.99 (s, 1H), 6.98 (t, *J* = 4.9 Hz, 1H), 1.57 (s, 9H).

^{13}C NMR (101 MHz, $CDCl_3$) δ 158.4, 157.9, 150.5, 115.7, 81.6, 28.2.

Synthesis of Pyridinium and Collidinium Salts

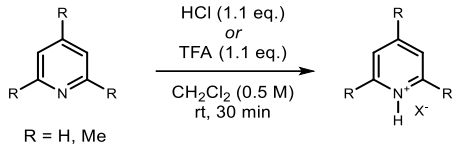

Scheme 3.19. Synthesis of pyridinium and 2,4,6-collidinium salts.

To a solution of the azine (5.5 mmol) in CH_2Cl_2 (10 mL, 0.5 M) was added conc. HCl (400 µL, 1.1 equiv.) or trifluoroacetic acid (424 µL, 1.1 equiv.) dropwise. After stirring for 30 min, the solvent was removed under reduced pressure to afford the pure pyridine hydrochloride salt.

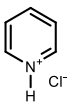

1a.HCl

Pyridinium hydrochloride (1a·HCl) Using pyridine (445 µL, 5.5 mmol). **1a·HCl** was obtained as a white powder (460 mg, 72% yield).

^{1}H NMR (400 MHz, $CDCl_3$) δ 8.94 (d, *J* = 5.5 Hz, 2H), 8.51 (t, *J* = 7.7 Hz, 1H), 8.04 (t, *J* = 6.9 Hz, 2H).

^{13}C NMR (101 MHz, $CDCl_3$) δ 145.8, 141.2, 127.3.

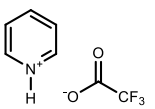

1a.TFA

Pyridinium trifluoroacetate (1a·TFA) Using pyridine (445 µL, 5.5 mmol). **1a·TFA** was obtained as a white powder (931 mg, 88% yield).

^{1}H NMR (400 MHz, $CDCl_3$) δ 8.87 (br s, 2H), 8.27 (tt, *J* = 7.8, 1.6 Hz, 1H), 7.81 (dd, *J* = 7.8, 6.4 Hz, 2H).

^{13}C NMR (101 MHz, $CDCl_3$) δ 143.4, 143.2, 126.3.

^{19}F{^{1}H} NMR (376 MHz, $CDCl_3$) δ -75.8.

[43] Deetz, M. J.; Forbes, C. C.; Jonas, M.; Malerich, J. P.; Smith, B. D.; Wiest, O. Unusually Low Barrier to Carbamate C−N Rotation. *J. Org. Chem.* **2002**, *67*, 3949–3952.

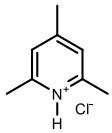

collidine.HCl

2,4,6-Collidinium hydrochloride (collidine·HCl) Using 2,4,6-collidine (728 µL, 5.5 mmol). **Collidine·HCl** was obtained as a white powder (620 mg, 71% yield).

^{1}H NMR (400 MHz, $CDCl_3$) δ 7.22 (s, 2H), 2.93 (s, 6H), 2.54 (s, 3H).

^{13}C NMR (101 MHz, $CDCl_3$) δ 157.7, 153.1, 125.1, 22.0, 19.3.

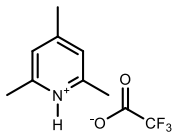

collidine.TFA

2,4,6-Collidinium trifluoroacetate (collidine·TFA) Using 2,4,6-collidine (728 µL, 5.5 mmol). **Collidine·TFA** was obtained as a white powder (1.23, 95% yield).

^{1}H NMR (400 MHz, $CDCl_3$) δ 7.19 (s, 2H), 2.74 (s, 6H), 2.50 (d, J = 0.7 Hz, 3H).

^{13}C NMR (101 MHz, $CDCl_3$) δ 157.6, 153.2, 124.9, 21.9, 19.2.

^{19}F NMR (376 MHz, $CDCl_3$) δ -75.9.

Electrochemical, Photophysical and Spectroscopic studies

Electrochemical Studies

For all cyclic voltammetry (CV) measurements, a platinum disk electrode (diameter 3 mm) was used as working electrode. A silver wire coated with AgCl immersed in a 3 M aqueous solution of NaCl and separated from the analyte by a fritted glass disk was employed as the reference electrode. A Pt wire counter-electrode completed the electrochemical setup. The scan rate used in each CV experiment is indicated case by case. Potentials are quoted with the following notation: E_p^C refers to the cathodic peak potential, E_p^A refers to the anodic peak potential

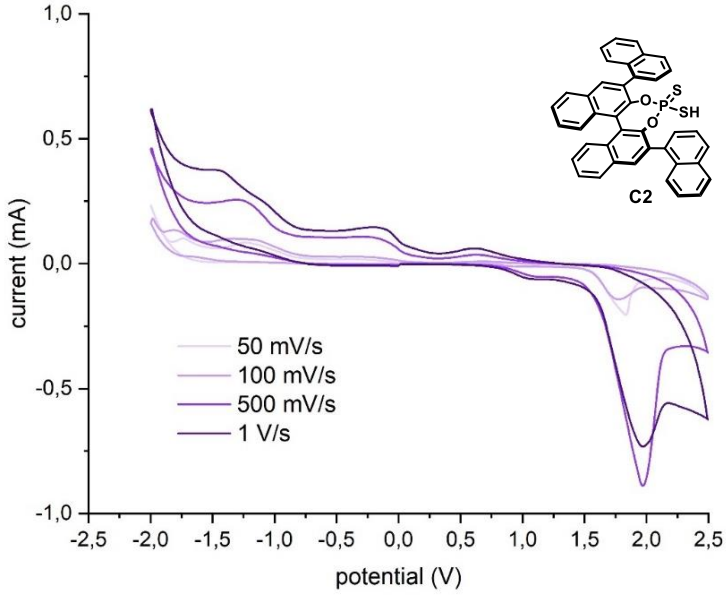

Figure 3.31. Cyclic voltammogram for catalyst C2 [0.02M] in [0.1 M] $TBAPF_6$ in CH_3CN. Measurement started by oxidation from 0 to +2.0 V and finishing at 0 V. Platinum disk working electrode, Ag/AgCl (NaCl 3 M) reference electrode, Pt wire auxiliary electrode. One irreversible oxidation observed at +1.12 V.

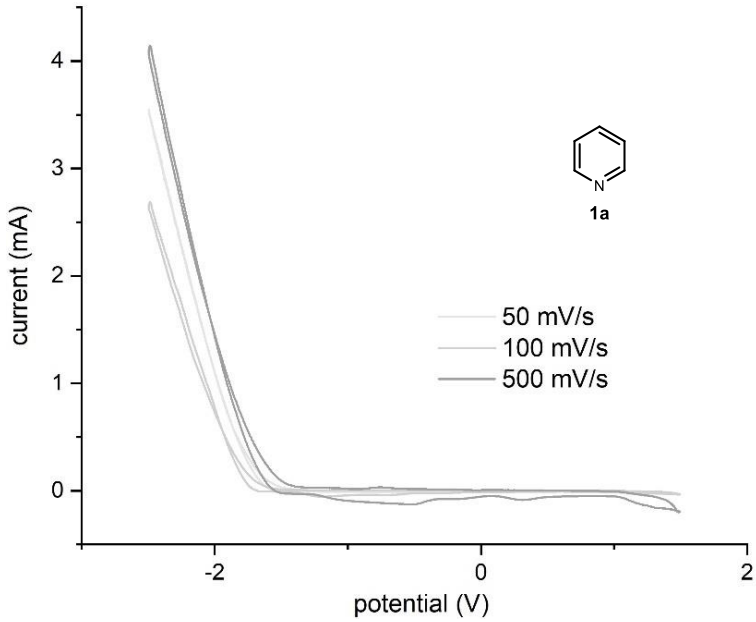

Figure 3.32. Cyclic voltammogram for pyridine 1a [0.025M] in [0.1 M] $TBAPF_6$ in CH_3CN. Measurement started by reduction from 0 to -2.5 V and finishing at 0 V. Platinum disk working electrode, Ag/AgCl (NaCl 3 M) reference electrode, Pt wire auxiliary electrode. No reduction wave was observed.

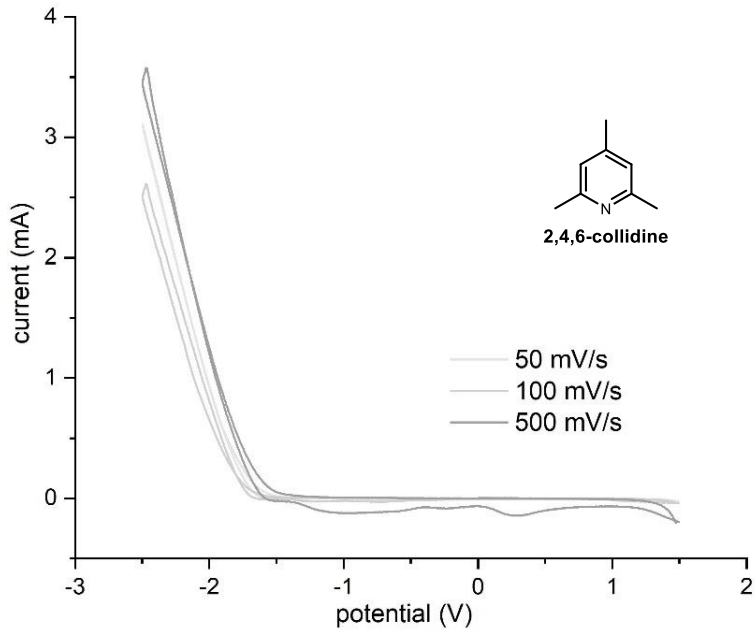

Figure 3.33. Cyclic voltammogram for 2,4,6-collidine [0.025M] in [0.1 M] $TBAPF_6$ in CH_3CN. Measurement started by reduction from 0 to -2.5 V and finishing at 0 V. Platinum disk working electrode, Ag/AgCl (NaCl 3 M) reference electrode, Pt wire auxiliary electrode. No reduction wave was observed.

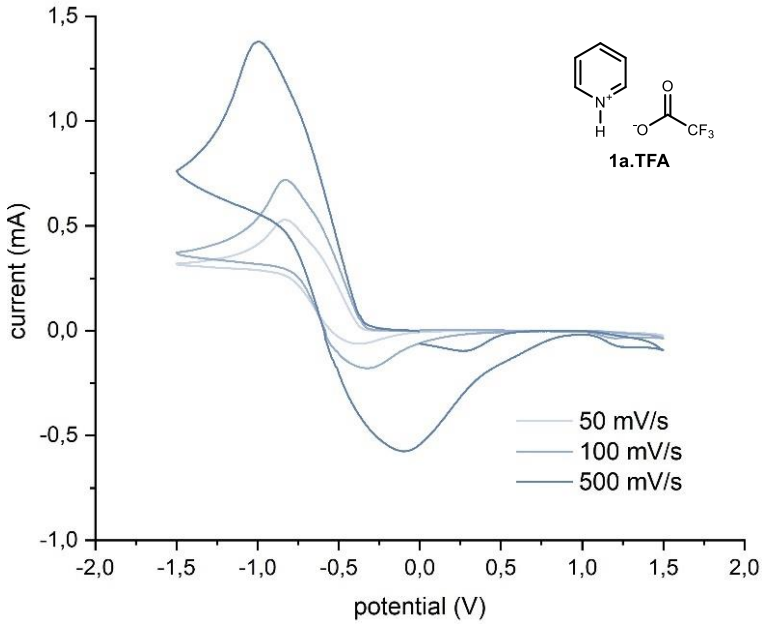

Figure 3.34. Cyclic voltammogram for **1a**·TFA [0.025M] in [0.1 M] $TBAPF_6$ in CH_3CN. Measurement started by reduction from 0 to -1.5 V and finishing at 0 V. Platinum disk working electrode, Ag/AgCl (NaCl 3 M) reference electrode, Pt wire auxiliary electrode. One reversible reduction wave observed at -0.6 V.

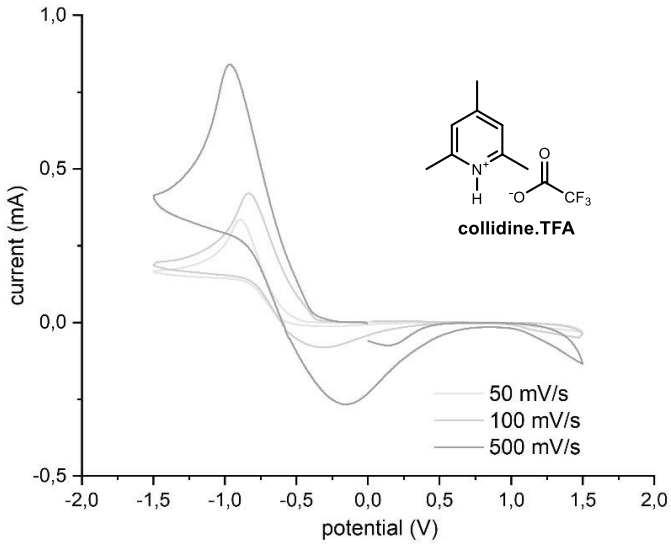

Figure 3.35. Cyclic voltammogram for collidine·TFA [0.025M] in [0.1 M] $TBAPF_6$ in CH_3CN. Measurement started by reduction from 0 to -1.5 V and finishing at 0 V. Platinum disk working electrode, Ag/AgCl (NaCl 3 M) reference electrode, Pt wire auxiliary electrode. One reversible reduction wave observed at -0.6 V.

Absorption Spectroscopy Analysis

The absorption profiles of the different reaction component were recorded in order to identify the photoactive species (Figure 3.36). 1:1 mixtures of **A2** + **1a** (green line) and **A2** + 2,4,6-collidine (orange line) display the same absorption as $\mathbf{A2}^-$ (light blue line) thus excluding the formation of EDA complexes between **A2** and pyridine **1a** or **A2** and 2,4,6-collidine.

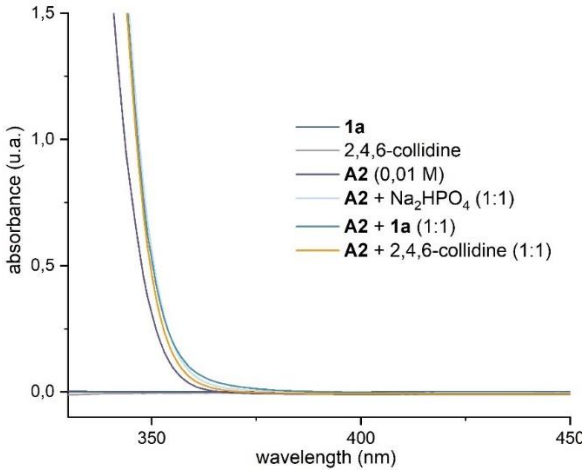

Figure 3.36. Optical absorption spectra of the reaction components, recorded in acetone in 1 mm path quartz cuvettes using a Shimadzu 2401PC UV−vis spectrophotometer.

Evaluation of the Excited-State Potential of A2$^-$

Using the data collected from the cyclic voltammetry (CV) studies (Section F.1) and from the absorption spectra (Section F.2) of catalyst **A2**, we could estimate the redox potential relative to its excited state **[A2$^-$]***, by means of the following Equation 1:

$$E(\mathbf{A2^\bullet/[A2^-]^*}) = E(\mathbf{A2^\bullet/A2^-}) - E_{0\text{-}0}(\mathbf{[A2^-]^*/A2^-}) \quad \text{[Eq. 1]}$$

Since the electrochemical oxidation of **A2$^-$** 1a is irreversible (Figure 3.31), the irreversible peak potential E_p^{anode} was used for E(**A2$^\bullet$/A2$^-$**). $E_{0\text{-}0}$([**A2$^-$]*/A2$^-$**), which is the excited state energy of the anion of the catalyst **A2**, was estimated spectroscopically from the position of the long wavelength tail of the absorption spectrum recorded in acetone (370 nm, Figures 3.9).

For the catalyst **A2**, the E_p^{anode}, which provides the E(**A2$^\bullet$/A2$^-$**), is *1.12 V* (Figures 3.31), while the position of the long wavelength tail of the absorption spectrum corresponds to *370 nm* (Figure 3.31), which translates into an $E_{0\text{-}0}$(**[A2$^-$]*/A2$^-$**) of *3.350 eV*.

$$E(\mathbf{A2^\bullet/[A2^-]^*}) = 1.12 - 3.35 = \mathbf{-2.23\ V}\ \text{(vs Ag/AgCl)}$$

Transient Absorption Spectroscopy (TAS)

Studies with microsecond transient absorption spectroscopy (TAS) were performed using an excitation source of NdYAG (neodymium-doped yttrium aluminium garnet) Opolette laser with an optical parametric oscillator (OPO) system that allows variable wavelength excitation from 400 -1800 nm, pulse width of 6 ns, up to 2 mJ of energy from OPO output with fiber optic coupled, and high energy output from direct NdYAG harmonics 355 (20 mJ, 5 ns) and 532 (45mJ, 6 ns). The system is completed with 150 W tungsten lamp as probe; 2 monochromators Minuteman MM151; Si amplified photodetector module for VIS; DSPDAU high speed data rate recorder and interface software from RAMDSP. Laser intensity for the chosen wavelength was 355 nm – 1.30 mJ.

In a typical transient absorption spectroscopy experiment, a solution of catalyst **A2** in acetone was prepared under an argon atmosphere and transferred into a screw-top 3.0 mL quartz cuvette for measurement. Upon irradiation with the appropriated wavelength, the decay of absorption at 625 nm of the transient excited state [**A2$^-$]*** was recorded. The same signal was observed upon irradiation from 400 nm to 800 nm but in lower intensity and higher noise.

As shown on Figure 3.37, **[A2$^-$]*** displayed a first order exponential with a half-lifetime of ~5 µs.

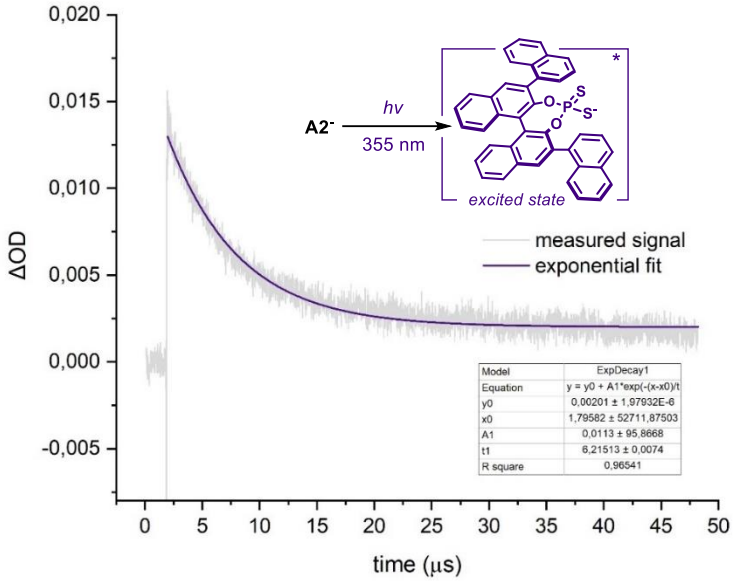

Figure 3.37. Absorption at 625 nm of the transient excited state of A2$^-$ generated upon 355 nm laser excitation. [A2] = 0.01 M in acetone. A first order exponential fit (purple line) was applied to the signal to facilitate the lifetime measurement. ΔOD: optical density variation.

Emission Spectrum and Stern-Volmer Quenching Studies

Emission Spectrum of [A2$^-$]*

The emission spectra were recorded in a Fluorolog Horiba Jobin Yvon spectrofluorimeter equipped with a photomultiplier detector, a double monochromator, and a 350W xenon light source. 2 mL of a 5 mM solution of **A2·Et$_3$N** (obtained by dissolving **A2** and Et$_3$N in CH_2Cl_2 in a 1:1 ratio, followed by solvent removal) in thoroughly degassed acetone were placed in a 10 x10 mm light path quartz fluorescence cuvette equipped with Silicone/PTFE 3.2 mm septum under an argon atmosphere. The excitation wavelength was fixed at 350 nm (incident light slit regulated to 5 mm), while the emission light was acquired from 355 nm to 500 nm (emission light slit regulated to 5 mm). A solvent blank was subtracted from all the measurements.

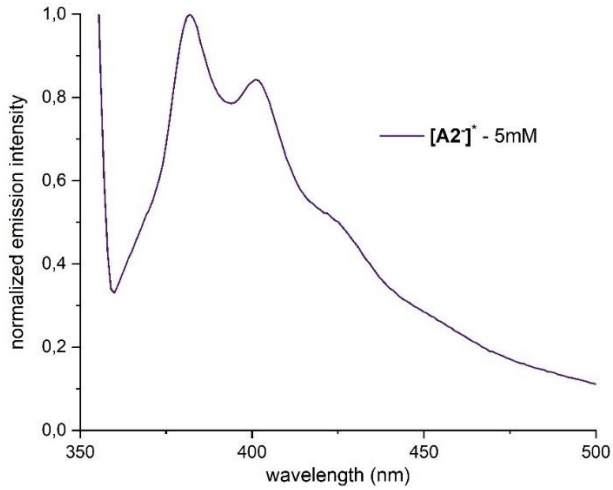

Figure 3.38. Normalized emission of [**A2**-]* upon 350 nm irradiation in acetone.

Stern-Volmer Quenching Studies using 1a·HCl as the Quencher

A 5.10^{-2} M solution of **1a·HCl** in acetone was prepared, and 5 µL of this stock solution were added to the solution of catalyst salt **A2·Et$_3$N**, prepared as described above. The addition of this solution of **1a·HCl** was repeated five consecutive times. After each addition, an absorption spectrum and an emission spectrum of the solution were recorded. The excitation wavelength was fixed at 350 nm (incident light slit regulated to 5 mm); the emission light was acquired from 355 nm to 500 nm (emission light slit regulated to 5 mm). A solvent blank was subtracted from all the measurements. The excitation wavelength was chosen in order to avoid saturation of the emission detector. The results shown in Figure 3.39 indicate that **1a**$^+$**-H** quenches the excited state of **A2**$^-$ and its emission. No change in the absorption spectra of the solution was observed during the addition of **1a·HCl**.

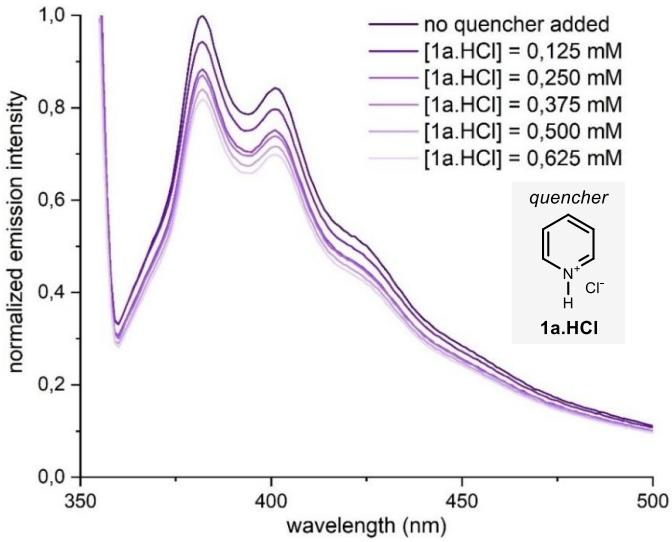

Figure 3.39. Quenching of the emission of $[A2^{-}]^{*}$ (5 mM in acetone) in the presence of increasing amounts of 1a.HCl.

The Stern-Volmer plot, reported in Figure 3.40, shows a linear correlation between the amounts of **1a·HCl** and the ratio I^0/I. On the basis of the following Equation 1, it is possible to calculate the Stern-Volmer constant K_{SV}.

$$I^0/I = 1 + K_{SV}[Q] \quad \textbf{Eq. 1}$$

We calculated a Stern-Volmer quenching constant of **346.4 M^{-1}**.

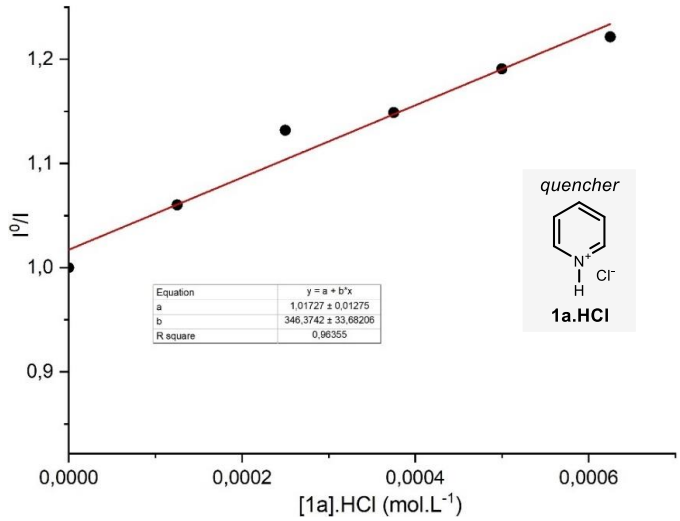

Figure 3.40. Stern-Volmer quenching plot using 1a.HCl as a quencher.

Stern-Volmer Quenching Studies Using Collidine.HCl as the Quencher

A 2.10^{-2} M solution of 2,4,6-collidine hydrochloride in acetone was prepared, and 10 μL of this stock solution were added to the solution of catalyst salt **A2·Et$_3$N**, prepared as described above. The addition of this 2,4,6-collidine hydrochloride solution was repeated five consecutive times. After each addition, an absorption spectrum and an emission spectrum of the solution were recorded. The excitation wavelength was fixed at 350 nm (incident light slit regulated to 5 mm); the emission light was acquired from 355 nm to 500 nm (emission light slit regulated to 5 mm). A solvent blank was subtracted from all the measurements. The excitation wavelength was chosen in order to avoid saturation of the emission detector. The results shown in Figure S20 indicate that 2,4,6-collidinium quenches the excited state of **A2$^-$** and its emission. No change in the absorption spectra of the solution was observed during the addition of 2,4,6-collidine hydrochloride.

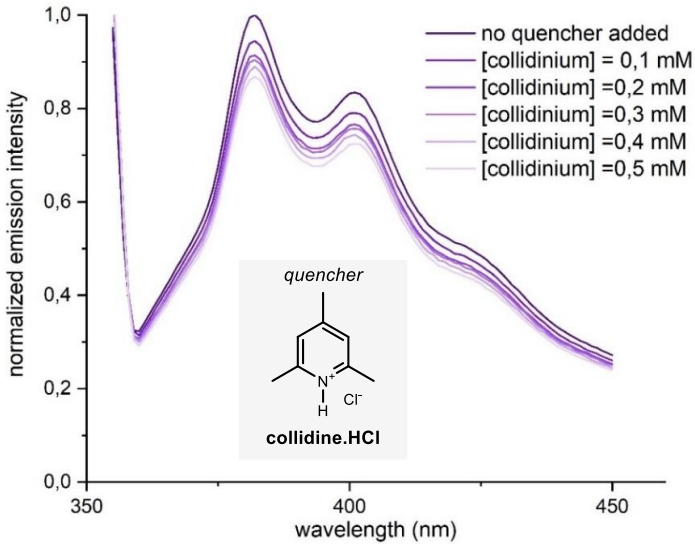

Figure 3.41. Quenching of the emission of [A2·]* (5 mM in acetone) in the presence of increasing amounts of collidine.HCl (collidinium on the graph).

The Stern-Volmer plot, reported in Figure S21, shows a linear correlation between the amounts of 2,4,6-collidine hydrochloride and the ratio I^0/I. On the basis of the following Equation 1, it is possible to calculate the Stern-Volmer constant K_{SV}.

$$I^0/I = 1 + K_{SV}[Q] \quad \textbf{Eq. 1}$$

We calculated a Stern-Volmer quenching constant of **283.4 M^{-1}**.

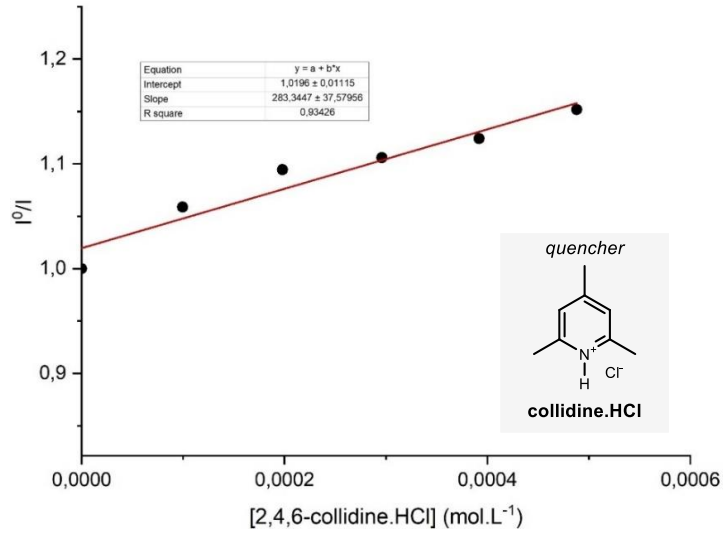

Figure 3.42. Stern-Volmer quenching plot using collidine.HCl as a quencher.

Emission Spectrum of $[Ir(ppy)_2dtbbpy]PF_6$

The emission spectra were recorded in a Fluorolog Horiba Jobin Yvon spectrofluorimeter equipped with a photomultiplier detector, a double monochromator, and a 350W xenon light source. 10 µL of a 1 mM solution of $[Ir(ppy)_2dtbbpy]PF_6$ in thoroughly degassed acetone were placed in a 10 x10 mm light path quartz fluorescence cuvette equipped with Silicone/PTFE 3.2 mm septum under an argon atmosphere. 2 mL acetone were added to this solution to reach a final concentration of 5 µM. The excitation wavelength was fixed at 390 nm (incident light slit regulated to 5 mm), while the emission light was acquired from 450 nm to 680 nm (emission light slit regulated to 5 mm). A solvent blank was subtracted from all the measurements.

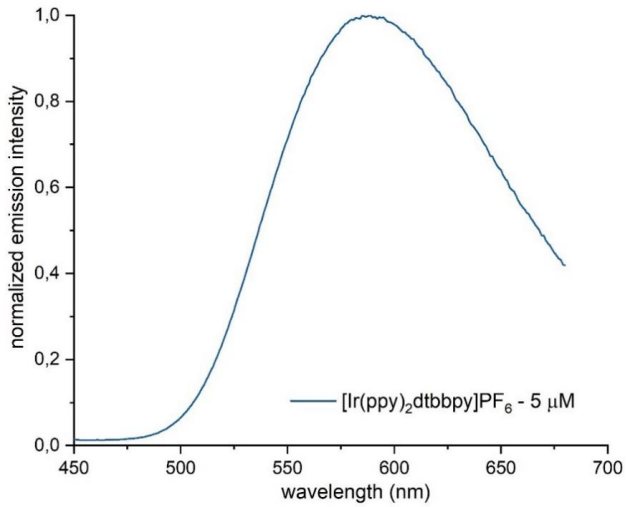

Figure 3.43. Normalized emission of $[Ir(ppy)_2dtbbpy]PF_6$ upon 390 nm irradiation in acetone.

Stern-Volmer Quenching Studies Using 1a·HCl as the Quencher

A 0.1 M solution of **1a·HCl** in acetone was prepared, and 5 μL of this stock solution were added to the solution of $[Ir(ppy)_2dtbbpy]PF_6$, prepared as described above. The addition of this solution of **1a·HCl** was repeated five consecutive times. After each addition, an absorption spectrum and an emission spectrum of the solution were recorded. The excitation wavelength was fixed at 390 nm (incident light slit regulated to 5 mm); the emission light was acquired from 450 nm to 680 nm (emission light slit regulated to 5 mm). A solvent blank was subtracted from all the measurements. The excitation wavelength was chosen in order to avoid saturation of the emission detector. The results shown in Figure 3.44 indicate that **1a$^+$-H** quenches the excited state of $[Ir(ppy)_2dtbbpy]PF_6$ and its emission. No change in the absorption spectra of the solution was observed during the addition of **1a·HCl**.

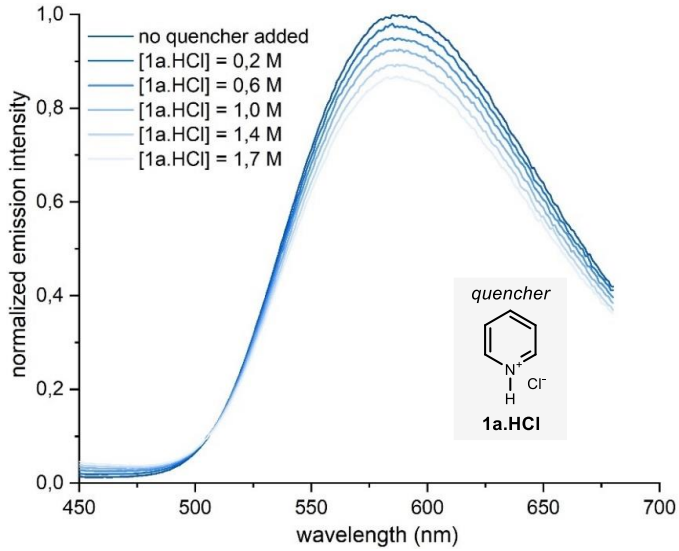

Figure 3.44. Quenching of the emission of $[Ir(ppy)_2dtbbpy]PF_6$ (5 μM in acetone) in the presence of increasing amounts of 1a.HCl.

The Stern-Volmer plot, reported in Figure S24, shows a linear correlation between the amounts of **1a.HCl** and the ratio I^0/I. On the basis of the following Equation 1, it is possible to calculate the Stern-Volmer constant K_{SV}.[16]

$$I^0/I = 1 + K_{SV}[Q] \quad \textbf{Eq. 1}$$

We calculated a Stern-Volmer quenching constant of **90.0 M^{-1}**.

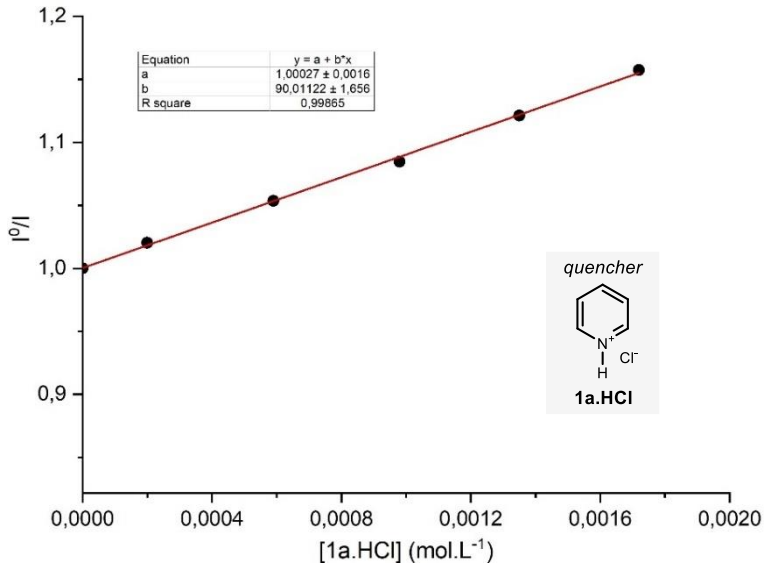

Figure 3.45. Stern-Volmer quenching plot using 1a.HCl as a quencher.

Electron Paramagnetic Resonance (EPR)

Continuous wave (CW) EPR spectra were acquired on a Bruker EMX Micro X-band spectrometer operating at 9.385e^9 using a Bruker ER 1164 HS resonator. A 150 mL Suprasil offset liquid nitrogen dewar flask (Wilmad-LabGlass) was used for low-temperature measurements. Individual EPR tubes were filled with ~0.7 mL of the solution and were placed at the same position of the resonant cavity for EPR spectral acquisition. The spectral data were collected at 77 K with the following spectrometer settings: microwave power = 0.5305 mW; center field = 3354.2 G, sweep width = 300 G, sweep time = 22.5 s, modulation frequency = 100 KHz, modulation amplitude = 1 G, power attenuation = 25 dB, time constant = 0.01 ms.

The pyridinyl radical **II** was generated by premixing pyridine **1a** (8 μL, 0.100 mmol) with catalyst **A2** (12.7 mg, 0.020 mmol) in 0.7 mL methanol in an EPR tube under inert atmosphere. The EPR sample was measured first in the absence of light at 77K using liquid N_2. As expected, no signal was observed. The same sample was allowed to reach room temperature and was irradiated for 15 min using a 365PF EvoluChemTM LED spotlight. The sample was immediately frozen using liquid N_2 and was inserted into the EPR cavity. A new signal at 3347.4 G was observed with a g-value of 2.00324 (Figure 3.46).

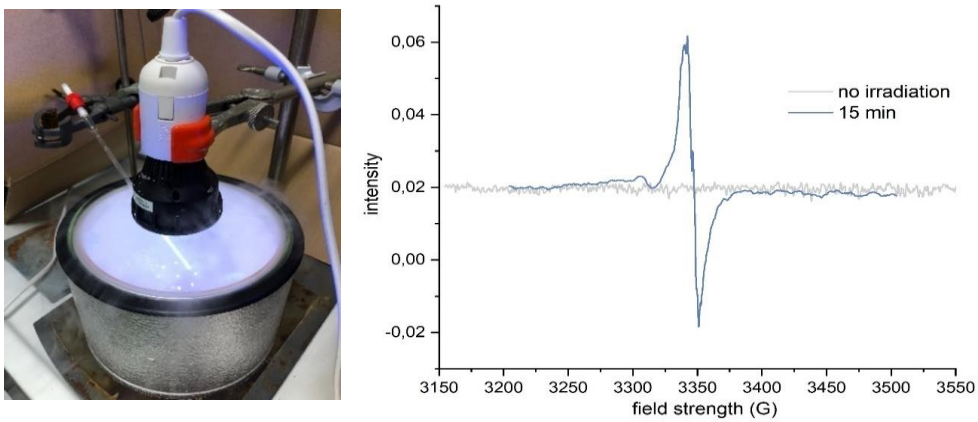

Figure 3.46. Experimental setup for the EPR experiment (*left*) and measured EPR spectra of a 5:1 mixture of 1a and C2 in methanol in the absence and after 15 min of irradiation (*right*).

The measured g-value of 2.00324 is in accordance with reports from the literature for the same radical. The hyperfine coupling constants could not be calculated due to the poor resolution of the spectrum.

Radical Clock Experiments

GP5 – General procedure for the radical clock experiments

To an argon-purged glass vial, containing the dithiophosphoric acid catalyst **A2** (12.7 mg, 0.02 mmol), and the appropriate (2,2-diphenylcyclopropyl)pyridine **4** (0.1 mmol), was added 2,4,6-collidine (6.6 µL, 0.05 mmol), followed by cyclohexene **2a** (101 µL, 1.0 mmol) and argon-sparged HPLC grade acetone (2 mL, 0.05M). The vial was sealed with Parafilm, and placed in the 365 nm irradiation setup. The reaction was stirred for 16 h, then the solvent was evaporated and the crude mixture purified by flash column chromatography on silica gel.

The formation of products **5a** and **5b** supports the formation of the delocalized pyridinyl radical **II** which then undergoes a rapid radical ring-opening to generate the highly stabilized bis-benzylic radical **IV**. The latter is then able to couple with a cyclohexene radical **III** generated in the meantime (Figure 3.47).

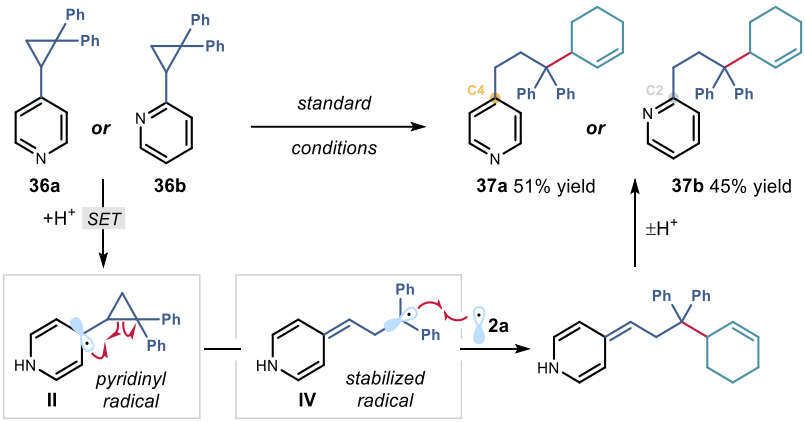

Figure 3.47. Radical clock experiments to probe the formation of the key pyridinyl radical II.

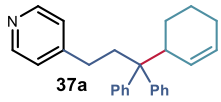

4-(3-(cyclohex-2-en-1-yl)-3,3-diphenylpropyl)pyridine (37a)
Prepared according to GP5 using 4-(2,2-diphenylcyclopropyl)pyridine **36a** (27.1 mg, 0.1 mmol). Purification by column chromatography (SiO_2, 1:10:89 Et_3N/EtOAc/hexanes) afforded product **37a** (18.0 mg, 51% yield) as a colorless oil.

^{1}H NMR (400 MHz, $CDCl_3$) δ 8.44 – 8.42 (m, 2H), 7.33 – 7.20 (m, 10H), 6.98 – 6.95 (m, 2H), 5.84 (dp, *J* = 10.4, 2.1 Hz, 1H), 5.61 (ddt, *J* = 10.2, 5.0, 2.5 Hz, 1H), 3.26 (dtq, *J* = 9.8, 4.8, 2.4 Hz, 1H), 2.47 – 2.33 (m, 2H), 2.31 – 2.15 (m, 2H), 1.93 – 1.82 (m, 2H), 1.73 – 1.48 (m, 4H).

^{13}C NMR (101 MHz, $CDCl_3$) δ 151.9, 149.6, 145.6, 143.3, 129.7, 129.4, 129.0, 129.0, 127.7, 127.1, 126.1, 126.0, 123.7, 54.4, 41.1, 40.5, 30.5, 25.0, 24.8, 22.4.
HRMS (ESI$^+$) Calculated for $C_{26}H_{28}N$ $[M+H]^+$: 354.2216, found: 354.2216.

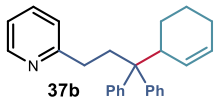

2-(3-(cyclohex-2-en-1-yl)-3,3-diphenylpropyl)pyridine (37b)
Prepared according to GP5 using 2-(2,2-diphenylcyclopropyl)pyridine **36b** (27.1 mg, 0.1 mmol). Purification by column chromatography (SiO_2, 1:10:89 Et_3N/EtOAc/hexanes) afforded product **37b** (15.8 mg, 45% yield) as a colorless oil.

^{1}H NMR (400 MHz, $CDCl_3$) δ 8.53 (d, *J* = 4.0 Hz, 1H), 7.54 (td, *J* = 7.7, 1.9 Hz, 1H), 7.35 – 7.28 (m, 8H), 7.27 – 7.20 (m, 2H), 7.09 (dd, *J* = 6.4, 4.9 Hz, 1H), 6.94 (d, *J* = 7.8 Hz, 1H), 5.92 – 5.84 (m, 1H), 5.66 – 5.58 (m, 1H), 3.36 – 3.26 (m, 1H), 2.66 – 2.36 (m, 4H), 2.03 – 1.94 (m, 1H), 1.92 – 1.82 (m, 1H), 1.76 – 1.61 (m, 2H), 1.62 – 1.47 (m, 2H).

^{13}C NMR (101 MHz, $CDCl_3$) δ 162.6, 149.1, 145.9, 143.6, 136.3, 129.9, 129.5, 129.4, 128.7, 127.7, 127.0, 125.9, 125.8, 122.7, 120.9, 54.4, 41.4, 39.5, 33.6, 29.7, 25.1, 24.8, 22.5.
HRMS (ESI$^+$) Calculated for $C_{26}H_{28}N$ $[M+H]^+$: 354.2216, found: 354.2218.

Computational Studies

All calculations were performed using Gaussian 09W (version 7.0). Gaussview 5.0.9 was used to generate input files for geometry and energy optimizations, and to visualize the output files. Spin density contour maps were generated from output (.chk) files. Mulliken spin densities were obtained directly from the output (.chk) files. NBO analysis was performed after full geometry and energy optimization. All calculations were performed without geometry restrictions and using unrestricted B3LYP functional unless otherwise stated. Energy values are given in atomic units (a.u.). *A*(X) values are literature values for the experimentally verified equilibrium constant between equatorial and axial conformations of a substituted cyclohexane.

Table 3.4. Calculated molecular orbitals of the pyridinyl radical II.

MO of II	**MO visualization**	**Electron density contour map** (0.15 Å above plane)
uB3LYP/6-311G+(d) **SOMO** (orbital 22) Energy = -0.11812	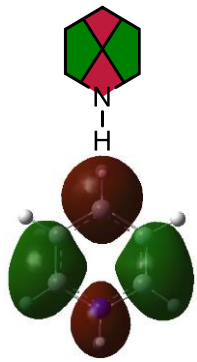	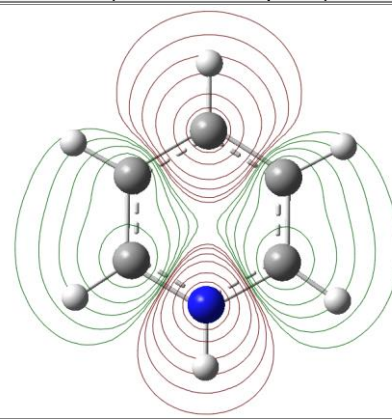
uB3LYP/6-311G+(d) **SOMO–1** (orbital 21) Energy = -0.27560	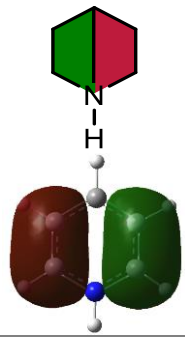	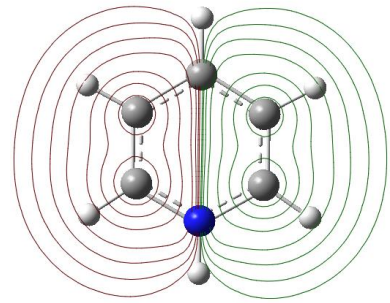

NBO analysis

A full NBO analysis was performed on the pyridinyl radical **II**. Using this approach, the wavefunction is analysed in terms of localised orbitals. Since the system is open-shell with doublet multiplicity, the α and β spins are treated separately. Both α and β orbitals indicate

localised density about the C4 atom in the model pyridinyl radical, with minimal denisty located at the C2 position.

Table 3.5. NBO analysis of the pyridinyl radical I.

Substrate	**NBO analysis of the SOMO**	**Electron density contour map** (positive values only, 0.06 Å above plane)
1a NBO 22α occupancy = 0.94357 Energy = -0.14039	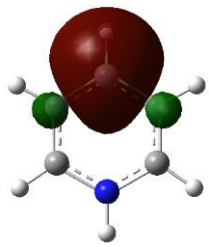	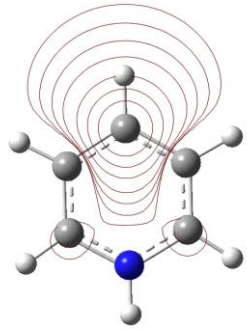
1a NBO 22β occupancy = 0.35099 Energy = -0.05085	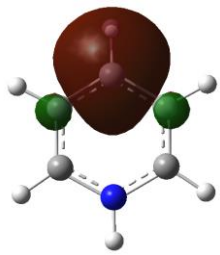	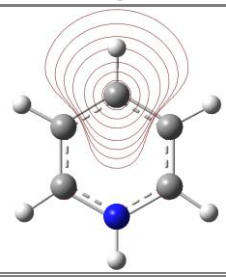

Spin density calculations

Table 3.6. Calculates spin densities on the pyridinyl-type radicals for different classes of substrates.

Substrate	**Mulliken spin densities**	**Contour map of spin density** (positive values only, 0.15 Å above plane)	**Total Energy** / a.u.	**Dipole moment**/ debye
3a 5.6 : 1 rr C4/C2	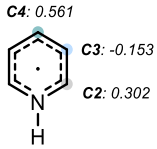	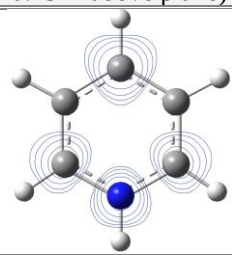	-248.84962	2.0395 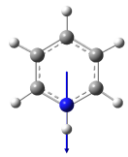
3a 5.6 : 1 rr C4/C2	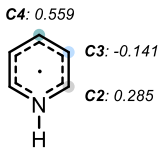 SCI-PCM(acetone) solvation model	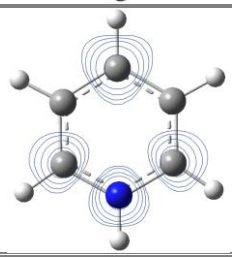	-248.85550	2.7639 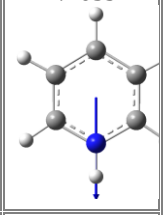
3a 5.6 : 1 rr C4(major) /C2(minor)	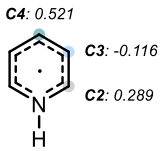 uB3LYP/6-311G+(d)	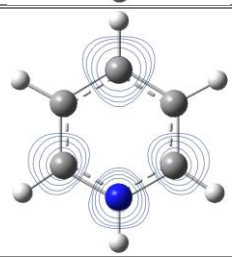	-248.89864	2.0144 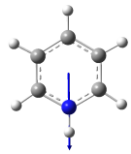
3a 5.6 : 1 rr C4(major) /C2(minor)	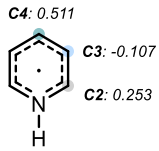 uB3LYP/cc-pVDZ[26]	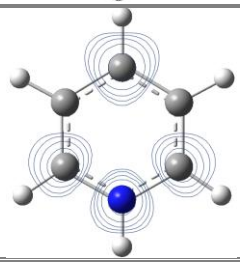	-248.85512	2.0490 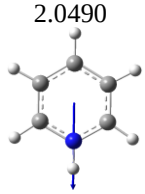

3a 5.6 : 1 rr C4(major) /C2(minor)	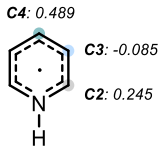 uB3LYP/cc-pVTZ [26]	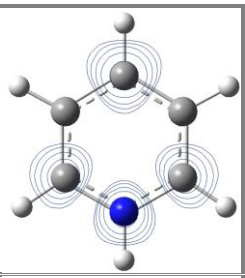	- 248.9328 6	1.9879 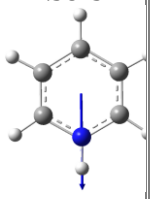
3d 5 : 1 r.r. C4(major) /C2(minor)	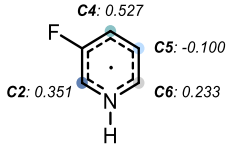 steric factor: *A*(F) = 0.15	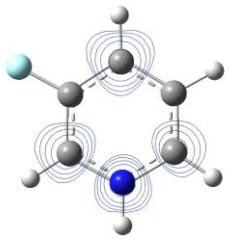	- 348.0899 0	3.2951 
3e 8:1 r.r. C4(major) /C2(minor)	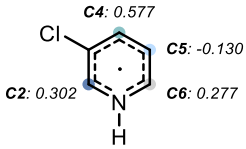 steric factor: *A*(Cl) = 0.43	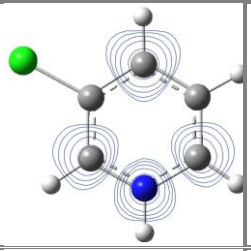	- 708.4448 3	3.4003 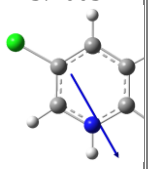
3f 9:1 r.r. C4(major) /C6(minor)	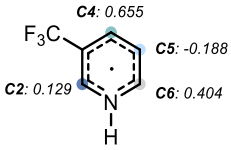 steric factor: *A*(CF_3) = 2.1	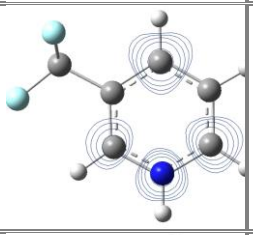	- 585.9121 0	4.5760 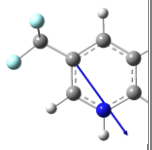
3b C4 only	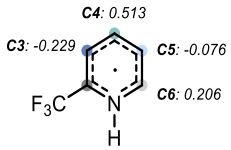 steric factor: *A*(CF_3) = 2.1	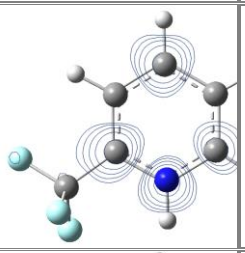	- 585.9132 7	2.8984 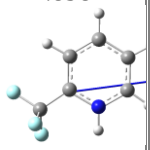
3g 14 : 1 C4(major) /C6(minor)	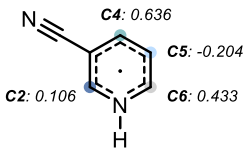 steric factor: *A*(CN) = 0.17	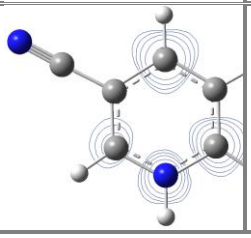	- 341.0978 7	6.2084 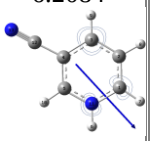

3j C6 only	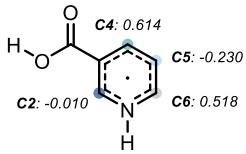 steric factor: $A(CO_2^-)$ = 1.92 $A(CO_2H)$ = 1.35	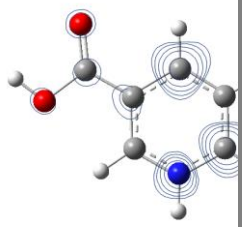	-437.55155	4.8603 
3l (Me instead of Et) C6 only	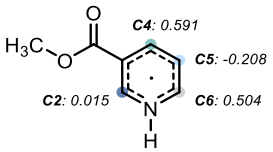 steric factor: $A(CO_2CH_3)$ = 1.27	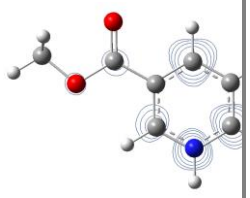	-476.71603	4.3854 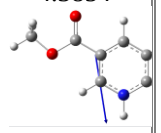
3o (Me instead of Et) C2 only	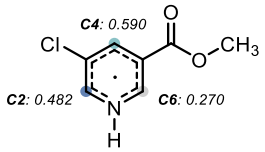 steric factor: A(Cl) = 0.43 $A(CO_2CH_3)$ = 1.27	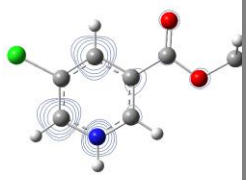	-936.33518	5.5148 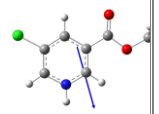
3aa C4/6 only	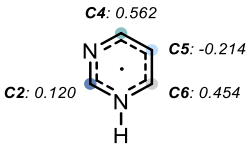	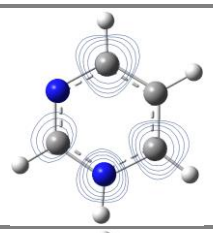	-264.89105	3.5256 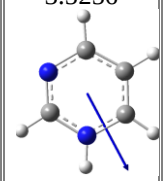
3cc C4/5 only	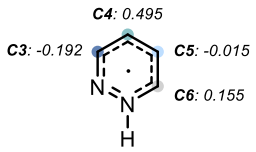	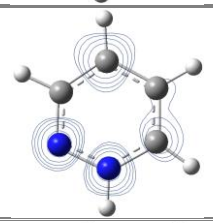	-264.87491	2.1416 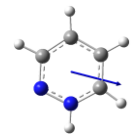
3x C1 only	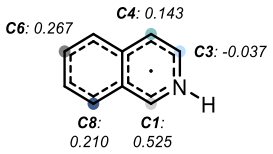	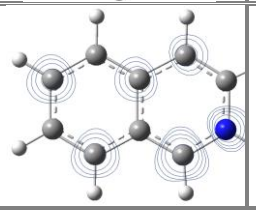	-402.50603	3.1094 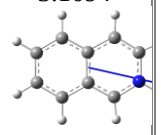

Input and optimized geometries of the computed structures

Table 3.7. Input and optimized geometries for different classes of pyridines used in this study.

uB3LYP/6-31G+(d)

Input orientation:

Center Number	Atomic Number	Atomic Type	Coordinates (Angstroms) X	Y	Z
1	6	0	1.064257	0.100402	0.000000
2	6	0	2.459417	0.100402	0.000000
3	6	0	3.156955	1.308153	0.000000
4	6	0	2.459301	2.516662	-0.001199
5	6	0	1.064476	2.516584	-0.001678
6	1	0	0.514498	-0.851915	0.000450
7	1	0	3.008925	-0.852111	0.001315
8	1	0	4.256635	1.308233	0.000634
9	1	0	3.009501	3.468805	-0.001258
10	1	0	0.514354	3.468865	-0.002631
11	1	0	-0.732729	1.308561	-0.000862
12	7	0	0.366875	1.308378	-0.000682

Output orientation:

Center Number	Atomic Number	Atomic Type	Coordinates (Angstroms) X	Y	Z
1	6	0	1.080128	0.093151	0.000076
2	6	0	2.447733	0.090813	0.000506
3	6	0	3.186109	1.308319	0.000030
4	6	0	2.447831	2.525981	-0.001049
5	6	0	1.080261	2.523744	-0.001481
6	1	0	0.472873	-0.804016	0.000380
7	1	0	2.961049	-0.866796	0.001215
8	1	0	4.269771	1.308304	0.000361
9	1	0	2.961289	3.483508	-0.001562
10	1	0	0.473068	3.420958	-0.002326
11	1	0	-0.622646	1.308558	-0.001276
12	7	0	0.385000	1.308491	-0.000783

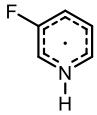

uB3LYP/6-31G+(d)

Input orientation:

Center Number	Atomic Number	Atomic Type	Coordinates (Angstroms) X	Y	Z
1	6	0	-0.053548	0.381526	0.000000
2	6	0	1.341612	0.381526	0.000000
3	6	0	2.039150	1.589277	0.000000
4	6	0	1.341496	2.797786	-0.001199
5	6	0	-0.053329	2.797708	-0.001678
6	1	0	-0.603307	-0.570791	0.000450
7	1	0	3.138830	1.589357	0.000634
8	1	0	1.891696	3.749929	-0.001258
9	1	0	-0.603451	3.749989	-0.002631
10	1	0	-1.850534	1.589685	-0.000862
11	7	0	-0.750930	1.589502	-0.000682
12	9	0	2.016220	-0.787834	0.001614

Output orientation:

Center Number	Atomic Number	Atomic Type	Coordinates (Angstroms) X	Y	Z
1	6	0	-0.283536	-1.186974	0.000014
2	6	0	-0.947190	0.009590	-0.000006
3	6	0	-0.306335	1.260773	-0.000037
4	6	0	1.122714	1.232024	0.000017
5	6	0	1.809714	0.051880	0.000028
6	1	0	-0.777228	-2.148581	0.000058
7	1	0	-0.876751	2.180463	-0.000050
8	1	0	1.684899	2.160694	0.000061
9	1	0	2.890693	-0.015836	0.000072
10	1	0	1.629579	-2.029428	0.000138
11	7	0	1.120467	-1.159622	-0.000078
12	9	0	-2.307406	-0.025968	0.000020

uB3LYP/6-31G+(d)

Input orientation:

Center Number	Atomic Number	Atomic Type	Coordinates (Angstroms) X	Y	Z
1	6	0	2.171732	-0.537123	0.000000
2	6	0	2.869270	0.670628	0.000000
3	6	0	2.171616	1.879137	-0.001199
4	6	0	0.776791	1.879059	-0.001678
5	6	0	0.079190	0.670853	-0.000682
6	1	0	0.226813	-1.489440	0.000450
7	1	0	2.721240	-1.489636	0.001315
8	1	0	2.721816	2.831280	-0.001258
9	1	0	0.226669	2.831340	-0.002631
10	1	0	-1.020414	0.671036	-0.000862
11	7	0	0.776572	-0.537123	0.000000
12	17	0	4.629270	0.670756	0.001015

Output orientation:

Center Number	Atomic Number	Atomic Type	Coordinates (Angstroms) X	Y	Z
1	6	0	0.137087	-1.175938	0.000009
2	6	0	-0.529869	0.018652	0.000005
3	6	0	0.142674	1.266263	0.000015
4	6	0	1.568040	1.222683	0.000002
5	6	0	2.245256	0.036851	-0.000008
6	1	0	2.034359	-2.044033	0.000145
7	1	0	-0.351691	-2.140787	-0.000044
8	1	0	-0.405517	2.199149	-0.000037
9	1	0	2.138570	2.146636	0.000002
10	1	0	3.325175	-0.044337	-0.000006
11	7	0	1.537166	-1.167340	-0.000026
12	17	0	-2.287070	-0.009194	-0.000001

uB3LYP/6-31G+(d)

Input orientation:

Center Number	Atomic Number	Atomic Type	Coordinates (Angstroms) X	Y	Z
1	6	0	-1.572959	1.077644	0.000000
2	6	0	-0.177799	1.077644	0.000000
3	6	0	0.519739	2.285395	0.000000
4	6	0	-1.572740	3.493826	-0.001678
5	6	0	-2.270341	2.285620	-0.000682
6	1	0	-2.122718	0.125327	0.000450
7	1	0	0.371709	0.125131	0.001315
8	1	0	1.619419	2.285475	0.000634
9	1	0	0.372285	4.446047	-0.001258
10	1	0	-2.122862	4.446107	-0.002631
11	6	0	-3.810341	2.285876	-0.000934
12	7	0	-0.177915	3.493904	-0.001199
13	9	0	-4.260264	3.381702	0.646550
14	9	0	-4.260130	2.298877	-1.273734
15	9	0	-4.260628	1.177275	0.624162

Output orientation:

Center Number	Atomic Number	Atomic Type	Coordinates (Angstroms) X	Y	Z
1	6	0	-0.717641	-1.265327	0.000203
2	6	0	-2.130730	-1.225039	-0.000111
3	6	0	-2.814249	-0.036887	-0.000204
4	6	0	-0.709081	1.172423	-0.000082
5	6	0	-0.023423	-0.006431	0.000041
6	1	0	-0.174242	-2.201587	0.000264
7	1	0	-2.701866	-2.148821	-0.000323
8	1	0	-3.892869	0.050245	-0.000062
9	1	0	-2.587776	2.049329	-0.003265
10	1	0	-0.227267	2.141317	-0.000294
11	6	0	1.473882	0.008186	0.000038
12	7	0	-2.093052	1.170782	0.000850
13	9	0	1.995157	1.262524	-0.000567
14	9	0	1.989316	-0.628937	1.086967
15	9	0	1.989176	-0.629976	-1.086575

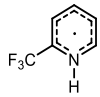

uB3LYP/6-31G+(d)

Input orientation:

Center Number	Atomic Number	Atomic Type	Coordinates (Angstroms) X	Y	Z
1	6	0	-3.291775	-0.925402	0.000000
2	6	0	-1.884897	-0.925402	0.000000
3	6	0	-1.218206	0.301205	0.000000
4	6	0	-1.972279	1.475992	-0.000241
5	6	0	-3.375481	1.373187	-0.000382
6	1	0	-0.119662	0.340981	-0.000950
7	1	0	-1.330165	-1.872303	0.000264
8	1	0	-1.488243	2.460916	-0.000342
9	1	0	-4.008830	2.278250	-0.000463
10	6	0	-4.080255	-2.248240	0.000170
11	9	0	-3.761881	-2.961740	1.101104
12	9	0	-5.403963	-1.983115	0.002987
13	9	0	-3.766123	-2.959494	-1.103432
14	1	0	-5.104747	0.221998	-0.000239
15	7	0	-4.035011	0.198236	-0.000197

Standard orientation:

Center Number	Atomic Number	Atomic Type	Coordinates (Angstroms) X	Y	Z
1	6	0	0.033837	0.093336	-0.041109
2	6	0	0.770766	1.261582	-0.025599
3	6	0	2.171473	1.230159	0.006485
4	6	0	2.820733	-0.047183	0.015425
5	6	0	2.085975	-1.194840	0.001467
6	1	0	2.747272	2.148145	0.007951
7	1	0	0.238324	2.206782	-0.040334
8	1	0	3.903587	-0.118800	0.030185
9	1	0	2.520898	-2.187467	0.001618
10	6	0	-1.446482	0.033845	-0.000841
11	9	0	-2.020090	1.223760	-0.273400
12	9	0	-1.938659	-0.879232	-0.900888
13	9	0	-1.938534	-0.376430	1.211105
14	1	0	0.174978	-1.984492	-0.206886
15	7	0	0.696095	-1.148350	0.020162

uB3LYP/6-31G+(d)

Input orientation:

Center Number	Atomic Number	Atomic Type	Coordinates (Angstroms) X	Y	Z
1	6	0	1.328226	0.368139	0.000000
2	6	0	2.025764	1.575890	0.000000
3	6	0	1.328110	2.784399	-0.001199
4	6	0	-0.066715	2.784321	-0.001678
5	6	0	-0.764316	1.576115	-0.000682
6	1	0	-0.616693	-0.584178	0.000450
7	1	0	1.877734	-0.584374	0.001315
8	1	0	3.125444	1.575970	0.000634
9	1	0	1.878310	3.736542	-0.001258
10	1	0	-1.863920	1.576298	-0.000862
11	7	0	-0.066934	0.368139	0.000000
12	6	0	-0.837054	4.117804	-0.003012
13	7	0	-1.410605	5.110643	-0.004006

Output orientation:

Center Number	Atomic Number	Atomic Type	Coordinates (Angstroms) X	Y	Z
1	6	0	-2.160826	0.018270	-0.000003
2	6	0	-1.490305	1.216739	0.000005
3	6	0	-0.082895	1.280550	-0.000005
4	6	0	0.639720	0.024941	0.000000
5	6	0	-0.043011	-1.164778	0.000006
6	1	0	-1.900503	-2.065995	0.000092
7	1	0	-3.237246	-0.087854	0.000019
8	1	0	-2.074038	2.132775	0.000013
9	1	0	0.451855	2.221246	0.000009
10	1	0	0.454751	-2.127197	0.000014
11	7	0	-1.417309	-1.180287	-0.000026
12	6	0	2.068614	-0.005003	0.000000
13	7	0	3.234081	-0.005040	0.000001

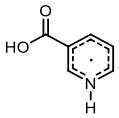

uB3LYP/6-31G+(d)

Input orientation:

Center Number	Atomic Number	Atomic Type	Cordinates (Angstroms) X	Y	Z
1	6	0	-1.957447	0.687943	0.000000
2	6	0	-0.562287	0.687943	0.000000
3	6	0	0.135251	1.895694	0.000000
4	6	0	-0.562403	3.104203	-0.001199
5	6	0	-2.654829	1.895919	-0.000682
6	1	0	-2.507206	-0.264374	0.000450
7	1	0	-0.012779	-0.264570	0.001315
8	1	0	-0.012203	4.056346	-0.001258
9	1	0	-2.507350	4.056406	-0.002631
10	1	0	-3.754433	1.896102	-0.000862
11	6	0	1.675251	1.895806	0.000888
12	8	0	2.323586	3.024099	0.000886
13	8	0	2.323750	0.767608	0.001637
14	1	0	3.268006	0.940753	0.001975
15	7	0	-1.957228	3.104125	-0.001678

Output orientation:

Center Number	Atomic Number	Atomic Type	Coordinates (Angstroms) X	Y	Z
1	6	0	-1.846517	1.235758	-0.000009
2	6	0	-0.451769	1.268688	-0.000015
3	6	0	0.258534	0.002882	-0.000003
4	6	0	-0.457573	-1.162464	0.000011
5	6	0	-2.547568	0.049417	0.000003
6	1	0	-2.411275	2.160866	-0.000014
7	1	0	0.094889	2.198772	-0.000023
8	1	0	0.036220	-2.125354	0.000020
9	1	0	-2.310211	-2.033397	0.000023
10	1	0	-3.622328	-0.038086	0.000002
11	6	0	1.720499	-0.122840	-0.000005
12	8	0	2.351904	-1.163205	-0.000025
13	8	0	2.345118	1.087968	0.000027
14	1	0	3.295374	0.903602	0.000025
15	7	0	-1.816069	-1.156164	0.000008

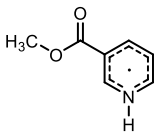

uB3LYP/6-31G+(d)

Input orientation:

Center Number	Atomic Number	Atomic Type	Coordinates (Angstroms) X	Y	Z
1	6	0	-1.957447	0.687943	0.000000
2	6	0	-0.562287	0.687943	0.000000
3	6	0	0.135251	1.895694	0.000000
4	6	0	-0.562403	3.104203	-0.001199
5	6	0	-2.654829	1.895919	-0.000682
6	1	0	-2.507206	-0.264374	0.000450
7	1	0	-0.012779	-0.264570	0.001315
8	1	0	-0.012203	4.056346	-0.001258
9	1	0	-2.507350	4.056406	-0.002631
10	1	0	-3.754433	1.896102	-0.000862
11	6	0	1.675251	1.895806	0.000888
12	8	0	2.323586	3.024099	0.000886
13	8	0	2.323750	0.767608	0.001637
14	7	0	-1.957228	3.104125	-0.001678
15	6	0	3.730299	1.025522	0.002140
16	1	0	3.989774	1.586288	0.875704
17	1	0	4.263063	0.097588	0.002689
18	1	0	3.990511	1.585675	-0.871598

Output orientation:

Center Number	Atomic Number	Atomic Type	Coordinates (Angstroms) X	Y	Z
1	6	0	-2.138094	-1.380207	-0.000002
2	6	0	-0.744762	-1.250449	-0.000007
3	6	0	-0.185310	0.091579	-0.000004
4	6	0	-1.034638	1.167651	0.000000
5	6	0	-2.974550	-0.280520	0.000005
6	1	0	-2.592131	-2.367549	-0.000002
7	1	0	-0.092714	-2.113141	-0.000010
8	1	0	-0.659430	2.184914	0.000003
9	1	0	-2.981746	1.818899	0.000009
10	1	0	-4.055100	-0.316860	0.000009
11	6	0	1.256636	0.389958	-0.000006
12	8	0	1.752436	1.509939	-0.000006
13	8	0	2.008487	-0.741379	0.000003
14	7	0	-2.387534	1.002855	0.000005
15	6	0	3.431092	-0.545118	0.000007
16	1	0	3.741627	0.007801	0.891015
17	1	0	3.860972	-1.547706	0.000008
18	1	0	3.741632	0.007801	-0.890998

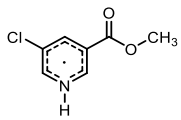

uB3LYP/6-31G+(d)

Input orientation:

Center Number	Atomic Number	Atomic Type	Coordinates X	Y	Z
1	6	0	-1.770117	0.175950	0.000000
2	6	0	-0.374957	0.175950	0.000000
3	6	0	0.322581	1.383701	0.000000
4	6	0	-0.375073	2.592210	-0.001199
5	6	0	-1.769898	2.592132	-0.001678
6	1	0	-2.319876	-0.776367	0.000450
7	1	0	1.422261	1.383781	0.000634
8	1	0	-2.320020	3.544413	-0.002631
9	1	0	-3.567103	1.384109	-0.000862
10	7	0	-2.467499	1.383926	-0.000682
11	6	0	0.395431	3.925598	-0.001282
12	8	0	-0.023430	5.082368	-0.002229
13	8	0	1.740095	3.743149	-0.000171
14	6	0	2.418807	5.001819	-0.000296
15	1	0	2.143449	5.555602	0.872861
16	1	0	3.476028	4.836949	0.000599
17	1	0	2.144790	5.554706	-0.874441
18	17	0	0.504531	-1.348548	0.002105

Standard orientation:

Center Number	Atomic Number	Atomic Type	Coordinates (Angstroms) X	Y	Z
1	6	0	2.204339	1.126388	-0.000011
2	6	0	1.794309	-0.196259	-0.000013
3	6	0	0.457391	-0.581541	-0.000003
4	6	0	-0.539362	0.481035	-0.000007
5	6	0	-0.117231	1.791214	-0.000028
6	1	0	3.228673	1.464149	-0.000004
7	1	0	0.164566	-1.621059	0.000012
8	1	0	-0.817758	2.616874	-0.000025
9	1	0	1.469753	3.079556	-0.000012
10	7	0	1.197652	2.105876	-0.000018
11	6	0	-1.984003	0.236485	0.000010
12	8	0	-2.856220	1.106130	0.000074
13	8	0	-2.276439	-1.086570	-0.000036
14	6	0	-3.674974	-1.435722	-0.000019
15	1	0	-4.166777	-1.041903	-0.892301
16	1	0	-3.700611	-2.524649	-0.000064
17	1	0	-4.166735	-1.041979	0.892320
18	17	0	3.048459	-1.432836	0.000019

Photochemical Reactions

Experimental Setups

Two different photochemical setups were used in this study, for UV- or blue light irradiation. Figure S6 depicts the emission spectra of the light sources used in these setups: a 365PF EvoluChem™ LED spotlight from HepatoChem, and a commercial 14 W 455 nm LEDs strip.

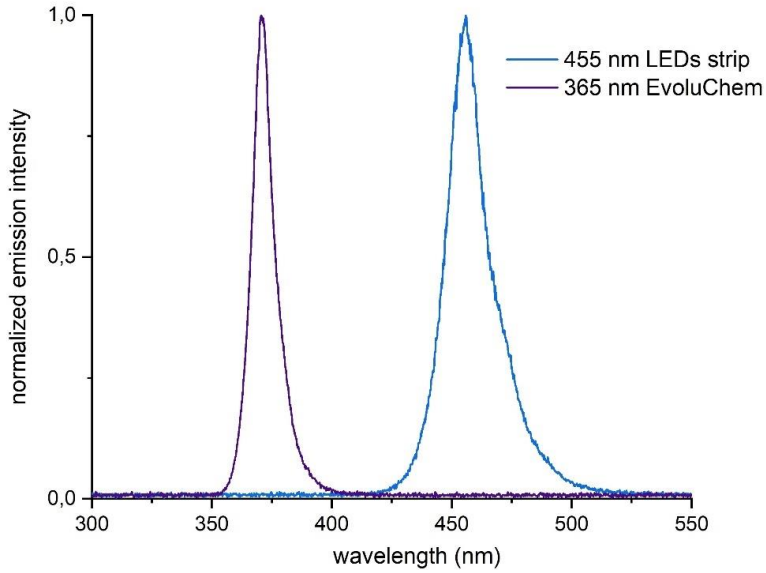

Figure 3.48. Emission spectra of the light sources used in this study.

365 nm Setup

The setup used for the reactions under UV-light consisted of two 365PF EvoluChem™ LED spotlights placed on two opposite sides of a rack. The vials were placed at ~1 cm of the lamps, with a maximum of 3 vials per lamp, allowing 6 reactions to run at the same time. A fan was placed on top of the vials, in order to dissipate the heat, thus maintaining the temperature at ~35ºC (Figure S7).

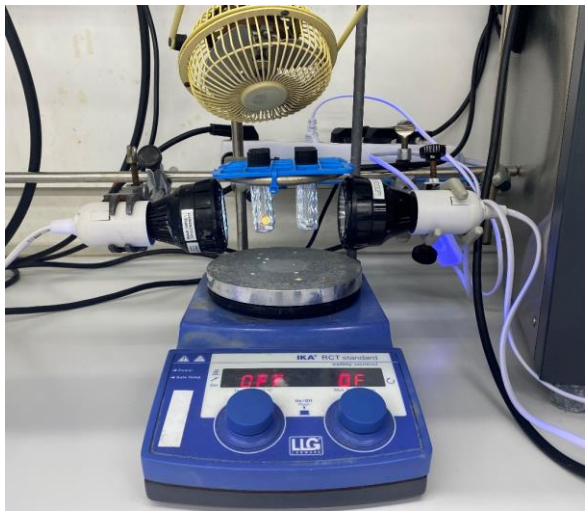

Figure 3.49. 365 nm setup in operation.

455 nm Photoreactor

The photoreactor used for the reactions under blue light consisted of a 12.5 cm diameter jar fitted with 4 standard B29 size quickfit-glass joints arranged around a central B29 size joint (Figure S6). A commercial 1-meter LEDs strip was wrapped around the jar, followed by a layer of aluminium foil and cotton for insulation. An inlet/outlet system provided circulation of liquid (ethylene glycol/water 1:1 mixture) from a Huber Minichiller 300 inside the jar. This setup allowed the performance of reactions at temperatures ranging from –20 ºC to 80 ºC with accurate control of the reaction temperature (± 1ºC, Figure S8).

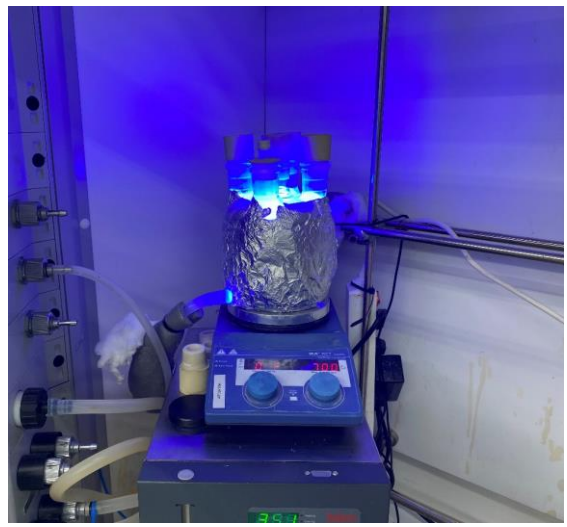

Figure 3.50. Fully assembled temperature-controlled photoreactor in operation.

In order to maintain consistent illumination between different experiments, only the four external positions were used to perform reactions. The central position was used to monitor the temperature using a thermometer inside an inserted Schlenk tube, ensuring that the reaction mixtures were at the desired temperature.

General Procedure of the direct allylation of azines

General Procedure A

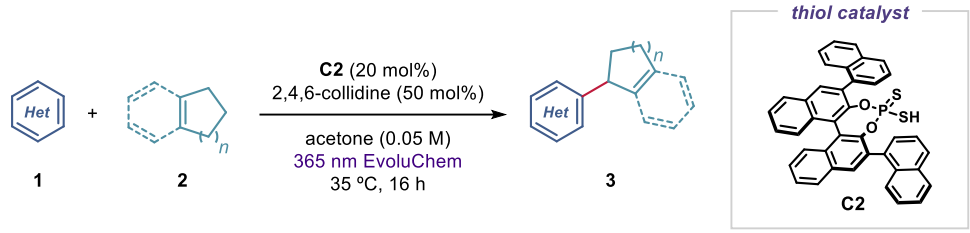

To an argon-purged glass vial, containing the dithiophosphoric acid catalyst **C2** (25.3 mg, 0.04 mmol), and azine **1** (0.2 mmol)**,** was added 2,4,6-collidine (13.2 µL, 0.1 mmol), followed by the allylic precursor **2** (2.0 mmol) and argon-sparged HPLC grade acetone (0.05 M). The vial was sealed with Parafilm, and placed in the 365 nm irradiation setup. The reaction was stirred for 16h, then the solvent was evaporated and the crude mixture purified by flash column chromatography on silica gel to furnish the product **3**.

General Procedure B

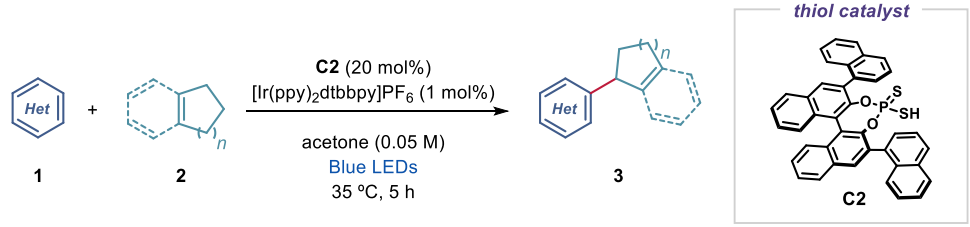

To an argon-purged glass vial, containing the dithiophosphoric acid catalyst **C2** (25.3 mg, 0.04 mmol), $[Ir(ppy)_2dtbbpy]PF_6$ (1.8 mg, 2.0 µmol), and azine **1** (0.2 mmol)**,** was added the allylic precursor **2** (2.0 mmol) followed by argon-sparged HPLC grade acetone (0.05 M). The vial was sealed with Parafilm, and placed in the 455 nm irradiation setup. The reaction was stirred for 5h, then the solvent was evaporated and the crude mixture purified by flash column chromatography on silica gel to furnish the product **3**.

Characterization of Products

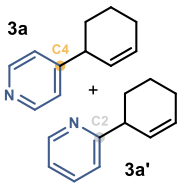

4-(cyclohex-2-en-1-yl)pyridine (3a) + 2-(cyclohex-2-en-1-yl)pyridine (3a')

Prepared according to General Procedure A using pyridine **1a** (16.2 µL, 0.2 mmol) and cyclohexene **2a** (203 µL, 2.0 mmol). The regioisomeric ratio **3a**/**3a'** (6:1) of the crude mixture was measured by ^1H NMR analysis. Purification by column chromatography (SiO_2, 1:10:89

Et_3N/EtOAc/hexanes) afforded product **3a** as a colorless oil (17.6 mg, 55% yield, > 20:1 *r.r.*). The minor regioisomer **3a'** was not isolated after column chromatography. **3a** displayed spectroscopic data consistent with those reported previously.[14]

^{1}H NMR (400 MHz, $CDCl_3$) δ 8.53 – 8.49 (m, 2H), 7.17 – 7.14 (m, 2H), 5.97 (m, 1H), 5.70 – 5.65 (m, 1H), 3.40 (m, 1H), 2.16 – 2.09 (m, 2H), 2.08 – 1.98 (m, 1H), 1.80 – 1.71 (m, 1H), 1.69 – 1.61 (m, 1H), 1.61 – 1.51 (m, 1H).

^{13}C NMR (126 MHz, $CDCl_3$) δ 155.3, 149.7, 129.7, 128.2, 123.1, 41.1, 31.7, 24.9, 20.8.

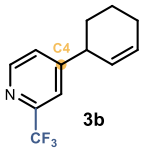

4-(cyclohex-2-en-1-yl)-2-(trifluoromethyl)pyridine (3b)

Prepared according to General Procedure A using 2-(trifluoromethyl)pyridine (23.0 µL, 0.2 mmol) and cyclohexene **2a** (203 µL, 2.0 mmol). No other regioisomer was detected in the crude mixture. Purification by column chromatography (SiO_2, 1:5:96 Et_3N/EtOAc/hexanes) afforded product **3b** as a colorless oil (29.3 mg, 65% yield, > 20:1 *r.r.*).

^{1}H NMR (500 MHz, $CDCl_3$) δ 8.64 (d, *J* = 5.0 Hz, 1H), 7.56 (d, *J* = 1.6 Hz, 1H), 7.36 (dd, *J* = 5.0, 1.6 Hz, 1H), 6.04 (m, 1H), 5.68 (m, 1H), 3.54 – 3.47 (m, 1H), 2.18 – 2.11 (m, 2H), 2.11 – 2.05 (m, 1H), 1.77 – 1.71 (m, 1H), 1.71 – 1.64 (m, 2H), 1.61 – 1.52 (m, 1H).

^{13}C NMR (126 MHz, $CDCl_3$) δ 157.5, 149.9, δ 148.3 (q, *J* = 34.0 Hz), 130.6, 127.1, 125.8, 119.8 (q, *J* = 2.9 Hz), 41.2, 31.8, 29.7, 24.8, 20.7.

^{19}F NMR (471 MHz, $CDCl_3$) δ -67.9.

HRMS (ESI$^+$) Calculated for $C_{12}H_{13}F_3N$ $[M+H]^+$: 228.0995 found: 228.0988.

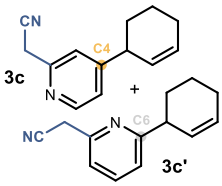

2-(4-(cyclohex-2-en-1-yl)pyridin-2-yl)acetonitrile (3c) + 2-(6-(cyclohex-2-en-1-yl)pyridin-2-yl)acetonitrile (3c')

Prepared according to General Procedure A using 2-pyridylacetonitrile (23.6 mg, 0.2 mmol) and cyclohexene **2a** (203 µL, 2.0 mmol). The regioisomeric ratio **3c**/**3c'** (8:1) of the crude mixture was measured by ^{1}H NMR analysis. Purification by column chromatography (SiO_2, 1:50:49 Et_3N/EtOAc/hexanes) afforded product **3c** as a colorless oil (17.4 mg, 44% yield, > 20:1 *r.r.*). The minor regioisomer **3c'** was not isolated after column chromatography.

^{1}H NMR (500 MHz, $CDCl_3$) δ 8.48 (d, *J* = 5.1 Hz, 1H), 7.30 (s, 1H), 7.14 (dd, *J* = 5.1, 1.6 Hz, 1H), 6.06 – 5.97 (m, 1H), 5.71 – 5.62 (m, 1H), 3.94 (s, 2H), 3.49 – 3.39 (m, 1H), 2.17 – 2.09 (m, 2H), 2.08 – 2.00 (m, 1H), 1.80 – 1.70 (m, 1H), 1.70 – 1.61 (m, 1H), 1.60 – 1.50 (m, 1H).

^{13}C NMR (126 MHz, $CDCl_3$) δ 157.3, 150.4, 149.8, 130.2, 127.6, 122.5, 121.6, 117.2, 41.2, 31.7, 26.6, 24.8, 20.8.

HRMS (ESI$^+$) Calculated for $C_{13}H_{15}N_2$ $[M+H]^+$: 199.1230 found: 199.1229.

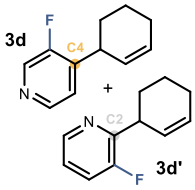

4-(cyclohex-2-en-1-yl)-3-fluoropyridine (3d) + 2-(cyclohex-2-en-1-yl)-3-fluoropyridine (3d')

Prepared according to General Procedure A using 3-fluoropyridine (17.2 µL, 0.2 mmol) and cyclohexene **2a** (203 µL, 2.0 mmol). The regioisomeric ratio **3d/3d'** (5:1) of the crude mixture was measured by ^{1}H NMR analysis. Purification by column chromatography (SiO_2, 1:4:95 Et_3N/EtOAc/hexanes) afforded a mixture of products **3d** and **3d'** as a colorless oil (16.5 mg, 47% yield, 6:1 *r.r.*). An analytically pure sample of **3d** was obtained by preparative TLC (SiO_2, 1:4:95 Et_3N/EtOAc/hexanes, >20:1 *r.r.*). Only the major product **3d** is described.

^{1}H NMR (400 MHz, $CDCl_3$) δ 8.39 (s, 1H), 8.35 (d, *J* = 4.9 Hz, 1H), 7.21 (dd, *J* = 6.5, 4.9 Hz, 1H), 6.06 – 5.98 (m, 1H), 5.68 – 5.57 (m, 1H), 3.85 – 3.74 (m, 1H), 2.18 – 2.10 (m, 2H), 2.09 – 2.03 (m, 1H), 1.76 – 1.66 (m, 2H), 1.63 – 1.53 (m, 1H).

^{13}C NMR (126 MHz, $CDCl_3$) δ 145.7 (d, *J* = 5.1 Hz), 141.7 (d, *J* = 12.4 Hz), 137.7, 137.5, 130.45, 126.9, 123.8, 33.8, 29.8, 24.8, 20.6.

^{19}F{^{1}H} NMR (471 MHz, $CDCl_3$) δ -59.03, -134.28 (d, *J* = 6.4 Hz).

HRMS (APCI$^+$) Calculated for $C_{11}H_{13}FN$ $[M+H]^+$: 178.1027 found: 178.1029.

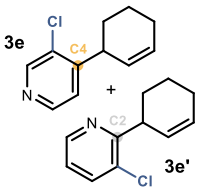

3-chloro-4-(cyclohex-2-en-1-yl)pyridine (3e) + 3-chloro-2-(cyclohex-2-en-1-yl)pyridine (3e')

Prepared according to General Procedure A using 3-chloro pyridine (22.7 mg, 0.2 mmol) and cyclohexene **2a** (203 µL, 2.0 mmol). Purification by column chromatography (SiO_2, 1:5:94 Et_3N/EtOAc/hexanes) afforded products **3e** + **3e'** (14.9 mg, 39% yield, 8:1 *r.r.*) as a colorless oil. Only the major product **3e** is described.

^{1}H NMR (400 MHz, $CDCl_3$) δ 8.54 (s, 1H), 8.41 (d, *J* = 5.0 Hz, 1H), 7.21 (d, *J* = 5.0 Hz, 1H), 6.09 – 6.02 (m, 1H), 5.67 – 5.58 (m, 1H), 3.91 – 3.83 (m, 1H), 2.17 – 2.06 (m, 3H), 1.73 – 1.65 (m, 2H), 1.58 – 1.44 (m, 1H).
^{13}C NMR (101 MHz, $CDCl_3$) δ 152.1, 149.3, 147.7, 131.7, 130.6, 127.2, 123.8, 37.6, 29.1, 24.9, 20.5.

HRMS (ESI$^+$) Calculated for $C_{11}H_{13}ClN$ $[M+H]^+$: 94.0731 found: 94.0732.

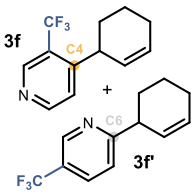

4-(cyclohex-2-en-1-yl)-3-(trifluoromethyl)pyridine (3f) + 6-(cyclohex-2-en-1-yl)-3-(trifluoromethyl)pyridine (3f')

Prepared according to General Procedure A using 3-(trifluoromethyl)pyridine (23.0 µL, 0.2 mmol) and cyclohexene **2a** (203 µL, 2.0 mmol). The regioisomeric ratio **3f/3f'** (9:1) of the crude mixture was measured by ^{1}H NMR analysis. Purification by column chromatography (SiO_2, 1:4:95 Et_3N/EtOAc/hexanes) afforded product **3f** as a colorless oil (20.1 mg, 44% yield, > 20:1 *r.r.*). The minor regioisomer **3f'** was not isolated after column chromatography.

^{1}H NMR (500 MHz, $CDCl_3$) δ 8.84 (s, 1H), 8.70 (d, *J* = 5.2 Hz, 1H), 7.38 (d, *J* = 5.2 Hz, 1H), 6.08 – 5.95 (m, 1H), 5.62 – 5.51 (m, 1H), 3.87 – 3.80 (m, 1H), 2.20 – 2.13 (m, 2H), 2.13 – 2.08 (m, 1H), 1.88 – 1.77 (m, 1H), 1.77 – 1.65 (m, 1H), 1.51 – 1.43 (m, 1H).
^{13}C NMR (126 MHz, $CDCl_3$) δ 155.0, 152.9, 146.8 (q, *J* = 6.5 Hz), 130.0, 127.9, 124.0, 37.6 (d, *J* = 1.8 Hz), 31.9, 24.7, 21.2.

^{19}F{^{1}H} NMR (376 MHz, $CDCl_3$) δ -59.1, -59.1.

HRMS (ESI^+) Calculated for $C_{12}H_{13}F_3N$ $[M+H]^+$: 228.0995 found: 228.0987.

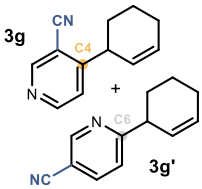

4-(cyclohex-2-en-1-yl)nicotinonitrile (3g) + 6-(cyclohex-2-en-1-yl)nicotinonitrile (3g')

Prepared according to General Procedure A using nicotinonitrile (20.8 mg, 0.2 mmol) and cyclohexene **2a** (203 µL, 2.0 mmol). The regioisomeric ratio **3g**/**3g'** (14:1) of the crude mixture was measured by ^{1}H NMR analysis. Purification by column chromatography (SiO_2, 1:4:95 Et_3N/EtOAc/hexanes) afforded product **3g** as a colorless oil (18.0 mg, 50% yield, > 20:1 *r.r.*). The minor regioisomer **3g'** was not isolated after column chromatography.

^{1}H NMR (400 MHz, $CDCl_3$) δ 8.81 (s, 1H), 8.69 (d, *J* = 5.3 Hz, 1H), 7.34 (d, *J* = 5.2 Hz, 1H), 6.10 – 6.05 (m, 1H), 5.63 – 5.58 (m, 1H), 3.86 – 3.80 (m, 1H), 2.20 – 2.11 (m, 3H), 1.76 – 1.67 (m, 2H), 1.58 – 1.49 (m, 1H).
^{13}C NMR (101 MHz, $CDCl_3$) δ 159.0, 153.2, 152.9, 131.6, 126.1, 123.0, 116.0, 110.1, 39.9, 30.9, 24.8, 20.7.

HRMS ($APCI^+$) Calculated for $C_{12}H_{13}N_2$ $[M+H]^+$: 185.1073 found: 185.1075.

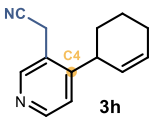

2-(4-(cyclohex-2-en-1-yl)pyridin-3-yl)acetonitrile (3h)

Prepared according to General Procedure A using 3-pyridylacetonitrile (21.3 µL, 0.2 mmol) and cyclohexene **2a** (203 µL, 2.0 mmol) prolonging the reaction time to 48 hours. No other regioisomer was detected in the crude mixture. Purification by column chromatography (SiO_2, 1:9:90 Et_3N/EtOAc/hexanes) afforded product **3h** as a colorless oil (13.0 mg, 33% yield, > 20:1 *r.r.*).

^{1}H NMR (400 MHz, $CDCl_3$) δ 8.50 (d, *J* = 2.4 Hz, 1H), 7.64 (dd, *J* = 8.1, 2.4 Hz, 1H), 7.25 (d, *J* = 8.1 Hz, 1H), 6.00 – 5.93 (m, 1H), 5.81 – 5.75 (m, 1H), 3.74 (s, 2H), 3.64 – 3.57 (m, 1H), 2.17 – 2.04 (m, 3H), 1.79 – 1.63 (m, 3H).
^{13}C NMR (101 MHz, $CDCl_3$) δ 153.6, 150.2, 150.1, 130.7, 127.5, 124.2, 123.5, 117.2, 37.8, 30.5, 24.8, 21.0, 18.8.

HRMS (ESI^+) Calculated for $C_{13}H_{15}N_2$ $[M+H]^+$: 199.1230 found: 199.1233.

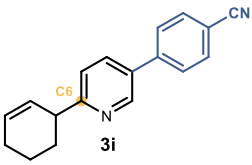

4-(6-(cyclohex-2-en-1-yl)pyridin-3-yl)benzonitrile (3i)

Prepared according to General Procedure A using 4-(pyridin-3-yl)benzonitrile **1i** (36.0 mg, 0.2 mmol) and cyclohexene **2a** (203 µL, 2.0 mmol).). No other regioisomer was detected in the crude

mixture. Purification by column chromatography (SiO_2, 1:10:89 Et_3N/EtOAc/hexanes) afforded product **3i** as a white solid (16.1 mg, 31% yield, > 20:1 *r.r.*).

^{1}H NMR (400 MHz, $CDCl_3$) δ 8.81 (dd, *J* = 2.5, 0.9 Hz, 1H), 7.84 (dd, *J* = 8.1, 2.5 Hz, 1H), 7.80 – 7.76 (m, 2H), 7.72 – 7.68 (m, 2H), 7.35 (dd, *J* = 8.1, 0.8 Hz, 1H), 6.04 – 5.97 (m, 1H), 5.89 – 5.81 (m, 1H), 3.72 – 3.64 (m, 1H), 2.20 – 2.09 (m, 3H), 1.88 – 1.63 (m, 3H).

^{13}C NMR (101 MHz, $CDCl_3$) δ 165.9, 147.7, 142.5, 134.9, 132.8, 132.3, 129.4, 128.2, 127.6, 122.0, 118.7, 111.6, 43.8, 30.7, 25.0, 21.1.

HRMS (ESI$^+$) Calculated for $C_{18}H_{17}N_2$ $[M+H]^+$: 261.1386 found: 261.1398.

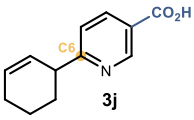

3j

6-(cyclohex-2-en-1-yl)nicotinic acid (3j)

Prepared according to General Procedure A using nicotinic acid (24.6 mg, 0.2 mmol) and cyclohexene **2a** (203 µL, 2.0 mmol). No other regioisomer was detected in the crude mixture. The yield (65%, single regioisomer) of **3j** was inferred by ^{1}H NMR analysis of the crude reaction mixture using trichloroethylene as the internal standard. Purification by column chromatography (SiO_2, 1:4:95 AcOH/MeOH/CH_2Cl_2) afforded an analytical amount of 92% pure product **3j** (estimated by ^{1}H NMR integration) as an off-white solid.

^{1}H NMR (400 MHz, MeOD) δ 9.10 (d, *J* = 1.4 Hz, 1H), 8.40 (dd, *J* = 8.2, 2.2 Hz, 1H), 7.51 (d, *J* = 8.2 Hz, 1H), 6.06 (dtd, *J* = 9.9, 3.7, 2.3 Hz, 1H), 5.88 – 5.79 (m, 1H), 3.73 (tq, *J* = 5.6, 2.8 Hz, 1H), 2.30 – 2.11 (m, 3H), 1.92 – 1.70 (m, 3H).
^{13}C NMR (101 MHz, MeOD) δ 169.3, 166.6, 149.6, 138.3, 129.4, 127.1, 125.0, 121.8, 43.7, 30.2, 24.5, 20.7.

HRMS (ESI$^+$) Calculated for $C_{12}H_{14}NO_2$ $[M+H]^+$: 204.1019 found: 204.1028.

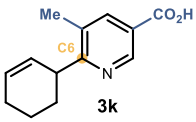

3k

6-(cyclohex-2-en-1-yl)-5-methylnicotinic acid (3k)

Prepared according to General Procedure A using 5-methylnicotinic acid (27.4 mg, 0.2 mmol) and cyclohexene **2a** (203 µL, 2.0 mmol). No other regioisomer was detected in the crude mixture. Purification by column chromatography (SiO_2, 1:49:50 AcOH/EtOAc/hexanes) afforded product **3k** as a white solid (21.0 mg, 48% yield, > 20:1 *r.r.*).

^{1}H NMR (400 MHz, MeOD) δ 8.86 (d, *J* = 2.1 Hz, 1H), 8.14 (dd, *J* = 2.1, 0.9 Hz, 1H), 5.97 – 5.90 (m, 1H), 5.70 – 5.63 (m, 1H), 3.95 – 3.88 (m, 1H), 2.45 (s, 3H), 2.17 (ddd, *J* = 12.7, 6.1, 3.0 Hz, 2H), 2.07 – 1.99 (m, 1H), 1.90 (ddd, *J* = 11.9, 5.4, 2.9 Hz, 1H), 1.80 – 1.62 (m, 2H).
^{13}C NMR (101 MHz, MeOD) δ 168.4, 148.4, 140.9, 133.0, 129.7, 129.1, 41.8, 30.0, 25.8, 22.9, 18.6.

HRMS (ESI$^-$) Calculated for $C_{13}H_{14}NO_2$ $[M-H]^+$: 216.1030 found: 216.1027.

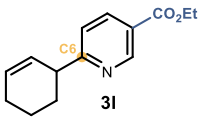

3l

ethyl 6-(cyclohex-2-en-1-yl)nicotinate (3l)

Prepared according to General Procedure A using ethyl nicotinate (27.3 µL, 0.2 mmol) and cyclohexene **2a** (203 µL, 2.0 mmol). No other regioisomer was detected in the crude mixture. Purification by column chromatography (SiO_2, 1:5:94 Et_3N/EtOAc/hexanes) afforded product **3l** as a yellowish oil (30.4 mg, 66% yield, > 20:1 *r.r.*).

^{1}H NMR (400 MHz, $CDCl_3$) δ 9.13 (dd, *J* = 2.2, 0.9 Hz, 1H), 8.19 (dd, *J* = 8.2, 2.2 Hz, 1H), 7.26 (dd, *J* = 8.2, 0.9 Hz, 1H), 5.95 (dtd, *J* = 9.8, 3.7, 2.2 Hz, 1H), 5.80 – 5.75 (m, 1H), 4.38 (q, *J* = 7.1 Hz, 2H), 3.67 – 3.61 (m, 1H), 2.17 – 2.02 (m, 3H), 1.79 – 1.60 (m, 3H), 1.38 (t, *J* = 7.1 Hz, 3H).

^{13}C NMR (101 MHz, $CDCl_3$) δ 169.9, 165.4, 150.6, 137.4, 129.5, 127.8, 123.9, 121.3, 61.1, 44.1, 30.5, 24.8, 21.0, 14.2.

HRMS: (ESI$^+$) calculated for $C_{14}H_{18}NO_2$ [M+H$^+$]: 232.1332, found 235.1326.

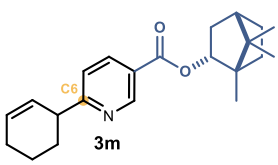

3m

1,7,7-trimethylbicyclo[2.2.1]heptan-2-yl 6-(cyclohex-2-en-1-yl)nicotinate (3m)

Prepared according to General Procedure A using 1,7,7-trimethylbicyclo[2.2.1]heptan-2-yl nicotinate **1m** (52.0 mg, 0.2 mmol) and cyclohexene **2a** (203 µL, 2.0 mmol). No other regioisomer was detected in the crude mixture. Purification by column chromatography (SiO_2, 2:98 EtOAc/hexanes) afforded product **3m** as a colorless oil (49.0 mg, 72% yield, > 20:1 *r.r.*).

^{1}H NMR (500 MHz, $CDCl_3$) δ 9.19 (dd, *J* = 2.2, 0.8 Hz, 1H), 8.22 (dd, *J* = 8.2, 2.2 Hz, 1H), 7.29 (dd, *J* = 8.2, 0.9 Hz, 1H), 5.99 – 5.95 (m, 1H), 5.80 – 5.77 (m, 1H), 5.13 – 5.10 (m, 1H), 3.68 – 3.65 (m, 1H), 2.47 (dddd, *J* = 13.5, 9.9, 4.7, 3.3 Hz, 1H), 2.15 – 2.04 (m, 4H), 1.84 – 1.63 (m, 5H), 1.44 – 1.36 (m, 1H), 1.32 – 1.24 (m, 1H), 1.10 (ddd, *J* = 13.8, 3.5, 1.3 Hz, 1H), 0.96 (s, 3H), 0.90 (d, *J* = 4.8 Hz, 6H).

^{13}C NMR (126 MHz, $CDCl_3$) δ 170.0, 165.8, 150.8, 137.6, 129.6, 128.0, 124.5, 121.6, 81.0, 49.3, 48.0, 45.1, 44.3, 37.0, 30.7, 28.2, 27.5, 25.0, 21.2, 19.8, 19.0, 13.7.

HRMS: (ESI$^+$) calculated for $C_{22}H_{30}NO_2$ [M+H$^+$]: 340.2271, found 340,2274.

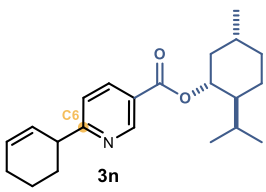

3n

(1R,2S,5R)-2-isopropyl-5-methylcyclohexyl 6-(cyclohex-2-en-1-yl)nicotinate (3n)

Prepared according to General Procedure A using (1R,2S,5R)-2-isopropyl-5-methylcyclohexyl nicotinate **1n** (52.3 mg, 0.2 mmol) and cyclohexene **2a** (203 µL, 2.0 mmol). No other regioisomer was detected in the crude mixture. Purification by column chromatography (SiO_2, 1:99 EtOAc/hexanes) afforded product **3n** as a colorless oil (34.0 mg, 50% yield, > 20:1 *r.r.*).

^{1}H NMR (400 MHz, $CDCl_3$) δ 9.14 (dd, *J* = 2.2, 0.9 Hz, 1H), 8.20 (dd, *J* = 8.2, 2.2 Hz, 1H), 7.28 (d, *J* = 0.8 Hz, 1H), 5.99 – 5.94 (m, 1H), 5.80 – 5.75 (m, 1H), 4.93 (td, *J* = 10.9, 4.4 Hz,

1H), 3.68 – 3.62 (m, 1H), 2.14 – 2.06 (m, 4H), 1.96 – 1.88 (m, 1H), 1.80 – 1.65 (m, 6H), 1.58 – 1.51 (m, 2H), 1.17 – 1.05 (m, 2H), 0.91 (dd, *J* = 8.7, 6.8 Hz, 6H), 0.78 (d, *J* = 6.9 Hz, 3H).

^{13}C NMR (101 MHz, $CDCl_3$) δ 170.0, 165.1, 150.7, 137.6 (d1,d2), 129.6 (d1,d2), 128.0, 124.4, 121.6 (d1,d2),, 75.4, 47.4, 44.3, 41.1, 34.4, 31.6, 30.7 (d1,d2), 26.7 (d1,d2), 25.0, 23.8(d1,d2), 22.1, 21.2(d1,d2), 20.9, 16.7(d1,d2).

HRMS: (ESI$^+$) calculated for $C_{22}H_{32}NO_2$ [M+H$^+$]: 342.2428, found 342,2439.

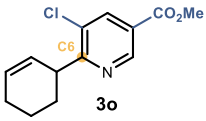

3o

Methyl 5-chloro-6-(cyclohex-2-en-1-yl)nicotinate (3o)

Prepared according to General Procedure A using methyl 5-chloronicotinate (34.3 mg, 0.2 mmol) and cyclohexene **2a** (203 µL, 2.0 mmol). No other regioisomer was detected in the crude mixture. Purification by column chromatography (SiO_2, 1:2:97 Et_3N/EtOAc/hexanes) afforded product **3o** as a colorless oil (23.0 mg, 46% yield, > 20:1 *r.r.*).

^{1}H NMR (400 MHz, $CDCl_3$) δ 9.05 (d, *J* = 1.9 Hz, 1H), 8.23 (d, *J* = 1.9 Hz, 1H), 6.03 – 5.96 (m, 1H), 5.77 – 5.70 (m, 1H), 4.17 – 4.09 (m, 1H), 3.94 (s, 3H), 2.24 – 2.05 (m, 3H), 1.93 – 1.85 (m, 1H), 1.77 – 1.64 (m, 2H).

^{13}C NMR (101 MHz, $CDCl_3$) δ 166.5, 165.0, 148.6, 137.9, 130.9, 129.2, 127.5, 125.1, 52.7, 40.6, 28.6, 24.8, 21.8.

HRMS (ESI$^+$) Calculated for C13H15ClNO2 [M+H]$^+$: 252.0786 found: 252.0785.

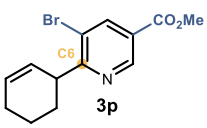

3p

Methyl 5-broro-6-(cyclohex-2-en-1-yl)nicotinate (3p)

Prepared according to General Procedure A using methyl 5-bromonicotinate (43.2 mg, 0.2 mmol) and cyclohexene **2a** (203 µL, 2.0 mmol) prolonging the reaction time to 24 hours. No other regioisomer was detected in the crude mixture. Purification by column chromatography (SiO_2, 1:2:97 Et_3N/EtOAc/hexanes) afforded product **3p** as a colorless oil (18.5 mg, 31% yield, > 20:1 *r.r.*).

^{1}H NMR (400 MHz, $CDCl_3$) δ 9.09 (d, *J* = 1.9 Hz, 1H), 8.41 (d, *J* = 1.9 Hz, 1H), 6.03 – 5.95 (m, 1H), 5.77 – 5.71 (m, 1H), 4.18 – 4.10 (m, 1H), 3.94 (s, 3H), 2.24 – 2.09 (m, 3H), 1.93 – 1.87 (m, 1H), 1.75 – 1.60 (m, 2H).

^{13}C NMR (101 MHz, $CDCl_3$) δ 167.6, 164.8, 149.2, 141.3, 129.1, 127.7, 125.2, 120.9, 52., 42.7, 28.8, 24.8, 21.8.

HRMS (ESI$^+$) Calculated for C13H15BrNO2 [M+H]$^+$: 296.0281 found: 296.0283.

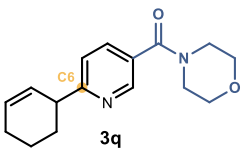

3q

(6-(cyclohex-2-en-1-yl)pyridin-3-yl)(morpholino)methanone (3q)

Prepared according to General Procedure A using morpholino(pyridin-3-yl)methanone **1q** (38.4 mg, 0.2 mmol) and cyclohexene **2a** (203 µL, 2.0 mmol). No other regioisomer was detected in the crude mixture. Purification by column chromatography (SiO_2, 1:99 Et_3N/EtOAc) afforded product **3q** as a colorless oil (21.6 mg, 40% yield, > 20:1 *r.r.*).

^{1}H NMR (500 MHz, $CDCl_3$) δ 8.62 (d, *J* = 2.4 Hz, 1H), 7.71 (dd, *J* = 8.0, 2.3 Hz, 1H), 7.29 (d, *J* = 8.0, 1H), 6.03 – 5.94 (m, 1H), 5.82 – 5.76 (m, 1H), 3.95 – 3.40 (m, 9H), 2.17 – 2.05 (m, 3H), 1.82 – 1.74 (m, 1H), 1.73 – 1.64 (m, 2H).
^{13}C NMR (126 MHz, $CDCl_3$) δ 168.2, 167.3, 147.6, 135.7, 129.5, 128.6, 128.0, 121.8, 66.8, 44.0, 30.6, 24.9, 21.0.
HRMS (ESI$^+$) Calculated for $C_{16}H_{21}N_2O_2$ $[M+H]^+$: 273.1598 found: 273.1595.

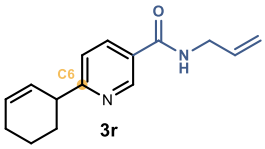

3r

N-allyl-6-(cyclohex-2-en-1-yl)nicotinamide (3r)

Prepared according to General Procedure A using *N*-allylnicotinamide **1r** (32.4 mg, 0.2 mmol) and cyclohexene **2a** (203 µL, 2.0 mmol). No other regioisomer was detected in the crude mixture. Purification by column chromatography (SiO_2, 1:9:90 Et_3N/EtOAc/hexanes to 1:24:75 Et_3N/EtOAc/hexanes) afforded product **3r** as a colorless oil (16.0 mg, 33% yield, > 20:1 *r.r.*).

^{1}H NMR (400 MHz, $CDCl_3$) δ 8.90 (dd, *J* = 2.4, 0.9 Hz, 1H), 8.05 (dd, *J* = 8.1, 2.4 Hz, 1H), 7.28 (dd, *J* = 8.1, 0.9 Hz, 1H), 6.24 (s, 1H), 5.99 – 5.88 (m, 2H), 5.80 – 5.74 (m, 1H), 5.27 (dq, *J* = 17.1, 1.6 Hz, 1H), 5.20 (dq, *J* = 10.2, 1.4 Hz, 1H), 4.10 (tt, *J* = 5.8, 1.6 Hz, 2H), 3.68 – 3.60 (m, 1H), 2.15 – 2.05 (m, 3H), 1.79 – 1.63 (m, 3H).

^{13}C NMR (101 MHz, $CDCl_3$) δ 169.0, 165.8, 147.5, 135.7, 134.0, 129.7, 128.1, 127.9, 121.9, 117.1, 44.2, 42.6, 30.7, 25.1, 21.2.

HRMS (ESI$^+$) Calculated for $C_{15}H_{19}N_2O$ $[M+H]^+$: 243.1492 found: 243.1501.

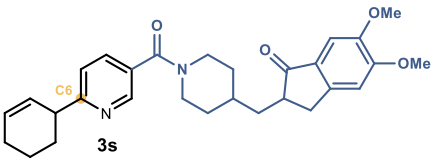

3s

2-((1-(6-(cyclohex-2-en-1-yl)nicotinoyl)piperidin-4-yl)methyl)-5,6-dimethoxy-2,3-dihydro-1H-inden-1-one (3s)

Prepared according to General Procedure A using donepezil nicotinate **1s** (78.9 mg, 0.2 mmol) and cyclohexene **2a** (203 µL, 2.0 mmol). No other regioisomer was detected in the crude mixture. Purification by column chromatography (SiO_2, 1:1:98 Et_3N/MeOH/CH_2Cl_2) afforded product **3s** (48.6 mg, 51% yield, > 20:1 *r.r.*) as a colorless oil.

^{1}H NMR (400 MHz, $CDCl_3$) δ 8.62 (dd, *J* = 2.3, 0.9 Hz, 1H), 7.71 (dd, *J* = 8.0, 2.3 Hz, 1H), 7.28 (d, *J* = 8.1 Hz, 1H), 7.18 (s, 1H), 6.88 (s, 1H), 6.02 – 5.95 (m, 1H), 5.86 – 5.76 (m, 1H), 4.74 (br s, 1H), 3.98 (s, 3H), 3.92 (s, 3H), 3.88 – 3.73 (m, 1H), 3.70 – 3.59 (m, 1H), 3.29 (dd, *J* = 17.4, 8.0 Hz, 1H), 3.10 (br s, 1H), 2.85 (br s, 1H), 2.77 – 2.68 (m, 2H), 2.17 – 2.06 (m, 3H), 2.02 – 1.82 (m, 3H), 1.82 – 1.64 (m, 2H), 1.48 – 1.37 (m, 2H).
^{13}C NMR (101 MHz, $CDCl_3$) δ 207.2, 168.0, 166.8, 155.6, 149.6, 148.6, 147.4, 135.5, 129.5, 129.4, 129.2, 128.1, 121.7, 107.3, 104.4, 56.3, 56.1, 44.0, 30.6, 24.9, 21.1.
HRMS: (ESI$^+$) calculated for $C_{29}H_{34}N_2NaO_4$ $[M+Na^+]$: 497.2411, found 497.2415.

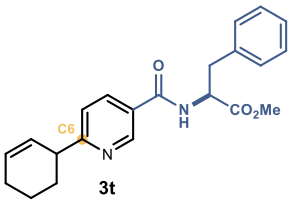

3t

Methyl (6-(cyclohex-2-en-1-yl)nicotinoyl)-L-phenylalaninate (3t)

Prepared according to General Procedure A using methyl nicotinoyl-L-phenylalaninate **1t** (26.0 mg, 0.2 mmol) and cyclohexene **2a** (203 µL, 2.0 mmol). No other regioisomer was detected in the crude mixture. Purification by column chromatography (SiO_2, 1:9:90 Et_3N/EtOAc/hexanes to 1:19:80 Et_3N/EtOAc/hexanes) afforded product **3t** as a white solid (30.0 mg, 41% yield, 1:1 *d.r.*, > 20:1 *r.r.*). The diastereomeric ratio was determined by UPC^2 analysis on a Daicel Chiralpak ID-3 column (gradient: 1 min 100% CO_2; 5 min from 100% CO_2 to 60% CO_2 - 40% MeOH; flow rate 2.0 mL/min; λ = 268 nm: τ_1 = 5.6 min, τ_2 = 5.9 min).

^{1}H NMR (400 MHz, $CDCl_3$) δ 8.83 (dt, *J* = 2.2, 1.0 Hz, 1H), 7.95 (dd, *J* = 8.2, 2.4 Hz, 1H), 7.31 – 7.22 (m, 4H), 7.13 – 7.11 (m, 2H), 6.57 (d, *J* = 7.6 Hz, 1H), 5.99 – 5.94 (m, 1H), 5.79 – 5.74 (m, 1H), 5.07 (dt, *J* = 7.6, 5.6 Hz, 1H), 3.77 (s, 3H), 3.65 – 3.60 (m, 1H), 3.24 (qd, *J* = 13.9, 5.6 Hz, 2H), 2.13 – 2.04 (m, 3H), 1.77 – 1.63 (m, 3H).

^{13}C NMR (101 MHz, $CDCl_3$) δ 172.0, 169.2, 165.4, 147.8, 147.8, 135.7, 135.6, 129.6, 129.4, 128.9, 128.0, 127.5, 127.3, 121.8, 53.6, 52.6, 44.2, 37.9, 30.7, 25.0, 21.1.

HRMS: (ESI$^+$) calculated for $C_{22}H_{25}N_2O_3$ [M+H$^+$]: 365.1860, found 365,1864.

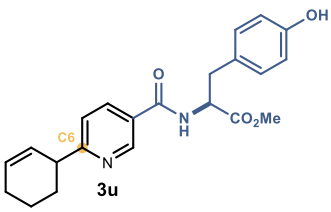

3u

Methyl (6-(cyclohex-2-en-1-yl)nicotinoyl)-L-tyrosinate (3u)

Prepared according to General Procedure A using methyl nicotinoyl-L-tyrosinate **1u** (60.0 mg, 0.2 mmol) and cyclohexene **2a** (203 µL, 2.0 mmol). No other regioisomer was detected in the crude mixture. Purification by column chromatography (SiO_2, 1:29:70 Et_3N/acetone/hexanes) afforded product **3u** as a white solid (31.8 mg, 42% yield, 1:1 id.r., > 20:1 *r.r.*). The diastereomeric ratio was determined by UPC^2 analysis on a Daicel Chiralpak ID-3 column (gradient: 1 min 100% CO_2; 5 min from 100% CO_2 to 60% CO_2 - 40% MeOH; flow rate 2.0 mL/min; λ = 268 nm: τ_1 = 10.8 min, τ_2 = 11.3 min).

^{1}H NMR (400 MHz, $CDCl_3$) δ 8.80 (d, *J* = 1.5 Hz, 1H), 8.03 (ddd, *J* = 8.1, 2.4, 1.5 Hz, 1H), 7.29 (d, *J* = 8.1 Hz, 1H), 6.98 – 6.94 (m, 2H), 6.76 – 6.71 (m, 2H), 6.65 (d, *J* = 7.8 Hz, 1H), 5.98 – 5.93 (m, 1H), 5.78 – 5.70 (m, 1H), 5.04 (dt, *J* = 7.7, 5.6 Hz, 1H), 3.78 (s, 3H), 3.69 – 3.60 (m, 1H), 3.16 (qd, *J* = 14.1, 5.7 Hz, 2H), 2.13 – 2.04 (m, 3H), 1.77 – 1.62 (m, 3H).
^{13}C NMR (101 MHz, $CDCl_3$) δ 172.2, 169.2, 165.4, 156.0, 147.3, 136.2, 130.5, 129.9, 127.7, 127.6, 126.9, 122.1, 115.9, 53.8, 52.7, 44.0, 37.1, 30.7, 25.0, 21.1.

HRMS: (ESI$^+$) calculated for $C_{22}H_{24}N_2NaO_4$ [M+Na$^+$]: 403.1628, found 403,1627.

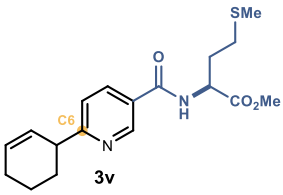

3v

Methyl (6-(cyclohex-2-en-1-yl)nicotinoyl)-L-methioninate (3v)

Prepared according to General Procedure A using methyl nicotinoyl-L-methioninate **1v** (53.7 mg, 0.2 mmol) and cyclohexene **2a** (203 µL, 2.0 mmol). No other regioisomer was detected in the crude mixture. Purification by column chromatography (SiO_2, 1:9:90 Et_3N/EtOAc/hexanes to 1:23:76 Et_3N/EtOAc/hexanes) afforded product **3v** as a white solid (31.0 mg, 44% yield, 1:1 *d.r.*, > 20:1 *r.r.*). The diastereomeric ratio was determined by UPC^2 analysis on a Daicel Chiralpak ID-3 column (gradient: 1 min 100% CO_2; 5 min from 100% CO_2 to 60% CO_2 - 40% EtOH; flow rate 2.0 mL/min; λ = 268 nm: τ_1 = 11.7 min, τ_2 = 12.0 min).

^{1}H NMR (400 MHz, $CDCl_3$) δ 8.96 (d, *J* = 2.4 Hz, 1H), 8.04 (dd, *J* = 8.1, 2.4 Hz, 1H), 7.27 (d, *J* = 8.2 Hz, 1H), 7.14 (d, *J* = 7.6 Hz, 1H), 5.98 – 5.93 (m, 1H), 5.78 – 5.74 (m, 1H), 4.91 (td, *J* = 7.3, 5.0 Hz, 1H), 3.78 (s, 3H), 3.65 – 3.60 (m, 1H), 2.58 (t, *J* = 7.2 Hz, 2H), 2.31 – 2.22 (m, 1H), 2.17-2.04 (m, 4H), 2.10 (s, 3H), 1.77 – 1.63 (m, 3H).
^{13}C NMR (101 MHz, $CDCl_3$) δ 172.5, 169.2, 165.6, 148.0, 135.7, 129.6, 128.0, 127.1, 121.8, 52.8, 52.3, 44.1, 31.3, 30.7, 30.3, 25.0, 21.1, 15.7.
HRMS: (ESI$^+$) calculated for $C_{18}H_{23}N_2O_3S$ [M+H$^+$]: 347.1435, found 347,1439.

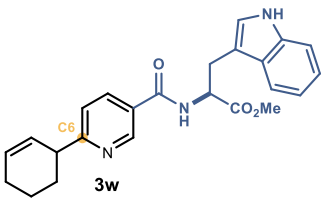

3w

Methyl (6-(cyclohex-2-en-1-yl)nicotinoyl)-L-tryptophanate (3w)

Prepared according to General Procedure A using methyl nicotinoyl-L-tryptophanate **1w** (64.7 mg, 0.2 mmol) and cyclohexene **2a** (203 µL, 2.0 mmol). No other regioisomer was detected in the crude mixture. Purification by column chromatography (SiO_2, 1:19:80 Et_3N/EtOAc/hexanes to 1:59:40 Et_3N/EtOAc/hexanes) afforded product **3w** as a white solid (32.5 mg, 40% yield, 1:1 *d.r.*, > 20:1 *r.r.*). The diastereomeric ratio was determined by UPC^2 analysis on a Daicel Chiralpak IA-3 column (gradient: 1 min 100% CO_2; 5 min from 100% CO_2 to 60% CO_2 - 40% EtOH; flow rate 2.0 mL/min; λ = 268 nm: τ_1 = 6.9 min, τ_2 = 7.2 min).

^{1}H NMR (400 MHz, $CDCl_3$) δ 8.81 (ddd, *J* = 3.3, 2.3, 0.8 Hz, 1H), 8.40 (br s, 1H), 7.90 (dt, *J* = 8.2, 1.9 Hz, 1H), 7.53 (d, *J* = 7.9 Hz, 1H), 7.33 (d, *J* = 8.1 Hz, 1H), 7.20 (d, *J* = 8.2 Hz, 1H), 7.19 – 7.15 (m, 1H), 7.08 (ddd, *J* = 8.0, 7.0, 1.0 Hz, 1H), 6.99 (d, *J* = 2.4 Hz, 1H), 6.69 (d, *J* = 7.7 Hz, 1H), 5.98 – 5.93 (m, 1H), 5.78 – 5.73 (m, 1H), 5.12 (dt, *J* = 7.6, 5.3 Hz, 1H), 3.72 (s, 3H), 3.64 – 3.59 (m, 1H), 3.45 – 3.43 (m, 2H), 2.12 – 2.03 (m, 3H), 1.77 – 1.61 (m, 3H).
^{13}C NMR (101 MHz, $CDCl_3$) δ 172.4, 169.1, 165.5, 147.9, 147.9, 136.3, 135.7, 135.7, 129.7, 129.6, 128.0, 127.7, 127.3, 123.0, 122.5, 121.7, 119.9, 118.6, 111.5, 109.9, 53.5, 52.7, 44.1, 30.7, 30.7, 27.7, 25.0, 21.1.
HRMS: (ESI$^+$) calculated for $C_{24}H_{26}N_3O_3$ [M+H$^+$]: 404.1969, found 404,1979.

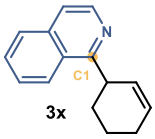

3x

1-(cyclohex-2-en-1-yl)isoquinoline (3x)

Prepared according to General Procedure A using isoquinoline (23.5 µL, 0.2 mmol) and cyclohexene **2a** (203 µL, 2.0 mmol). No other regioisomer was detected in the crude mixture. Purification by column chromatography (SiO_2, 1:99 Et_3N/hexanes to 1:5:94 Et_3N/EtOAc/hexanes) afforded product **3x** as a colorless oil (16.6 mg, 40% yield, > 20:1 *r.r.*).

^{1}H NMR (500 MHz, $CDCl_3$) δ 8.51 (d, *J* = 5.7 Hz, 1H), 8.25 (d, *J* = 8.5 Hz, 1H), 7.82 (dt, *J* = 8.2, 1.0 Hz, 1H), 7.66 (ddd, *J* = 8.2, 6.9, 1.2 Hz, 1H), 7.58 (ddd, *J* = 8.3, 6.9, 1.4 Hz, 1H), 7.50 (dd, *J* = 5.7, 1.0 Hz, 1H), 6.04 – 5.99 (m, 1H), 5.95 (dtdd, *J* = 10.1, 2.5, 1.6, 1.1 Hz, 1H), 4.48 – 4.43 (m, 1H), 2.31 – 2.11 (m, 3H), 1.96 – 1.75 (m, 3H).
^{13}C NMR (126 MHz, $CDCl_3$) δ 164.6, 142.1, 136.5, 129.6, 129.1, 128.2, 127.6, 126.9, 126.5, 125.0, 119.2, 40.3, 30.2, 24.9, 22.1.

HRMS: (ESI$^+$) calculated for $C_{15}H_{16}N$ [M+H$^+$]: 210.1277, found 210.1271.

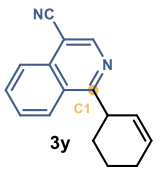

3y

1-(cyclohex-2-en-1-yl)isoquinoline-4-carbonitrile (3y)

Prepared according to General Procedure A using isoquinoline-4-carbonitrile (30.8 mg, 0.2 mmol) and cyclohexene **2a** (203 µL, 2.0 mmol). No other regioisomer was detected in the crude mixture. Purification by column chromatography (SiO_2, 10:90 EtOAc/hexanes) afforded product **3y** as a white solid (14.6 mg, 31% yield, > 20:1 *r.r.*).

^{1}H NMR (400 MHz, $CDCl_3$) δ 8.87 (s, 1H), 8.35 (ddt, *J* = 8.5, 1.3, 0.7 Hz, 1H), 8.20 (ddd, *J* = 8.4, 1.3, 0.7 Hz, 1H), 7.89 (ddd, *J* = 8.3, 7.0, 1.3 Hz, 1H), 7.75 (dddd, *J* = 8.6, 7.0, 1.3, 0.3 Hz, 1H), 6.08 – 6.03 (m, 1H), 5.88 (dtdd, *J* = 10.1, 2.4, 1.8, 1.1 Hz, 1H), 4.54 – 4.46 (m, 1H), 2.30 – 2.12 (m, 3H), 1.97 – 1.74 (m, 3H).
^{13}C NMR (101 MHz, $CDCl_3$) δ 169.9, 147.7, 135.0, 132.2, 129.0, 128.8, 127.8, 125.7, 125.6, 125.1, 116.4, 104.3, 40.7, 30.2, 24.8, 21.8.

HRMS: (ESI$^+$) calculated for $C_{16}H_{15}N_2$ [M+H$^+$]: 235.1230, found 235.1234.

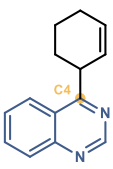

3z

4-(cyclohex-2-en-1-yl)quinazoline (3z)

Prepared according to General Procedure A using quinazoline (26.0 mg, 0.2 mmol) and cyclohexene **2a** (203 µL, 2.0 mmol). No other regioisomer was detected in the crude mixture. Purification by column chromatography (SiO_2, 1:10:89 Et_3N/EtOAc/hexanes) afforded product **3z** (8.3 mg, 20% yield, > 20:1 *r.r.*) as a colorless oil.

^{1}H NMR (400 MHz, $CDCl_3$) δ 9.28 (s, 1H), 8.22 (d, *J* = 8.4 Hz, 1H), 8.06 (d, *J* = 8.5 Hz, 1H), 7.88 (ddd, *J* = 8.4, 6.9, 1.4 Hz, 1H), 7.64 (ddd, *J* = 8.3, 6.9, 1.3 Hz, 1H), 6.11 – 6.02 (m, 1H), 5.93 – 5.84 (m, 1H), 4.44 (ddp, *J* = 8.4, 5.6, 2.7 Hz, 1H), 2.31 – 2.11 (m, 3H), 2.02 – 1.71 (m, 3H).
^{13}C NMR (101 MHz, $CDCl_3$) δ 174.1, 154.9, 150.2, 133.4, 129.4, 129.3, 127.5, 127.4, 124.4, 123.5, 40.0, 29.9, 24.8, 21.8.
HRMS (ESI$^+$) Calculated for $C_{14}H_{15}N_2$ [M+H]$^+$: 211.1230 found: 211.1236.

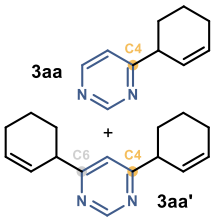

4-(cyclohex-2-en-1-yl)pyrimidine (3aa) + 4,6-di(cyclohex-2-en-1-yl)pyrimidine (3aa')

Prepared according to General Procedure B using pyrimidine (15.6 µL, 0.2 mmol) and cyclohexene **2a** (203 µL, 2.0 mmol). Purification by column chromatography (SiO_2, 1:5:94 Et_3N/EtOAc/hexanes) afforded products **3aa** (8.8 mg, 27% yield, > 20:1 *r.r.*) as a colorless oil.

^{1}H NMR (500 MHz, $CDCl_3$) δ 9.16 (d, *J* = 1.4 Hz, 1H), 8.65 (d, *J* = 5.2 Hz, 1H), 7.25 (dd, *J* = 5.2, 1.4 Hz, 1H), 6.08 – 5.97 (m, 1H), 5.86 – 5.75 (m, 1H), 3.59 – 3.52 (m, 1H), 2.21 – 2.07 (m, 3H), 1.81 – 1.65 (m, 3H).
^{13}C NMR (126 MHz, $CDCl_3$) δ 173.7, 158.8, 156.9, 130.2, 126.7, 119.5, 43.5, 29.9, 24.8, 20.8.
HRMS (ESI$^+$) Calculated for $C_{10}H_{13}N_2$ $[M+H]^+$: 161.1073 found: 161.1076.

Product **3aa'** (3.8 mg, 8% yield, > 20:1 *r.r.*) was also isolated as a colorless oil.

^{1}H NMR (500 MHz, $CDCl_3$) δ 9.09 (d, *J* = 1.3 Hz, 1H), 7.12 (d, *J* = 1.3 Hz, 1H), 6.07 – 5.99 (m, 2H), 5.82 – 5.74 (m, 2H), 3.59 – 3.47 (m, 2H), 2.22 – 2.04 (m, 6H), 1.86 – 1.63 (m, 6H).
^{13}C NMR (126 MHz, $CDCl_3$) δ 173.7, 158.5, 130.0, 127.1, 117.2, 43.5, 30.0, 24.9, 21.0.
HRMS (ESI$^+$) Calculated for $C_{16}H_{21}N_2$ $[M+H]^+$: 241.1699 found: 241.1699.

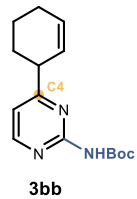

tert-butyl (4-(cyclohex-2-en-1-yl)pyrimidin-2-yl)carbamate (3bb)

Prepared according to General Procedure A using tert-butyl pyrimidin-2-ylcarbamate **1bb** (39.0 mg, 0.2 mmol) and cyclohexene **2a** (203 µL, 2.0 mmol). No other regioisomer was detected in the crude mixture. Purification by column chromatography (SiO_2, 1:10:89 Et_3N/EtOAc/hexanes) afforded product **3bb** (17.9 mg, 27% yield, > 20:1 *r.r.*) as a colorless oil.

^{1}H NMR (400 MHz, $CDCl_3$) δ 8.53 (d, *J* = 5.1 Hz, 1H), 7.54 (brs, 1H), 6.88 (d, *J* = 5.1 Hz, 1H), 6.04 – 5.93 (m, 1H), 5.80 – 5.72 (m, 1H), 3.54 – 3.40 (m, 1H), 2.17 – 2.04 (m, 3H), 1.82 – 1.63 (m, 3H), 1.55 (s, 9H).
^{13}C NMR (101 MHz, $CDCl_3$) δ 175.4, 158.2, 157.6, 150.6, 129.9, 126.9, 113.8, 81.2, 43.3, 29.6, 28.2, 24.8, 20.9.

HRMS (ESI$^+$) Calculated for $C_{15}H_{21}N_3NaO_2$ $[M+Na]^+$: 298.1526 found: 298.1522.

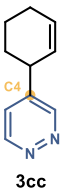

4-(cyclohex-2-en-1-yl)pyridazine (3cc)

Prepared according to General Procedure A using pyridazine (14.5 µL, 0.2 mmol) and cyclohexene **2a** (203 µL, 2.0 mmol). No other regioisomer was detected in the crude mixture. Purification by column chromatography (SiO_2, 1:40:59 Et_3N/EtOAc/hexanes) afforded product **3cc** (10.0 mg, 31% yield, > 20:1 *r.r.*) as a brown oil.

^{1}H NMR (400 MHz, $CDCl_3$) δ 9.10 (s, 1H), 9.08 (d, *J* = 5.5 Hz, 1H), 7.33 (dd, *J* = 5.3, 2.4 Hz, 1H), 6.05 (dq, *J* = 9.8, 3.4 Hz, 1H), 5.70 – 5.61 (m, 1H), 3.45 (m, 1H), 2.17 – 2.11 (m, 2H), 2.10 – 2.04 (m, 1H), 1.77 – 1.62 (m, 2H), 1.61 – 1.52 (m, 1H).

^{13}C NMR (101 MHz, $CDCl_3$) δ 152.3, 151.1, 145.6, 131.1, 126.3, 125.2, 38.8, 31.3, 24.7, 20.4.

HRMS (ESI$^+$) Calculated for $C_{10}H_{13}N_2$ $[M+H]^+$: 161.1073 found: 161.1073.

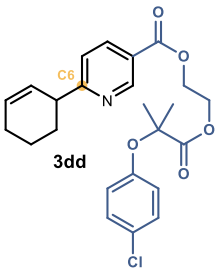

3dd

2-((2-(4-chlorophenoxy)-2-methylpropanoyl)oxy)ethyl 6-(cyclohex-2-en-1-yl)nicotinate (3dd)

Prepared according to General Procedure A using Etofibrate **1dd** (72.8 mg, 0.2 mmol) and cyclohexene **2a** (203 µL, 2.0 mmol). No other regioisomer was detected in the crude mixture. Purification by column chromatography (SiO_2, 1:10:89 Et_3N/EtOAc/hexanes) afforded product **3dd** as a colorless oil (47.8 mg, 54% yield, > 20:1 *r.r.*).

^{1}H NMR (400 MHz, $CDCl_3$) δ 9.10 (dd, *J* = 2.3, 0.9 Hz, 1H), 8.07 (dd, *J* = 8.2, 2.2 Hz, 1H), 7.28 (dd, *J* = 8.2, 0.9 Hz, 1H), 7.13 – 7.08 (m, 2H), 6.79 – 6.74 (m, 2H), 6.05 – 5.97 (m, 1H), 5.85 – 5.77 (m, 1H), 4.58 – 4.49 (m, 4H), 3.73 – 3.63 (m, 1H), 2.22 – 2.03 (m, 3H), 1.86 – 1.65 (m, 3H), 1.60 (s, 6H).

^{13}C NMR (101 MHz, $CDCl_3$) δ 173.9, 170.5, 165.1, 153.9, 150.7, 137.4, 129.6, 129.1, 127.8, 127.2, 123.1, 121.5, 120.2, 79.4, 63.0, 62.5, 44.2, 30.5, 25.3, 24.9, 21.0.

HRMS (ESI$^+$) Calculated for $C_{24}H_{27}ClNO_5$ $[M+H]^+$: 444.1572 found: 444.1565.

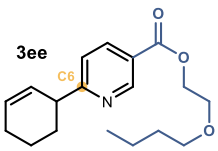

3ee

2-butoxyethyl 6-(cyclohex-2-en-1-yl)nicotinate (3ee)

Prepared according to General Procedure A using Nicoboxil **1ee** (44.7 mg, 0.2 mmol) and cyclohexene **2a** (203 µL, 2.0 mmol). No other regioisomer was detected in the crude mixture. Purification by column chromatography (SiO_2, 1:2:97 Et_3N/EtOAc/hexanes) afforded product **3ee** as a light-yellow oil (32.3 mg, 53% yield, > 20:1 *r.r.*).

^{1}H NMR (500 MHz, $CDCl_3$) δ 9.19 (d, *J* = 2.2 Hz, 1H), 8.25 (dd, *J* = 8.1, 2.2 Hz, 1H), 7.30 (d, *J* = 8.2 Hz, 1H), 6.05 – 5.96 (m, 1H), 5.88 – 5.79 (m, 1H), 4.53 – 4.45 (m, 2H), 3.81 – 3.75 (m, 2H), 3.72 – 3.65 (m, 1H), 3.53 (t, *J* = 6.6 Hz, 2H), 2.22 – 2.06 (m, 3H), 1.83 – 1.64 (m, 3H), 1.64 – 1.55 (m, 2H), 1.45 – 1.35 (m, 2H), 0.93 (t, *J* = 7.4 Hz, 3H).

^{13}C NMR (126 MHz, $CDCl_3$) δ 170.1, 165.5, 150.8, 137.6, 129.6, 127.9, 123.7, 121.4, 71.3, 68.5, 64.4, 44.2, 31.7, 30.6, 24.9, 21.0, 19.3, 13.9.

HRMS (ESI$^+$) Calculated for $C_{18}H_{26}NO_3$ $[M+H]^+$: 304.1907 found: 304.1904.

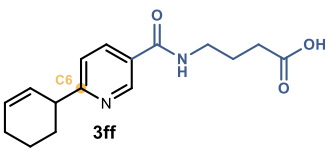

3ff

4-(6-(cyclohex-2-en-1-yl)nicotinamido)butanoic acid (3ff)

Prepared according to General Procedure A using Picamilon (41.6 mg, 0.2 mmol) and cyclohexene **2a** (203 µL, 2.0

mmol). No other regioisomer was detected in the crude mixture. Purification by column chromatography (SiO_2, 1:40:59 AcOH/EtOAc/hexanes to 1:99 AcOH/EtOAc) afforded product **3ff** as a white solid (43.4 mg, 75% yield, > 20:1 *r.r.*).

^{1}H NMR (400 MHz, Acetone) δ 9.05 (d, *J* = 2.7 Hz, 1H), 8.39 (s, 1H), 8.27 (dd, *J* = 8.2, 2.4 Hz, 1H), 7.37 (d, *J* = 8.2 Hz, 1H), 5.95 – 5.89 (m, 1H), 5.82 – 5.75 (m, 1H), 3.71 – 3.61 (m, 1H), 3.52 (q, *J* = 6.7 Hz, 2H), 2.43 (t, *J* = 7.0 Hz, 2H), 2.07 (p, *J* = 2.2 Hz, 4H), 1.93 (p, *J* = 7.1 Hz, 2H), 1.83 – 1.71 (m, 2H), 1.70 – 1.59 (m, 1H).
^{13}C NMR (101 MHz, Acetone) δ 147.8, 136.1, 128.8, 128.1, 121.3, 5
4.1, 43.5, 39.2, 24.6, 20.8.
HRMS (ESI$^+$) Calculated for $C_{16}H_{21}N_2O_3$ $[M+H]^+$: 289.1547 found: 289.1543.

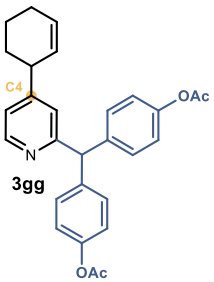

((4-(cyclohex-2-en-1-yl)pyridin-2-yl)methylene)bis(4,1-phenylene) diacetate (3gg)

Prepared according to General Procedure B using bisacodyl (72.3 mg, 0.2 mmol) and cyclohexene **2a** (203 µL, 2.0 mmol). No other regioisomer was detected in the crude mixture. Purification by column (SiO_2, 1:9:90 Et_3N/EtOAc/hexanes) afforded product **3gg** as a colorless oil (29.0 mg, 33% yield, > 20:1 *r.r.*).

^{1}H NMR (400 MHz, $CDCl_3$) δ 8.48 (d, *J* = 5.1 Hz, 1H), 7.21 – 7.17 (m, 4H), 7.03 – 6.98 (m, 6H), 5.94 – 5.89 (m, 1H), 5.63 – 5.59 (m, 2H), 3.35 – 3.30 (m, 1H), 2.27 (s, 6H), 2.09 – 2.04 (m, 2H), 2.00 – 1.94 (m, 1H), 1.73 – 1.63 (m, 2H), 1.62 – 1.59 (m, 1H), 1.52 – 1.42 (m, 1H).
^{13}C NMR (101 MHz, $CDCl_3$) δ 169.6, 162.5, 156.4, 149.6, 149.4, 140.4, 140.3, 130.4, 130.4, 129.8, 128.2, 123.5, 121.5, 121.2, 58.2, 41.3, 31.9, 25.0, 21.3, 21.0.
HRMS: (ESI$^+$) calculated for $C_{28}H_{28}NO_4$ $[M+H^+]$: 442.2013, found 442,2031.

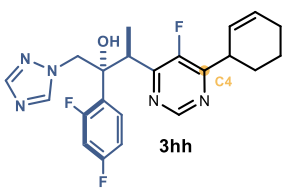

3-(6-(cyclohex-2-en-1-yl)-5-fluoropyrimidin-4-yl)-2-(2,4-difluorophenyl)-1-(1H-1,2,4-triazol-1-yl)butan-2-ol (3hh)

Prepared according to General Procedure A using voriconazole (69.9 mg, 0.2 mmol) and cyclohexene **2a** (203 µL, 2.0 mmol). No other regioisomer was detected in the crude mixture. Purification by column chromatography (SiO_2, 1:50:49 Et_3N/EtOAc/hexanes) afforded product **3hh** (37.6 mg, 44% yield, 1:1 *d.r.*, > 20:1 *r.r.*) as an off-white solid.

^{1}H NMR (400 MHz, $CDCl_3$) *1:1 mixture of diastereoisomers* δ 8.85 (dd, *J* = 7.4, 1.8 Hz, 1H), 7.99 (d, *J* = 4.3 Hz, 1H), 7.67 – 7.58 (m, 1H), 7.54 (d, *J* = 5.2 Hz, 1H), 6.90 – 6.79 (m, 2H), 6.73 (s, 0.5H), 6.68 (s, 0.5H), 6.10 – 6.02 (m, 1H), 5.77 – 5.67 (m, 1H), 4.72 (dd, *J* = 14.2, 3.5 Hz, 1H), 4.32 (dd, *J* = 17.3, 14.1 Hz, 1H), 4.19 – 4.10 (m, 1H), 4.04 – 3.92 (m, 1H), 2.27 – 2.14 (m, 2H), 2.14 – 2.05 (m, 1H), 1.99 – 1.89 (m, 1H), 1.86 – 1.71 (m, 2H), 1.12 – 1.08 (m, 3H).

^{13}C NMR (101 MHz, $CDCl_3$) *1:1 mixture of diastereoisomers* δ 162.07 (d, *J* = 4.5 Hz), 161.94 (d, *J* = 4.6 Hz), 152.96 (d, *J* = 3.7 Hz), 152.86 (d, *J* = 3.7 Hz), 130.67 (dd, *J* = 9.4, 5.8 Hz), 111.67 (d, *J* = 2.6 Hz), 111.46 (d, *J* = 3.2 Hz), 104.07 (d, *J* = 27.6 Hz), 57.52 (d, *J* = 5.1 Hz).

^{19}F{^{1}H} NMR (376 MHz, $CDCl_3$) *1:1 mixture of diastereoisomers* δ -109.17 (d, *J* = 8.2 Hz), -109.19 (d, *J* = 8.0 Hz), -110.55 (d, *J* = 8.1 Hz), -138.87, -139.00.

HRMS (ESI$^+$) Calculated for $C_{22}H_{23}F_3N_5O$ [M+H]$^+$: 430.1849 found: 430.1854.

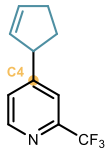

3ii

4-(cyclopent-2-en-1-yl)-2-(trifluoromethyl)pyridine (3ii)

Prepared according to General Procedure A using 2-(trifluoromethyl)pyridine (23.0 µL, 0.2 mmol) and cyclopentene (183 µL, 2.0 mmol). No other regioisomer was detected in the crude mixture. Purification by column chromatography (SiO_2, 5:95 EtOAc/hexanes) afforded product **3ii** as colorless oil (17.1 mg, 40% yield, > 20:1 *r.r.*).

^{1}H NMR (400 MHz, $CDCl_3$) δ 8.60 (d, *J* = 5.0 Hz, 1H), 7.49 (d, *J* = 1.7 Hz, 1H), 7.30 (dd, *J* = 5.0, 1.7 Hz, 1H), 6.09 – 6.05 (m, 1H), 5.76 – 5.72 (m, 1H), 4.00 – 3.93 (m, 1H), 2.60 – 2.40 (m, 3H), 1.77 – 1.67 (m, 1H).

^{13}C NMR (101 MHz, $CDCl_3$) δ 157.5, 150.0, 148.4 (q, *J* = 34.1 Hz), 134.4, 131.6, 125.2, 121.7 (q, *J* = 274.2 Hz), 119.3 (q, *J* = 2.8 Hz), 50.6, 33.1, 32.4.

^{19}F NMR (376 MHz, $CDCl_3$) δ -68.0.

HRMS: (ESI$^+$) calculated for $C_{11}H_{11}F_3N$ [M+H]$^+$: 214.0838, found 214.0829.

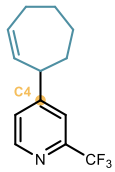

3jj

4-(cyclohept-2-en-1-yl)-2-(trifluoromethyl)pyridine (3jj)

Prepared according to General Procedure A using 2-(trifluoromethyl)pyridine (23.0 µL, 0.2 mmol) and cycloheptene (233 µL, 2.0 mmol) prolonging the reaction time to 24 hours. No other regioisomer was detected in the crude mixture. Purification by column chromatography (SiO_2, 5:95 EtOAc/hexanes) afforded product **3jj** as colorless oil (21.2 mg, 44% yield, > 20:1 *r.r.*).

^{1}H NMR (400 MHz, $CDCl_3$) δ 8.62 (d, *J* = 5.0 Hz, 1H), 7.55 (d, *J* = 2.2 Hz, 1H), 7.35 (dd, *J* = 5.0, 1.9 Hz, 1H), 5.96 (dddd, *J* = 11.2, 6.9, 5.5, 2.3 Hz, 1H), 5.64 (dddt, *J* = 11.3, 4.2, 1.9, 0.8 Hz, 1H), 3.66 – 3.60 (m, 1H), 2.29 – 2.19 (m, 2H), 1.97 – 1.88 (m, 1H), 1.88 – 1.66 (m, 4H), 1.53 – 1.42 (m, 1H).

^{13}C NMR (101 MHz, $CDCl_3$) δ 158.2, 150.1, 148.4 (q, *J* = 34.1 Hz), 133.9, 133.6, 125.3, 121.7 (q, *J* = 274.5 Hz), 119.5 (q, *J* = 2.9 Hz), 46.3, 35.2, 29.7, 28.7, 26.6.

^{19}F NMR (376 MHz, $CDCl_3$) δ -68.03.

HRMS: (ESI$^+$) calculated for $C_{13}H_{15}F_3N$ [M+H]$^+$: 242.1151, found 242.1157.

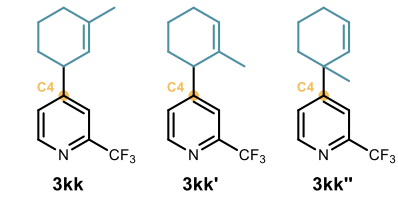

4-(3-methylcyclohex-2-en-1-yl)-2-(trifluoromethyl)pyridine (3kk) + 4-(2-methylcyclohex-2-en-1-yl)-2-(trifluoromethyl)pyridine (3kk') + 4-(1-methylcyclohex-2-en-1-yl)-2-(trifluoromethyl)pyridine (3kk'')

Prepared according to General Procedure A using 2-(trifluoromethyl)pyridine (23.0 µL, 0.2 mmol) and 1-methylcyclohex-1-ene (237 µL, 2.0 mmol). Purification by column chromatography (SiO_2, 1:99 Et_3N/hexanes) afforded mixture of products **3kk, 3kk', and 3kk''** as colorless oil (29.7 mg, 61% yield, 2:0.75:1 allylic *r.r.*). For NMR characterization where possible the peaks are correlated with parent compound (COSY and HSQC spectra used for correlations).

^{1}H NMR (400 MHz, $CDCl_3$) δ 8.61 (dm, *J* = 5.0 Hz, 1H, **3kk'**), 8.61 (dm, *J* = 5.0 Hz, 1H, **3kk''**), 8.60 (dp, *J* = 5.0 Hz, 0.7 Hz, 1H, **3kk**), 7.65 (dd, *J* = 1.8, 0.8 Hz, 1H, **3kk''**), 7.52 – 7.51 (m, 1H, **3kk**), 7.51 – 7.50 (m, 1H, **3kk'**), 7.46 (ddq, *J* = 5.2, 1.8, 0.6 Hz, 1H, **3kk''**), 7.32 (ddt, *J* = 5.0, 1.7, 0.6 Hz, 1H, **3kk**), 7.30 (ddt, *J* = 5.0 Hz, 1.6, 0.5 Hz, 1H, **3kk'**), 5.96 (dtd, *J* = 10.1, 3.7, 0.6 Hz, 1H, **3kk''**), 5.79 (tp, *J* = 3.9, 1.4 Hz, 1H, **3kk'**), 5.64 (dtd, *J* = 10.1, 2.2, 1.1 Hz, 1H, **3kk''**), 5.36 (ddtd, *J* = 2.9, 2.2, 1.5, 0.7 Hz, 1H, **3kk**), 3.45 (ddp, *J* = 8.0, 5.5, 2.5 Hz, 1H, **3kk**), 3.32 (t, *J* = 5.9 Hz, 1H, **3kk'**), 2.15 – 1.26 (m, nH, CH_2) 1.77 – 1.76 (m, 3H, **3kk**), 1.50 – 1.49 (m, 3H, **3kk'**), 1.40 (s, 3H, **3kk''**)

^{13}C NMR (101 MHz, $CDCl_3$) δ 161.0, 158.2, 156.7, 149.8, 149.8, 149.7, 148.2 (q, *J* = 34.0 Hz), 148.2 (q, *J* = 34.0 Hz, **3kk**), 148.1 (q, *J* = 33.6 Hz), 137.9, 132.5 (**3kk''**), 131.9, 128.9 (**3kk''**), 126.4 (**3kk'**), 125.8 (q, *J* = 1.0 Hz), 124.6 (q, *J* = 1.1 Hz, **3kk''**), 121.8 (q, *J* = 273.9 Hz, **3kk''**), 121.7 (q, *J* = 274.2 Hz, **3kk**), 121.7 (q, *J* = 274.1 Hz, **3kk'**), 121.4 (**3kk**), 120.4 (q, *J* = 2.5 Hz), 119.8 (q, *J* = 2.5 Hz), 118.6 (q, *J* = 2.8 Hz), 45.4 (**3kk'**), 41.6 (**3kk**), 39.7 (**3kk''**), 38.3, 31.9, 31.5 (**3kk**), 29.7, 28.5 (**3kk''**), 25.1, 24.8, 23.9 (**3kk**), 22.5 (**3kk'**), 21.1 (**3kk**), 18.8, 18.3 (**3kk'**).

^{19}F NMR (376 MHz, $CDCl_3$) δ 67.89 (**3kk''**), 67.96 (**3kk'**), 67.96 (**3kk**)

HRMS: (ESI$^+$) calculated for $C_{13}H_{15}F_3N$ $[M+H]^+$: 242.1151, found 242.1152.

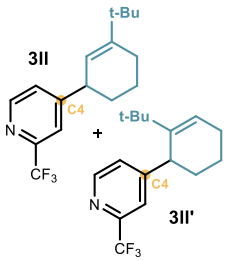

4-(3-(tert-butyl)cyclohex-2-en-1-yl)-2-(trifluoromethyl)pyridine (3ll) and 4-(2-(tert-butyl)cyclohex-2-en-1-yl)-2-(trifluoromethyl)pyridine (3ll')

Prepared according to General Procedure A using 2-(trifluoromethyl)pyridine (23.0 µL, 0.2 mmol) and 1-(tert-butyl)cyclohex-1-ene (330 µL, 2.0 mmol). Purification by column chromatography (SiO_2, 5:95 EtOAc/hexanes) afforded products **3ll** + **3ll'** as colorless oil (25.8 mg, 46% yield, 8:1 allylic *r.r.*). Only the major product **3ll** is described.

^{1}H NMR (400 MHz, $CDCl_3$) δ 8.61 (dt, *J* = 5.0, 0.7 Hz, 1H), 7.50 (dt, *J* = 1.5, 0.7 Hz, 1H), 7.31 (ddt, *J* = 5.0, 1.7, 0.7 Hz, 1H), 5.44 – 5.42 (m, 1H), 3.49 (ddq, *J* = 8.4, 5.5, 2.7 Hz, 1H),

2.16 – 2.09 (m, 2H), 2.00 (dtd, *J* = 13.1, 6.6, 2.8 Hz, 1H), 1.79 – 1.69 (m, 1H), 1.65 – 1.55 (m, 1H), 1.44 (dddd, *J* = 13.1, 10.6, 8.2, 3.0 Hz, 1H), 1.09 (s, 9H).

^{13}C NMR (101 MHz, $CDCl_3$) δ 158.5, 149.8, 149.5, 148.2 (q, *J* = 34.0 Hz), 125.7, 121.7 (q, *J* = 273.9 Hz), 119.9 (q, *J* = 2.8 Hz), 41.6, 35.6, 31.6, 30.0, 29.1, 24.3, 21.5.

^{19}F NMR (376 MHz, $CDCl_3$) δ -68.03.

HRMS: (ESI$^+$) calculated for $C_{16}H_{21}F_3N$ $[M+H]^+$: 284.1621, found 284.1623.

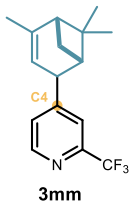

3mm

2-(trifluoromethyl)-4-(4,6,6-trimethylbicyclo[3.1.1]hept-3-en-2-yl)pyridine (3mm)

Prepared according to General Procedure A using 2-(trifluoromethyl)pyridine (23.0 µL, 0.2 mmol) and alpha-Pinene (318 µL, 2.0 mmol) prolonging the reaction time to 60 hours. The yield (39%, single regioisomer) of **3mm** was inferred by ^{1}H NMR analysis of the crude reaction mixture using trichloroethylene as the internal standard. Purification by column chromatography (SiO_2, 1:40 Et_2O/Hexanes) afforded an analytical amount product **3mm** as colorless oil (17.8 mg, 31%, ca. 90% purity).

^{1}H NMR (400 MHz, $CDCl_3$) δ 8.60 (dt, *J* = 5.0, 0.7 Hz, 1H), 7.54 (dt, *J* = 1.6, 0.7 Hz, 1H), 7.35 (ddt, *J* = 5.1, 1.7, 0.7 Hz, 1H), 5.32 (td, *J* = 2.9, 1.6 Hz, 1H), 3.62 (h, *J* = 2.3 Hz, 1H), 2.17 – 2.13 (m, 1H), 1.81 (t, *J* = 1.9 Hz, 3H), 1.35 (s, 3H), 1.21 – 1.14 (m, 1H), 1.01 (s, 3H).

^{13}C NMR (101 MHz, $CDCl_3$) δ 156.3, 149.6, 148.6, 148.0 (q, *J* = 34.3 Hz), 126.4, 121.8 (q, *J* = 274.1 Hz), 120.5 (q, *J* = 2.6 Hz), 115.6, 47.6, 46.8, 45.1, 42.1, 26.3, 26.2, 23.2, 20.5.

^{19}F NMR (376 MHz, $CDCl_3$) δ -67.5.

HRMS: (ESI$^+$) calculated for $C_{16}H_{19}F_3N$ $[M+H]^+$: 282.1464, found 282.1473.

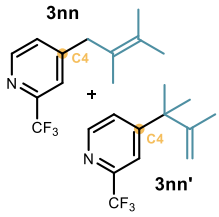

4-(2,3-dimethylbut-2-en-1-yl)-2-(trifluoromethyl)pyridine (3nn) and 4-(2,3-dimethylbut-3-en-2-yl)-2-(trifluoromethyl)pyridine (3nn')

Prepared according to General Procedure A using 2-(trifluoromethyl)pyridine (23.0 µL, 0.2 mmol) and tetramethylethylene (238 µL, 2.0 mmol) prolonging the reaction time to 60 hours. Purification by column chromatography (SiO_2, 5:95 EtOAc) afforded the mixture of products **3nn** + **3nn'** as a colorless oil (22.4 mg, 43% yield, 3:2 allylic *r.r.*).

^{1}H NMR of **3nn** (400 MHz, $CDCl_3$) δ 8.58 (dt, *J* = 5.0, 0.7 Hz, 1H), 7.47 – 7.42 (m, 1H), 7.27 – 7.24 (m, 1H), 3.47 – 3.45 (m, 2H), 1.76 – 1.75 (m, 6H), 1.63 – 1.56 (m, 3H).

^{13}C NMR of **3nn** (101 MHz, $CDCl_3$) δ 152.4, 149.8, 148.2 (q, *J* = 34.2 Hz), 128.5, 126.3 (q, *J* = 1.1 Hz), 123.6, 121.7 (q, *J* = 274.5 Hz), 120.5 (q, *J* = 2.7 Hz), 39.6, 20.7, 20.6, 18.5.

^{19}F NMR of **3nn** (376 MHz, $CDCl_3$) δ -68.1.

^{1}H NMR of **3nn'** (400 MHz, $CDCl_3$) δ 8.62 (dp, *J* = 5.1, 0.6 Hz, 1H), 7.59 (dd, *J* = 1.8, 0.7 Hz, 1H), 7.41 (ddq, *J* = 5.1, 1.8, 0.6 Hz, 1H), 5.03 (dq, *J* = 1.4, 0.7 Hz, 1H), 5.00 (p, *J* = 1.4 Hz, 1H), 1.52 (dd, *J* = 1.4, 0.7 Hz, 3H), 1.44 (s, 6H).

^{13}C NMR of **3nn'** (101 MHz, $CDCl_3$) δ 159.9, 149.9, 149.8, 148.3 (q, *J* = 34.0 Hz), 124.1 (q, *J* = 1.1 Hz), 121.7 (q, *J* = 274.1 Hz), 118.2 (q, *J* = 2.7 Hz), 111.7, 44.2, 27.6, 20.0.

^{19}F NMR of **3nn'** (376 MHz, $CDCl_3$) δ -67.9.

HRMS of **3nn** + **3nn'**: (ESI^+) calculated for $C_{12}H_{15}F_3N$ $[M+H]^+$: 230.1151, found 230.1161.

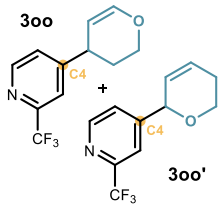

4-(3,4-dihydro-2H-pyran-4-yl)-2-(trifluoromethyl)pyridine (3oo) + 4-(5,6-dihydro-2H-pyran-2-yl)-2-(trifluoromethyl)pyridine (3oo')

Prepared according to General Procedure A using 2-(trifluoromethyl)pyridine (23.0 µL, 0.2 mmol) and 3,4-dihydropyran (182 µL, 2.0 mmol). Purification by column chromatography (SiO_2, 10:90 EtOAc/hexanes) afforded products **3oo** + **3oo'** as a colorless oil (19.8 mg, 43% yield, 7:1 allylic *r.r.*). Only the major product **3oo** is described.

^{1}H NMR (400 MHz, $CDCl_3$) δ 8.65 – 8.63 (m, 1H), 7.60 – 7.58 (m, 1H), 7.40 (dddd, *J* = 5.0, 2.2, 1.1, 0.6 Hz, 1H), 6.64 (dd, *J* = 6.3, 1.9 Hz, 1H), 4.72 (dddd, *J* = 6.3, 3.3, 0.7 Hz, 1H), 4.03 (dddt, *J* = 11.0, 8.0, 3.0, 0.4 Hz, 1H), 3.96 (ddd, *J* = 11.1, 6.9, 3.2 Hz, 1H), 2.25 (dddddd, *J* = 13.8, 6.9, 6.3, 3.0, 1.1, 0.5 Hz, 1H), 1.84 (m, 1H).

^{13}C NMR (101 MHz, $CDCl_3$) δ 156.6, 150.0, 148.4 (q, *J* = 34.3 Hz), 146.3, 125.6, 121.6 (q, *J* = 274.2 Hz), 119.7 (q, *J* = 2.7 Hz), 100.7, 63.4, 35.8, 31.1.

^{19}F NMR (376 MHz, $CDCl_3$) δ -68.0.

HRMS: (ESI^+) calculated for $C_{11}H_{11}F_3NO$ $[M+H]^+$: 230.0787, found 230.0788.

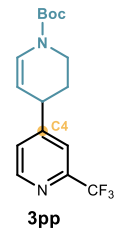

tert-butyl 2'-(trifluoromethyl)-3,4-dihydro-[4,4'-bipyridine]-1(2H)-carboxylate (3pp)

Prepared according to General Procedure A using 2-(trifluoromethyl)pyridine 23.0 µL, 0.2 mmol) and tert-butyl 3,4-dihydropyridine-1(2H)-carboxylate (367 mg, 2.0 mmol). Purification by column chromatography (SiO_2, 5:95 to 12:88 EtOAc/hexanes) afforded product **3pp** as colorless oil (24.8 mg, 38% yield, 20:1 allylic *r.r.*) and recovered olefin (311 mg, 1.7 mmol). Due to presence of N-Boc rotamers the ^{1}H NMR and ^{13}C NMR spectra were recorded at 328K which produced singular broad singlets for these peaks.

^{1}H NMR (500 MHz, $CDCl_3$, 328K) δ 8.63 (d, *J* = 5.0 Hz, 1H), 7.55 (d, *J* = 2.0 Hz, 1H), 7.36 (dd, *J* = 5.0, 1.9 Hz, 1H), 7.08 (br. s, 1H), 4.82 (br. s, 1H), 3.67 – 3.51 (m, 3H), 2.19 (dtd, *J* = 13.4, 6.2, 3.6 Hz, 1H), 1.82 (dtd, *J* = 13.5, 7.4, 4.0 Hz, 1H), 1.52 (s, 9H).

^{13}C NMR (126 MHz, $CDCl_3$, 328K) δ 156.3, 152.2, 150.1, 148.8 (q, *J* = 34.5 Hz), 128.1, 125.5, 121.7 (q, *J* = 274.3 Hz), 119.7 (q, *J* = 2.7 Hz), 104.5, 81.3, 39.7, 37.8, 30.4, 28.3.

^{19}F NMR (376 MHz, $CDCl_3$) δ -68.0.

HRMS: (ESI$^+$) calculated for $C_{16}H_{20}F_3N_2O_2$ $[M+H]^+$: 329.1471, found 329.1471.

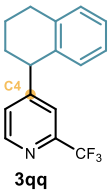

3qq

4-(1,2,3,4-tetrahydronaphthalen-1-yl)-2-(trifluoromethyl)pyridine (3qq)

Prepared according to General Procedure A using 2-(trifluoromethyl)pyridine (23.0 µL, 0.2 mmol) and 1,2,3,4-tetrahydronaphthalene (273 µL, 2.0 mmol). No other regioisomer was detected in the crude mixture. Purification by column chromatography (SiO_2, 1:100 Et_3N/hexanes to 1:3:96 Et_3N/EtOAc/hexanes) afforded product **3qq** as pale-yellow oil (27.3 mg, 49% yield, > 20:1 *r.r.*).

^{1}H NMR (400 MHz, $CDCl_3$) δ 8.60 (d, *J* = 5.0 Hz, 1H), 7.46 (d, *J* = 1.7 Hz, 1H), 7.21 – 7.17 (m, 3H), 7.12 – 7.05 (dt, *J* = 7.7, 4.2 Hz, 1H), 6.75 (dd, *J* = 7.6, 1.0 Hz, 1H), 4.23 (t, *J* = 6.4 Hz, 1H), 3.00 – 2.82 (m, 2H), 2.27 – 2.17 (m, 1H), 1.90 – 1.77 (m, 3H).

^{13}C NMR (101 MHz, $CDCl_3$) δ 158.5, 149.9, 148.3 (q, *J* = 34.1 Hz), 137.6, 136.2, 129.8, 129.5, 126.9, 126.7, 126.1, 121.6 (q, *J* = 274.3 Hz), 120.6 (q, *J* = 2.7 Hz), 45.1, 32.6, 29.4, 20.4.

^{19}F NMR (376 MHz, $CDCl_3$) δ -68.0.

HRMS: (ESI$^+$) calculated for $C_{16}H_{15}F_3N$ $[M+H]^+$: 278.1151, found 278.1152.

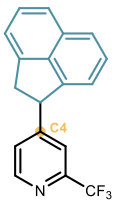

3rr

4-(1,2-dihydroacenaphthylen-1-yl)-2-(trifluoromethyl)pyridine (3rr)

Prepared according to General Procedure A using 2-(trifluoromethyl)pyridine (23.0 µL, 0.2 mmol) and 1,2-dihydroacenaphthylene (308 mg, 2.0 mmol). No other regioisomer was detected in the crude mixture. Purification by column chromatography (SiO_2, 5:95 EtOAc/hexanes) afforded product **3rr** as colorless oil (25.4 mg, 42% yield, > 20:1 *r.r.*).

^{1}H NMR (400 MHz, $CDCl_3$) δ 8.66 – 8.62 (m, 1H), 7.75 (t, *J* = 7.2 Hz, 2H), 7.60 – 7.54 (m, 2H), 7.51 (t, *J* = 7.6 Hz, 1H), 7.37 (d, *J* = 7.1 Hz, 1H), 7.31 – 7.27 (m, 1H), 7.12 (d, *J* = 7.1 Hz, 1H), 5.00 – 4.94 (m, 1H), 4.04 (dd, *J* = 17.6, 8.8 Hz, 1H), 3.39 (d, *J* = 17.3 Hz, 1H).

^{13}C NMR (101 MHz, $CDCl_3$) δ 156.5, 150.3, 148.6 (q, *J* = 34.3 Hz), 145.8, 142.5, 138.6, 131.6, 128.4, 128.1, 125.5, 123.9, 123.0, 121.5 (q, *J* = 274.3 Hz), 120.2, 119.8, 119.7 (q, *J* = 2.8 Hz), 48.7, 41.0.

^{19}F NMR (376 MHz, $CDCl_3$) δ -67.6.

HRMS: (ESI$^+$) calculated for $C_{18}H_{13}F_3N$ $[M+H]^+$: 300.0995, found 300.0997.

1.0 mmol Scale Reaction

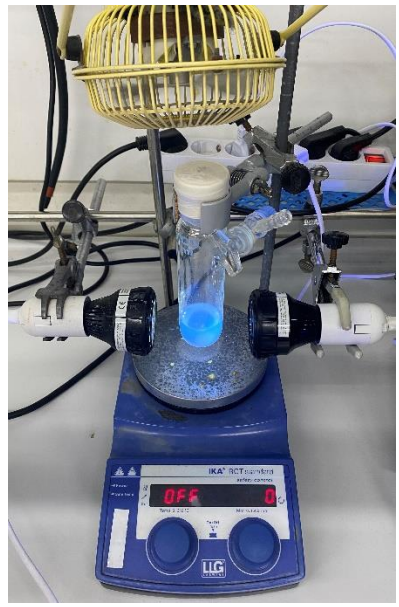

Figure 3.51. 1 mmol scale reaction using two 365 nm EvoluChem lamps.

To an argon-purged glass vial, containing the dithiophosphoric acid catalyst **C2** (127 mg, 0.2 mmol), and pyridine **1a** (81 µL, 1 mmol), was added 2,4,6-collidine (66 µL, 0.5 mmol), followed by cyclohexene **2a** (1 mL. 10 mmol) and argon-sparged HPLC grade acetone (20 mL, 0.05 M). The vial was sealed with Parafilm, and placed in the 365 nm irradiation setup as shown on Figure S9. The reaction was stirred for 16h, then the solvent was evaporated.The regioisomeric ratio **3a**/**3a'** (2.6:1) of the crude mixture was measured by ^{1}H NMR analysis. Purification by column chromatography (SiO_2, 1:10:89 Et_3N/EtOAc/hexanes) afforded product **3a** as a light-yellow oil (81.2 mg, 51% yield, > 20:1 *r.r.*). The minor regioisomer **3a'** was not isolated after column chromatography.

Chapter IV

General Conclusions

During my doctoral studies, I have explored new photocatalytic strategies for the functionalization of pyridines and other azaarenes. In a first project, detailed in Chapter II of the thesis, I developed a photocatalytic system for the chemodivergent benzylation of 4-cyanopyridines. Our initial plan focused on the C4-selective functionalization of pyridines proceeding through an established *ipso*-substitution radical mechanism. A serendipitous discovery led to the development of a complementary C2-selective strategy. The two protocols used a single photoredox catalyst to generate benzyl radicals upon N−F bond activation of 2-alkyl *N*-fluorobenzamides. The judicious choice of different photocatalyst quenchers allowed us to select between mechanistically divergent processes: an *ipso*-substitution path, proceeding *via* radical coupling, and a Minisci-type addition, which enabled selective access to regioisomeric C4 or C2 benzylated pyridines, respectively. These complementary strategies grant access, at will, to orthogonal substitution pattern on the pyridine moiety leading to complex substitution. Our mechanistic investigation, by means of pH measurements, Stern-Volmer quenching experiments and reaction profile analysis, allowed us to rationalize the chemoselective switch.

Chapter II details the development of a method for the selective C-H allylation of pyridines. The method harnessed the unique reactivity of pyridinyl radicals, generated upon single-electron reduction of pyridinium ions, which undergo effective coupling with allylic radicals. Crucial for reaction development was the identification of a dithiophosphoric acid organocatalyst, which mastered three distinct catalytic roles. In a sequential manner, it acted as *i*) a Brønsted acid to protonate and activate the pyridine, *ii*) a strong reductant in the excited state, able to reduce the resulted pyridinium ion, and *iii*) a hydrogen atom abstractor to deliver an allylic radical from cyclic alkenes. The resulting pyridinyl and allylic radicals then coupled with a distinct positional selectivity for pyridine functionalisation, which diverged from classical Minisci chemistry. Overall, two substrates underwent C-H functionalization to form a new C(sp^2)-C(sp^3) bond.

Overall, during my PhD research investigations, I identified new photochemical methods to functionalize pyridines with control over site selectivity.

UNIVERSITAT ROVIRA I VIRGILI
PHOTOCATALYTIC STRATEGIES FOR THE FUNCTIONALIZATION OF PYRIDINES
Eleni Georgiou

UNIVERSITAT ROVIRA i VIRGILI

ICIQ
Institut Català d'Investigació Química